LEGIBILITY NOTICE

A major purpose of the Technical Information Center is to provide the broadest dissemination possible of information contained in DOE's Research and Development Reports to business, industry, the academic community, and federal, state and local governments.

Although a small portion of this report is not reproducible, it is being made available to expedite the availability of information on the research discussed herein.

1

DISCLAIMER

This report was prepared as an account of work sponsored by an agency of the United States Government. Neither the United States Government nor any agency thereof, nor any of their employees, makes any warranty, express or implied, or assumes any legal liability or responsibility for the accuracy, completeness, or usefulness of any information, apparatus, product, or process disclosed, or represents that its use would not infringe privately owned rights. Reference herein to any specific commercial product, process, or service by trade name, trademark, manufacturer, or otherwise does not necessarily constitute or imply its endorsement, recommendation, or favoring by the United States Government or any agency thereof. The views and opinions of authors expressed herein do not necessarily state or reflect those of the United States Government or any agency thereof.

ORNL-6385
Distribution Category
UC-4

ORNL--6385

DE87 013361

CHEMISTRY DIVISION ANNUAL PROGRESS REPORT
for Period Ending March 31, 1987

M. L. Poutsma, Division Director
L. M. Ferris, Section Head - Organic, Inorganic, and Catalytic Chemistry
O. L. Keller, Section Head - Transuranium Element Chemistry
R. E. Wasmer, Section Head - Aqueous, Separations, and Structural Chemistry

Date of Issue: August 1987

Prepared by the
OAK RIDGE NATIONAL LABORATORY
Oak Ridge, Tennessee 37831
operated by
MARTIN MARIETTA ENERGY SYSTEMS, INC.
for the
U.S. DEPARTMENT OF ENERGY
under Contract No. DE-AC05-84OR21400

MASTER

Reports previously issued in this series are as follows:

ORNL-2386	Period Ending June 20, 1957
ORNL-2584	Period Ending June 20, 1958
ORNL-2782	Period Ending June 20, 1959
ORNL-2983	Period Ending June 20, 1960
ORNL-3176	Period Ending June 20, 1961
ORNL-3320	Period Ending June 20, 1962
ORNL-3488	Period Ending June 20, 1963
ORNL-3679	Period Ending June 20, 1964
ORNL-3832	Period Ending May 20, 1965
ORNL-3994	Period Ending May 20, 1966
ORNL-4164	Period Ending May 20, 1967
ORNL-4306	Period Ending May 20, 1968
ORNL-4437	Period Ending May 20, 1969
ORNL-4581	Period Ending May 20, 1970
ORNL-4706	Period Ending May 20, 1971
ORNL-4791	Period Ending May 20, 1972
ORNL-4891	Period Ending May 20, 1973
ORNL-4976	Period Ending May 20, 1974
ORNL-5111	Period Ending Nov. 1, 1975
ORNL-5297	Period Ending Mar. 31, 1977
ORNL-5485	Period Ending Aug. 31, 1978
ORNL-5665	Period Ending Feb. 29, 1980
ORNL-5817	Period Ending July 31, 1981
ORNL-5954	Period Ending Jan. 31, 1983
ORNL-6037	Period Ending Jan. 31, 1984
ORNL-6152	Period Ending Jan. 31, 1985
ORNL-6261	Period Ending Jan. 31, 1986

CONTENTS

1. INTRODUCTION AND DIVISIONAL OVERVIEW 1

2. COAL CHEMISTRY 4

2.1 Studies of Coal Structure by Ionization and Methylation of Acidic Sites: PSOC 1197 Low Volatile Bituminous Coal 4

2.1.1 O-Methylation of PSOC 1197: The Distribution of Acidic OH Sites . . 4

2.1.2 C-Methylation of PSOC 1197: The Distribution of Acidic CH Sites . . 5

2.2 Applications of Solid-State NMR to Studies of Coal Structure and Reactivity 7

2.2.1 Concentration Estimate of Chemically Reactive Methylene and Methine Carbon Centers of Defined C-H Acidity in Coal 7

2.2.2 ^{1}H-^{31}P-^{13}C-DCP/MAS-NMR: Polarization Dynamics of Model Compounds . . 9

2.3 Structural Studies of Texas Lignite by Acid Catalyzed Transalkylation 10

2.4 Thermolysis of Surface-Attached 1,3-Diphenylpropane: Implications for Free-Radical Chain Decomposition Pathways in Coal 11

3. AQUEOUS CHEMISTRY AT HIGH TEMPERATURES AND PRESSURES 14

3.1 Thermodynamics of Solutions 14

3.1.1 Isopiestic Measurements at High Temperatures 14

3.1.2 Isopiestic Measurements at 25°C 14

3.1.3 High-Temperature, High-Pressure Density Measurements 15

3.1.4 Thermodynamics of (Methanol + Water) 15

3.1.5 Thermodynamics of NaOH(aq) to High Temperatures and Pressures 16

3.1.6 Modeling of the Thermodynamics of HCl(aq) 17

3.2 Chemical Equilibria 18

3.2.1 Ionization of Water in Sodium Trifluoromethanesulfonate Solutions to Elevated Temperatures 18

3.2.2 Solubility of Magnetite in Aqueous Acetate Media from 100 to 250°C 18

3.2.3 The Protonation of Tris(hydroxymethyl)aminomethane in Aqueous NaCl Media to 200°C 19

3.3 Other Topics 19

3.3.1 Ionic Electrical Conductances 19

3.3.2 Speciation of Cr(VI)(aq) at High Temperatures by Raman Spectroscopy 19

3.3.3 Possible Geochemical Production of Biological Precursors: Amino Acids and Other Amines (also Hydrocarbons) from Aqueous Ammonium Carbonate Solutions and Metal Carbides at 200°-300°C 20

3.3.4 Modified Raoult's Law Applied to Potassium and Lithium Nitrate Solutions 20

3.3.5 Electrical Conductance of Liquid and Supercritical Water 21

4. GEOCHEMISTRY OF CRUSTAL PROCESSES TO HIGH TEMPERATURES AND PRESSURES 22

4.1 Hydrothermal Geochemistry 22

4.1.1 Aluminum Speciation and Solubility of Hydroxide Phases 22

4.1.2 Ferrous Acetate Complexing by Hydrogen Electrode EMF 23

4.1.3 High Temperature – High Pressure Vibrating Tube Densimeter 23

4.1.4 Kinetics of Isotopic Exchange at Elevated Temperatures and Pressures 23

4.1.5 Rates of Isotopic Exchange in the Basalt-Seawater System 23

4.1.6 Isotopic Studies of Icelandic Geothermal Systems 24

4.2 Silicate Melt Geochemistry 24

4.2.1 Hydrogen Leak Rates in the 1000 MPa Hydrogen-Service Internally Heated Pressure Vessel (IHPV) at High Hydrogen Pressures 24

4.2.2 An Improved Shaw Hydrogen Osmotic Membrane for Use in IHPV Apparatus 25

4.2.3 Hydrogen Permeation Through Platinum at $P_1 = P_{H_2} = 132$ MPa and 831°C 26

4.3 Methane Generation, Migration, and Accumulation 26

4.3.1 Rockford District, Alabama 26

4.3.2 Tallulah Falls Dome 26

4.4 Continental Scientific Drilling Program Activities 27

5. CHEMISTRY OF ADVANCED INORGANIC MATERIALS 28

5.1 Application of Ion Implantation to the Study of Electrocatalysis 28

5.1.1 Electrochemical Aspects of Cl_2 and O_2 Evolution at Ru-implanted Titanium Electrodes 28

5.1.2 Photoacoustic and Photocurrent Spectroscopy of Ruthenium-implanted Titanium Electrodes: the Semiconductor/Metal Transition 30

5.2 Research on Nonoxidic Ceramics and Superconducting Oxides 31

5.2.1 Ammonolysis of Transition Metal Halides 31

5.2.2 Ammonolysis of Transition Metal Dialkylamides 32

5.2.3 Photoassisted Preparation of Ceramic Precursors 33

5.2.4 Thermal Decomposition of Bis(cyclopentadienyl) Compounds of Titanium 33

5.2.5 Studies on the Reaction of SiO_2 with NaOH at 1000°C, and Synthesis and Characterization of Sodium Titanates 34

5.2.6 Synthesis and Characterization of Titanium Phosphates and Their Reactions with NaOH at 1000°C 35

5.2.7 Attempts to Prepare Cubic BN at Atmospheric Pressure 36

5.2.8 Study of High Tc Superconductors 37

5.2.9 Study of the Reaction Chemistry of Gaseous and Solid Silicon Monosulfide 37

5.2.10 Study of Alternate Sintering Aids 37

5.2.11 Raman Microprobe Study of Phase Transformations in Ceria Stabilized Zirconia 38

6. STRUCTURE AND DYNAMICS OF ADVANCED POLYMERIC MATERIALS 41

6.1 Experimental Equipment and Methods 41

6.2 Diffraction Studies of Crystalline Polymer Fibers 41

6.3 The Structure of Dichloro(tetrapyridine)platinum(II) Trihydrate Based on Combined X-ray and Neutron Diffraction Data 42

6.4 Tricarbonyl(styrene)chromium: A Structure Study Related to the Design of Polymeric Second-Harmonic Generators 43

6.5 Evidence for Extensive Graphite Monolayers in Wyodak Coal from X-ray Diffraction 44

6.6 Evidence from X-ray Diffraction for a Covalent Bond to Bromine in Conducting Polyaniline 47

6.7 Spectra of Polymeric Systems 47

6.8 Self-Diffusion Constants of Atoms and Small Molecules Dissolved in Polymer Systems 49

6.9 Dynamic Properties of Polymer Systems Using Lattice Models 51

6.10 Structural and Thermodynamic Properties of Liquid Systems Using Lattice Models 52

7. CHEMISTRY OF TRANSURANIUM ELEMENTS AND COMPOUNDS 54

7.1 Chemistry and Physics of 5f Solids 54

7.1.1 High Temperature Thermochemical Studies 54

7.1.2 Solution Thermochemical Studies 56

7.1.3 Synthesis and Characterization of Transplutonium Monobismuthides and Monoantimonides 57

7.1.4 Magnetic Studies of Californium Chloride and Oxide, and Curium Bismuthide 59

7.1.5 Behavior of Actinide Materials Under Pressure 61

7.2 Solution Chemistry 66

7.2.1 Volumes of Aqua Ions from Measured Radial Distribution Functions 66

7.3 Transeinsteinium Chemistry 67

7.3.1 The Search for Monovalent Mendelevium 67

8. SEPARATIONS CHEMISTRY 70

8.1 Molecular Design and Synthesis 70

8.2 Synergistic Extraction of Mn(II) from Nitric Acid by Combinations of t-butylcyclohexano-15-crown-5 (tBC15C5) and t-butylbenzo-15-crown-5 (tBB15C5) with Didodecylnaphthalene Sulfonic Acid (HDDNS) 71

8.3 Radium Extraction with Dicyclohexano-21-crown-7 (DC21C7) and Neo-carboxylic Acids 71

8.4 Cesium Extraction with Crown Ether, Cation Exchanger Combination 72

8.5 Selective Extraction of Cu(II) and Ag(I) from Sulfuric Acid by a Synergistic Extraction System 72

8.6 Spectral Studies and Equilibrium Analysis of the Didodecylnaphthalene Sulfonic Acid, Dicyclohexano-18-crown-6, Sr^{2+} Extraction System 72

8.7 Spectral and Equilibrium Studies of the Hydration of Crown Ethers in CCl_4 73

8.8 Molecular Mechanics Studies of Crown Ether Complexes of Alkaline-Earth Metals 73

8.9 Crystal Structures of $Sr((CH_3)_3C_2O_2)_2 \cdot H_2O \cdot DC$-18-crown-6 and $Ba((CH_3)_3C_2O_2)_2 \cdot (H_2O)_2 \cdot DC$-18-crown-6-$H_2O$ 74

8.10 FTIR Analysis of the Hydration of Di-2-ethylhexyl Sulfoxide (DEHSO) in Dodecane 75

8.11 Extraction of Al(III) by Dibenzoylmethane 76

8.12 Computer Modeling of Solvent Extraction Data 77

8.13 Improved Apparatus for Isothermal Titration Calorimetry 77

8.14 Dual Mechanism Bifunctional Polymers: Design, Synthesis, and Application of a New Category of Metal Ion Complexing Agents 78

9. REACTIONS AND CATALYSIS IN MOLTEN SALTS 79

9.1 Protonation of Arenes in $AlCl_3$-1-Ethyl-3-Methyl-1H-Imidazolium Chloride at Ambient Temperature 79

9.2 Instrumentation for Rapid Spectrophotometry 82

10. SURFACE SCIENCE RELATED TO HETEROGENEOUS CATALYSIS 83

10.1 The Structure of Carburized W(001) Surface 83

10.2 Evidence for Sub-Surface Carbon on Mo(111) 84

10.3 Adsorption and Reaction of Methanethiol on Ni(110) 85

10.4 Structure and Composition of the Surface of NiAl(110) and NiAl(100) 86

11. ELECTRON SPECTROSCOPY 88

11.1 Electronic Structure and Dynamics of Free Atoms 88

11.2 Photoelectron Dynamics of Free Molecules 90

12. CHEMISTRY RELATED TO NUCLEAR WASTE DISPOSAL 94

12.1 An Evaluation of Retardation Parameters for Nuclide Migration in Geological Media 94

12.2 Solubility and Electrochemical Studies of Tc(IV) Oxides 95

12.3 Sorption of Radionuclides on Shales 96

12.4 Review and Evaluation of Literature on Geochemical Issues Pertinent to the Disposal of High-Level Radioactive Wastes: Technical Assistance to Geotechnical Staff of the Nuclear Regulatory Commission (NRC) 96

12.5 Solubility Issues Related to the Performance of a High-Level Nuclear Waste Repository in Bedded Salt: A Survey of Data Needs on Solubilities and Aqueous Species of Radium, Technetium and Iodine 97

13. COMPUTATIONAL MODELING OF SECURITY DOCUMENT PRINTING 99

13.1 Web Currency Inspection and Finishing Systems 99

13.1.1 Web Currency Inspection System (WCIS) 99

13.1.2 Web Currency Finishing System 100

13.2 Printing Flaw Characterization 101

13.2.1 Flaw Specification Language 101

13.2.2 Currency Flaw Severity Survey and Model 102

13.2.3 Postage Stamp Flaws 104

13.2.4 International Workshop 104

13.3 Printing Ink Chemistry and Technology 105

13.3.1 Ink Formulation 105

13.3.2 Ink Adhesion Determination 106

13.4 International Conference Organization 106

13.4.1 Machine Inspection of Printed Security Documents 107

13.4.2 Security Documents for the 21st Century 107

14. SPECIAL TOPICS 108

14.1 Conservation Programs 108

14.1.1 Hypereutectic Heat Storage Alloy 108

14.1.2 Solution Thermodynamics for Modeling Ideal Absorption Heat Pump Fluids 108

14.1.3 Lithium Hydride Properties for Thermal Energy Storage 110

14.2 Regeneration of Spent Activated Carbon 111

14.3 Microemulsion Fuels 112

14.4 The Expert System for Chemistry: Planning Syntheses and Polymer Degradation 113

14.5 Development of DNA-Specific Cytochemical Stains for Electron Microscopy 115

PUBLICATIONS, PRESENTATIONS, AND PATENTS 117

DIVISIONAL STAFFING AND FINANCIAL SUMMARY FY 1986 135

ORGANIZATION CHART 137

1. INTRODUCTION AND DIVISIONAL OVERVIEW

The Chemistry Division emphasizes research aimed at broadening the base of fundamental understanding of materials and phenomena of relevance to future energy technologies. It also conducts some shorter-range studies of more immediate energy interest in cases where the expertise of its staff and its facilities are appropriate. A broad range of chemical specialties is covered, except for analytical chemistry which is organizationally separate at ORNL. This report briefly describes recent progress in all current divisional project areas. Some selected highlights are summarized below; the number in parentheses after each entry refers to the section of this report where more details can be found.

1. The combined use of carbanion-promoted alkylation, isotopic labeling, and CP/MAS-^{13}C-NMR revealed a remarkably narrow distribution of surprisingly acidic C-H sites in a low-volatile bituminous coal and provided additional evidence for the importance of five-membered hydroaromatic ring systems in coals. Novel NMR methodology allowed subdivision of these acidic C-H sites into CH_2 ($\gtrsim$20%) and CH ($\lesssim$80%) centers. (2)

2. Studies of the thermolysis of surface-immobilized 1,3-diphenylpropane demonstrated that free-radical chain decomposition can occur at reasonable rates at 375°C even under diffusionally restricted conditions and, hence, provides a facile means for cleavage of such polymethylene linkages in coal. (2)

3. Analysis of data on the heats of dilution of methanol-water to 300°C and 400 bars provided the first set of high-temperature thermodynamic properties for a small, highly polar molecule in aqueous solution. The results show the strong dependence of thermodynamic properties on molecular size and serve as a model for the thermodynamics of the polar ion pairs which tend to form in aqueous electrolyte solutions at high temperatures. (3)

4. Potentiometric data on the dissociation quotient of water in solutions of $CF_3SO_3^-Na^+$ over the ranges 25-250°C and 0.2-6.5 molal revealed that this salt is suitable as a highly dissociated, relatively noncomplexing, stable supporting electrolyte for high-temperature studies of aqueous transition metal chemistry. (3, 4)

5. Potentiometric titrations in a hydrogen-electrode EMF cell have yielded formation quotients for the 1:1 and 1:2 complexes of Fe^{2+} with $CH_3CO_2^-$ in aqueous systems at high temperatures. The extent of coordination with acetate, both absolutely and compared with Cl^-, becomes increasingly important as temperature increases. (3, 4)

6. Aqueous solubilities of $Al(OH)_3$ (gibbsite) were measured in NaOH solutions (0.01 and 0.1 molal) up to 80°C and 5.0 molal NaCl. These new data have given an accurate measure of the stability of the $Al(OH)_4^-$ species as a function of temperature and ionic strength and of the Na^+ - $Al(OH)_4^-$ interaction parameters. (4)

7. A correlation between the rate of Cl_2 evolution and the Ru concentration-depth profile of Ru-implanted Ti electrodes has enabled, for the first time, an evaluation of the <u>in situ</u> surface concentration of the catalytically active Ru(IV) component of the "dimensionally stable anode," $Ru_xTi_{1-x}O_2/Ti$. A study of the variations in optical absorption, photocurrent, and Tafel slope with Ru content place the transition from a semiconducting to a metallic electrode, a prerequisite for efficient electrocatalysis, at a Ru/Ti ratio as low as 0.1. (5)

8. Reaction of the dialkylamides of Ti(IV), Zr(IV), and Nb(V) with liquid ammonia produced polymeric solids with high metal content. Pyrolysis converted these ammonolysis products quantitatively to refractory metal nitrides or carbonitrides. The conversion temperature and the amount of residual carbon in the final product are both lowered by the presence of H_2. (5)

9. X-ray diffraction studies of polyaniline doped with HBr showed that the bromine atoms are covalently bonded to ring carbons. This result renders all current models for the electrical conductivity of this organic polymer system untenable because they are based on an assumed ionic structure. (6)

10. Large-scale computer simulations by molecular dynamics methods of models of long polymer chains have given new insights into the dynamics of polymer melting and of bond breaking by laser irradiation. (6)

11. The hydration numbers of trivalent lanthanide ions, which have been obtained from neutron diffraction studies, have been used successfully to calculate the partial molar volumes of the ions, which are normally obtained from densimetric data. This new development in relating microscopic and macroscopic insights into aqueous solutions has also been successful for most divalent and small univalent cations. (7)

12. Two new techniques have been developed and successfully applied to the synthesis of the bismuthides of Am, Cm, and Cf. Because of the unusually large actinide-actinide separation distances afforded by the large radius of bismuth, these compounds will be useful for systematic probing of magnetic and high-pressure interactions in the actinide pnictogen series. (7)

13. Molecular mechanics modeling and further x-ray crystallographic studies of 18-crown-6 ether complexes of alkaline earth cations showed that the observed selectivities in solvent extraction originate predominantly in the balance between electrostatic bonding and dehydration energy, whereas the conformational energy of the flexible crown ether ligand plays only a secondary role. (8)

14. A solvent extraction system selective for Ra^{2+} over alkali and alkaline-earth cations has been developed based on a synergistic combination of the macrocyclic dicyclohexano-21-crown-7 ether with organophilic neocarboxylic acids. (8)

15. A method has been developed to measure the Bronsted acidity of HCl toward arene bases in chloroaluminate systems, a fundamental but until now elusive variable in Friedel-Crafts catalysis. Preliminary data show that HCl at 1 atm in liquid mixtures of $AlCl_3$ and 1-ethyl-3-methyl-1H-imidazolium chloride (55:45 molar ratio) at 25°C has an acidity similar to that of liquid HF at 0°C. (9)

16. The structure of the carburized W(001) and Mo(111) surfaces was analyzed by low-energy ion scattering. Contrary to literature hypotheses, the W surface is not grossly reconstructed, and the carbon adatoms remain above the surface to high temperatures. In contrast, carbon adatoms on the Mo surface undergo irreversible migration above 650 K to a previously unknown adsorption site localized just below the surface, where they remain stable to very high temperatures. (10)

17. A novel experimental approach based on synchrotron radiation and angle-resolved electron spectrometry has allowed, for the first time, an unambigous analysis of the resonant Auger process. Thus a wealth of new data on the electronic structure of small molecules becomes potentially available, especially for highly excited spectator electron states with core shell vacancies. (11)

18. Photoelectron spectroscopic results on the multiplet structure within the 3s and 3p levels of free manganese atoms revealed the purely atomic nature of level splitting and negated solid-state arguments, which had previously been proposed in the literature to rationalize results for transition metal salts. (11)

19. Studies aimed at generating and evaluating data which will be needed in calculations of radionuclide retardation factors in groundwaters in the geological formations under consideration as nuclear waste repository sites have continued. Examples include studies of sorption of radionuclides on representative shales and a comparison of sorption on tuff by batch and column techniques. (12)

20. The severity of flaws in printed currency, as judged by a panel of experts, has been correlated with the physical parameters of these flaws by a novel analytical model. This is a critical first step along the path to developing a system of machine inspection for security document printing operations of the U. S. Bureau of Engraving and Printing. (13)

21. Small-angle neutron scattering studies of water-in-oil microemulsion fuels, formulated both from pure model compounds and from economically realistic components, have continued to clarify important relationships between colloidal structure and performance. (14)

Summaries of staffing, organization, and funding sources are provided at the end of this report. The major source of funding is the Office of Basic Energy Sciences of the Department of Energy (DOE), but work is also carried out for other parts of DOE, for the Nuclear Regulatory Commission, and for other Federal agencies. The productivity of the division is enhanced by a significant number of guests: postdoctoral fellows, university professors on sabbatical leave, graduate students, and undergraduate students in special training programs; their contributions are acknowledged individually in the text of this report.

Additional information on any of the research projects described herein can be obtained by contacting individual members of the division.

2. COAL CHEMISTRY

The goal of this research is to gain new information at the molecular level concerning the organic chemical structure and reactivity of coals. Structurally diagnostic organic reactions are developed and used to quantify specific structural features of coals. Carbon-13 and carbon-14 double labelling techniques, solid-state ^{13}C NMR, and parallel studies with model compounds are also central to this theme. Acid catalyzed transalkylation chemistry is being used to probe aliphatic substituents and linking groups in native coals, coal extracts, and coal products. Acidic O-H and C-H sites in coal are being quantitatively probed by reactions with bases of well-defined strengths. Of particular interest is the use of carbanion bases to further assess the importance of five-membered-ring hydroaromatic structures in coals. Solid-state NMR techniques are also being developed for the study of coal structure, particularly in concert with selective chemical modifications. Current emphases are the development of ^{1}H-^{31}P-^{13}C double cross polarization techniques, and the use of CP/MAS-^{13}C-NMR to estimate the number of chemically reactive, acidic methylene and methine carbon centers in bituminous coals. Reaction mechanisms that underlie the thermal reactivity of coal are also being investigated. The thermal reaction pathways for surface-attached 1,3-diphenylpropane are being probed to further examine the impact of restricted mobility on free-radical reactivity. The information derived from these fundamental studies will contribute to the body of knowledge necessary for the development of novel processes for the utilization of coal as a source of liquid fuels and chemicals.

2.1 Studies of Coal Structure by Ionization and Methylation of Acidic Sites: PSOC 1197 Low Volatile Bituminous Coal

2.1.1 O-Methylation of PSOC 1197: The Distribution of Acidic OH Sites

(R. R. Chambers, E. W. Hagaman, M. C. Woody)

An important step in the characterization of the acidic OH sites in coal is the initial conversion of the phenols and carboxylic acids to methyl ethers and methyl esters, respectively. This O-methylation reaction serves to suppress the ionization and methylation of these acidic OH sites during the subsequent base-promoted C-methylation studies.

To evaluate the distribution of acidic OH sites in PSOC 1197, a low volatile bituminous coal from Eastern Pennsylvania, this coal was methylated with C-13, C-14 double labelled dimethyl sulfate at pH 12 or pH 7 using n-Bu_4NOH as the base. For further structural characterization, the methylated coals were subjected to base hydrolysis using n-Bu_4NOH in aqueous THF.[1] The number of base labile methyl groups was taken as a measure of the maximum number of methyl esters produced during the alkylation. The results from this study are presented below in Table 2.1.

Table 2.1 pH Dependence of O-methylation of PSOC-1197

pH	No. $^{14}CH_3$/100 coal C: Total	No. $^{14}CH_3$/100 coal C: Base Labile	Site Specificity
12	0.096 ± 0.007	0.029 ± 0.003	30 ± 6%
7	0.068 ± 0.002	0.028 ± 0.003	41 ± 6%

Two important observations emerge from the ^{14}C combustion data. First, the methylation reaction is found to be highly pH dependent, the total number of introduced methyl groups increasing with pH. Raising the solution pH from 7 to 12 results in a net increase of 0.028 ± 0.009 methyl/100 coal C, a value which is statistically significant. This pH dependence establishes that methylation of PSOC 1197 requires the removal of acidic protons. And secondly, the base hydrolysis results indicate that a small but detectable number of base labile methyl groups, 0.028 ± 0.003/100 coal C, are introduced at either pH value. However, all of these base labile methyls can be added at the lower pH value, namely pH 7. In other words, it appears that these methyls are

attached to those sites which form the most stable anions. From the data, the maximum number of methyl esters formed under these conditions is 0.028 ± 0.003/100 coal C. And finally, the data can be used to evaluate the selectivity of the reaction as a function of pH. This is done by evaluating the ratio, base labile methyls to total methyls. As shown in the last column of Table 2.1, if we adopt the midpoint values for the 'site specificity' then the data suggest a loss in selectivity as the pH is raised.

The pH dependence of this methylation reaction and the existence of base labile methyl groups in the coal derivatives implicate the ionization and methylation of acidic OH sites. On the other hand, the ^{14}C results alone do not preclude the reaction of other sites of comparable acidity. To establish whether this is important, the pH 12 O-methyl derivative of PSOC 1197 was analyzed by solid state ^{13}C NMR. In the difference spectrum, pH 12 O-methyl coal minus parent coal, methyls are detected in two distinct (but arbitrarily defined) spectral regions, those with δ >50 ppm and those with δ <50 ppm, in a measured ratio of 60:40, respectively. The resonance band at 54.6 ppm (line width at half height = 200 Hz, 8 ppm), which accounts for 0.06 methyl/100 coal C, suggests the formation of a variety of OCH_3 functional groups such as non-hindered, aromatic methyl ethers which derive from the methylation of phenols.[2] The resonance envelope with δ <50 ppm can be explained in terms of methyl groups attached to nitrogen, sulfur and carbon atoms. Using the ^{13}C NMR integration and the ^{14}C values for the pH 12 sample, the maximum number of C-methyls formed under these conditions is 0.04/100 coal C. Alternatively, if the methyl groups in O-methyl PSOC 1197 adopt the O/C discrimination ratio, 1.4/1.0, which was found for O-methyl Illinois No. 6,[2] then the calculated maximum for C-methyls increases to 0.05/100 coal C. In either case, the extent of C-methylation under these conditions is minimal and will have a negligible impact on the subsequent base-promoted C-methylation studies.

1. L. M. Stock and R. S. Willis, Am. Chem. Soc. Div. Fuel Chem. Preprints 30(1), 21-28 (1985).
2. E. W. Hagaman, R. R. Chambers, Jr., and M. C. Woody, Anal. Chem. 58,387-394 (1986).

2.1.2 C-Methylation of PSOC 1197: The Distribution of Acidic CH Sites

(R. R. Chambers, E. W. Hagaman, M. C. Woody)

To examine the distribution of acidic CH sites in PSOC 1197, a sample of pH 12 O-methyl coal (see Section 2.1.1) was treated at 0°C, in separate experiments, with an excess of the conjugate bases of 9-phenylfluorene (pK_a, 18.5),[1] fluorene (pK_a, 22)[1] and triphenylmethane (pK_a, 31)[1] as their lithium salts using tetrahydrofuran as the solvent. After quenching the reaction mixtures with C-13, C-14, double labelled CH_3I and isolating the coal derivatives, the samples were analyzed for their ^{14}C contents, with appropriate corrections made for the amount of reagent incorporation. The isolated derivatives were treated repetitively with base and $^{13,14}CH_3I$ a total of three times. The results are depicted in Table 2.2 below. The important trends to be noted from the data are as follows. First, the reactivity of O-methyl PSOC 1197 towards these bases, as measured by the numbers of introduced methyl groups, follows the order 9-phenylfluorenyllithium << fluorenyllithium ≈ trityllithium. In other words, most of the alkylation chemistry can be accomplished using fluorenyllithium as the base. These results suggest that the acidic CH sites in PSOC 1197 have a narrow range of acidities, and we conclude that the pK_a values for these sites are comparable to that of fluorene (pK_a, 22).[1] More specifically, we can bracket the pK_a values of these sites in the approximate range of 19 < pK_a <22 since this coal is virtually unreactive towards 9-phenylfluorenyllithium (pK_a, 18.5).[1]

Table 2.2. pK_a Dependence of C-Methylation of PSOC 1197

Base, B (pK_a, BH)[1]	Treatment No.	No. $^{14}CH_3$/100 Coal C
	1	0.024 ± 0.002
9-phenylfluorenyllithium (18.5)	2	0.042 ± 0.004
	3	0.061 ± 0.006
	1	0.71 ± 0.07
fluorenyllithium (22)	2	1.6 ± 0.2
	3	1.9 ± 0.2
	1	0.71 ± 0.07
trityllithium (31)	2	1.2 ± 0.1
	3	1.7 ± 0.2

Of particular interest, we note that the ^{14}C data for fluorenyllithium and trityllithium are identical within experimental error. This establishes that acidic sites with 22 < pK_a <31 are absent or at least below the detection limit. For this reason, we conclude that 9,10-dihydroanthracene (pK_a = 30) and its analogs are not important structural features in PSOC 1197.

The second feature evident from the data in Table 2.2 is the requirement for multiple treatments to achieve exhaustive alkylation.[2,3] In fact, the data suggest that a minimum of three treatments is necessary before exhaustive alkylation can be achieved. This feature of the chemistry implicates the reaction of acidic $-CH_2-$ sites in PSOC 1197. Supporting evidence for this conclusion is obtained from the CP/MAS ^{13}C NMR spectra of these methylated coal derivatives (see Section 2.2.1).

All of the data presented here indicate that the acidic CH sites in PSOC 1197 have acidities approximately represented by the range 19 < pK_a <22. Within the context of coal structure, this result is surprising. Structural types such as fluorenes and others which form aromatic anions upon proton removal as well as structures which contain acidic CH bonds adjacent to electron withdrawing substituents (e.g., carbonyl) are implicated by our results. From the ^{14}C data and using fluorene as a model structure, it is possible to estimate that as much as ~9% (0.71 x 13 carbons = 9%) of the carbon in PSOC 1197 could derive from fluorene-like structures. Clearly, these results suggest that future pictures of coal structure need to highlight the importance of five-membered cyclopentadiene-type rings, a structural feature which is common to all fluorene derivatives.

---

1. D. A. Bors, M. J. Kaufman, and A. Streitwieser, Jr., J. Am. Chem. Soc. 107, 6975-6982 (1985).
2. R. R. Chambers, Jr., E. W. Hagaman, M. C. Woody, K. E. Smith, and D. R. McKamey, Fuel 64, 1349-1354 (1985).
3. R. R. Chambers, Jr., E. W. Hagaman, and M. C. Woody, Fuel 65, 895-898 (1986).

2.2 Applications of Solid-State NMR to Studies of Coal Structure and Reactivity

2.2.1 Concentration Estimate of Chemically Reactive Methylene and Methine Carbon Centers of Defined C-H Acidity in Coal

(E. W. Hagaman, R. R. Chambers, M. C. Woody, L. L. Brown)

The methylation of carbon sites in a low volatile bituminous coal, PSOC 1197, was performed using a fluorenyllithium/THF reaction system to generate coal carbanions that were quenched by further reaction with methyl iodide (see Section 2.1.2). The CP/MAS-^{13}C-NMR spectra of coal derivatives generated by serial treatments using highly enriched $^{13}CH_3I$ show striking resonance band changes in the methyl region of the spectrum as a function of alkylation step number. From an analysis of these spectra both methylene (CH_2) and methine (CH) carbon centers have been identified. A minimum estimate for this CH_2/CH site ratio is obtained from the methyl group chemical shift redistribution delineated in this study as a function of methylation step number. Separate experiments which employ ^{13}C(9) fluorene as the precursor for the alkylation base establish that the indicated fluorenyl sites are a part of the native organic coal matrix and not artifacts of reagent incorporation in the coal. The following sections expand on the experiments that lead to these conclusions.

Evidence for alkylation of methylene and methine sites in the coal. In order to monitor the accumulating number of methyl groups introduced into the coal in consecutive alkylations, the CP/MAS-^{13}C-NMR spectra of the labelled products can be subtracted from that of the [illegible] coal. The subtraction criterion that is applied is nulling the aromatic resonance area in the difference spectrum. If the methyl resonance area is evaluated by the integral over the entire aliphatic resonance band, this procedure is equivalent to the numerical evaluation from the change in aromaticity, Δf_a, between the samples.

Analysis of the NMR difference spectra (obtained at 2.35 T; 25.16 MHz for ^{13}C) yields the accumulating sum of methyl groups, 0.8, 1.8, and 2.1 per 100 coal carbons, found in the organic matrix of the coal following the first, second, and third alkylations, respectively. Two striking observations can be made from this series of difference spectra. As the number of added methyl groups increases with serial alkylation, the peak methyl resonance chemical shift moves to lower field and the full width at half-height of the methyl resonance band, $\nu_{1/2}$, monotonically decreases. Peak chemical shifts (and $\nu_{1/2}$) for the first, second, and third serial methylations are 18.8 ppm (420 Hz), 25.1 ppm (380 Hz), and 25.7 ppm (360 Hz), respectively. The unusual linewidth narrowing announces a reorganization of the high field methyl resonance component in the spectra of subsequently alkylated products such that the predominant fraction of introduced methyl resonances have or attain chemical shift values centered at 26 ppm. The evolution in local structure which accounts for the fraction of reorganized chemical shifts is

$$\underset{\text{i}}{>CH_2} \rightarrow \underset{\text{ii}}{>CHCH_3} \rightarrow \underset{\text{iii}}{>C(CH_3)_2}.$$

The labelled methyl group in ii is shifted downfield in iii, yielding after 3 passes, a rather symmetric resonance band with major spectral contributions from 19-33 ppm (26 ± 7 ppm; peak max ± 0.5 $\nu_{1/2}$). This chemical shift reorganization can be used as a measure of the concentration of reactive methylene sites in the coal as discussed below.

Methyl Group Concentration. The accumulating sum of methyl groups introduced into the coal is 0.8, 1.8 and 2.1 CH_3/100 coal C for the first, second, and third alkylation passes, respectively, as evaluated from the set of difference spectra obtained by subtraction of the spectrum of the common precursor coal from the spectra of the first, second, and third pass

alkylation products. An alternate set of difference spectra which yields the incremental increase in the methyl resonance contribution for each methylation step can be generated by progressive subtraction of spectra for sequential alkylation products. These results in principle differ from those determined using a common precursor coal spectrum only with respect to a different error distribution among the samples which arises from extraneous (reagent) area contributions to each spectrum. The results of these two evaluations compare well with values for the methyl group concentrations determined from an isotope difference method and also with the values determined by C-14 combustion analysis. The concentration of CH_3/100 coal C is similar for all analysis methods to within ±0.1 CH_3/100 coal C. We establish in the next section the levels of reagent incorporation and independently determine that errors in methyl group concentrations resulting from the reagent incorporation amount to no more than about 10%.

Extent of Methylation at Artifactual Fluorenyl Sites. In a restrictive interpretation of the results presented above, we suggest that a substantial fraction of the alkylated sites in the coal are fluorenyl centers. This result could be true and of little consequence in terms of coal structure if it happened that the methyl groups being monitored were bound to fluorenyl residues chemically or physically entrained in the products during the course of the derivatization.

To ascertain the level of reagent incorporated in the products, the parent O-protected coal (P) was alkylated serially with natural abundance methyl iodide in reactions that used 92.1% ^{13}C(9)-fluorenyllithium to generate the coal anions. The products were then subjected to NMR analysis. The added fluorene concentration is assessed from Δf_a, the difference between the theoretical f_a (f_a of P = 0.82, adjusted for added methyls; 0.8, 1.0, 0.3 for passes, 1, 2, and 3; no reagent incorporation) and the experimental value of f_a measured from the products made with ^{13}C(9)-enriched fluorene. The accumulating fluorene incorporation for the first, second, and third alkylation products is 0.2, 0.3, and 0.9 fluorene molecules/100 coal carbons, respectively. It is clear from a consideration of the chemical shift of the C(9) resonance and the C(9) shifts of the numerous fluorene model compounds we have studied that the reagent cannot be physically entrained fluorene, 9-methylfluorene or 9,9-dimethylfluorene; it must be chemically bound to the organic coal matrix.

The models indicate that the 53 ppm chemical shift for C(9) is compatible with both C(9) mono- and C(9) disubstituted fluorene derivatives. The fraction of fluorenes added to the coal that are C(9)-protonated cannot have reacted with the alkylating reagent. It is the fraction of C(9) disubstituted fluorenes that provides an upper limit estimate of the extent to which methylation may occur on the chemically introduced fluorenyl moieties. This fraction measured by dipolar dephasing experiments reaches 0.2 residues/100 coal carbons after three passes and represents the upper limit estimate for the concentration of methyl groups which can be involved in this side reaction. Hence, of the 2.1 CH_3/100 coal carbons introduced into this coal, only 0.2/100 are likely to be attached to reagent derived fluorenyl residues.

Methyl resonance band shape deconvolution: estimate of reactive methylene/methine sites in the coal. An estimate of the concentration of reacted methylene and methine sites in the coal for the first pass alkylation can be made from the difference spectrum generated from the spectrum of the first pass methylation product (54.6% $^{13}CH_3I$) and that of the second pass methylation product derived from the labelled material but produced using natural abundance methyl iodide in the second pass. The large ^{13}C-enhancement factor gained by the use of $^{13}CH_3I$ in the first pass (54.6/1.108 = 49.3) means that to a good approximation, the natural abundance methyl groups added in the second pass alkylation can be considered transparent. Within this approximation, the difference

spectrum monitors the reorganization of first pass methyl resonances as effected by the second pass alkylation. The integral over the aliphatic spectral region is zero and occurs at the aromatic carbon resonance null condition. The difference spectrum graphically depicts the ca. 19 to 26 ppm chemical shift redistribution and constitutes a proof that a fraction of the reactive sites alkylated in the first pass are re-alkylated in the second alkylation step. One-half the value of the second integral of this pseudo-dispersion signal, normalized to the total introduced methyl area, indicates that 19% of the methyl resonance area undergoes the shift. Thus, of the 0.8 CH_3/100 coal C added in the first pass, 0.15 of these are at methylene centers. The same isotope-difference technique used to evaluate the second pass methylation reveals that 0.16 of 1.0 CH_3/100 coal C added in this pass are methylene centers. No new methylene component is found in the third methylation step. Hence, over three alkylation passes 0.3 methylene sites are identified. These consume 2 x 0.3 = 0.6 of the 2.1 methyl groups added over the course of three alkylation passes, the balance (1.5 CH_3/100 coal C) reacting at methine centers. Thus 0.3/1.8 or 20% of the reacting sites in the coal matrix are methylene carbon centers (of the 1.8 total coal sites, a maximum of 0.2 could result from reagent incorporation, and none of these artifactual sites would be of the methylene type), which in light of the chemical shift behavior observed, are likely to include 9-unsubstituted fluorenyl moieties in the coal matrix. This analysis provides a lower limit estimate of the methylene concentration. This is equated with the area of redistributed methyl chemical shifts, and partial cancellation of this difference area will occur if overlap of the initial and shifted resonance bands exists. While minimal overlap is expected for individual methyl resonances, based on the magnitude of the β-effect and typical resonance line widths in coals, an additional chemical shift dispersion of the mono-methyl and gem-dimethyl [fluorenyl] moieties will result from differences in local substitution patterns. This effect introduces a degree of uncertainty in the extent of overlap of the resonance bands, and imposes the lower limit estimate condition given above.

2.2.2 ^{1}H-^{31}P-^{13}C-DCP/MAS-NMR: Polarization Dynamics of Model Compounds

(E. W. Hagaman, R. R. Chambers, M. C. Woody)

Our DCP-NMR studies have centered on the characterization of the ^{31}P-^{13}C cross polarization dynamics with the use of some isotopically enriched model compounds. The cross polarization process between spin 1/2 nuclei that are not in spin diffusion contact with homonuclear neighbors, by virtue of chemical and/or isotopic dilution, is no longer characterized by a single exponential time constant. Transient oscillations of the spin magnetization between the isolated nuclei characterize the short time behavior of the polarization transfer. In order to simplify the time constant characterization of the CP process and to define the experimental DCP methodology, experiments have been devised which suppress the oscillatory behavior in the magnetization spin order transfer step. This is effected by preventing the accumulation of spin order for the ^{31}P partner of the ^{31}P-^{13}C spin pair by periodic inversion of the r.f. phase of the ^{31}P r.f. field used in the CP step. The spin order which grows along this field is effectively averaged to zero and the transfer process is driven unidirectionally from ^{13}C to ^{31}P. At the end of the cross polarization time period the ^{13}C magnetization is decreased by that amount drained to the ^{31}P nuclei. If this signal is subtracted from the ^{13}C-magnetization developed and treated identically except for the ^{13}C-^{31}P drain step, the difference signal is the ^{13}C-^{31}P drain signal. From measurements of this drain signal intensity as a function of drain time, the cross polarization time constant between the two nuclei is obtained. For 1 the process is exponential with T_{IS} = 2.1 ± 0.1 ms. Hence, effectively complete cross polarization between directly bonded

^{31}P-^{13}C pairs will require ca. 6 ms ($3T_{IS}$). Measurements are in progress to determine T_{IS} for nonbonded ^{31}P-^{13}C pairs as in 2.

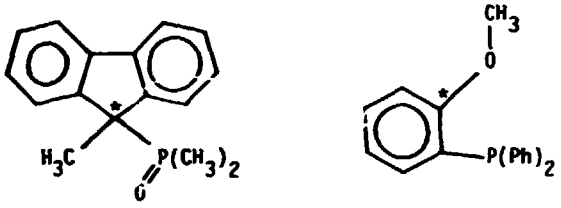

1 2

* = 90 atom % ^{13}C

2.3 Structural Studies of Texas Lignite by Acid Catalyzed Transalkylation

(B. M. Benjamin, E. C. Douglas, E. W. Hagaman)

We have previously developed the acid-catalyzed transalkylation reaction into a successful probe of certain aliphatic structures in coals.[1] Pendant, connecting, and cross-linking aliphatic groups that are attached to aromatic rings are carved out of the coal network and transferred to toluene solvent by the action of trifluoromethanesulfonic acid as a catalyst. The resulting alkyl-substituted toluenes can then be quantitatively analyzed by gas chromatography-mass spectrometry. Application of this and other techniques to a Texas lignite has now provided evidence for structural moieties that we did not observe in our earlier studies of higher rank coals: long polymethylene chains that exist in the lignite to a major extent as carboxylic acids.

The pyridine insoluble part of Texas lignite gives a transalkylation product mixture similar to those for bituminous coals.[1b] However transalkylation of the pyridine soluble portion of Texas lignite gives many new products not found in other coals. The prominent, unanticipated feature in the transalkylation products was a homologous series of alkyl-substituted toluenes with linear chains ranging in length from 2 to 34 carbons, with the even numbers from C-24 to C-34 dominant. Since the precursors to these products could be extracted from the lignite by pyridine, they must be incorporated into the pores rather than being covalently bonded to the cross-linked coal network. That these precursors are largely long-chain aliphatic carboxylic acids was demonstrated most directly by their quantitative analysis (GC and GC-MS) as volatile methyl esters after methylation of a hexane-soluble subfraction of the pyridine extract. Up to 0.1% of the whole lignite is comprised of these fatty acids. ^{13}C-NMR data also confirmed the linear paraffinic structural assignment (intense resonance at 30 ppm) and suggested, in addition, that even further amounts of such chains with different terminal functionality are likely to be present (e.g., esters, ketones, and hydrocarbons). The close correspondence of the carbon number distribution of the fatty acids detected in this lignite with that found in some plant waxes[2] has significant implications for coal genesis.

This conclusion, of course, demands that fatty acids give alkyl-substituted toluenes under the transalkylation conditions by a combination of acylation and hydrogen transfer. Model compound studies employing stearic (C-18) and capric (C-10) acids indeed confirmed this but also showed that some secondary cyclization of the alkyl-substituted toluenes occurs to form alkyl-substituted methylnaphthalenes and methyltetralins. The latter materials had been observed previously by others among the products from thermal liquefaction of Texas lignite in tetralin as a model hydrogen donor solvent,[3] and they had been interpreted as indicating the presence of a series of long-chain aliphatic substituted naphthalenes in the lignite. Given our new information about long-chain acids, we repeated the liquefaction studies with ^{13}C-labeled tetralin both with and without added fatty acids. Results show that fatty acids react with the tetralin solvent thermally (425°C) to give alkylated naphthalenes (and tetralins). Hence, it is not possible to draw firm conclusions whether alkylated naphthalenes

occur in native Texas lignite, along with the fatty acids.

1. (a) B. M. Benjamin, E. C. Douglas, and D. M. Canonico, Fuel 63, 888 (1984). (b) B. M. Benjamin, E. C. Douglas, P. M. Hershberger, and J. W. Mohoes, Fuel 64, 1340 (1985).
2. T. Robinson, "The Organic Constituents of Higher Plants," Burgess Publishing Co., Minneapolis, 1963, pp. 80-81.
3. Z. Mudamburi and P. H. Given, Org. Geochem. 8, 221,441 (1985).

2.4 Thermolysis of Surface-Attached 1,3-Diphenylpropane: Implications for Free-Radical Chain Decomposition Pathways in Coal

(A. C. Buchanan, III, C. A. Biggs)

A complicating feature in the interpretive extrapolation of model compound thermal reaction behavior to coal is the possible modifications in free-radical reactivity patterns resulting from restricted translational mobility in the coal where breaking one bond in the macromolecular structure will result in radical centers that are still attached to the residual framework. We are modeling this phenomenon by studying the thermolysis of model compounds that are immobilized by covalent attachment to an inert surface.[1] In this report we describe preliminary results on the effects of surface immobilization on the thermolysis of 1,3-diphenylpropane, whose fluid phase behavior has been previously investigated.[2]

Surface-immobilized 1,3-diphenylpropane (~~DPP) was prepared at saturation coverage by the condensation at 225°C of excess p-HOPh$(CH_2)_3$Ph with the surface hydroxyl groups of a fumed silica according to the procedure described previously for surface-immobilized bibenzyl.[1] GC analysis of two different preparations following a base hydrolysis assay procedure[1] gave coverages of 0.586 (Batch A) and 0.566 (Batch B) mmol ~~DPP per gram of final product. Thermolysis experiments in sealed, evacuated tubes typically employed 0.3-0.4 g of surface-attached material (0.17-0.23 mmol ~~DPP). Volatile products were collected in a cold trap and then analyzed by GC and GC-MS. In a separate procedure surface-attached products were liberated as phenols following digestion of the silica in 1 N NaOH, silylated to the corresponding trimethylsilyl ethers, and analyzed as above.

The thermolysis product distribution was determined as a function of ~~DPP conversion. The two lowest conversion runs (1.50 and 1.94%) were obtained at 345°C, while the remainder of the data was obtained at 375°C. Results from the two different high coverage batches of ~~DPP were consistent in terms of products detected and their relative yields. We find that at low conversions (<~3%) ~~DPP cracks to form four major products in essentially equal amounts as shown below.

$$\sim\!\!Ph(CH_2)_3Ph \rightarrow \underset{1}{\sim\!\!PhCH_3} + \underset{2}{PhCH{=}CH_2} + \underset{3}{\sim\!\!PhCH{=}CH_2} + \underset{4}{PhCH_3} \qquad (1)$$

Thermolysis of liquid DPP at very low conversions also gave a correspondingly simple product distribution as shown in Eq. 2.[2]

$$Ph(CH_2)_3Ph \rightarrow PhCH_3 + PhCH{=}CH_2 \qquad (2)$$

Hence at low conversions, the surface-immobilized DPP is reacting in an analogous fashion to liquid DPP. The additional product pair observed in the thermolysis of ~~DPP results from the fact that the two ends of the DPP molecule are no longer equivalent upon covalent surface attachment. The initial rate of the ~~DPP reaction is 15-20% h^{-1} at 375°C for the two batches (based on a 2.3-3.0% conversion after a 9 min reaction period), and this decomposition rate is comparable to that measured for liquid DPP (ca. 19% h^{-1}).[2] This further indicates that surface immobilization at high coverage is not perturbing the initial reaction behavior of the DPP moiety.

The facile decomposition of liquid DPP was demonstrated to arise from a radical chain route whose chain propagation steps are shown in Eqs. 3 and 4.[2]

$$\dot{PhCH_2} + PhCH_2CH_2CH_2Ph \rightarrow PhCH_3 + \dot{PhCH}CH_2CH_2Ph \quad (3)$$

$$\dot{PhCH}CH_2CH_2Ph \rightarrow PhCH{=}CH_2 + \dot{PhCH_2} \quad (4)$$

In the case of ~DPP, two distinct benzylic radicals can be formed by hydrogen abstraction (Eq. 6) following a small amount of initial homolysis (Eq. 5). Each radical can then undergo a rapid β-scission process (Eqs. 7 and 8) to produce the surface bound and free styrene products (3 and 2 respectively) analogous to Eq. 4. The free and surface-immobilized benzyl radicals propagate the chain by reacting with ~DPP (Eq. 6; R = $PhCH_2$) to form the free and surface bound toluene products (4 and 1 respectively) while regenerating 5 and 6.

$$\sim Ph(CH_2)_3Ph \rightarrow \sim Ph\dot{CH_2} + PhCH_2\dot{CH_2} \quad (5a)$$

$$\sim Ph(CH_2)_3Ph \rightarrow \sim PhCH_2\dot{CH_2} + Ph\dot{CH_2} \quad (5b)$$

$$\sim Ph(CH_2)_3Ph + R\cdot \ (\text{or } \sim R\cdot) \rightarrow \underset{5}{\sim Ph\dot{C}HCH_2CH_2Ph} + RH \ (\text{or } \sim RH) \quad (6a)$$

$$\sim Ph(CH_2)_3Ph + R\cdot \ (\text{or } \sim R\cdot) \rightarrow \underset{6}{\sim PhCH_2CH_2\dot{C}HPh} + RH \ (\text{or } \sim RH) \quad (6b)$$

$$\underset{5}{\sim Ph\dot{C}HCH_2CH_2Ph} \rightarrow \sim PhCH{=}CH_2 + \dot{PhCH_2} \quad (7)$$

$$\underset{6}{\sim PhCH_2CH_2\dot{C}HPh} \rightarrow \sim Ph\dot{CH_2} + PhCH{=}CH_2 \quad (8)$$

No selectivity is observed for the two possible decay routes that form the product pairs 1 and 2 or 3 and 4. This suggests that at low conversions, radicals 5 and 6 are formed with equal probability and that their β-scission reactions (Eqs. 7 and 8) occur at equal rates. Trace quantities of other primary products (each <0.05 mol% of the products) including free and surface bound PhC_2H_5 (Eq. 6; R = PhC_2H_4) and free bibenzyl (from benzyl radical coupling) are also detected.

As the conversion of ~DPP increases, there is a divergence in the yields of the four main products, and several secondary products are formed in small but increasing yields. The most significant of these (reaching about 2.8 mol % of the products at 23% conversion) is $\sim Ph(CH_2)_3Ph\sim$, 7. The formation of this doubly attached product arises from a secondary reaction that consumes 3, perhaps via addition of surface-attached benzyl radical (which would normally have reacted to form 1) to the surface-attached styrene. However even at the highest conversion studied (23%), all secondary products sum to only 5 mol % of the total products. The radical chain decomposition of surface-immobilized DPP is a very efficient process with an estimated kinetic chain length (c.l.≡ (PhVi + ~PhVi)/4PhEt) of 200 at 345°C. This calculation assumes that there is no selectivity in the initial homolysis (Eq. 5) and that all $PhC_2H_4\cdot$ start chains.

One of the most interesting features to emerge from this study is an observed selectivity for the radical chain reaction path that forms 1 and 2 relative to that which forms 3 and 4 as the conversion increases. This is most clearly seen in the styrene to toluene yield ratio (these products are not consumed in secondary reactions), which can be used as an indicator of this selectivity. The ratio increases monotonically from a value of 1.00 (±0.02) indicating no selectivity at conversions <1% to a value of 1.41 (±0.04) at 23% conversion. We previously observed in the case of surface-immobilized bibenzyl that reaction rates of radical chain pathways are very sensitive to changes in surface coverage.[1] These studies also indicated that unimolecular steps

such as Eqs. 7 and 8 should be unaffected by such surface coverage changes. The observed regiospecificity in the reaction of —OPP at higher conversions may indicate that, as the molecules of —OPP become spread apart on the surface, hydrogen abstraction at the benzylic carbon that is farthest from the surface is becoming favored, i.e., selectivity for formation of 6 (Eq. 6b) relative to 5 (Eq. 6a). However the complication resulting from the formation of secondary products, which likely involves the reaction of 5 and 6, does not allow a firm conclusion to be reached at this time. Experiments are in progress to determine if this selectivity is a result of regiospecific hydrogen transfer on the surface at lower surface coverages. The current investigation of the thermolysis of surface-immobilized 1,3-diphenylpropane has shown that facile decomposition of the trimethylene link in coal by means of a radical chain process can still occur under conditions of restricted mobility.

---

1. (a) A. C. Buchanan, III, T. D. J. Dunstan, E. C. Douglas, M. L. Poutsma, J. Am. Chem. Soc. 108, 7703 (1986). (b) M. L. Poutsma, E. C. Douglas, J. E. Leach, Ibid. 106, 1136 (1984).
2. M. L. Poutsma, C. W. Dyer, J. Org. Chem. 47, 4903 (1982), and references therein.

3. AQUEOUS CHEMISTRY AT HIGH TEMPERATURES AND PRESSURES

The purpose of this program is to conduct experimental research on reactions and thermodynamic properties of important classes of solutes in water at high temperatures and pressures. Systems chosen for study often have immediate applicability in energy related technologies but always form a basis for the evaluation of theoretical models that can advance understanding and predictability of chemical reactivity. Subjects addressed include thermodynamic properties of (single and mixed) electrolytes and non-electrolytes in addition to equilibrium and kinetic studies providing enthalpies, volume changes, and equilibrium constants for reactions such as ion-association, acid and base ionization, complexation, oxidation-reduction, hydrolysis, and solubilities in aqueous solutions. Progress is strongly dependent on a continuing development of new apparatus and techniques to complement the broad spectrum of capabilities already in hand. Research is conducted with a high level of precision on real systems selected for their practical and fundamental significance. Experimental capabilities include flow calorimetry, isopiestic and electrochemical measurements, electrical conductivity, vibrating-tube densimetry, and Raman and UV-visible spectrophotometry to extremes of temperature and pressure. Results have application in steam generation, nuclear and chemical waste disposal, chemical processing, the extraction of heat and material resources, and basic hydrothermal geochemistry.

3.1 Thermodynamics of Solutions

3.1.1 Isopiestic Measurements at High Temperatures

(H. F. Holmes, R. E. Mesmer)

The HSO_4^- anion and its equilibrium with SO_4^{2-} are important in natural systems and in models for the representation and prediction of, e.g., solubilities, and ore deposition. Very little information is available concerning aqueous solutions of the alkali metal bisulfates at elevated temperatures. We have undertaken a high-temperature isopiestic study to provide basic excess Gibbs energy data for this important family of electrolytes and to compare the properties of complex, ionizable anions with those of the simple monatomic anions. Molalities of $LiHSO_4$(aq), $KHSO_4$(aq), $CsHSO_4$(aq), and NaCl(aq), all at isopiestic equilibrium, have been measured as a function of temperature from 110 to 225°C. Osmotic coefficients were calculated from the results assuming that the metal bisulfates behave as simple 1-1 electrolytes in this temperature range, i.e., neglecting ionization of the HSO_4^-(aq) anion. Isopiestic results for the mixed electrolyte system $\{(1-y)NaHSO_4^- + yNa_2SO_4\}$(aq) were obtained during the same series of experiments with the alkali metal bisulfates. Interaction parameters for mixing HSO_4^-(aq) and SO_4^{2-}(aq) can be obtained from these latter results. With the mixing parameters and the known second ionization constant of H_2SO_4(aq), one can calculate the contribution of HSO_4^-(aq) ionization to the thermodynamics of aqueous metal bisulfates in this temperature range. Sulfuric acid and the alkali metal bisulfates (results for H_2SO_4(aq) and $NaHSO_4$(aq) were taken in a related study) behave, in this temperature range, more like HCl(aq) and the alkali metal chlorides rather than like the alkali metal sulfates.

3.1.2 Isopiestic Measurements at 25°C

(D. A. Palmer, F. H. Sweeton)

Isopiestic measurements at 25°C were initiated to complement the high temperature program which is restricted to temperatures above 110°C and thereby provide reliable data for the ion-interaction model to ambient conditions. The osmotic coefficients of the sulfate salts of the alkali metals (lithium, sodium, potassium, rubidium, and cesium) have been determined from isopiestic measurements using a sodium chloride reference solution. The results for the sodium salt are in excellent agreement with those of a recently published study over the entire concentration range of 0.2 to 3.8 molal. Similar agreement was found with much older work for the lithium and potassium salts, whereas the osmotic coef-

ficients of the rubidium and cesium sulfates showed marked departure from these previously accepted values. The discrepancy in the latter case was predicted from an earlier high-temperature study conducted in this group. Inclusion of these 25°C data in the fit of the high temperature results should lead to an improved model for the alkali metal sulfates. Finally, in view of the increasing importance of the sodium trifluoromethanesulfonate salt as a noncomplexing electrolyte, its osmotic coefficients have also been measured at 25°C from 0.4 to 3.6 molal.

3.1.3 High-temperature, High-Pressure Density Measurements

(H. F. Holmes, J. M. Simonson, R. E. Mesmer, C. S. Patterson[1])

A high-temperature (to 773 K), high-pressure (100 MPa) densimeter has been constructed and is currently being tested with several prototype tube assemblies in an effort to maximize the precision and sensitivity of the instrument. In this apparatus, a U-shaped tube is mounted in a heavy nickel-alloy holder. Two Alnico magnets are attached to the tube. Electromagnetic coils mounted on the tube holder are used in an amplifier circuit to drive and monitor the oscillation of the tube at its resonance frequency. The tube assembly is mounted in a heavy-walled aluminum sleeve suspended in the bore of a tube furnace. Testing completed to date has shown that the resonant frequency of the vibrating tube is strongly affected by mechanical losses within the apparatus and by coupling to the surroundings introduced in mounting the equipment. The importance of precise measurement and control of temperature and pressure has also been demonstrated. Individual measurements of the vibration frequency have been made with the desired precision of a few parts in 10^7; the uncertainty in replicate measurements is about ten times larger due to hysteresis and temperature instability. Modification in the tube mounting method and the construction of a solution preheater, currently underway, are expected to improve the performance of the densimeter. A number of tube assemblies are needed to optimize system performance over wide ranges of temperature and pressure with a variety of electrolyte systems.

Aqueous electrolyte systems to be studied early in the experimental program include NaOH(aq) and $CaCl_2$(aq). The high densities of these solutions at high concentrations make them attractive choices for use as secondary standards for measurements over wide density ranges. An effort will be made to extend measurements to the lowest possible concentrations, particularly in the high temperature region where small changes in solution composition lead to large changes in densities.

---

1. Furman University, Greenville, S.C.

3.1.4 Thermodynamics of (Methanol + Water)

(J. M. Simonson, D. J. Bradley[1], R. H. Busey[2])

Dilution enthalpies of aqueous "strong" electrolytes measured at high temperatures by flow microcalorimetry show dilution behavior at low molalities which is not consistent with assumed complete dissociation of the solute. Two related effects must be considered in modeling this behavior: the enthalpy of dilution and the enthalpy of dissociation of ion pairs. Due to experimental limitations, these effects are not completely separable on the basis of a set of electrolyte dilution measurements. However, it is important in describing a wide variety of measurements at high temperatures to be able to separate the contributions of reaction and excess properties.

As a model compound of ion pairs (small, polar molecules) at high temperatures, we have measured the enthalpy of mixing of methanol and water to 373 K and 40 MPa. Analysis of these results has recently been completed. Literature data were included with the results obtained in our experiments in a thermodynamically consistent analysis, giving a

representation of the thermodynamic properties of this system over the complete composition range as a function of temperature and pressure. The composition dependence of the mixing properties was found to be simpler than that for aqueous solutions of longer-chain aliphatic alcohols, indicating an increased importance of packed structures of a particular geometry for the higher alcohols. Relative magnitudes of the exothermic formation of water-water, methanol-methanol, and methanol-water hydrogen bonds are considered to be primarily responsible for the gross changes noted in the mixing enthalpies with temperature.

The relative importance of the enthalpy of dilution of neutral ion pairs on the overall excess thermodynamic properties of incompletely dissociated electrolytes is indicated by comparing these results with the dilution enthalpy of an electrolyte at high temperatures. The enthalpies of dilution of (methanol + water) are compared in Figure 3.1 with those for NaCl(aq) as functions of temperature and composition. The dilution enthalpies of the polar molecular solute are negligible compared with those for the electrolyte. In addition, the polar molecular dilution enthalpy has the opposite sign of the observed heat effect for dilution of incompletely dissociated electrolytes. This comparison indicates that the large enthalpies of dilution noted for a number of electrolytes at high temperatures are due to a very large exothermic dissociation enthalpy of ion pairs, and not to excess thermodynamic effects associated with the dilution of the polar molecules (ion pairs) present in aqueous electrolytes at high temperatures.

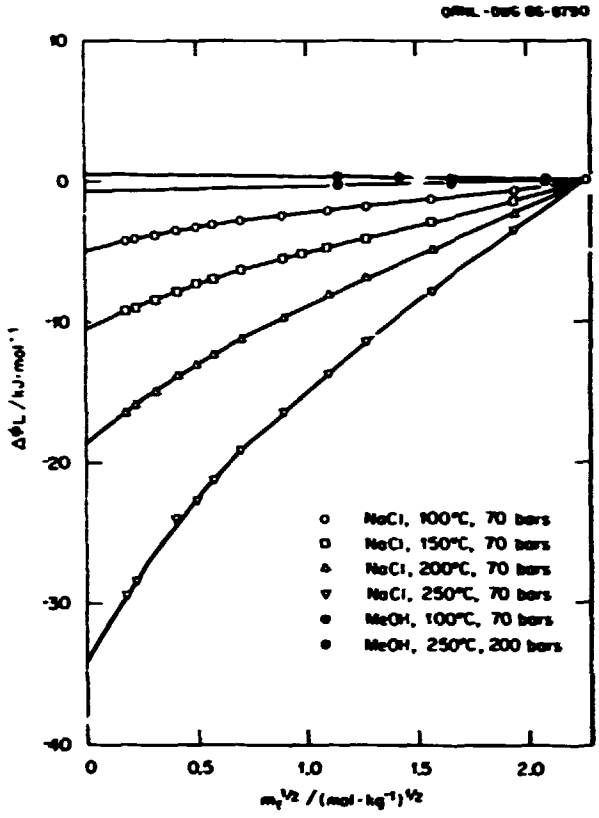

Fig. 3.1 Comparisons of the enthalpy of dilution of 5.5 m NaCl(aq) with that of aqueous methanol from 373 to 523 K.

3.1.5 Thermodynamics of NaOH(aq) to High Temperatures and Pressures

(J. M. Simonson, R. E. Mesmer)

There are a number of reactions or processes, including hydrolysis of metal ions, solubilities of solids in basic media, and measurements of the reaction thermodynamics of aqueous weak acids, for which information on the high temperature thermodynamic properties of aqueous base is required. To address this need, the enthalpies of dilution of NaOH(aq) were measured with the flow microcalorimeter developed in this program to 673 K at pressures to 40 MPa.

A preliminary analysis of our dilution enthalpy measurements has been carried out to 523 K and 40 MPa. The data were fitted with the standard ion interaction treatment, assuming complete dissociation of the solute.

1. Montana College of Mineral Science and Technology, Butte, MT.
2. ORNL Chemistry Division, retired.

Temperature and pressure dependences were assigned to the parameters of the model. Literature values of heat capacity and free energy at temperatures below 373 K were included in the analysis. The dilution enthalpies measured in this program were adequately represented by the model and were consistent with the available values of other excess thermodynamic properties. At temperatures above 373 K, activity and osmotic coefficients calculated from integration of the dilution enthalpies are not in good agreement with the available free energy results. Published values of activity and osmotic coefficients above 373 K from various investigators are not in agreement; thus it is not possible to evaluate the accuracy of the dilution enthalpies based on comparison with the free energy measurements. Isopiestic measurements on NaOH(aq) at temperatures above 373 K are planned. This new, complementary experimental information should resolve the discrepancies between the free energy and enthalpy results.

The dilution enthalpy curves for NaOH(aq) indicate that ion association is important in these solutions at temperatures above 523 K. This same general behavior has been noted previously for NaCl(aq). Dilution enthalpies above 523 K will be modeled using the ion association-interaction treatment developed earlier. This approach requires values of the association constant of NaOH(aq) at high temperatures which are currently unavailable. Electrical conductance measurements, to be made in the near future, will make available the equilibrium constants needed for this analysis.

3.1.6 Modeling of the Thermodynamics of HCl(aq)

(H. F. Holmes, R. H. Busey[1], J. M. Simonson, R. E. Mesmer, D. G. Archer[2], R. H. Wood[2])

A comprehensive model for the thermodynamic properties of HCl(aq) has been completed and accepted for publication. The model is valid over the temperature range of 0 to 375°C for pressures to 400 bars and molalities to 16 $mol \cdot kg^{-1}$. Pressure dependence of the excess Gibbs energy of HCl(aq) at the reference temperature (25°C) was calculated from PVT data and could be represented by a single term containing one adjustable parameter. A qualitative explanation for the comparative behavior of HCl(aq) and NaCl(aq) is that H^+(aq) is hydrated more strongly than Na^+(aq) at low temperatures resulting in a larger activity coefficient for HCl(aq). With increasing temperature the dielectric constant and hydration energy both decrease causing the activity coefficient of both electrolytes to decrease, albeit at a faster rate for HCl(aq). Above about 250°C, ionic association becomes greater for HCl(aq) than for NaCl(aq), resulting in a lower activity coefficient for HCl(aq). This explanation is consistent with the apparent relative molar enthalpies of these two electrolytes as shown in Figure 3.2. At 350°C the larger contribution from dissociation in the case of HCl(aq), as compared to NaCl(aq), results in a much steeper approach to infinite dilution.

Modeling of the thermodynamic properties of $CaCl_2$(aq) has been initiated. The initial phase consists of isothermal fitting of various data sets to the ion-interaction model in order to select compatible sets of experimental results. Difficulties are anticipated at high ionic strengths where hydration is incomplete, and at high-temperatures where ion association can no longer be neglected. The use of various models is expected to provide some information concerning the dependence of derived thermodynamic properties on the particular model used to obtained them.

---

1. ORNL Chemistry Division, retired.
2. University of Delaware.

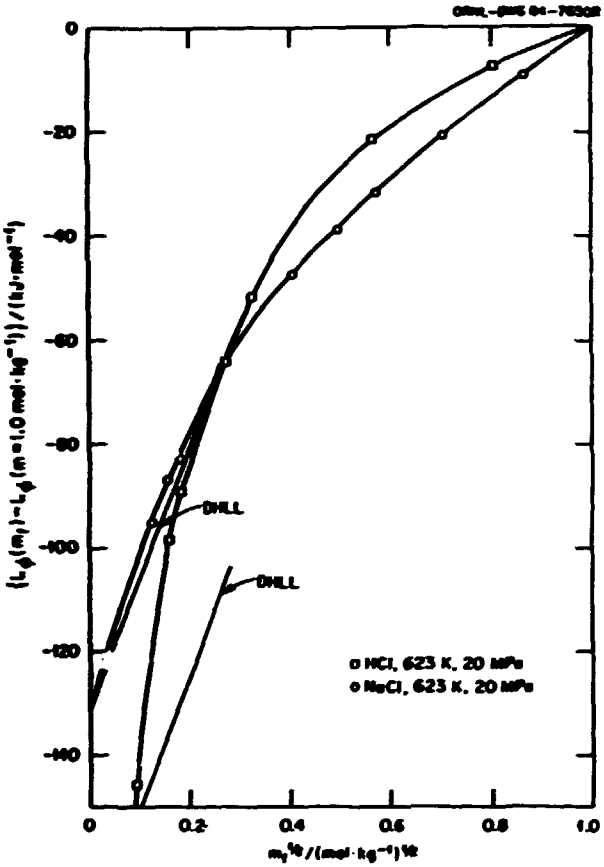

Figure 3.2. The enthalpy of dilution of HCl(aq) and NaCl(aq) at 623 K and 20 MPa plotted as the apparent relative molar enthalpy L_ϕ at the final molality m_f relative to L_ϕ at an initial molality of 1.0 mol·kg^{-1}. The thin lines are the Debye-Hückel limiting law (DHLL) at these conditions □, HCl(aq); ○, NaCl(aq).

3.2 Chemical Equilibria

3.2.1 Ionization of Water in Sodium Trifluormethanesulfonate Solutions to Elevated Temperatures

(D. A. Palmer, S. E. Drummond)

As the field of high temperature aqueous chemistry has developed to embrace the more complicated processes involved in complexation and redox reactions, the need arose for an inert, strong electrolyte to provide a constant ionic strength medium in which the concentrations of the participating ions could be varied. Given the established stability of sodium trifluoromethanesulfonate in near neutral solutions to at least 300°C[1], the first system to be investigated involved the ionization of water to provide comparative evidence of the degree of association of this salt to NaCl[2] and KCl.[3] Thus emf experiments were carried out in a concentration cell fitted with hydrogen electrodes from 25 to 250°C at six salt molalities ranging from 0.2015 to 6.4147 m. The equilibrium quotients, $Q_w = [H^+][OH^-]$, derived from these data were subjected to a regressional analysis in which were also included literature results for the equilibrium constants, enthalpies of ionization from calorimetric studies and apparent molar volumes, all determined in the absence of added salts. The equilibrium quotients and associated thermodynamic parameters are consistent with those reported for the ionization of water in NaCl and KCl within experimental error up to 3 m ionic strength, but diverge outside these limits at higher molalities; although it must be remembered that the previous measurements with KCl and NaCl were limited to 3 m. Nevertheless, the deviations observed are consistent with sodium trifluoromethanesulfonate being a stronger electrolyte than NaCl. However, the relative degree of association of these two salts cannot be determined quantitatively without knowledge of the activity coefficients for former and mixtures thereof.

1. L. Fabes and T. W. Swaddle, Can. J. Chem., 53, 3053 (1975).
2. R. H. Busey and R. E. Mesmer, J. Solution Chem., 5, 147 (1976).
3. F. H. Sweeton, R. E. Mesmer, and C. F. Baes, Jr., J. Solution Chem., 3, 191 (1974).

3.2.2 Solubility of Magnetite in Aqueous Acetate Media from 100 to 250°C

(D. A. Palmer, S. E. Drummond)

Carboxylic acids, particularly acetic, are now recognized for their potential role in mobilizing metals by complexation both in natural hydrothermal systems and in power generating facilities. Accordingly, analyses of these waters has confirmed the presence of

acetate in many of these systems. However, the stabilities of metal acetates are unknown above 25°C.

The batch method for studying the solubility of magnetite, Fe_3O_4, was employed originally in order to obtain the formation quotients for the ferrous acetate complexes. An extensive series of experiments has now been completed over the above-mentioned temperature range and at pressures of 250 and 1250 bars. These results establish the existence of the 1:1 and 1:2 species, with some evidence for the $Fe(CH_3COO)_3^-$ complex at 250°C. In order to extract the temperature dependences of the formation constants for these complexes, knowledge of the thermodynamics of the equilibria controlling the hydrogen fugacity and the pH via the acetic acid/acetate buffer are required. Using the literature values for these systems, as well as assumptions as to the magnitude of the activity coefficients, the log K_1 and log K_2 values have been derived. These results are compatible with the preliminary quantities obtained by potentiometry. However, as the latter are inherently more precise, the solubility data can now be better utilized in redetermining the thermodynamics of the magnetite/hematite hydrogen fugacity buffer as they are currently very uncertain and have not actually been measured below 300°C.

3.2.3 The Protonation of Tris(hydroxymethyl)-aminomethane in Aqueous NaCl Media to 200°C

(D. A. Palmer, D. Wesolowski)

The Tris buffer system has been used extensively in biological and oceanographic studies to control the pH of solutions. However, this system also has potential for application in high temperature aqueous studies because of its reasonable thermal stability, at least to 200°C, and its weak interaction with anions, and finally its buffering capacity which extends from the near neutral to the basic range where few other buffer systems are operative. In fact, the Tris buffer will be of immediate use in aluminum hydrolysis experiments that were recently initiated. The molal association quotients of Tris were determined potentiometrically in the concentration cell from 5 to 200°C at approximately 25° intervals, and at 6 ionic strengths from 0.0759 to 4.960. The low temperature results are in excellent agreement with those in the literature, which are generally available from 0 to 45°C. This entire data set was then fitted by nonlinear least squares regression to a six-parameter equation from which the thermodynamic quantities were subsequently derived. Thus, this treatment allows the pH of any Tris buffer mixture to be calculated up to 5 molal ionic strength and probably to 300°C with an average precision of better than 0.01.

3.3 Other Topics

3.3.1 Ionic Electrical Conductances

(W. L. Marshall)

A reduced state relationship for limiting electrical conductances of aqueous ions to high temperatures and pressures has been obtained based on our recent discovery that isothermal limiting conductances extrapolate to a common (for several temperatures) value at high density where the conductance equals zero. Walden's rule (conductance x viscosity nearly constant) is not observed. At 400°C this product increases by 70% when the solvent density is increased from 0.40 to 0.95 $g \cdot cm^{-3}$. Specific parameters for 12 ions have been obtained that can be used to calculate ionic conductances by the relationship. From these values, limiting equivalent conductances of many single and mixed aqueous electrolyte systems at 0-800°C and pressures to 400 MPa may be obtained.

3.3.2 Speciation of Cr(VI)(aq) at High Temperatures by Raman Spectroscopy

(D. A. Palmer, G. M. Begun)

The newly developed micro Raman cell was used to record spectra of chromate solutions as a function of temperature, pressure, chromate concentration, chloride concentration,

and nature of supporting electrolyte. This was the first practical test of the cell which was found to be fully functional to 300°C and 100 MPa. No attempt was made to extend this range so that this does not necessarily represent its operational limit. In the presence of high chloride concentrations at a pH of 4, a band could be assigned to the bichromate ion. This band increased in intensity with temperature and pressure. This is the first spectroscopic evidence for the existence of the bichromate ion; however, the reason for its exclusive appearance in chloride media is not fully understood at this time.

A potentiometric study[1] of the hydrolysis of chromate (VI) in sodium chloride solutions was completed recently in this laboratory. Four chromium species were identified to exist within the range of conditions investigated, namely, 25-175°C, chloride concentrations of 0.1 to 5.0 molal, total chromium concentrations of 0.001 to 0.1 molal, and pH of 2.5 to 10.0. The dominant species at most of these conditions proved to be the bichromate ion, $HCrO_4^-$. However, a recently reported study[2] of the Raman spectra of chromate solutions at room temperature over a similar range of chromium concentrations, but in the absence of added chloride ion, failed to detect any band assignable to the $HCrO_4^-$ ion.

1. D. A. Palmer, D. Wesolowski and R. E. Mesmer, J. Solution Chem., in press.
2. G. Michel and R. Cahay, J. Raman Spect. 17, 79 (1986).

3.3.3 Possible Geochemical Production of Biological Precursors: Amino Acids and Other Amines (also Hydrocarbons) from Aqueous Ammonium Carbonate Solutions and Metal Carbides at 200°-300°C

(W. L. Marshall)

Aqueous ammonium carbonate solutions under reducing conditions at 200-300°C have been reacted with iron and calcium carbides (Fe_3C, CaC_2) to produce amines (also hydrocarbons). Some amino acids (glycine, alanine, lysine) were produced by inclusion of oxygen with CaC_2, while dissolved $(NH_4)_2SO_4$ increased the amine production of Fe_3C. Products were identified by chromatographic, infrared, and colorimetric techniques. These experiments are believed to be the first to show these types of amine-forming reactions in high temperature aqueous solutions, with their potential significance to biological precursor production. The early conjectures of Oparin and others on crustal carbides and primordial organics are expanded here to include reactions with aqueous ammonium carbonates at high temperatures. It is hypothesized here that these types of reactions may have occurred at primitive, hot crust-seawater interfaces at depths where high pressure prevents boiling. Carbides in rock (or magma) might have reacted rapidly with dissolved ammonium carbonates, water, and included gases (H_2, O_2) in primitive oceans to form amino acids and other amines. Carbides are found in the earth's crust, in meteorites, and in lunar soils. These experiments were thus performed to test the possibility for such reactions. Their success suggests the need for further study. Reactive carbides under the above conditions would have disappeared in early earth history, and therefore would not be observed in recently formed rocks.

3.3.4 Modified Raoult's Law Applied to Potassium and Lithium Nitrate Solutions

(W. L. Marshall)

The modified Raoult's law (MRL) has been used to describe water activities of aqueous solutions of potassium nitrate and lithium nitrate. These activities were those of Simonson and Pitzer at 120°C together with other literature values. The MRL model fitted the activities with average deviations of 0.7% and 1.0% over ranges of molality of 0-24 and 0-14 for KNO_3 and $LiNO_3$, respectively. The description of the water activity by MRL over such a wide range of composition further indicates the power of this one-term function.

3.3.5 Electrical Conductance of Liquid and Supercritical Water

(W. L. Marshall)

A new approach to the description of the electrical conductance of (pure) water has been presented based on previous results from this activity. Briefly, a set of isothermal conductances for a given electrolyte can be extrapolated on a straight line to a very high density at which the conductance equals zero. Sets of isothermal conductances for the same electrolyte at other temperatures from 0°C to above the critical temperature (374°C) extrapolate also to zero at the same high density. With the new relationship and the earlier work, the electrical conductance of liquid and supercritical water to high temperatures and pressures is now represented by a simplified, reduced state equation. Calculations with the equation are believed to describe the specific conductance of liquid water within ±1 to ±5% at temperatures from 0°C to 374°C and at pressures from saturated to 1000 MPa (10 kbars). For supercritical water at fluid densities from about 0.3 to 1 $g.cm^{-3}$ and at temperatures from 374°C to 1000°C, the uncertainties probably increase to perhaps 15% at the highest temperatures and pressures.

4. GEOCHEMISTRY OF CRUSTAL PROCESSES TO HIGH TEMPERATURES AND PRESSURES

The primary focus of this program is the study of high temperature and high pressure hydrothermal and igneous processes that control heat and material transport in the earth's crust. Our goal is to attain an understanding of these processes that is sufficient for modeling the evolution of natural systems pertinent to DOE magma/hydrothermal and hydrocarbon energy programs. Studies of phase equilibria, crystallization kinetics and element partitioning are conducted in rock-forming silicate melt systems to 1200°C and 4 kb using facilities developed to perform these experiments under controlled redox conditions. Aqueous systems are investigated at temperatures to 600°C and 1.4 kb with a unique array of hydrothermal facilities that permit study of metal hydrolysis, mineral solubilities, acid ionization, activity coefficients and reaction kinetics. Theoretical modeling complements the experimental approach by extending the data to experimentally inaccessible P-T-X regions and by establishing the critical relationship between experimental and complex natural processes. Recent results of this program have provided a greater understanding of the role of organic complexing in mobilizing metals in hydrothermal systems; the effect of oxidation states on silicate melt properties; methane generation, migration and accumulation; and isotopic exchange between rocks and geothermal fluids.

4.1 Hydrothermal Geochemistry

4.1.1 Aluminum Speciation and Solubility of Hydroxide Phases

(D. Wesolowski)

The behavior of aluminum in geothermal systems is critical since many important rock-forming and alteration minerals are aluminosilicates (clays, feldspars, zeolites, etc.). The stabilities of these minerals, which in turn have a major influence on permeability and the pH and major element compositions of brines in equilibrium with these phases, are directly dependent on the activity of aluminum species in the fluid. Previous studies at ORNL of the reaction

$$xAl^{3+} + yH_2O = Al_x(OH)_y^{3x-y} + yH^+ \qquad (1)$$

demonstrate that in natural fluids the dominant aluminum species will likely be $Al(OH)_y^{3-y}$, where y = 0-4, and that as temperature and ionic strength increase, $Al(OH)_3$ and $Al(OH)_4^-$ likely become the most important species at near-neutral and basic pH's. In fact, previous work at ORNL demonstrated that $Al(OH)_4^-$ was predominant at 0.003-0.006 m aluminum in the presence of 0.001-0.015 m free hydroxide at 150°C.

During the past year, the solubility of gibbsite was determined in 0.01 to 5.0 molal solutions of NaOH + NaCl (two sets of runs at 0.01 and 0.10 molal NaOH) from 6.4 to 80.0°C. The equilibrium concentration quotients for the reaction, $Al(OH)_4^- \rightleftharpoons Al(OH)_3 + OH^-$, ($Q = mOH^-/mAl(OH)_4^-$), have been mathematically modeled as follows:

$$\log Q = 31.607 - 329.38/T - 5.1540 \ln T - 0.032846 I - 7.869 \times 10^{-8}\, IT^2 \qquad (2)$$

where I is the stoichiometric ionic strength and T is the absolute temperature (°K). This curve fits 80% of the data within 0.01 log units (±2%) and the remainder within 0.016 log units (±4%). Equation (2) can be differentiated to obtain the thermodynamic properties of the reaction shown above. At 25°C and zero ionic strength, these are log K = 1.137 ± 0.015, ΔH = -5.52 ± 0.30 $kJmol^{-1}$, ΔS = -13.3 ± 0.9 $JK^{-1}mol^{-1}$ and ΔC_p = -24 ± 15 $JK^{-1}mol^{-1}$.

The small ionic strength dependence and heat capacity for this reaction are due to the zero net change in charge of the reactants versus products. The linear isothermal ionic strength dependence and the very small temperature dependence of the ionic strength effect are also typical for such

"isocoulombic" reactions. These results can be used to determine the Na^+-$Al(OH)_4^-$ interaction parameters in NaCl brines.

4.1.2 Ferrous Acetate Complexing by Hydrogen Electrode EMF

(S. E. Drummond, D. A. Palmer)

In this study, EMF techniques have been developed which allow precise and direct measurement of metal complexes with hydrolyzing ligands such as acetate and other carboxylates. This method is more accurate and more rapid than conventional solubility studies and will make it possible in the near future to assess the role of organic ligands in enhancing secondary permeability in oil and gas reservoirs. The current results for the ferrous acetate complexes extend from 50 to 300°C and over a range of concentrations of sodium triflate (NaF_3CSO_3) media and acetate. Both the $FeCH_3COO^+$ and the $Fe(CH_3COO)_2$ species were observed, and the formation constants calculated from the data are in good agreement with those derived from the magnetite solubility results obtained in 1986. In general, the ferrous acetate complexes are very strong and there is every indication from these experiments that acetate is a major factor in the mobility of iron in sedimentary basin settings.

4.1.3 High Temperature — High Pressure Vibrating Tube Densimeter

(S. E. Drummond, B. E. Mesbitt[1])

During this period we have designed, built, and tested a vibrating tube densimeter that is capable of making precise measurements of the volumetric properties of fluids to 500°C and 4000 bars. This device represents a breakthrough in P-V-T measurements at elevated conditions and is designed for routine experimentation on C-O-H supercritical fluids. Preliminary experiments at 100 and 200°C and pressures up to 1000 bars, using published data for H_2O and CH_4 to calibrate the instrument, have produced density measurements for CO_2 which are well within the errors of the accepted values (±0.2%). Studies underway include an examination of the P-V-T properties of the components of natural fluids (H_2O, CO_2, CH_4, H_2) to 4000 bars and 500°C.

1. University of Alberta, Edmonton.

4.1.4 Kinetics of Isotopic Exchange at Elevated Temperatures and Pressures

(D. R. Cole)

A knowledge of the rates and mechanisms of stable isotope exchange between various geologic media is needed for the interpretation of isotopic disequilibrium processes commonly observed in geothermal systems and petroleum and natural gas reservoirs. A comprehensive review of the literature, published as Chapter 2 in Volume 16 of Reviews in Mineralogy entitled "Stable Isotopes in High Temperature Geological Processes," discusses the experimental and computational techniques used in determining the rates and mechanisms of isotope exchange for a wide variety of geological systems, including gas-gas reactions, interaction of solutes in aqueous solution, and the reaction of solids (or melts) with either gases or fluids. This work demonstrates, among other things, (1) how isotopic rate laws vary according to the type of system studied, (2) the requirements for successful exchange experiments in both homogeneous and heterogeneous systems, (3) the pitfalls in some of the techniques, and (4) the advantage of using activation parameter plots in understanding mechanism of exchange. The techniques described in this chapter lay the foundation upon which future studies will be based.

4.1.5 Rates of Isotopic Exchange in the Basalt-Seawater System

(D. R. Cole)

Calculations of water/rock ratios and the origin of water in geothermal systems are commonly made assuming that the fluids and rocks have equilibrated isotopically. However, we have observed isotopic disequilibrium in several geothermal systems, most notably in Iceland and at various sea-floor hot spring sites. In order to quantify fluid/rock

interaction at these areas, we have experimentally investigated the mechanisms and rates of isotopic exchange between basalt and seawater as a function of temperature, solution composition, rock composition and crystallinity, time, and surface area. Isotopic redistribution of both oxygen and hydrogen during experimental basalt-seawater interaction is controlled by alteration reactions similar to those observed in natural systems. In general, depletion of ^{18}O and enrichment of D in basalts occurred at all temperatures, with the magnitudes of change being greater as temperature, time, and to a lesser degree, glass content increases. Rates of oxygen isotope exchange between basalt and seawater are similar to rates observed in various silicate mineral-fluid systems in which isotope exchange is accompanied by the formation of new phases. The rate data can be used to model the duration of isotopic exchange in natural basalt-seawater systems, which in turn is related to the residence time of fluid in the system.

4.1.6 Isotopic Studies of Icelandic Geothermal Systems

(D. R. Cole)

We have examined the relationships between the extent and style of alteration and isotopic exchange resulting from fluid-rock interaction in six geothermal systems in Iceland. In each system studied we found evidence of isotopic disequilibrium. Although our experimental basalt-seawater rate data tell us equilibration times are relatively fast (e.g., months to years), the fact that we observe disequilibrium in systems known to be several thousands of years old implies that local self-sealing of the fracture system commonly occurs prior to isotopic equilibration. The ability for fractures or pores to remain open or continue to propagate may be the deciding factor in whether isotopic equilibration takes place. The Iceland data suggest that once a local domain seals, it may remain closed for the duration of hydrothermal activity or at least until the hydrothermal regime declines in temperature to a point where reaction rates are too slow to allow for reequilbration.

Recent unpublished experimental studies of hydrogen and oxygen isotope partitioning between water and 1 and 4 m NaCl solutions from 100 to 350°C by S. Matsuo and K. Kazahaya at Tokyo Institute of Technology tend to agree qualitatively with earlier studies by A. Truesdell.[1] These results were used to model the isotopic compositions of brines in several geothermal fields in Iceland. In the case of the dilute, meteoric-domonated Icelandic geothermal systems, we have observed an excellent correlation between measured bore-hole temperatures and isotopic temperatures calculated from secondary mineral-fluid fractionation factors. These data imply that secondary minerals such as quartz and calcite have equilibrated isotopically with the reservoir fluid at temperatures consistent with those currently measured down hole. However, we observe poorer agreement between calculated and measured temperatures in Icelandic systems with high salinities (e.g., Reykjanes, Svartsengi). Consequently, we readjusted the oxygen isotope fractionation factors measured between secondary alteration phases such as quartz, calcite, and smectite, and the brine for this salt effect. As a consequence of the correction, we observed a much improved correlation between measured bore-hole temperatures and isotopic temperatures calculated from the mineral-water fractionation factors, thereby confirming the experimentally measured salinity effects.

1. A. Truesdell, Earth. Planet. Sci. Letters 23, 387 (1974).

4.2 Silicate Melt Geochemistry

4.2.1 Hydrogen Leak Rates in the 1000 MPa Hydrogen-Service Internally Heated Pressure Vessel (IHPV) at High Hydrogen Pressures

(M. T. Maney)

The hydrogen-service internally heated pressure vessel (IHPV) system was developed to study magmatic and hydrothermal processes under controlled redox conditions. A rigorous

test of the ability of the system to maintain constant f_{H_2} for extended periods of time was needed to demonstrate that equilibrium f_{H_2} conditions can be attained during experiments. Hydrogen leak rate studies were conducted in conjunction with experiments designed to measure the hydrogen permeation rate through a platinum membrane. These studies were conducted to test the assumption that a pressure vessel of "cold wall" design eliminates hydrogen loss by diffusion through the vessel wall as observed in experiments using "hot wall" Cold Seal Pressure Vessel (CSPV) apparatus. Confirmation of this assumption is a prerequisite for simplifying the experimental procedures adopted by Hewitt[1] to counteract leakage due to hydrogen diffusion in Shaw bomb (modified CSPV) experiments. Hydrogen leak rates were measured at the following conditions: $P_{Tot} = P_{H_2} = 132$ MPa and T = 831°C; $P_{Tot} = P_{H_2} = 250$ MPa, and T = 600, 800, 862, and 1000°C. In all cases, observed pressure decreases in the IHPV could be accounted for by temperature decreases caused by controller or thermocouple drift, hydrogen transfer across the platinum membrane, or pressure gauge drift. For example, a pressure decrease of 1.9 MPa during the 600°C experiment can be correlated with a 1.3°C change in the furnace canister wall temperature — 187.6 to 186.3°C — that occurred during the 8.5-day experiment; and a pressure decrease of 0.3 MPa during the 800°C, 1.7-day experiment is apparently due solely to hydrogen transfer and/or gauge drift. In both of these cases the decrease is less than 0.2 MPa (2 bars) or 0.1% of the total pressure per day.

1. D. A. Hewitt, Contrib. Mineral Petrol. 65, 165 (1977).

4.2.2 An Improved Shaw Hydrogen Osmotic Membrane for Use in IHPV Apparatus

(M. T. Naney)

A number of variations on Shaw's[1,2] original hydrogen osmotic diffusion membrane design are in use (e.g., Frantz et al.[3], Hewitt[4], and Gunter et al.[5]). However, some additional design changes were made to accommodate the extended operating temperature range capabilities of IHPV experimentation. Several features are incorporated in this design that contribute to the longevity of membrane operational life. First, the internal support is designed to minimize deformation of the platinum membrane. This is accomplished by substituting a single-bore soft-fired, crushable alumina thermocouple insulator for the loose grain Al_2O_3 powder used in a membrane designed for use in IHPV apparatus by Piwinskii.[6] To provide rigidity to the membrane tip and to eliminate membrane deformation caused by differential movement of the stainless steel and ceramic supports during pressurization, structural constraint for the porous ceramic was incorporated into the design. The trifold crimp termination used in the Piwinskii design to seal the ends of the membrane is eliminated to reduce the potential for brittle failure. The low temperature end of the membrane is brazed to the supporting stainless steel capillary tubing and the small diameter stainless steel capillary tubing. The high temperature end of the membrane is sealed by welding a flat disk of the membrane metal into the open end of the membrane tubing. A laser beam weld produced a very clean joint without observable platinum-stainless steel interaction. This blunt-end termination eleminates the necessity for crimping the membrane, and provides a rugged membrane tip that is not readily damaged during sample loading operations.

1. H. R. Shaw, Science 139, 1220 (1963).
2. H. R. Shaw, "Hydrogen Osmosis in Hydrothermal Experiments," in Researches in Geochemistry, ed. P. H. Abelson, John Wiley and Sons, New York, 2, 521 (1967).
3. J. D. Frantz, J. M. Ferry, R. K. Popp and D. A. Hewitt, Carnegie Instit. Washington Yearbook, 76, 660 (1977).
4. D. A. Hewitt, Contrib. Mineral. Petrol., 65, 165 (1977).
5. W. D. Gunter, J. Myers, J. R. Wood, Contrib. Mineral. Petrol., 70, 23 (1979).

6. A. J. Piwinskii, J. R. Weidner and J. H. Carman, Phys. E: Sci. Instr., 6, 603 (1973).

4.2.3 Hydrogen Permeation Through Platinum at $P_T = P_{H2} = 132$ MPa and 831°C

(M. T. Maney)

Experiments were conducted at $P_{tot} = P_{H_2} = 132$ MPa, with samples maintained at 831°C — the melting point of NaCl at 132 MPa. Hydrogen pressure in a platinum Shaw diffusion membrane equilibrated with the hydrogen atmosphere of the IHPV in approximately 400 minutes for three initial ΔP ($P_{IHPV} - P_{Shaw}$ membrane) conditions: 12.1, 50.6, and 79.4 MPa. Initial estimates of H_2 permeation rates based on the observed incremental pressure changes in the platinum Shaw diffusion membrane over short periods of time agree well with values predicted by extrapolations of the the data of Ebisuzaki et al.[1] and Chou.[2]

1. Y. Ebisuzaki, W. J. Kass and M. O'Keeffe, Chem. Phys., 49, 3329 (1968).
2. I-Ming Chou, Amer. Jour. of Sci., 286, 638 (1986).

4.3 Methane Generation, Migration, and Accumulation

4.3.1 Rockford District, Alabama

(D. Wesolowski)

New carbon isotopic data for granitoids and their graphite-bearing metasedimentary host rocks in the Rockford District, Alabama Piedmont, demonstrate the possibility for generation of a methane-rich metamorphic fluid under amphibolite-grade metamorphic conditions, which could then migrate to a site of accumulation. In collaboration with Dr. Mark Drummond of the University of Alabama at Birmingham, the carbon isotopic ratios of graphite in 21 samples of metasediment and 24 granitoids from the Rockford District were measured. Previous work by Drummond and Wesolowski demonstrated that the granitoids in the district are synmetamorphic granites which were formed by partial melting of a metasedimentary protolith, were emplaced in their present host rocks, and were subsequently altered to Na-rich trondjhemite by the action of a circulating Na-rich metamorphic fluid. Alteration took place at temperatures of 450-550°C and pressures of 4-5 kb. Metagraywackes and granitoids have similar ^{13}C and total carbon contents. Metapelites are considerably enriched in both ^{13}C and total carbon. These observations support our earlier conclusion, made without the benefit of isotopic data, that the metagraywackes were the most likely parent rock for the Rockford Granite. While the metapelites have fairly constant ^{13}C contents, the granitoids and metagraywackes both show strong positive correlations between and ^{13}C and ^{18}O contents. The most plausible explanation for these trends is that circulating metamorphic fluids reacted with graphite and clays in the metapelites, acquiring enriched levels of ^{18}O, ^{13}C, total carbon and sodium. Upon encountering the volumetrically less abundant metagraywackes and granites, the fluids reacted with these rocks, causing mineralogical alteration and isotopic enrichment. This explanation is entirely consistent with the major element chemistry. These results clearly document both the reactivity of graphite and the high fluid flux in high P-T metamorphic regimes. Preliminary calculations indicate that fluids in the Rockford District probably contained 15 mole percent CH_4.

4.3.2 Tallulah Falls Dome

(D. Wesolowski, D. R. Cole)

In a collaborative effort with Professor Robert Bodnar of Virginia Polytechnic Institute, abundant methane-rich inclusions were discovered in late tectonic veins and structures at several sites including the Tallulah Falls Dome, about 20 miles northwest of the ADCOH target area. Detailed seismic, gravity and magnetic data collected by NSF-funded ADCOH scientists indicate that the

Blue Ridge basal detachment fault may lie within 3 km of the surface beneath the Tallulah Falls Dome. This fault appears to separate overlying amphibolite to granulite faces metamorphics of the Blue Ridge Province from underlying unmetamorphosed Cambro-Ordovician clastics and carbonates of the Valley and Ridge platform sequence. These observations suggest that the Tallulah Falls Dome may be a favorable site for accumulation of methane or other hydrocarbons in a domal feature beneath the Blue Ridge-Inner Piedmont thrust sheet. A subgroup of the ADCOH team, including Wesolowski and Cole, is currently investigating the possibility of a DOE/BES-funded exploratory drill hole into the Tallulah Falls Dome to test this hypothesis.

4.4 Continental Scientific Drilling Program Activities

(D. Wesolowski, M. T. Maney, D. R. Cole)

These activities principally involved the participation in various CSDP workshops and meetings. Specifically, Wesolowski and Cole participated in the ADCOH Workshop held in Helen, Georgia, where Wesolowski chaired the discussion on Stable Isotope Geochemistry/ Hydrothermal Processes which has been incorporated into the DOSECC format preproposal. In addition, Wesolowski helped present the ADCOH Plan to the DOSECC Science Advisory Committee in Denver. Maney and Cole participated in the Katmai workshop held in Durango, Colorado, and contributed directly to the Science Drilling Plan in the areas of geochemical evolution of the early vapor system and the use of kinetic isotope exchange models in quantifying the temporal relationships of fluid-rock interaction, respectively. Further involvement in CSDP activities on a research level will be contingent upon the successful acquisition of funding from CSDP-related proposals.

5.0 CHEMISTRY OF ADVANCED INORGANIC MATERIALS

The research activities encompassed by this program are centered on two broad classes of inorganic materials of importance to a variety of energy-related technologies: (1) electrocatalysts, and (2) nonoxidic ceramics. Research in the area of electrocatalysis has as its objective the acquisition of a thorough knowledge of the fundamental physicochemical processes involved and of the properties required of an effective catalyst. In a novel and systematic approach to the attainment of the aforementioned objective, modern surface-modification techniques (ion implantation, ion-beam mixing, ion-beam plating, etc.), coupled with nondestructive Rutherford backscattering, are utilized in the preparation and characterization of well-defined electrocatalytically active surfaces. The kinetics and mechanistics of the catalyzed reaction, the electronic characteristics and stability of the catalyst, and the specific function of the catalytically active species are determined for prototypic systems (e.g., Cl_2 and O_2 evolution at $M_xTi_{1-x}O_2$/Ti (M = Ru, Ir, Rh, Os, etc.) electrodes) by means of electrochemical techniques and photoacoustic/photocurrent spectroscopies. The objective of research in the ceramic field is the development of new generalized methodologies for the synthesis of nonoxidic ceramic materials (BN, Si_3N_4, SiC, and the borides, nitrides, carbides, carbonitrides, and silicides of the transition metals of groups 4, 5 and 6). Emphasis is placed upon low-temperature methods for the preparation of inorganic or organometallic precursors which may be thermally or photochemically converted to ceramic powders, fibers, or films. This approach is exemplified by the synthesis of titanium, zirconium, and niobium nitrides and carbonitrides *via* pyrolysis (<800°C) of the ammonolysis products of the corresponding transition metal halides or dialkylamides. High-temperature methodologies are illustrated by the reactions of molten NaCN with TiO_2 or titanium pyrophosphates to yield TiN. Research on the synthesis and characterization of high T_c superconductors in the Y-Ba-Cu-O system, and on improved sintering aids has been initiated. Intermediate and final products synthesized in the ceramic program are characterized by Raman and UV-Vis-FTIR spectroscopies, x-ray diffraction, and thermal analysis (DTA/TGA-mass spectrometry).

5.1 Application of Ion Implantation to the Study of Electrocatalysis

5.1.1 Electrochemical Aspects of Cl_2 and O_2 Evolution at Ru-implanted Titanium Electrodes

(E. J. Kelly, D. E. Heatherly, C. W. White[1])

A detailed study has been made of the electrocatalysis of the chlorine and oxygen evolution reactions at Ru-implanted titanium electrodes in aqueous media.[2] Ru-implanted titanium near-surface alloys were generated by ion implantation of ^{102}Ru ions into zone-refined titanium and characterized (Ru concentration/depth profiles) by Rutherford backscattering. A judicious selection of multiple beam energies (40, 70, and 120 keV) and fluences (number of ions implanted per cm^2 of surface) at each energy enabled the generation of near Gaussian profiles extending over a depth of approximately 100 nm and having a rather broad Ru concentration peak located at 20-40 nm from the surface. The peak Ru concentrations ranged from 1.94×10^{21} to 1.77×10^{22} atoms cm^{-3}.

The electrochemical behavior of the Ru-implanted titanium electrodes in the potential region of interest for Cl_2 and O_2 evolution ($E^0_{Cl^-/Cl_2}$ = 1.36 V vs SHE and $E^0_{H_2O/O_2}$ = 1.23 V vs SHE) was determined in acidic (pH = 1.0) chloride, perchlorate, and sulfate solutions by means of conventional potentiostatic and potentiodynamic polarization techniques. Under the prevailing experimental conditions, the near-surface alloys are anodically oxidized to form a thin (3-5 nm) film of electrocatalytically active $Ru_xTi_{1-x}O_2$ on the alloy substrate. As a consequence of the continuous formation and dissolution of the $Ru_xTi_{1-x}O_2$ film (at constant film thickness) which occurs when an implanted electrode is immersed in an electrolyte (e.g., 1 M [Cl^-]), the oxide/solution interface at which the Cl_2 and

O_2 evolution reactions occur passes through the original implant region. Simultaneously, the current density (i) corresponding to the rate of the Cl_2 evolution reaction increases (moving up the Gaussian) from zero to a peak value (i_p) associated with the peak concentration ($C_{Ru,p}$) of Ru in the implant profile, and then decreases as the surface moves beyond the peak (moving down the Gaussian). As shown in Fig. 5.1, i_p is a linear function of $C_{Ru,p}$, i.e., $i_p = kC_{Ru,p}$. The concentration of Ru(IV) cations in the oxide film ($C_{Ru(IV)}$) is proportional to the concentration of ruthenium (C_{Ru}) in the volume element of alloy from which the oxide is formed, i.e., $C_{Ru(IV)} = \lambda C_{Ru}$ (λ = 0.50). Consequently, the proportionality between i_p and $C_{Ru,p}$ provides unequivocal proof that the rate of Cl_2 evolution is first order in the concentration of the catalytically active Ru(IV) cation in the oxide at the oxide/solution interface and enables, for the first time, an <u>in situ</u> evaluation of the latter quantity <u>via</u> the equation, $C_{Ru(IV)} = (\lambda/k)i$. In Fig. 5.1 (Δ points), the linear relation observed between i_p and the total Ru fluence is an artifact deriving from the proportionality between $C_{Ru,p}$ and the total fluence when

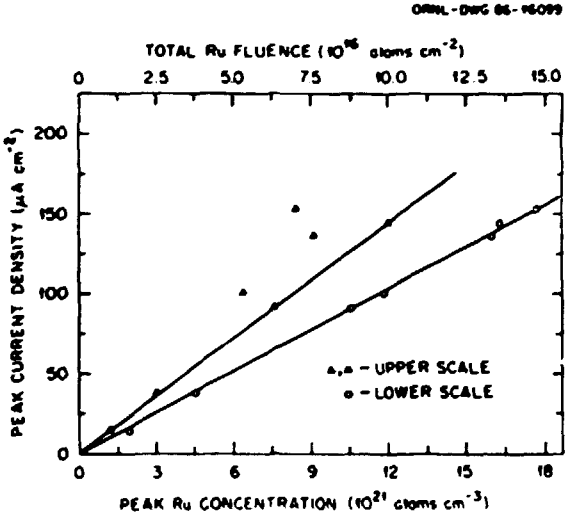

Fig. 5.1. Peak current density (i_p) as a function of: O, peak Ru concentration ($C_{Ru,p}$); Δ and ▲, total Ru fluence under constant and variable implantation conditions, respectively. 1 M [Cl^-] (pH = 1.0), E = 1.10 V <u>vs</u> SCE.

constant implantation conditions are maintained. When the implantation conditions were changed, the proportionality between i_p and the total fluence was destroyed (see ▲ points in Fig. 5.1) while that between i_p and $C_{Ru,p}$ was retained. Consequently, the rate of the Cl_2 evolution reaction depends only upon the Ru concentration and not upon fluence-dependent factors such as the implantation or radiation damage.

The Tafel slope for the Cl_2 evolution reaction at $Ru_xTi_{1-x}O_2/Ti$ electrodes was shown to be equal to 40 mV, i.e., $\partial E/\partial \log i = 2.303(2RT/3F)$, where E is the electrode potential. The reaction order with respect to chloride ion concentration, $\partial \log i/\partial \log [Cl^-]$, was found to approach 1.0 and 2.0 at high and low chloride concentrations, respectively. The aforementioned diagnostic criteria characterizing the Cl_2 evolution reaction were shown to be consistent with a modified Volmer-Heyrovsky mechanism: (1) $S + Cl^- \rightleftharpoons S - Cl^-_{ad}$, (2) $S - Cl^-_{ad} \rightleftharpoons S - Cl_{ad} + e^-$, (3) $Cl^- + S - Cl_{ad} \rightarrow S + Cl_2 + e^-$ (rate-determining step), where S represents Ru(IV) sites at the oxide/solution interface. Similarly, the 40 mV Tafel slope for the O_2 evolution reaction was shown to be consistent with the well-known mechanism: (4) $S + H_2O \rightleftharpoons S - OH + H^+ + e^-$, (5) $S - OH \rightarrow S - O + H^+ + e^-$ (rate-determining step), (6) $2S - O \rightarrow O_2 + 2S$. According to the above mechanisms, the current densities corresponding to the rates of Cl_2 evolution (i_{Cl}) and O_2 evolution (i_O) are given by the equations,

$$i_{Cl}/[S]F = 2k_3[Cl^-]K_2\{K_1[Cl^-]/(K_1[Cl^-] + 1)\}\cdot Z$$

and

$$i_O/[S]F = 2k_5(k_4/k_{-4})a^{-1}_{H^+}\cdot Z$$

where $Z = \exp(3FE/2RT)$.

It should be noted that although $Ru_xTi_{1-x}O_2$ is a highly effective catalyst for the Cl_2 evolution reaction, it is much less effective for the O_2 evolution reaction. For example, in 1 <u>M</u> [Cl^-](pH = 1.0), the current efficiency for Cl_2

evolution, $100i_{Cl}/(i_{Cl} + i_O)$, was shown to exceed 98%.

---

1. Solid State Division, ORNL.
2. E. J. Kelly, D. E. Heatherly, C. E. Vallet, and C. W. White, J. Electrochem. Soc., in press.

5.1.2 Photoacoustic and Photocurrent Spectroscopy of Ruthenium-implanted Titanium Electrodes: the Semiconductor/Metal Transition (C. E. Vallet, S. E. Borns[1] C. W. White[2])

In situ photoacoustic/photocurrent spectroscopies in conjunction with potentiodynamic polarization measurements[3] were initiated at Ru-implanted titanium electrodes in order to explore the possibility of monitoring the transition from a semiconducting n-TiO_2 layer to a metallic-oxide layer through measurements of the $Ru_xTi_{1-x}O_2$ layer optical absorption and photocurrent.

An electrode implanted with a low dose of 0.8×10^{16} Ru cm^{-2} was used to locate a possible threshold value of the ruthenium content at which metallic behavior and electrocatalytic activity appear. Properties of the oxide layer, formed at 0.9 V/SCE in (1 M $[Cl^-]$, pH = 1.0) solution, were monitored over a time period (about 10 days) during which the near-Gaussian Ru-implant profile was progressively brought to the surface by dissolution. Slow scan rate potentiodynamic measurements were made in the potential region of chlorine evolution after each spectroscopic measurement. The Tafel slopes observed at 1.1 V/SCE decreased from 400 mV (typical of a semiconducting electrode) at the beginning of the experiment to a value of about 45 mV, i.e., to a value close to that expected for a metallic electrode, and the chlorine evolution current increased. Simultaneously, the photoacoustic spectra evolved from the characteristic n-TiO_2 spectrum with an absorption edge at 350 nm to spectra with smaller absorption (less than half) in the TiO_2 absorption band but increasing absorption in the 550-400 nm range. During the same period, the photocurrent under band-gap illumination decreased. Since the peak concentration of Ru(IV) in the oxide (measured by backscattering) was ~1.2×10^{21} at cm^{-3}, and since a 40 mV value of the Tafel slope is characteristic of a metallic electrode, these results suggested that the $Ru_xTi_{1-x}O_2$ oxide may behave in a metallic-like fashion when the ruthenium concentration reaches a value somewhat larger than the aforementioned peak concentration. A more detailed study was carried out on a sample having a near-Gaussian implant profile and a total fluence of 4.6×10^{16} Ru cm^{-2}. Characterization was made over a prolonged time period of 40 days during the slow corrosion (0.15-0.20 nm h^{-1}) through the entire implant profile. The mixed oxide layer was formed at 1 V/SCE in a (1 M $[Cl^-]$, pH = 1.0) solution. In Fig. 5.2.a, the variations with time of the exchange current in the chlorine evolution region and of the photocurrent for n-TiO_2 band gap illumination are compared with the original ruthenium implant profile. The exchange current curve for the first 10 days reproduces almost perfectly the ruthenium concentration profile. The similarity holds over a region which includes the concentration peak and the exchange current peak. The known proportionality[4] between the current and the Ru(IV) surface concentration was used to calculate the Ru(IV) surface concentration scales in Figs. 5.2.b and 5.2.c. Figure 5.2.b shows the dependence upon ruthenium surface concentration of the measured photocurrent for a 300 nm light. A sharp boundary between two near-constant regions is found at a Ru(IV) surface concentration of 1.9×10^{21} at cm^{-3}. Figure 5.2.c gives the corresponding variations of the optical absorptions measured by photoacoustic spectroscopy. The dimensionless band gap absorptions of mixed oxides (PAS_{300nm} - PAS_{400nm}/PAS_{300nm}) are compared to the one (✱ in Fig. 5.2.c) calculated for a semiconducting n-TiO_2 layer of similar thickness and provide a means to illustrate the composition dependence of the band to band transition. Both spectroscopies qualitatively agree with a

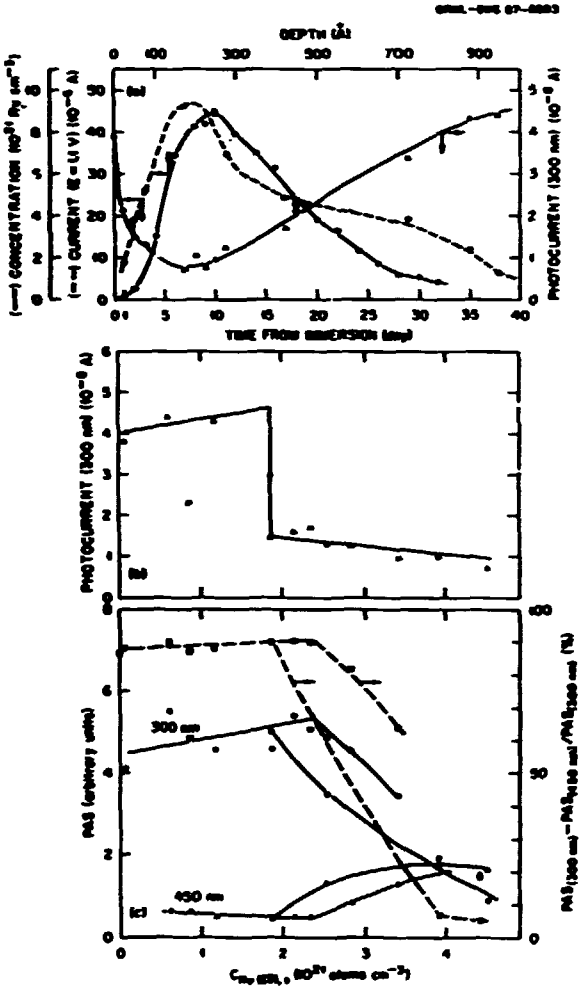

Fig. 5.2. (a) --O-- chlorine evolution current and —▲— photocurrent vs time; —●— ^{102}Ru implant profile. (b) photocurrent vs Ru surface concentration. (c) ——— optical absorption and ---- dimensionless band gap absorption vs Ru surface concentration. Solid symbols denote measurements taken before the peak concentration is reached.

critical ruthenium concentration of about 2 x 10^{21} at cm^{-3}. During the course of the experiment, a Tafel slope of 40 mV was observed for surface concentrations larger than 2.6 x 10^{21} at cm^{-3}. This value falls within the diffuse transition of the dimensionless band gap absorption.

Ion implantation combined with characterization of the alloy by Rutherford backscattering made possible the survey of variations with ruthenium content of optical absorption, photocurrent, and Tafel slope from measurements at a single electrode. Photoacoustic and Tafel slope measurements agree with a critical content of ruthenium of ~10% for the transition from a semiconducting to a metallic electrode. A transition, explained in terms of the formation of an infinite cluster of conducting RuO_2, was observed[5] for a ruthenium content of 30% in conventionally prepared mixed oxides. The lower percolation limit in the implanted samples may arise[6] from a different microstructure involving links between the conducting RuO_2 particles.

1. GLCA/ACM student, Albion College, Michigan, Fall 1986.
2. Solid State Division, ORNL.
3. Chem. Div. Annu. Prog. Rep. Jan. 31, 1986, ORNL-6261 (May 1986), pp. 74-76.
4. Section 5.1.1, this report.
5. Yu E. Roginskaya, B. Sh. Galyamov, I. D. Belova, R. R. Shifrina, V. B. Kozhevnikov, and V. I. Bystrov, Elektrokhimyia 18, 1327 (1982).
6. G. E. Pike in "Electrical Transport and Optical Properties in Inhomogeneous Media," J. C. Garland, and D. B. Tanner, editors, New York: American Institute of Physics (1978) pp. 366-71.

5.2 Research on Nonoxidic Ceramics and Superconducting Oxides

5.2.1 Ammonolysis of Transition Metal Halides (L. Maya)

Research on the use of ammonolytic products of transition metal halides as reactants for the preparation of precursors of nitrides or carbonitrides has continued. Previous work on the Ti(III) and Ti(IV) halides demonstrated that it was possible to replace residual halide not removed by ammonolysis by either amide or acetylide in liquid ammonia. The resulting derivatives could then be pyrolyzed to produce the corresponding nitrides or carbonitrides. This synthetic approach appeared to be applicable to other transition metals of interest such as niobium, vanadium, tungsten, or molyb-

...num. This assumption was tested in some detail in the case of niobium and briefly for vanadium. The ammonolysis of niobium (V) bromide produces the instantaneous displacement of two equivalents of bromide as ammonium bromide and the formation of a soluble niobium ammonolytic product. Long-term ammonolysis leads, after a few days, to the deposition of a precipitate containing only one bromide equivalent per niobium. The long-term ammonolysis product can be obtained readily after a few hours in the presence of excess potassium borohydride which acts as a mild base to consume the ammonium halide by-product which otherwise prevents the ammonolysis from proceeding beyond the displacement of two bromide equivalents. Evaporation of the short-term ammonolytic mixture, followed by sublimation of ammonium bromide, produced additional elimination of ammonium bromide and left a residue with a Br/Nb ratio of 1.5. The residue proved to be an interesting compound containing a hexanuclear niobium cluster and having an empirical formula corresponding to $Nb_6Br_9N_7$. Direct pyrolysis of the material left a residue of niobium nitride. Acetylide treatment of $Nb_6Br_9N_7$ and the long-term ammonolytic product, $NbBr(NH_2)_2NH$, produced derivatives which upon pyrolysis at 800°C yielded niobium carbonitride. The nitride and carbonitrides of niobium in the cubic form are ceramic materials of considerable interest because of their superconducting properties. Similar experiments were performed with VBr_3 which produced upon ammonolysis $VBr_2NH_2 \cdot 4NH_3$. The acetylide derivative of this intermediate produced V_4C_3 at 800°C. However, in this case the residue contained in addition to the carbide a considerable amount (~30% by weight) of amorphous carbon. The above experiments demonstrated the generality of the synthetic approach involving the use of intermediate ammonolytic products. The advantage of this methodology resides in the relative simplicity of a low-temperature approach involving materials readily available in high purity.

5.2.2 Ammonolysis of Transition Metal Dialkylamides

(Gilbert M. Brown, L. Maya)

Ammonolysis of titanium and niobium halides in liquid ammonia results in the formation of imide-amide-halide compounds. These compounds can be thermally converted to nitrides or carbonitrides following treatment with sodium acetylide. The ammonolysis of the dialkylamides of groups 4 and 5 in liquid ammonia has been shown to produce high metal content precursor compounds which can be thermally converted to refractory materials. Metal dialkylamides of general formula $M(NR_2)_n$, where M is Ti, Zr, or Nb, R is CH_3 or C_2H_5, and n is the highest valence of the metal, react with NH_3 to liberate a large fraction of the dialkylamine. Infrared spectroscopy and elemental analysis indicate these ammonolysis products are nitrido- or imido-bridged polymers. The formulas of the titanium, zirconium, and niobium products are $Ti_3(NR_2)(NH_2)_2(N)_3$, $Zr_5(NR_2)(NH_2)_3(NH)_5(N)_2$, and $Nb_2(NR_2)(NH)_3(N)$. Pyrolysis at <800°C converts the metal quantitatively to the corresponding nitride or carbonitride. The only products trapped following vacuum pyrolysis were ammonia and dialkylamine, with all condensable materials evolved by 400°C. Temperature-programmed pyrolysis (TPP) with analysis of the evolved gases by mass spectroscopy shows that the composition of the gaseous products depends on whether helium or hydrogen is used as the carrier gas. The presence of a hydrogen atmosphere compared to a helium environment or a dynamic vacuum results in a lower carbon content of the titanium and niobium products. The presence of hydrogen does not affect the analysis of the zirconium product. The conversion of $Ti_3[N(CH_3)_2](NH_2)_2N_3$ to TiN in helium or a vacuum proceeds through a postulated Ti(IV) intermediate, Ti_3N_4. Conversion of this Ti(IV) species to stoichiometric TiN results in the evolution of N_2, observed during TPP at ~660°C and ~760°C. Hydrogen seems to function as a reducing agent for Ti(IV), and an increase in

the amount of NH_3 evolved is observed along with suppression in N_2 evolution at higher temperatures. The carbon content of the refractory product is reduced in the presence of hydrogen because the hydrocarbon portion of the residual dialkylamine is not forced to serve as a source of hydrogen for ammonia or dialkylamine evolution. Hydrogen is apparently unable to act as a reducing agent for the zirconium precursor compound, and thus the presence of hydrogen has no effect on either the evolution of nitrogen or the carbon content of the ZrN product.

5.2.3 Photoassisted Preparation of Ceramic Precursors

(L. Maya, Gilbert M. Brown)

A new program was initiated to study the photoassisted formation of refractory materials of groups 4, 5, and 6 transition metals. We would like to discover systems in which the direct photolysis of a compound containing the appropriate elements in the desired stoichiometric ratio results in the formation of a refractory phase or a precursor thereof. The photochemically promoted reaction between a metal containing film and a reactive gaseous species is also a possible synthetic pathway. The metal carbonyl complexes of groups 4, 5, and 6 can be photochemically activated to eject CO. An investigation of the photolysis of organometallic compounds, adsorbed on a suitable substrate, has been undertaken. The surface bound molecule will be photochemically activated to react with an appropriate gas phase molecule (NH_3, CH_3CN, HCCH, B_2H_6, SiH_4, etc.) to produce a species which can be converted to a nitride, carbide, boride, or silicide. The photochemistry of $V(C_5H_5)(CO)_4$ in solution has been investigated in enough detail by others to suggest that high quantum yield substitution reactions can be expected. In our work, photolysis of $V(C_5H_5)(CO)_4$ at 450 nm (60 nm bandwidth) in hexane containing NH_3 has been shown to yield $V(C_5H_5)(CO)_3(NH_3)$ which precipitates as a brick red solid. The same compound is formed by photolysis of solid $V(C_5H_5)(CO)_4$ in the presence of NH_3 vapor (approximately 10 atmospheres pressure) above liquid NH_3 at room temperature. The infrared spectrum of a thin film of $V(C_5H_5)(CO)_4$ sublimed onto either a KBr or sapphire plate was followed during photolysis at 450 nm (60 nm bandwidth) in the presence of 200 torr of NH_3. Comparison of these *in situ* spectra with the KBr pellet spectrum of an isolated and analyzed sample of $V(C_5H_5)(CO)_3(NH_3)$ indicates that substitution of NH_3 for CO occurs in the film. Vacuum pyrolysis at 800°C of $V(C_5H_5)(CO)_3(NH_3)$ in a quartz reaction vessel resulted in the formation of a black shiny film on the walls of the vessel. This material was identified by XRD as V_4C_3. The thermal reaction appears to proceed in several stages with the initial formation of some $V(C_5H_5)(CO)_4$ and an unknown product. This unknown product reacts further to form the V_4C_3 film and a powdery residue. Further studies are required to identify the species which forms the V_4C_3 film. The only condensable species trapped during the pyrolysis reaction were NH_3 and C_5H_6. Under the conditions of the vacuum pyrolysis, $V(C_5H_5)(CO)_4$ would have completely sublimed out of the reaction vessel. The role of NH_3 in the formation of V_4C_3 is not evident, but it does activate this vanadium compound to form a refractory material. The disproportionation of $V(C_5H_5)(CO)_3(NH_3)$ could yield the starting tetracarbonyl and $V(C_5H_5)(CO)_2(NH_3)_2$, the latter of which might lose NH_3 to form a precursor to V_4C_3. The divanadium compound $V_2(C_5H_5)_2(CO)_5$ disproportionates in boiling THF to form $V(C_5H_5)(CO)_4$ and the cluster compound $V_4(C_5H_5)_4(CO)_4$. This tetravanadium compound is the type of compound that may yield V_4C_3, and the isolation and pyrolysis of this compound is clearly of interest.

5.2.4 Thermal Decomposition of Bis(cyclopentadienyl) Compounds of Titanium

(Gilbert M. Brown)

The controlled thermal decomposition of compounds of the type, $M(\pi - C_5H_5)_2L_2$, where M is Ti or V and L is an anionic ligand (NCS, NCO,

N_3, or CN), is being investigated as a possible method of making refractory nitrides or carbides of these metals. The NCS, NCO, and N_3 compounds of Ti have been studied by atmospheric pressure temperature-programmed pyrolysis (TPP) and by vacuum pyrolysis with trapping of evolved species at 77°K.

The TPP apparatus utilizes a furnace controller to ramp the temperature linearly with time, and the evolved gases are detected with a mass selective detector (Hewlett-Packard Model 5970). Helium or hydrogen is used as a carrier gas to remove volatile reaction products in these experiments. The TPP of the NCS, NCO, and N_3 compounds of $Ti(C_5H_5)_2$ show sharp maxima in plots of ion count from the mass spectrometer vs time (linear temperature ramp). The maxima occur at 325°C, 300°C, and 230°C for the NCS, NCO, and N_3 compounds, respectively. Mass spectroscopy demonstrates that all three titanium compounds evolve 1,3-cyclopentadiene (C_5H_6) and minor amounts of a species (m/e = 130) which may be the dimer of the cyclopentadiene radical, $(C_5H_5)_2$. The NCO and NCS compounds also evolve HCN, while the N_3 compound evolves N_2. Both the NCO and NCS compounds are reported to have nitrogen bound to titanium, so the evolution of HCN indicates the NCO and NCS groups may isomerize to become O or S bound as a part of the decomposition reaction. The temperatures of the maxima and the shapes of the gas evolution profiles for decomposition of the NCO and N_3 compounds, as measured by TPP, can be used to estimate a value for $\Delta H^{\ddagger}$ of the decomposition reaction. The estimated values (75-85 kcal/mol) are in reasonable agreement with the measured value of the mean bond dissociation energy of a π-C_5H_5-Ti bond (78 kcal/mol) in bis(cyclopentadienyl)titanium compounds. However, the TPP results indicate the C_5H_5 ligand and the other ligands are lost simultaneously from these $Ti(C_5H_5)_2L_2$ compounds, a result that would not have been predicted from a consideration of the mean bond dissociation energies of Ti-L and Ti-C_5H_5 bonds.

Vacuum pyrolysis of these $Ti(C_5H_5)_2L_2$ compounds presents a problem since the materials tend to sublime out of the hot zone. A tortuous path assembly of three nested quartz tubes, each sealed at one end and having their openings in opposite directions, forced the volatile material to the hotter outer zone of the pyrolysis assembly as it sublimed. The center of the furnace was heated as rapidly as possible to 500-550°C. There is an estimated 100°C temperature variation through the tortuous path assembly. The condensable reaction products were collected in a U-tube trap at 77°K for quantification and identification. Infrared and mass spectroscopy demonstrate the only condensable product from the decomposition of $Ti(C_5H_5)_2(N_3)_2$ is 1,3-cyclopentadiene (approximately one mole per mole of starting material). The dimer of the cyclopentadiene radical, $(C_5H_5)_2$, would have decomposed on the time scale of the analysis. Infrared spectroscopy indicated HCN, 1,3-cyclopentadiene, and at least one other product were condensed from the pyrolysis products of $Ti(C_5H_5)_2(NCO)_2$. The pyrolysis of $Ti(C_5H_5)_2(N_3)_2$ was completed without unreacted starting material escaping from the tortuous path assembly, and weight loss after pyrolysis shows the residue contains at least TiC_5. Pyrolysis of both the NCO and N_3 compounds resulted in the formation of a shiny black film on the walls of the quartz reaction tubes. This result suggests these compounds might be useful for chemical vapor deposition (CVD) of refractory films. Accordingly, a preliminary experiment demonstrated a shiny black film was deposited on a quartz heater, with the system at a base pressure of 5×10^{-3} torr, when the heater was almost at red heat. Experiments are in progress to produce these films in a reproducible manner and to determine if the film is titanium carbide.

5.2.5 Studies on the Reaction of TiO_2 with NaCN at 1000°C, and Synthesis and Characterization of Sodium Titanates

(C. E. Bamberger, G. M. Begun)

Earlier (unpublished) attempts by us to establish the stoichiometry of the reaction of TiO_2 with NaCN at high temperatures (>800°C)

revealed the formation of TiN and other compounds. Occasionally among the latter, a sodium titanate was identified by x-ray diffraction (XRD). It was inferred that other titanates were present which were unidentifiable by XRD because the literature appeared to contain spurious XRD data. Consequently, the syntheses of the sodium titanates listed in the literature were undertaken, and the identities of the titanates were established by complementing x-ray diffractometry with Raman spectroscopy. The results confirmed the existence of Na_4TiO_4, α-, β-, and γ-Na_2TiO_3, $Na_2Ti_3O_7$, $Na_8Ti_5O_{14}$, and $Na_2Ti_6O_{13}$. The Raman spectra are shown in Figs. 5.3 and 5.4 and indicate that the other titanates listed in the literature (e.g., $Na_2Ti_5O_{11}$, $Na_6Ti_2O_7$, and $Na_2Ti_2O_5$) do not exist but are mixtures of the above titanates. A preprint of the resulting manuscript was sent to the International Center for Diffraction Data and, upon review by an appointed editor, it was recommended to delete five cards (out of 14) and replace one. This unambiguous identification of the sodium titanates allowed for the completion of the study of the reaction of TiO_2 with NaCN. The results indicated that, contrary to claims in the literature,[1] "sodium tianide" (NaTiN) did not form. Instead, the products consisted of a mixture of TiN with $Na_2Ti_6O_{13}$ and $Na_8Ti_5O_{14}$ as major phases and $Na_2Ti_3O_7$ as a minor phase.

1. R. Skórksi, Hutnik 17, 26 (1950).

5.2.6 Synthesis and Characterization of Titanium Phosphates and Their Reactions with NaCN at 1000°C

(C. E. Bamberger, G. M. Begun)

The synthesis of TiN (a material of technological interest) via the reaction of TiO_2 with NaCN at 1000°C is accompanied by the formation of $Na_2Ti_6O_{13}$. The latter product, being quite insoluble in aqueous acid solutions, is extremely difficult to separate from TiN. Consequently, an attempt was made to find a titanium salt which when reacted with NaCN would yield TiN and a water-soluble sodium salt. A titanium phosphate, TiP_2O_7, was chosen

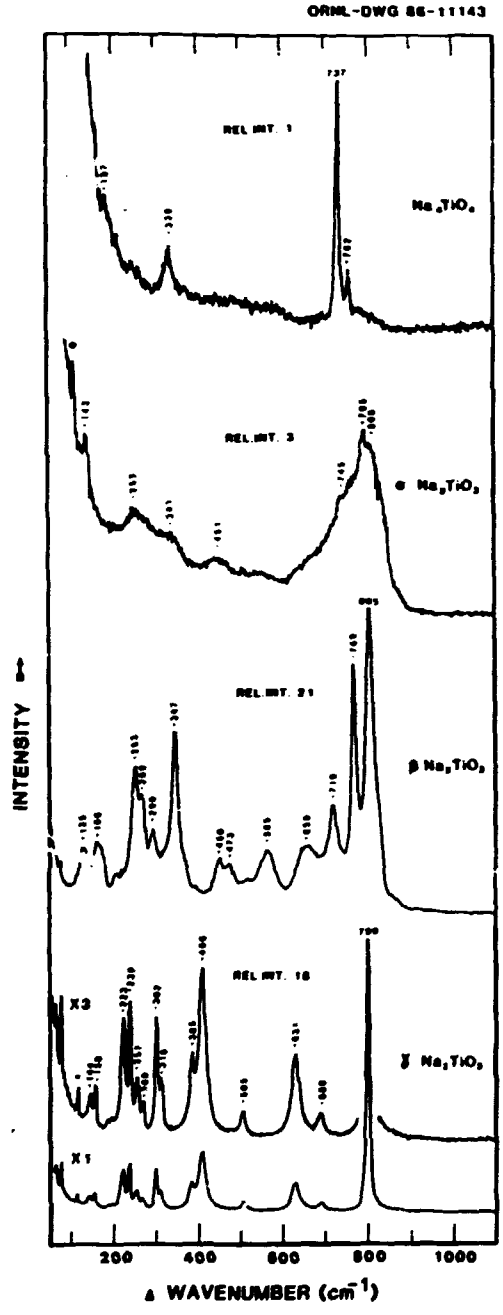

Fig. 5.3. Raman spectra, recorded with 514.5 nm excitation, of Na_4TiO_4 (top), α-Na_2TiO_3, β-Na_2TiO_3, and γ-Na_2TiO_3 (bottom). The values of the relative intensities were obtained by normalizing the scale factors of the signal averager to the values of 1 for the weakest and 100 for the strongest spectra. *Designates plasma lines.

for this purpose. When its synthesis was attempted, it was found that occasionally an additional unidentified phase formed. The unidentified material was studied and then

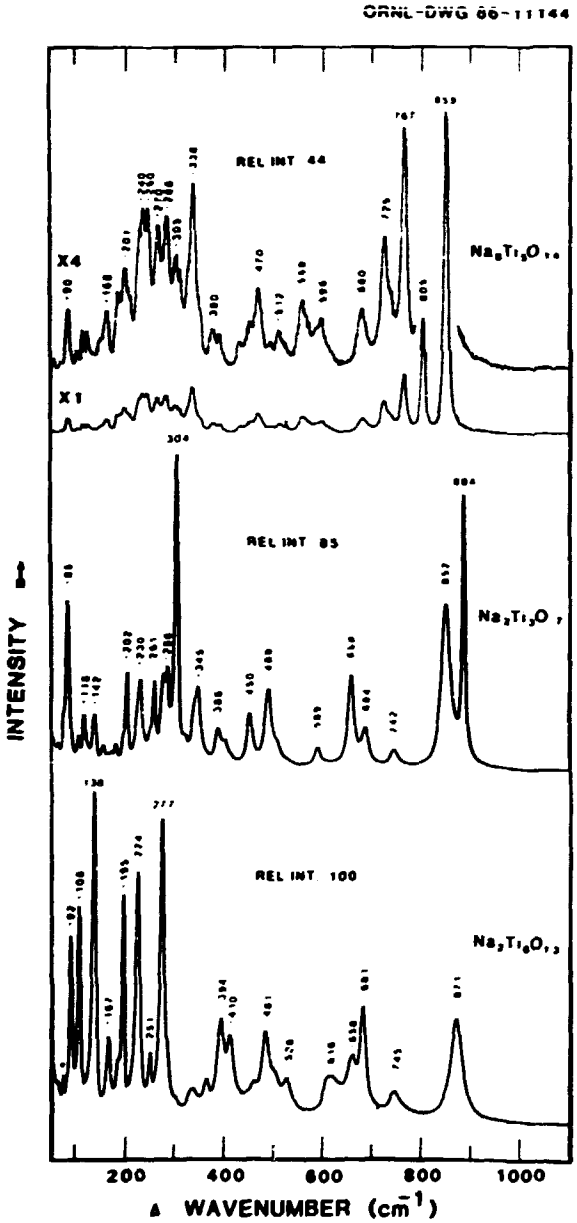

Fig. 5.4. Raman spectra, recorded with 514.5 nm excitation, of $Na_8Ti_5O_{14}$ (top), $Na_2Ti_3O_7$ (center), and $Na_2Ti_6O_{13}$ (bottom). The values of the relative intensities were obtained by normalizing the scale factors of the signal averager to the values of 1 for the weakest and 100 for the strongest spectra. *Designates plasma lines.

synthesized by means of different reactions. It was identified as titanyl pyrophosphate, $(TiO)_2P_2O_7$. The thermal stabilities of TiP_2O_7 and $(TiO)_2P_2O_7$ were determined. It was found that TiP_2O_7 decomposes into $(TiO)_2P_2O_7$ and P_2O_5 at 1150°C, and that $(TiO)_2P_2O_7$ decomposes at 1200°C into TiO_2 (rutile) and P_2O_5. A manuscript describing this work has been submitted for publication. A study of the reactions of NaCN with $(TiO)_2P_2O_7$ and with TiP_2O_7 was initiated with the expectation that the solid products would be TiN and sodium phosphates. It was found that, when the reactants were in low NaCN/Ti ratios (e.g., 1 or 2), several novel compounds were formed as intermediates. The latter were identified as "titanium bronze" (sodium titanates in which part of the titanium is reduced to the trivalent state) and double phosphates of sodium and titanium (IV) or titanyl ion, i.e. the known $NaTi_2(PO_4)_3$ and the new $Na_4(TiO)(PO_4)_2$. During the course of synthesizing these double phosphates an additional new compound, $Na(TiO)PO_4$, was also identified. With NaCN/Ti ratios of 3 to 4, the solid reaction products were TiN powder and Na_3PO_4.

5.2.7 Attempts to Prepare Cubic BN at Atmospheric Pressure

(C. E. Bamberger, J. Brynestad)

Two literature references[1,2] indicate that the reaction of thin coatings of BP with gaseous ammonia at reduced pressures at ~800°C yields thin coatings of cubic BN. Because that work is described very briefly, and because cubic BN is a very hard material which has industrial applications but is obtainable only at high pressures, the reaction was reexamined using gram quantities of BP. Under such conditions the reaction is slow and quite complex. It appears that some elemental phosphorous and/or PH_3 are evolved; however, the reacting powder gained weight at the beginning of the reaction (several days). After ca. 30 days of exposure to NH_3 at 800°C, the solid product consisted of poorly crystallized hexagonal BN, a P-N species tentatively identified by XRD as PN, and some unreacted BP. Reactions at temperatures higher than 800°C yielded well-crystallized hexagonal BN. Another series of tests consisted of reacting BP and $B_{13}P_2$ with molten NaCN at

800°-1000°C in an attempt to produce BCN or B_4C, both products of considerable industrial interest. The results indicated that hexagonal BN was the stable phase and the main product.

1. R. C. Vickery, Nature 184, 268 (1959).
2. Chih Chung Wang, "Studies on Aluminum-Phosphide and Boron-Phosphides and Cubic Boron-Nitride," PhD Thesis #63-1406 (1962), Univeristy Microfilms International, Ann Arbor, Michigan.

5.2.8 Study of High Tc Superconductors
(J. Brynestad, Staff Members in the Metals and Ceramics Division)

A study of high-temperature superconductors has been initiated. Several compositions in the system Y-Ba-Cu-O were synthesized, and pertinent properties were determined in cooperation with staff members in the Metals and Ceramics Division. The compound $YBa_2Cu_3O_{7\pm x}$ was tentatively identified as the most prominent superconducting phase in the mixed phase composition $Y_{1.2}Ba_{0.8}CuO_{4-\delta}$ reported by C. W. Chu et al.[1] When $YBa_2Cu_3O_{7\pm x}$ is equilibrated at 950°C in air, the composition is close to $YBa_2Cu_3O_{6.52\pm0.01}$, and it is not superconducting. However, when equilibrated at 600°C in pure oxygen at atmospheric pressure, the composition is close to $YBa_2Cu_3O_{7.1\pm0.03}$, and it is superconducting at 93K. The study of the optimum oxygen content of this phase is proceeding, as well as structural studies as a function of the oxygen content. The study of the effects of substitutions in the Y-sublattice and Ba-sublattice is also proceeding.

1. M. K. Wu, J. R. Ashburn, C. J. Torng, P. H. Hor, R. L. Meng, L. Gao, Z. J. Huang, Y. Q. Wang, and C. W. Chu, Phys. Rev. Letters 58, 908 (1987).

5.2.9 Study of the Reaction Chemistry of Gaseous and Solid Silicon Monosulfide
(J. Brynestad)

The study of the reaction chemistry of gaseous and solid SiS with NH_3, hydrocarbons, and monomethylamine (CH_3NH_2) has been completed. Whereas NH_3 reacts with both solid and gaseous SiS to form "$Si(NH)_2 \cdot xSiS_2$", the hydrocarbons and CH_3NH_2 yield unspecified reaction products that cannot be converted into pure refractory compounds. It was also observed that finely divided silicon disulfide (SiS_2) easily reacts with NH_3 at temperatures >~700°C to form practically pure $Si(NH)_2$. Both $Si(NH)_2$ and $Si(NH)_2 \cdot xSiS_2$ may be converted to high purity α-Si_3N_4 at 1500°C. Ultrapure SiS_2 powder can be made from impure silicon by forming SiS(g) according to the reaction scheme,

$$Si(s) + 2H_2S(g) \xrightarrow{T>1090°C} SiS_2(\ell) + 2H_2(g)$$

$$SiS_2(\ell) + Si(s) \xrightarrow{T>\sim1140°C} 2SiS(g)$$

Subsequently, the SiS(g) is brought to react with H_2S(g) (below ~1090°C, the melting point of SiS_2) to form SiS_2(s),

$$SiS(g) + H_2S(g) \xrightarrow{1050°C<T<\sim1090°C} SiS_2(s) + H_2(g)$$

Alternatively the SiS(g) may be quenched to form very finely divided SiS(s) powder which subsequently may be brought to react with H_2S in the temperature range ~600°C – ~700°C,

$$SiS(s) + H_2S(g) \xrightarrow{\sim600°C<T<\sim700°C} SiS_2(s) + H_2(g)$$

This may prove to be a route to synthesize high purity Si_3N_4 powders from impure silicon.

5.2.10 Study of Alternate Sintering Aids
(J. Brynestad)

A limiting factor for the successful development of sinterbodies of covalent refractories (Si_3N_4, SiC, TiB_2 etc.) is finding

effective sintering aids that do not impair the high temperature properties of the compacted refractory product. Ideally, a sintering aid should make it possible to achieve full theoretical density by pressureless sintering without damaging grain growth which affects its high-temperature properties. In the case of Si_3N_4, for example, the sintering aids presently used are oxides (MgO, Al_2O_3, Y_2O_3, etc.); they need hot pressing to be active. In these cases, the additives form liquid intergranular phases during the sintering process which convert to glassy intergranular phases at lower temperatures. Therefore, the high-temperature properties of these sinterbodies are limited by the inferior properties of the glassy phases present. Preliminary studies indicate that improved sinterbodies may be obtained by chemical routes utilizing sintering aids that form crystalline refractory intergranular phases. For example, it has been reported in the literature that a hot pressed 10 wt % "Zyttrite"-Si_3N_4 ceramic has a high-temperature strength at 1370°C nearly double that of a 1 wt % MgO-Si_3N_4 ceramic. The reason for this may be that ZrO_2 does not form glassy intergranular phases. A guiding principle may be to find compounds or mixtures of compounds that provide diffusion paths for the matrix material during the sintering process and form crystalline refractory intergranular phases at lower temperatures. As an example, a preliminary experiment revealed that the addition of Al_4C_3 to Si_3N_4 gave rise to partial pressureless sintering of a (cold-pressed) pellet at 1500°C. The main reactions are probably

$$Al_4C_3(s) + Si_3N_4(s) \xrightarrow{1500°C} 4AlN(s) + 3Si(\ell) + 3C(s)$$

$$3Si(\ell) + 3C(s) \xrightarrow{1500°C} 3SiC(s)$$

AlN, SiC, and as yet unidentified phase(s) were observed by X-ray diffraction. Other schemes are being developed.

5.2.11 Raman Microprobe Study of Phase Transformations in Ceria Stabilized Zirconia

(G. M. Begun, P. F. Becher,[1] E. F. Funkenbusch[2])

Transformation-toughened multiphase ceramics containing metastable tetragonal ZrO_2 are being widely investigated for use as technologically important materials. The ceramic samples are strengthened by the presence of the metastable tetragonal ZrO_2 phase which, when subjected to a tensile stress, converts to the higher volume monoclinic phase and inhibits crack propagation. Keramidas and White[3] and Benner and Nagelberg[4] obtained the Raman spectra of amorphous, tetragonal, monoclinic, and cubic zirconia. The tetragonal and monoclinic forms are easily characterized, and the ratio of tetragonal to monoclinic crystalline forms present in a sample can be determined by measurement of several of the non-overlapping Raman peaks assigned to the two species. Clarke and Adar[5] established that the ratio of monoclinic ZrO_2 to tetragonal ZrO_2 was equal to the sum of the intensities of the Raman peaks at 181 and 191 cm^{-1} divided by the sum of the intensities of the peaks at 148 and 264 cm^{-1}. The development of the Raman microprobe has made it possible to determine the microscopic state of ZrO_2 present in ceramic samples and to study its variation in the neighborhood of indentations and cracks.

We have applied this method to samples of ceria stabilized ZrO_2 (10-15 mol % CeO_2). Representative samples were impressed with square 30 Kg DPH indents. The samples were then examined with a Ramanor Microprobe using 488.0 nm radiation from an argon-ion laser. Figure 5.5 shows some of the Raman traces made at various distances perpendicular to the side of a square 30 Kg indentation. The tetragonal (t) to monoclinic (m) phase transformation proceeds by cooperative shear, forming extended bands in which neighboring tetragonal grains transform. The results show that less extensive transformation occurs along the extension of the indent diagonal than along the normal at the center of the side face of the indent.

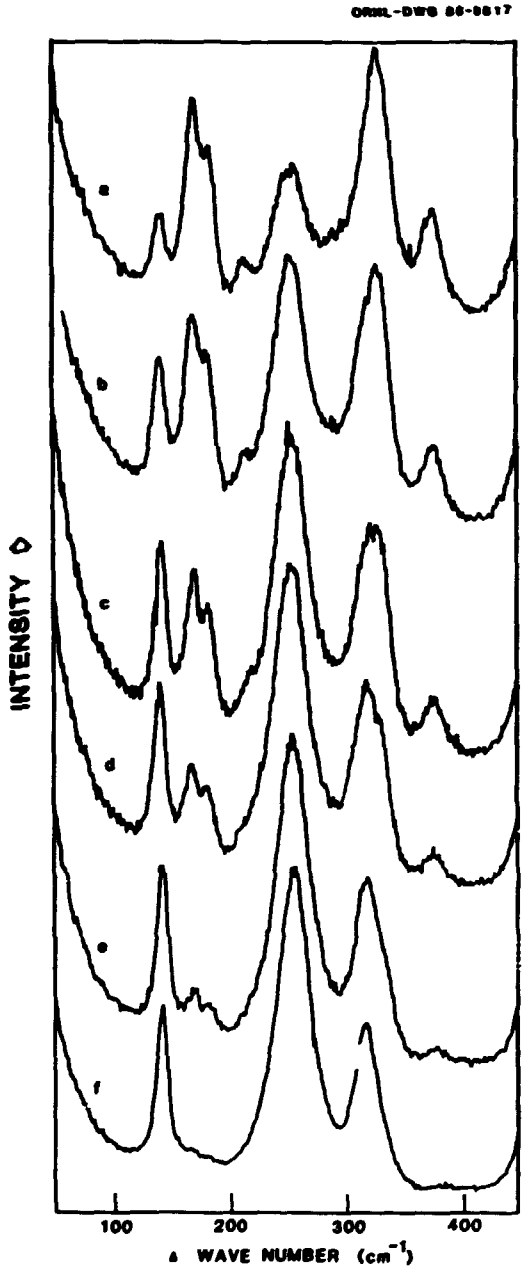

Fig. 5.5. Raman spectra of CeO_2 stabilized ZrO_2. a → f; 0, 60, 90, 140, 200, 300 μm from indent, respectively. 488.0 nm excitation.

Figure 5.6 shows a plot of the results obtained (% monoclinic, assuming the samples to contain only the monoclinic and tetragonal forms, vs the distance (μm) from the edge of the indent). Data is given for samples with 10.0, 12.5, and 15.0 mol % CeO_2. Increasing the CeO_2 content suppresses the t→m transformation. The 15.0

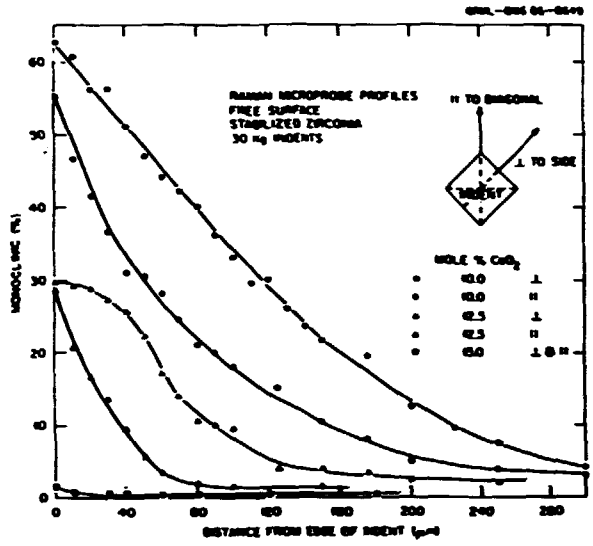

Fig. 5.6. Percent monoclinic vs distance from indent for CeO_2 stabilized zirconia. Free surface.

mol % sample shows very little transformation, while the 10.0 and 12.5 mol % samples exhibit the effect mentioned above, i.e., with more transformation taking place along the line normal to the indent. Figure 5.7 shows the results on the same samples which were care-

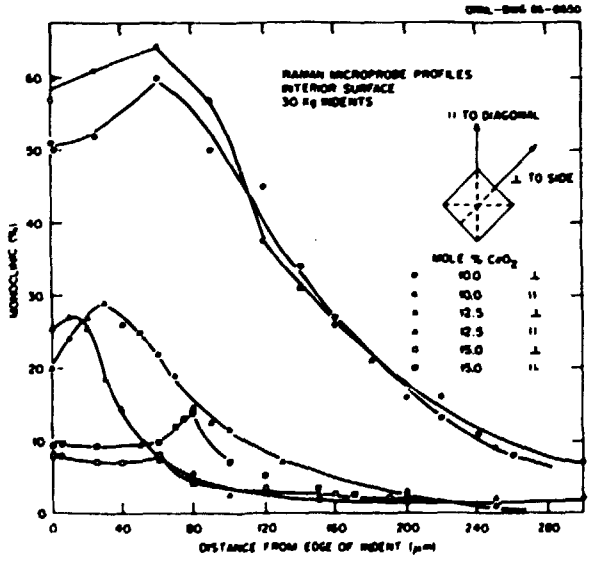

Fig. 5.7. Percent monoclinic vs distance from indent for CeO_2 stabilized zirconia. Interior surface.

fully polished down to a depth of ~20 μm after indentation in order to expose the interior surface. Examination of the interior surface at 15 mol % shows that the t→m transformation has occurred; t→m→t transformation occurs on the free surface due to stress relaxation. The zone shape and crack geometry is altered by the change in constraining forces (free vs interior surfaces).

---

1. Metals and Ceramics Division
2. 3M Company, Saint Paul, MN 55101.
3. V. G. Keramidas and W. B. White, J. Am. Ceram. Soc. 57, 22 (1974).
4. R. E. Benner and A. S. Nagelberg, Thin Solid Films 84, 89 (1981).
5. D. R. Clarke and F. Adar, J. Am. Ceram. Soc. 65, 284 (1982).

6. STRUCTURE AND DYNAMICS OF ADVANCED POLYMERIC MATERIALS

Advanced materials such as polymers and composites are replacing traditional materials. Future development of these new materials will be facilitated by fundamental understanding and characterization of them at the molecular level. With modern experimental and theoretical tools, it is becoming possible, for example, to predict polymer properties from a knowledge of molecular properties and to design polymers more r. ionally for specific uses. The achievement of these ambitious goals involves a long-term effort of an interdisciplinary group of scientists and a variety of techniques. Diffraction techniques are being used in studies of amorphous materials to determine precisely interatomic distances and angles, from which potential parameters for atom pair interactions are obtained through computing techniques. This work requires intense neutron beams from the HFIR and tunable x-rays from the NSLS as well as x-rays from conventional sources. Experimental results will be used to predict conformational, thermodynamic, and dynamic properties through advanced computing and statistical mechanical techniques. Studies are now in progress to locate dopant atoms in amorphous conducting polymers. Single-crystal techniques are being modified for collection of diffractometer data from crystalline polymer fibers for structure determination, and preliminary data sets have been obtained for two high-performance crystalline fibers. Single-crystal structure analyses are performed on crystals of small molecules relevant to questions of polymer structure. Computer simulation studies of the dynamics of long-chain molecules are also in progress.

6.1 Experimental Equipment and Methods

(B. K. Annis, George M. Brown, W. R. Busing, A. H. Narten)

The fast data acquisition system for neutron scattering from amorphous solid and liquid materials was fully tested and brought into operation. The system involves a one-dimensional curved position-sensitive detector which permits simultaneous measurement of diffraction data over an angular range of 130 degrees at moderate resolution. High precision neutron data can now be collected in hours, a major advance over conventional step-scanning techniques. The system was tested by measuring the diffraction pattern of amorphous carbon, a convenient test material for comparison of x-ray and neutron data from different laboratories.

The new x-ray diffractometer for single-crystal and fiber diffraction studies was brought into full operation, thoroughly tested, and used by members of this group to collect several sets of diffraction data (see below) and by J. H. Burns of the Separations Chemistry Group to collect additional sets of data. Three sets of single-crystal data have been used to determine three crystal structures quite precisely, indicating that the diffractometer can routinely be used to collect high quality data.

In cooperation with members of the Metals and Ceramics Division, we have designed and had constructed the necessary vacuum shroud and radiation shields for a Displex closed-cycle helium refrigerator to be used on the ORNL diffractometer at the Brookhaven Synchrotron Light Source. The equipment will be used to study the conformational changes of polymers during phase transitions.

6.2 Diffraction Studies of Crystalline Polymer Fibers

(W. R. Busing)

Diffractometer techniques have been developed for measuring diffuse x-ray and neutron scattering from partially oriented crystalline fibers. Data sets have been obtained from samples of Allied Spectra-1000 high-performance polyethylene and DuPont Kevlar-49 poly(paraphenylene terephthalamide) by sealed-tube x-ray, synchrotron x-ray, and neutron scattering. These results indicate that the diffractometer data show many more significant features than do the early x-ray diffraction

photographs from which the reported approximate structures were deduced. Furthermore, the recorded data counts are free of errors introduced by the photographic process and subsequent optical scanning. Initial calculations have been made which encourage us to believe that a least-squares technique can be developed for a precise refinement of the fiber crystal structure and morphology. For example, the conformation angles between the phenyl and amide groups in Kevlar are at present only known approximately. We expect to be able to measure them to the ±0.1 degree usually obtainable from single-crystal studies. Then the effects of temperature or tensile stress on these angles may be observable, and this should provide an improved understanding of the thermal and mechanical properties of these materials.

Figure 6.1 is a plot of intensities measured along the [001] direction in Kevlar-49 using

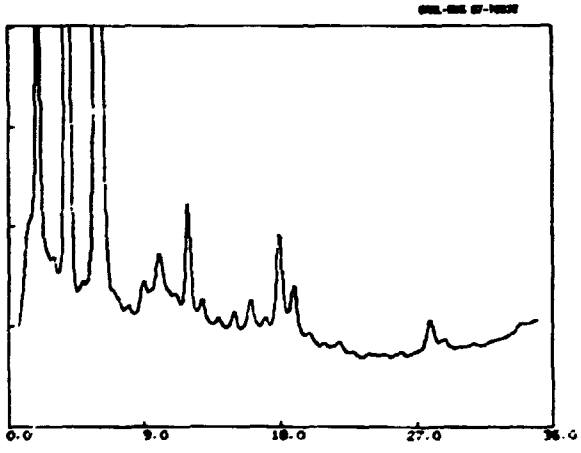

Fig. 6.1. X-ray diffraction intensities along the fiber axis of Kevlar-49.

monochromatic Mo Kα radiation. It shows peaks all the way out to the 0 0 34 reflection. The reported structure[1] is based on a few reflections with ℓ indices no higher than 8.

1. M. G. Northolt, Eur. Pol. J. 10, 799 (1974).

6.3 The Structure of Dichloro(tetrapyridine)-platinum(II) Trihydrate Based on Combined X-ray and Neutron Diffraction Data

(C. H. Wei,[1] W. R. Busing)

The compound $[Pt(C_5H_5N)_4]^{2+}\cdot 2Cl^-\cdot 3H_2O$ crystallizes with four formula units in a cell of symmetry Cc with a = 12.711(1), b = 12.856(1), c = 16.600(2) Å, and β = 118.544(8)°. Its structure by x-ray diffraction has been reported.[2] Although the final discrepancy factor R(F) was 0.021, the water H atoms were not found.

Recrystallization of the compound from a pyridine-water solution produced crystals suitable for a neutron-diffraction study. Neutron-diffraction data were collected at the HFIR to a resolution of 0.86 Å using neutrons of wavelength 1.537 Å. The six H atoms of the waters were located from a Fourier difference map. Parameters of 56 atoms with anisotropic thermal motion were refined based on a combination of 3429 x-ray data corrected for isotropic extinction and 1336 neutron data corrected for anisotropic extinction.[3] The 515 variables were adjusted by the least-squares program XFLS4.[4] A user subroutine was modified to select x-ray or neutron scattering factors for the different data sets. A final R(F) of 0.022 was obtained for the combined data. A drawing[5] of the structure is shown in Figure 6.2.

All water H atoms make hydrogen bonds to neighboring Cl^- ions, and each Cl^- is linked to three H atoms from different water molecules, thus forming a three-dimensional network. The $H\ldots Cl^-$ distances are between 2.16(1) and 2.38(1) Å, and the $H\ldots Cl^-\ldots H$ angles range from 65.6(4) to 134.9(4)°. The average C-H and O-H distances are 1.078(2) and 0.943(5) Å, respectively. The four N atoms of the pyridine rings that form a square-planar array around Pt are in a plane to within 0.026(1) Å.

1. Biology Division, ORNL.
2. C. H. Wei and B. E. Hingerty, Acta Cryst. A40 (sup.), C-309 (1984).

3. P. Coppens and W. C. Hamilton, Acta Cryst. A26, 71 (1970).
4. W. R. Busing, K. O. Martin, and H. A. Levy, ORNL/TM-305 (1963).
5. C. K. Johnson, ORNL-5138 (1976).

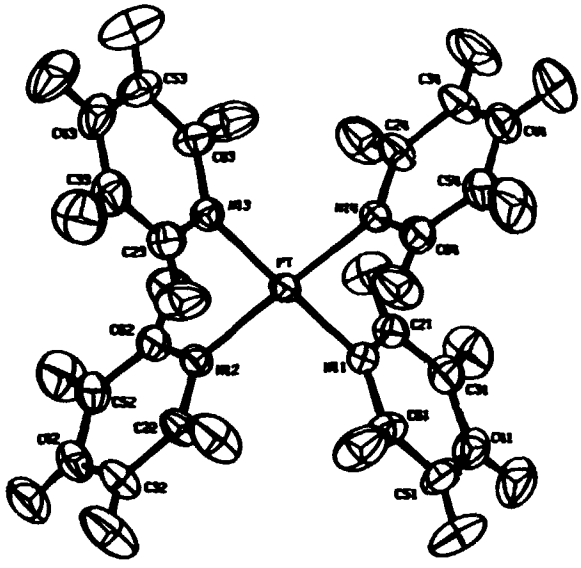

Fig. 6.2. The tetrapyridineplatinum moiety.

6.4 Tricarbonyl(styrene)chromium: A Structure Study Related to the Design of Polymeric Second-Harmonic Generators

(George M. Brown)

Because of the importance of technical applications of second-harmonic generators (s.h.g's), there has been recent interest in the s.h.g. properties of transition-metal-organometallic compounds[1] and of their inclusion compounds in host crystals.[2] Organic crystals that are strong second-harmonic generators are known to be acentric crystals of conjugated molecules having low-lying intramolecular charge-transfer states. Because transition-metal organic complexes are also conjugated systems that have low-lying charge transfer states, Frazier et al.[1] have recently surveyed the s.h.g. properties of about 60 such compounds as powders and have called attention to the need for knowledge of their crystal structures in interpreting the results. Understanding of the structural basis of second-harmonic generation in such compounds may lead to the design of new crystalline and polymeric generators.

This report describes the x-ray crystal-structure analysis of tricarbonyl(styrene)-chromium $(CO)_3(C_6H_5CHCH_2)Cr$, the strongest s.h.g. of the compounds surveyed by Frazier et al. The compound is a moderately strong s.h.g., showing a signal strength about 1.8 times that of ammonium dihydrogen phosphate.

Crystallographic data: orange-yellow orthorhombic crystals, space group $P2_12_12_1$; $\underline{a}$ = 11.5456(6), $\underline{b}$ = 12.3227(9), $\underline{c}$ = 7.3741(5), at −18°C. (λ = 0.70930 A); Z = 4, calculated density = 1.520 g/cc. R = 0.030 for 1306 reflection data ($F^2 > (\sigma F^2)$); σ_1 = 1.31. Figure 6.3 shows the molecular and crystal structures found.

ORNL-DWG. 87-10731

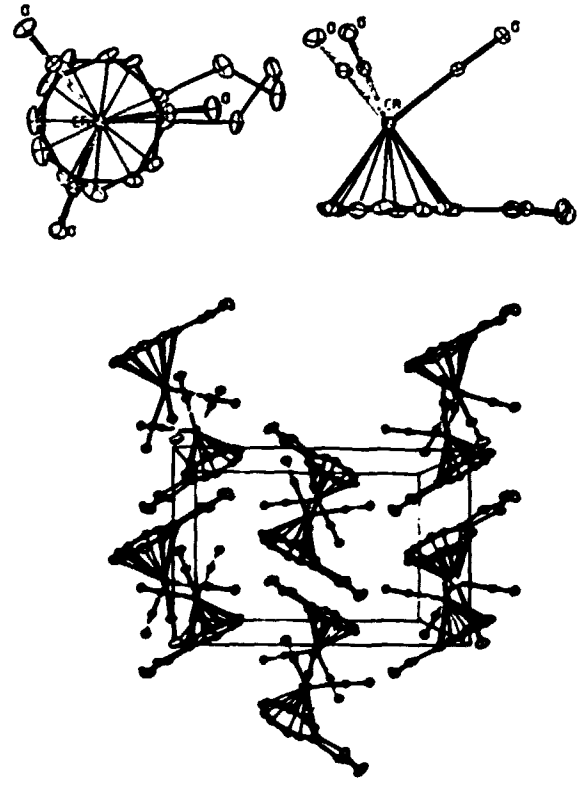

Fig. 6.3. Two views of the molecule of tricarbonyl(styrene)chromium, showing the disorder of the styrene ligand, and view of the crystal structure approximately in the $-\underline{b}$ direction.

There is disorder of the styrene ligand in the molecule, with two orientations (about equally populated) of the ligand relative to the $Cr(CO)_3$ moiety. The two different orientations were represented in least-squares refinement by idealized molecules with only a few degrees of freedom, and damping of parameter shifts was applied. In both orientations, the $Cr-C_{CO}$ linkages are nearly eclipsed with respect to $Cr-C_{ring}$ bonds, in contrast to the exactly staggered arrangement in tricarbonyl(benzene)chromium. The normal to the ring planes makes angles of 74°, -102°, and 29° with the base vectors $\underset{\sim}{a}$, $\underset{\sim}{b}$, $\underset{\sim}{c}$, respectively.

Further analysis of the structure is in progress, and similar studies on other metal-organic s.h.g.'s are planned.

1. C. C. Frazier, M. A. Harvey, M. P. Cockerham, H. M. Hand, E. A. Chauchard, and C. H. Lee, J. Phys. Chem. 90, 5703 (1986).
2. D. F. Eaton, A. G. Anderson, W. Tam, and Y. Wang, J. Am. Chem. Soc. 109, 1886 (1987).

6.5 Evidence for Extensive Graphite Monolayers in Wyodak Coal from X-ray Diffraction

(W. E. Thiessen, A. H. Narten)

There has been extensive interest in deducing the structures of European brown coal and its carbonization products from x-ray diffraction studies.[1,2] In this report, those results are compared with our measurements of an American subbituminous coal and synthetic glassy carbon.

Samples of powdered Wyodak (Rawhide Seam) coal were obtained from Prof. John W. Larsen along with analytical data giving a composition (atom per cent) of 48.25% C, 40.99% H, 10.14% O, 0.48% N, and 0.14% S. The density of the material was 0.78 g/ml.

Samples of "Vitreous Carbon Grade V10" were obtained commercially.[3] According to the manufacturer, the material was obtained by carbonization and subsequent thermal treatment of carbonaceous substances which, after carbonization, leave a coke in crystallographic disorder. The black glassy material has a density of 1.50 to 1.55 g/ml.

The x-ray measurements were made using reflection geometry[4] and Mo Kα radiation (λ = 0.7107 Å), with a crystal monochromator in the diffracted beam. The range of scattering angles covered the interval $0.6 < k < 16$ Å^{-1} of $k = (4\pi/\lambda)\sin\theta$, and the accumulated counts ranged from 5×10^4 at the lowest to 5×10^5 at the highest angles. Corrections for background, absorption,[5] polarization, incoherent scattering,[6] monochromator discrimination,[4] and multiple scattering[7] were applied. The corrected cross sections were normalized to the calculated self scattering from independent atoms,

$$S_s(k) = \sum_{i=1}^{n} c_i f_i^2(k), \qquad (1)$$

with c_i the atom fraction, $f_i(k)$ the coherent x-ray scattering factor of atom i, and summation over the types of atoms in the sample. The cross section thus obtained may be written as

$$S(k) = S_s(k) + S_d(k), \qquad (2)$$

with $S_d(k)$ the distinct scattering from correlated atom pairs.

The next step in the data reduction was to construct the structure function H(k), defined as

$$H(k) = M(k)\{S(k)-S_s(k)\}. \qquad (3)$$

The factor M(k) is given by

$$M(k) = [\sum_{i=1}^{n} c_i f_i]^{-2}. \qquad (4)$$

The functions H(k) derived from the x-ray data are shown in Fig. 6.4. The curves oscillate with decreasing amplitude around the asymptotic values H(∞) = 0, and are typical of amorphous materials. There is no indication of the sharp Bragg diffraction peaks characteristic of crystalline samples.

The short-range order or structure found in amorphous materials is described by probability

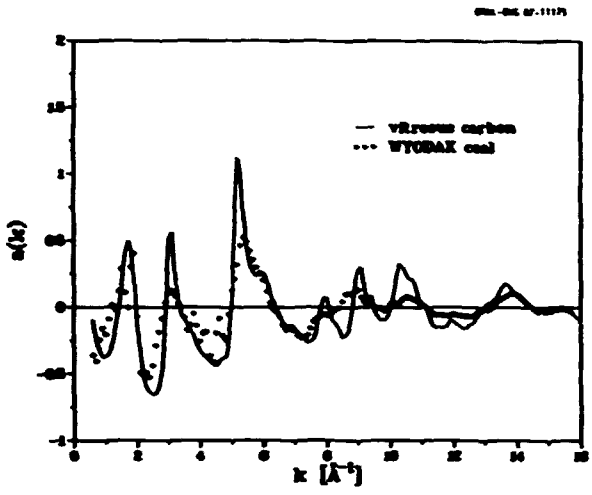

Fig. 6.4. Structure functions of amorphous carbon and Wyodak coal derived from x-ray diffraction.

functions of the relative positions of the particles. For the materials considered here, the atom pair distribution functions $g_{ij}(r)$ depend only on the scalar distances r between atoms of type ij, and are defined so that $\rho_j g_{ij}(r)$ is the average number of j atoms in the volume element $d\underset{\sim}{r}$ at a distance r from an origin atom of type i. The pair distribution functions are related to the partial structure functions $h_{ij}(k)$ by the Fourier integral

$$\hat{h}_{ij}(k) = 4\pi\int_0^\infty r^2 h_{ij}(r) j_0(kr)dr, \qquad (5)$$

with $j_0(x) = x^{-1}\sin x$, $h_{ij}(r) = g_{ij}(r)-1$, $k = (4\pi/\lambda)\sin\theta$, and 2θ the scattering angle. The total structure function H(k) accessible from scattering experiments can be written as

$$H(k) = M(k)\sum_{ij}\sum c_i c_j f_i f_j a_{ij}(k), \qquad (6)$$

with $a_{ij}(k) = \rho\hat{h}_{ij}(k)$. Fourier inversion of the function H(k) yields a radial distribution function

$$G(r) = 1 + (2\pi^2\rho r)^{-1}\int_0^\infty kH(k)\sin(kr)dr, \qquad (7)$$

which, from Eqs. 5 and 6, is seen to be a weighted sum of atom pair distribution functions modified by products of the atomic scattering factors. For monatomic materials the sum (5) consists of only one term, and the functions a(k) and g(r) can be extracted from a single diffraction experiment. Hence the radial distribution functions for carbon, shown in Fig. 6.5, are descriptive of carbon atom pair interactions. The function G(r) for the coal sample contains contributions from hydrogen atoms which are, however, not "seen" very well by x-rays in non-crystalline materials.

The radial distribution functions for carbon and for coal, shown in Fig. 6.5 are identical to radial distances of about 4 Å. Beyond this distance the curve for carbon shows further deviations from a uniform distance distribution (i.e., more structure), while the curve for coal rapidly approaches the uniform value G(r) = 1. The first peak at 1.42 Å in both curves is typical of the bonded C-C distance in condensed aromatic ring systems. The area under this peak corresponds to 3 C-C interactions. The first maximum is flanked on both sides by a series of "diffraction ripples" which arise from truncation of the Fourier integral in Eq. 7 at finite values of the variable k. Hence, the peak near 2 Å is of no physical significance. Further peaks in the

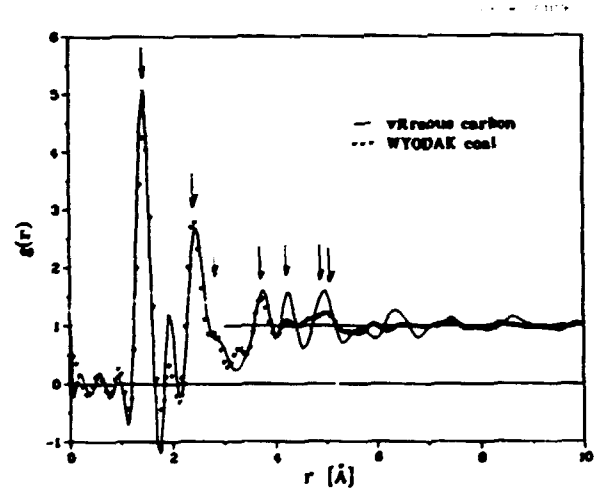

Fig. 6.5. Radial distribution functions of amorphous carbon and of Wyodak coal obtained by Fourier inversion of the data shown in Fig. 6.4. The arrows indicate calculated carbon-carbon distances for planar hexagonal sheets with a bond distance of 1.42 Å (graphite model).

radial distribution functions occur at distances given by the relationship

$$r_n = r_0 n^{1/2}, \quad n = 1,3,4,7,9,... \qquad (8)$$

with r_0 = 1.42 Å the bond distance between carbon atoms. This distance relationship[8] shows that the carbon atoms in the two samples studied are arranged in the planar hexagonal sheets found in crystalline graphite. In the crystal, the distance between carbon atoms in adjacent layers is 3.64.[9] No distinct peak is visible at this distance in the curves of Fig. 6.5. We conclude from this that the hexagonal layers of carbon atoms are only roughly parallel with neighboring sheets, leading to a wide distribution of interplanar distances. This would seem to result in a less efficient packing of carbon atoms than found in the graphite crystal and would explain the lower density of the vitreous carbon (1.5 g/ml) relative to crystalline graphite (2.25 g/ml).

To test this assumption quantitatively, we have calculated structure functions for the graphite model of amorphous carbon and of coal. The calculations were done using the Debye equation averaged over Gaussian distributions as described in detail elsewhere.[10] The distances r were taken from Eq. 8 to n = 9, and the rms-variations ℓ were adjusted by least-squares to seek a fit of the structure functions derived from experiment. For simplicity, a uniform distribution of distances was assumed for distances greater than 5.6 Å. The radial distribution function for the graphite model, obtained from the calculated structure function through Eq. 7, is compared with the experimental curve for amorphous carbon in Fig. 6.6. We thus conclude that an important component of the structure of Wyodak coal consists of essentially planar hexagonal sheets, roughly 75-80 Å^2 in area, which are only very roughly parallel with any neighboring sheets. This structure is very different from the stacked 20 Å^2 "clusters" ringed by amorphous material

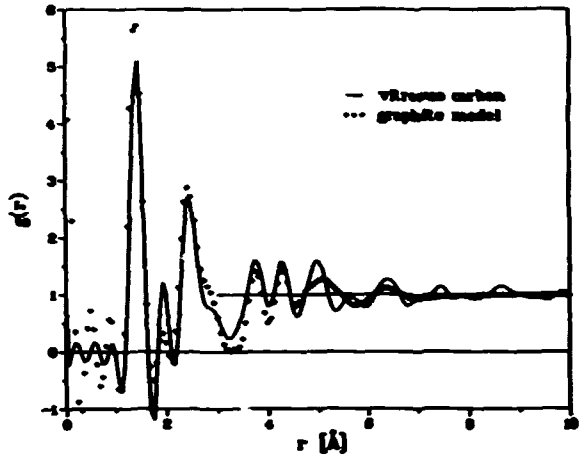

Fig. 6.6. Radial distribution functions calculated for the graphite model of amorphous carbon compare well with curves derived from experiment.

proposed by Cartz and Hirsch[2] for European brown coals.

1. R. Diamond, Phil. Trans. Royal Soc. (London) A251, 193 (1959).
2. L. Cartz and P. B. Hirsch, Phil. Trans. Royal Soc. (London) A252, 557 (1960).
3. Atomergic Chemetals Co., 100 Fairchild Ave., Planview, NY 11803.
4. A. H. Narten and H. A. Levy, in "Water: A Comprehensive Treatise," p. 314, Vol. I, F. Franks ed., Plenum Press, New York, 1972.
5. H. A. Levy, P. A. Agron, and M. D. Danford, J. Appl. Phys. 30, 2012 (1959).
6. Atomic Scattering Factors for C were taken from "International Tables for X-ray Crystallography," Kynoch, Birmingham, 1974, Vol. IV. Compton scattering factors were taken from D. T. Cromer and J. B. Mann, J. Chem. Phys. 47, 1893 (1967).
7. B. E. Warren and R. L. Mozzi, Acta Crystallogr. 21, 459 (1966).
8. G. D. Wignall and C. J. Pings, Carbon 12, 51 (1974).

9. S. Ergun, Carbon 6, 141 (1968).
10. A. Habenschuss and A. H. Narten, J. Chem. Phys. 85, 6022 (1986).

6.6 Evidence from X-ray Diffraction for a Covalent Bond to Bromine in Conducting Polyaniline

(B. K. Annis, A. H. Narten)

The emeraldine base form of polyaniline can be doped with dilute aqueous protonic acids to give a conductivity of approximately 5 (ohm cm)$^{-1}$ for a compressed pellet.[1] It has been thought that the doping process involves proton addition to the polymer which results in extensive conjugation of the chain accompanied by association of anions with the ring bridging NH^+ groups. However, direct confirmation of this aspect of the structure has not been available. Both the brominated and chlorinated versions of the polymer have been found to have similar conductivities, and since bromine has a more favorable cross section for x-ray scattering, we have investigated the former material.

Both doped and undoped samples of polyaniline were obtained from the University of Pennsylvania Conducting Polymers Group under the direction of Prof. A. G. MacDiarmid. X-ray diffraction measurements conducted in our laboratory established that both materials are amorphous. In the case of the doped polymer, measurements were made on samples from two different batches, and the conclusions were essentially the same. Analysis of the data in terms of radial distribution functions showed that the doped samples were characterized by a peak at 1.93 ± 0.03 Å which was not present in the undoped material.

One method of data reduction is to assume that all interatomic spacings which do not involve bromine are the same in both doped and undoped samples. The radial distribution function obtained by subtracting the two data sets should then depend only on those spacings involving bromine. The results of such an analysis are shown in Fig. 6.7. The area under the first peak provides information about the

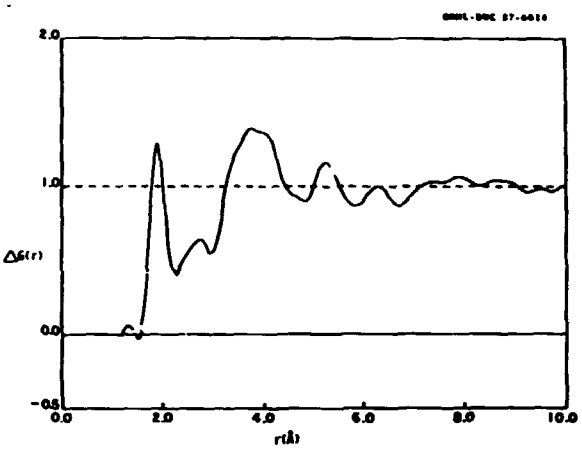

Fig. 6.7. Radial distribution function computed from difference of doped and undoped polyaniline.

coordination of the bromine atoms to carbon or nitrogen and suggests that most of the bromine is coordinated at a distance which is commensurate with a covalent rather than an ionic bond.

The significant amount of covalently bound bromine suggests that the proposed conduction mechanism in this material is in need of revision. The possibility that different dopants interact uniquely with the polymer chain will be a subject for future investigation.

1. A. G. MacDiarmid, J. C. Chiang, W. Huang, B. D. Humphrey, and N. L. D. Somasiri, Mol. Cryst. Liq. Cryst 125, 309 (1985).

6.7 Spectra of Polymeric Systems

(D. W. Noid, G. A. Pfeffer)

In this Section, we present some preliminary results concerning the transition from quasi-periodic to chaotic motion in a long linear polymeric chain $(AB)_n$. A few studies have been reported for linear atomic chains,[1] but even less work has been reported using polymeric diatomic chains.[2] We also further extended the previous research by studying longer chain lengths; the longest chains considered before have contained ~1000 atoms; we have employed 20-3200 atoms (10-1600 diatoms). The motivation for both our investigations and those

preceding us has been twofold: to find appropriate criteria to detect or predict the onset of chaos in systems with many modes and to examine the stochastic threshold as a function of chain length, initial excitation and other chain attributes. Such work is applicable to energy transfer in polymeric systems.

Our model chain mimics a linear array of AB beads where the A-B bond is a typical chemical bond and the B···A interaction is much weaker. A Morse oscillator is chosen for the AB bond and has the form

$$V(r) = D(e^{-2\alpha(r-re)} - 2e^{-\alpha(r-re)}), \qquad (1)$$

where r is the A-B distance. The B···A interaction is given by a Lennard-Jones potential

$$V(R) = 4\varepsilon[(\frac{\sigma}{R})^{12} - (\frac{\sigma}{R})^{6}] , \qquad (2)$$

where R is the distance between the molecular centers of mass.

A one-dimensional "temperature" was calculated from the kinetic energy at each time step. This temperature remained reasonably constant after an initial equilibration period. The spectra were generated by a fast Fourier transform of the sum of all the particle coordinates at each time step. A random displacement (either positive or negative) from the equilibrium position was then introduced to give the initial positions. By changing the maximum position-displacement parameter and the maximum momentum parameter, the temperature could be changed. The ends of the chain were not fixed, in contrast to several previous studies.

The spectra clearly showed a low frequency set of peaks ($\lesssim$100 cm^{-1}) and a high frequency set of peaks ($\sim$3000 cm^{-1}). The choice of initial conditions described above gives, in the low temperature case, nearly 100% excitation of the high frequency modes. The conclusions reported here deal only with these initial conditions, and conclusions for other choices of initial conditions may be different.

Figure 6.8 shows the power spectrum for 1280 particles at a nominal temperature of 1 K. The log of the intensity from the fast Fourier transform actually is displayed rather than the intensity itself, because the low frequency peaks are more easily seen in the log plot. Well separated sharp peaks can be seen in the range 0-1300 cm^{-1}, and in the range 3250 cm^{-1} - 3924 cm^{-1}. There is an intermediate region where no peaks and little noise are seen. Based upon the appearance of the spectrum, at this temperature the system appears to be quasiperiodic. Figure 6.9 shows the (log) power spectrum for the same system at 135 K

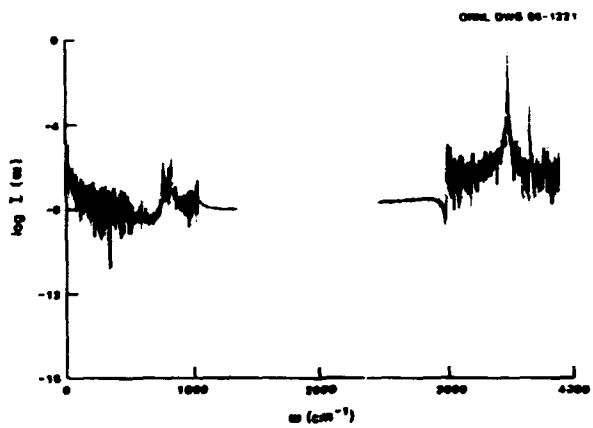

Fig. 6.8. Spectrum of a polymeric chain with 1280 atoms in the quasiperiodic regime and for a low temperature (1 K).

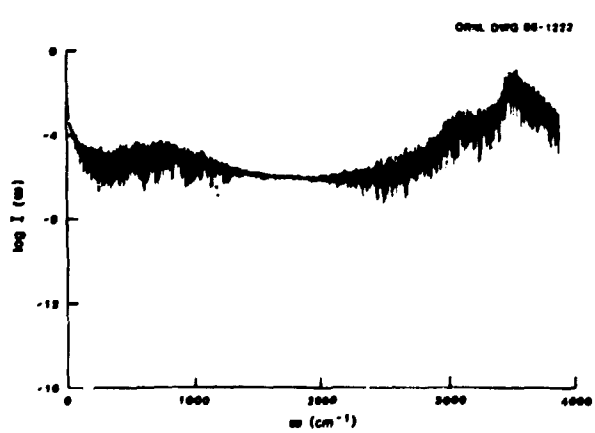

Fig. 6.9. Same as Fig. 6.8 but for a higher temperature (135 K) and chaotic motion.

where no sharp peaks are seen and the noise-free intermediate region has disappeared. Based upon the appearance of this spectrum, the system appears to be chaotic.

Furthermore, if the integral of the spectrum is taken from 0 to ~1982 cm^{-1} (the low frequency regime) and a second integral is taken from 1982 to 3924 cm^{-1} (the high frequency regime), then for Figure 6.8 the low frequency/high frequency percentages are 0/100, whereas for Figure 6.9, the ratio is 24/76. Clearly, the initial excitation (which evidently was of the high frequency modes only, because the low temperature spectrum shows only high frequency peaks) has remained localized in the quasi-periodic case and has begun to redistribute among all modes in the chaotic case. In solid polymeric materials, the low frequency modes are known as acoustical modes, and the high frequency modes are known as optical modes. The technique proposed here should be useful in studying the onset of efficient energy transfer from the optical modes (perhaps excited by laser light) to acoustical modes (which can lead, upon excitation, to damage in the solids).

We note as a final comment that in our studies we have found that the temperature at which the chaotic limit is reached has a more complicated dependence upon the chain length[1] than has been seen before for the atomic chains. Preliminary calculations indicate that the temperature at which the spectra become chaotic increases with increasing chain length up to a point and then essentially remains constant or drops somewhat as the chain length is further increased. Work is in progress to explore these results more fully, as well as to apply these energy transfer ideas to solid polyethylene.

---

1. (a) E. Diana, L. Galgani, M. Casartelli, G. Casati, and A. Scotti, Theor. Math. Phys. 29, 1022 (1977).
   (b) M. C. Carotta, C. Farrario, G. LoVecchio, and L. Galgani, Phys. Rev. A 17, 786 (1978).
   (c) E. A. Jackson, Rocky Mountain J. Math. 8, 127 (1978).
   (d) L. Galgani and G. LoVecchio, Nuovo Cimento B. 52, 1 (1979).
2. (a) B. I. Henry and J. Oitmaa, Aust. J. Phys. 38, 171 (1985).
   (b) B. I. Henry and J. Oitmaa, Aust. J. Phys. 38, 191 (1985).

6.8 Self-Diffusion Constants of Atoms and Small Molecules Dissolved in Polymer Systems

(E. Johnson)

A number of situations arise in which the rate of diffusion of a given atom or small molecule through a specific polymer determines whether or not the material is suitable for a particular application. An example of this is the use of polymers as containers for soft drinks. If carbon dioxide diffuses rapidly through a given polymer, then this polymer is not suitable as a container for soft drinks, because carbon dioxide is an important component of this beverage. The rate of diffusion of an atom or molecule through a polymer is determined by two properties of the atom or molecule in the polymer: (1) the solubility and (2) the self-diffusion constant. At this stage, we are concerned with obtaining the relevant self-diffusion constants. The method being used to obtain the self-diffusion constants is molecular dynamics.

Experimentally determined and computer simulation determined self-diffusion constants are compared below. The self-diffusion constants compared are for xenon dissolved in a series of different alkanes. The form of the potential energy function and the specific molecular dynamics method used are discussed. Periodic boundary conditions, box size and shape, the formula used for the self-diffusion constant, and uncertainties in the molecular dynamics self-diffusion constants are also discussed.

The self-diffusion constant of xenon in various alkanes has been determined.[1] The general formula for alkanes is C_nH_{2n+2}. The determinations were made for n = 5 through n =

16. In these results the value of the self-diffusion constant of xenon decreased as n increased. The determinations were made at 293 K. The concentrations of xenon in the alkanes were low, but values for the concentrations were not given. The pressure or densities were not given either. The systems were probably at one atmosphere pressure.

Self-diffusion constants for n = 5 and n = 6 were determined by molecular dynamics. The experimental and molecular dynamics values for n = 5 are 7.96×10^{-5} cm^2/sec and 3.6×10^{-5} cm^2/sec, respectively. The uncertainties in the molecular dynamics values are discussed below. The experimental and molecular dynamics values for n = 6 are 6.71×10^{-5} cm^2/sec and 7.7×10^{-5} cm^2/sec, respectively.

The potential energy functions used in the molecular dynamics calculations had five components. Four of these components were intramolecular interactions. The first was the bond stretching force. The form of the chemical bond potential energy function was the Morse function.[2] An angle bending force was associated with each set of three atoms for which two of these atoms were chemically bonded to the third atom. The angle bending potential[3] was the sum of two terms. A torsion force[3] was associated with each set of four atoms for which no atom of the set is bonded to more than two other atoms of the set and each atom of the set is chemically bonded to at least one other atom of the set. The torsion potential contains three parameters. The form for the intramolecular and intermolecular van der Waals interaction[4] was a Lennard-Jones potential. An intramolecular van der Waals force existed between all atoms in the same molecules which were not chemically bonded to each other and which were not both chemically bonded to a third atom.

The Morse and Lennard-Jones potentials were shifted so that no discontinuities were obtained in the resulting forces.[5] Without the shifts, periodic boundary conditions would produce these discontinuities.

The molecular dynamics method used was based on solving Newton's equations of motion under the condition of constant temperature. This method is examined in Reference 6. When determining forces and energies of interaction from the potential energy function, periodic boundary conditions were applied. Periodic boundary conditions were also used in determining the positi s of atoms.

In most molecula dynamics studies, the periodic boundary c ndition box is cubic. Other shapes have been used.[7] In the calculations described here, the boxes used were prisms. For example, in the calculations for the xenon and C_5H_{12} mixture, the length of the box along the x and y axes was 7.0711×10^{-8} cm. The box length along the z axis was 12.0×10^{-8} cm.

The self-diffusion constant D was determined from the following expression:[8] $\langle|\underset{\sim}{r}(t) - \underset{\sim}{r}(o)|^2\rangle/(6t)$ for large t. Here $\underset{\sim}{r}(t)$ is the position vector of the xenon atom at time t. The quantity $\langle|\underset{\sim}{r}(t) - \underset{\sim}{r}(o)|^2\rangle$ was fitted to the expression $(b_1 + 6b_2t)$ by least squares. Here b_1 and b_2 are least squares parameters. The self-diffusion constant D is equal to b_2.

The uncertainty in the value of the self-diffusion constants is probably about fifty percent of the value of the self-diffusion constants. Further calculations need to be done to obtain more accurate results.

---

1. G. L. Pollack and J. J. Enyeart, Phys. Rev. A 31, 980 (1985).
2. P. M. Morse, Phys. Rev. 34, 57 (1929).
3. E. M. Engler, J. D. Andose, and P. von R. Schleyer, J. Am. Chem. Soc. 95, 8005 (1973).
4. M. Levitt and S. Lifson, J. Mol. Biol. 46, 269 (1969).
5. W. B. Streett, D. J. Tildesley, and G. Saville, "Multiple Time Step Methods and an Improved Potential Function for Molecular Dynamics Simulations of Molecular Liquids" in Computer Modeling of Matter,

edited by Peter Lykos (American Chemical Society, Washington, 1978), p. 144.
6. J. M. Haile and S. Gupta, J. Chem. Phys. 79, 3067 (1983).
7. D. J. Adams, Chem. Phys. Lett. 62, 329 (1979).
8. J. P. Boon and S. Yip, Molecular Hydrodynamics (McGraw-Hill, St. Louis, 1980), p. 47.

6.9 Dynamic Properties of Polymer Systems Using Lattice Models

(E. Johnson, Jeffrey D. Kovac[4])

The effect on the structure and motion of a polymer molecule by other polymer molecules and by solvent molecules may be treated directly by the use of an appropriate potential energy function. These effects may also be treated indirectly. Using hydrodynamic interactions is one indirect way of treating these effects. The attractive feature of indirect methods is that they are more economical to use. Computation times are usually shorter.

At this time, the property of main interest to us is the variation of the self-diffusion constant of polymer molecules in a system as a function of the length of these molecules and the effect on this variation as the strength of the hydrodynamic interactions changes. The computational technique used here is the Brownian molecular dynamics method. The basic assumption in the method is that the forces that produce non-transient effects are random. This assumption is more appropriate for some properties than for others.

With no hydrodynamic interactions, the self-diffusion constant of a polymer is proportional to $N^{-\alpha}$ where $\alpha = 1$. This was determined some time ago.[1] Our calculations seem to agree with this result. Calculations were performed for molecules containing 12, 24, and 48 monomer units. The molecules were chains. This means that each monomer unit was chemically bonded to no more than two but at least to one other monomer unit and that only two of the monomers were chemically bonded to only one other monomer unit.

The values of the self-diffusion constant for N = 12, 24, and 48 are 1.6×10^{-2}, 1.7×10^{-3}, and 7.7×10^{-4} in (length unit)^2/(time unit), respectively, when the hydrodynamic interactions are equal to zero. The length unit and the time unit must be chosen on the basis of the polymer system being treated. These units will be left unspecified here. For moderately strong hydrodynamic interactions, the values of the self-diffusion constant for N equal to 12, 24, and 48 are 2.3×10^{-3}, 4.1×10^{-4}, and 5.3×10^{-4}, respectively. For strong hydrodynamic interactions, the values of the self-diffusion constant for N equal to 12 and 24 are 4.1×10^{-3} and 4.0×10^{-3}, respectively.

The $N^{-\alpha}$ dependence of the value of the self-diffusion constant on chain length is most closely obeyed for large values of N. With no hydrodynamic interactions, the value of α seems to be close to one. For strong hydrodynamic interactions, the value of α seems to be close to zero. For moderate values of the hydrodynamic interactions, the value of α seems to lie between zero and one. As the values of the hydrodynamic interactions increase, the value of α seems to vary roughly from one to zero. This observation seems to agree with previous results on this property.[2]

The only intramolecular potential energy interaction that was treated directly was particle exclusion. Each monomer unit was centered on a lattice site, so chemical bond length, bond angles, and bond torsion angles between monomer units were automatically restricted to certain values. A simple cubic lattice was used. Since only one polymer molecule was treated, it was not necessary to consider intermolecular forces. Particle exclusion required that no more than one monomer unit occupy a given lattice site.

The Brownian Dynamics algorithm used was a modification of that presented in Reference 3. The modifications were made to allow the simulation of a lattice system. The trajectories of the monomer units were determined largely by the random forces. The excluded volume forces come into effect only when the

Brownian forces would lead to two or more monomer units occupying the same lattice site. Periodic boundary conditions and a cubic box were used for the simulations. For the calculation of self-diffusion constants, probably neither the periodic boundary conditions nor the box size and shape affect the results if the dimensions of the box are longer than the length of the polymer molecule.

The self-diffusion constant was obtained from the expression[1] $\underset{\sim}{R}(t) - \underset{\sim}{R}(o)^{2}/(6t)$ where $\underset{\sim}{R}(t)$ is the vector position of the center of mass of the polymer molecule at time t. The center of mass of the polymer molecule is defined by $\underset{\sim}{R}(t) = \Sigma_{i=1}^{N} \underset{\sim}{r}_i(t)/N$ where $\underset{\sim}{r}_i(t)$ is the vector position of monomer unit i of the molecule. The quantity $\underset{\sim}{R}(t) - \underset{\sim}{R}(o)^{2}$ was fitted by least squares to the expression $(b_1 + 6b_2t)$. The least squares parameter b_2 is equal to the self-diffusion constant.

The size of the uncertainty in the values of the self-diffusion constants given must still be determined. This determination will be made by varying the initial conditions and the run times of the Brownian Dynamics calculations.

1. C. C. Crabb and J. Kovac, Macromolecules 18, 1430 (1985).
2. M. Bishop, M. H. Kalos, and H. L. Frisch, J. Chem. Phys. 70, 1299 (1979).
3. D. L. Ermak and J. A. McCammon, J. Chem. Phys. 69, 1352 (1978).
4. University of Tennessee.

6.10 Structural and Thermodynamic Properties of Liquid Systems Using Lattice Models

(E. Johnson)

This report is about a closed and exact set of equations[1,2] which may be used to obtain the particle distribution functions of statistical mechanics. Other such equations in statistical mechanics do not satisfy the condition of being closed and exact. A set of equations is closed if there are as many equations in the set as there are unknown functions in the equations. The set is exact if no approximations were used to derive any of the equations in the set.

Sets of equations that are not exact give unacceptable results for certain systems.[3] With appropriate methods for solving the equations involved, results of arbitrary accuracy may be obtained from a closed and exact set of equations. Three numerical methods for solving the set of equations have been used. The first method is inadequate for most systems.[1] The second method is adequate up to moderate densities.[1] The third method seems to be completely adequate. The third method has not been completely tested yet.

Applications to lattice fluids have been made. A lattice fluid is a fluid in which positions of particles are confined to sites on a lattice. The particles may occupy more than one lattice site. As the grid spacings decrease while the particle volume remains constant, the properties of a lattice fluid approach the properties of a regular fluid.[4] So the applications to lattice fluids have implications for such fluids as water and liquid argon.

Two of the three integral equations of the set used are applicable to systems with any kind of pair potential. The third equation is applicable to systems with a pairwise additive potential energy function. The third equation may be modified to treat systems which are not pairwise additive. The three equations are applicable to classical systems. All of the equations are exact.[1] The first equation of the set is the two particle Ornstein-Zernike equation.[3] The second equation is an integrated form of the Baxter equation.[5] The third equation is a system of nonhomogeneous linear equations. The third equation was obtained by applying the calculus of variations to an integral equation.[2] A detailed discussion of the set of three equations is presented in Reference 1.

The Gaussian elimination procedure is not always appropriate for solving the variational equation mentioned above. Accurate solutions to the equations are often not obtained using Gaussian elimination because the equation is ill-conditioned. With certain numerical

methods, ill-conditioned equations often cannot be solved accurately on a computer because of computer round-off error.[6]

The Jacobi method[7] is usually appropriate for solving the variational equation up to moderate densities. The Jacobi method is known to reduce the effects of computer round-off error relative to the Gaussian elimination method.

The least squares method[8] appears to be appropriate for solving the variational equation in all cases. This method has not yet been fully tested. For the variational equation given here, it appears to be far superior to the Gaussian elimination and the Jacobi method.

The technique discussed above is apparently ready to be used for solving a number of statistical mechanical problems. Examples are certain models for liquid crystals.[9] Because of the long computation times that would be required, the method presented here is probably not yet practical for the treatment of certain equilibrium problems in classical statistical mechanics. An example is the usual type of model for fluids such as water.

---

1. E. Johnson, J. Chem. Phys. (in press).
2. E. Johnson, J. Chem. Phys. 72, 3010 (1980).
3. J. A. Barker and D. Henderson, Rev. Mod. Phys. 48, 587 (1976).
4. G. M. Bell, J. Phys. A 13, 659 (1980).
5. R. J. Baxter, J. Chem. Phys. 41, 553 (1964).
6. H. Müller-Merbach, On Round-Off Errors in Linear Programming (Springer-Verlag, New York, 1970).
7. A. M. Cohen, J. F. Cutts, R. Fielder, D. E. Jones, J. Ribbans, and E. Stuart, Numerical Analysis (Wiley, New York, 1973), pp. 190-192.
8. Reference 7, pp. 284-285.
9. L. Borkowski and J. Stecki, Mol. Phys. 40, 333 (1980).

7. CHEMISTRY OF TRANSURANIUM ELEMENTS AND COMPOUNDS

This program is illuminating important areas of inorganic and physical chemistry through studies that are sensitive to the unusual or unique f-orbital and relativistic bonding effects associated with the actinide region of the periodic table. Most studies center on the isotopes of Cm through Es available from the DOE National Transplutonium Production Program. Since the chemistry of these heaviest elements can only be understood in relation to the lighter actinides and the lanthanides, work with these elements is also performed. An example of f-orbital bonding is found in experiments where extremely high pressures bring about a transition of the 5f electrons in Am, Cm, Bk, and Cf metals from an atomic non-bonding condition to a metallic bonding condition. These high pressure (up to 60 GPa) experiments on the pure metals are being extended to alloys and compounds. In our studies, we often select particular classes of compounds which we think may illuminate significant chemical differences between the lanthanides and the actinides. For example, the properties of the hydrides, pnictides, and chalcogenides are expected to differ significantly between the 4f and 5f electron series. Crystallographic, thermodynamic, and magnetic studies of such compounds are underway. Operation of a high temperature Knudsen cell-mass spectrometer system allows characterization of high temperature gaseous atoms and molecules. These high temperature studies provide enthalpies and entropies of various vaporization processes and determine the stability of various gaseous materials. Unique compounds that might be stabilized under special conditions include EsF_6 (5f half filled shell stabilization) and diatomic molecules (such as CfO and CfS). The theoretical understanding of relativistic f-electron systems has been hindered because of their inherent complexity. Characterizing gaseous diatomic compounds simplifies the molecular calculations and could lead to a much better understanding. We are also searching for unusual low oxidation states of the actinide elements through the development of new types of electrolyte chemistry in selected high boiling aprotic organic solvents. An extension of these investigations will employ selected organometallic compounds in an attempt to stabilize the lower oxidation states of the actinides.

7.1 Chemistry and Physics of 5f Solids

7.1.1 High Temperature Thermochemical Studies

(R. G. Haire and J. K. Gibson)

Enthalpies and entropies of vaporization may be derived by measuring the rate of effusion of material from a Knudsen cell as a function of temperature. From such data the "metallic valence" of a metal (which can be equated with the electronic configuration and bonding in the metal) can be inferred and used to compare with similar data for other actinide and lanthanide metals. The classical approach for such experiments consists of studying the effusate from a cell containing a pure element. The limited availability of the transcalifornium elements together with their higher volatility required that a modified experimental approach be used.

A useful technique is to employ alloys, where the element of interest is present as a dilute solute in a selected metallic solvent. The vapor pressure of the elemental solute over the alloy is then measured and the vapor pressure for the pure element is derived from these values and the composition of the alloy. In addition to being useful for highly radioactive and very small amounts of material, the technique also permits investigating the vaporization of solute from different solvents that may effect its metallic valence. Studies of several actinide-lanthanide and lanthanide-lanthanide alloys have been carried out. The alloy technique offers the additional advantage in that thin films of material that are very susceptibile to chemical changes are not employed. For example, attempts were made to study pure Es metal using 100 μg of Es-253 in

a thin film, but these were not successful. Major problems with the studies of pure Es were: (1) the high reactivity of the thin Es metal deposits with gaseous impurities and the tantalum backing material; and (2) the relatively low temperature range dictated by the high volatility of pure Es metal. Contributing to these experimental problems was the self-heating of the Es metal (1000 watts/gram, Es-253).

One recent application of this alloy technique was the study of a Cf-Es-Sm alloy where the Cf and Es solutes ($<10^{-4}$ atom %) were co-volatilized from the Sm solvent. The object of this study was to determine the enthalpy of vaporization of divalent Es metal from a trivalent Sm metal solvent. Studying an alloy containing both Cf and Es allowed a relative comparison of the amounts of Cf and Es evaporated under identical experimental conditions. Experimental data for the enthalpy of vaporization of Es metal have previously been obtained only from an alloy of divalent Yb metal. This work on the Sm alloy examined the influence of the metallic valence of the solvent on the vaporization behavior of the Es metal and also allowed Cf metal to serve as a reference material in the study.

In Fig. 7.1 the data from one study of a Es-Cf-Sm alloy are shown. From the slopes of the lines, enthalpies of vaporization for Es (34 kcal/mol) and Cf (46 kcal/mol) were calculated, which are in accord with

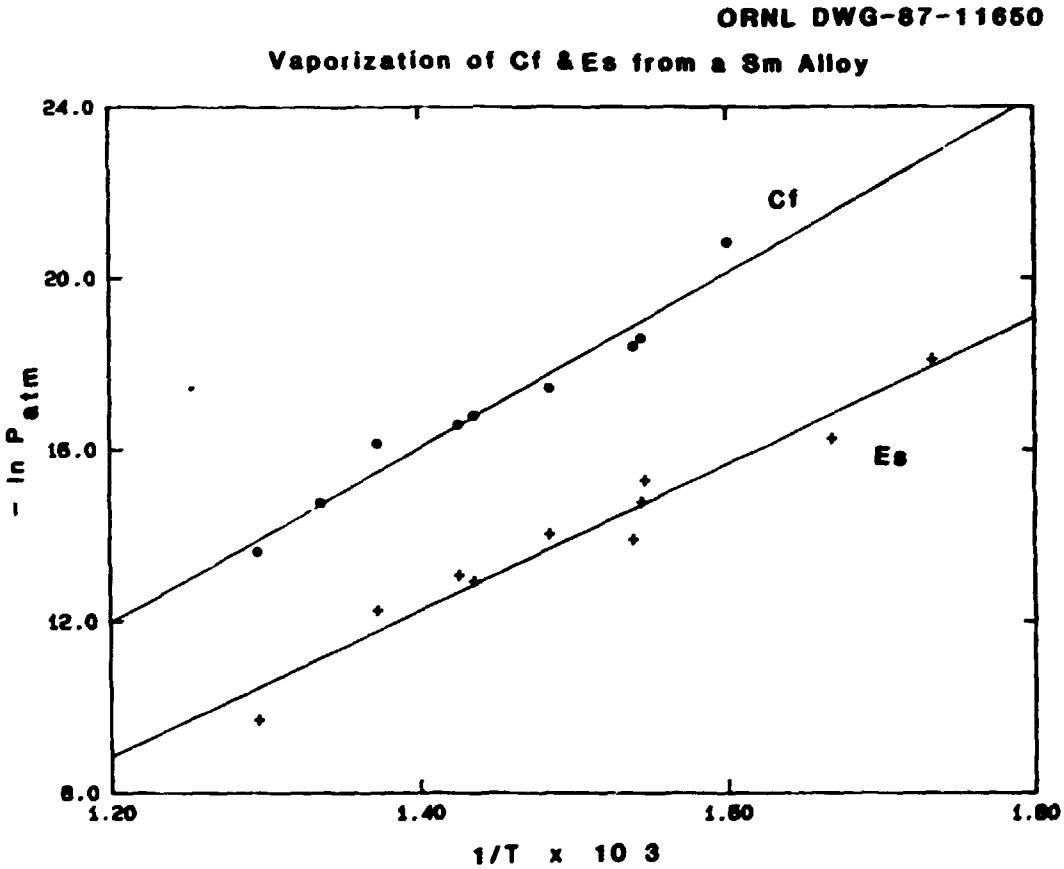

Fig. 7.1. Vapor pressure data for Es and Cf in an Es-Cf-Sm alloy as a function of temperature. The data show that Es metal is divalent even when vaporized from a trivalent Sm host solvent.

published values of 31.6 kcal/mol for Es (derived from the vaporization of Es from a divalent Yb solvent) and 46.9 kcal/mol obtained from studies of pure Cf metal. The value for Es in the Sm alloy indicates that Es metal maintains its divalent nature in the trivalent Sm solvent.

The technique of using alloys for enthalpy of vaporization studies will permit an extension of such studies to other actinides and will also provide a better understanding of the metallic valence of the transplutonium metals.

We have also initiated studies to investigate the vaporization and thermal stability of compounds using Knudsen cell mass spectrometric techniques. Results for the trifluorides of Pr, Eu, Tb, Dy, Ho, and Lu and the tetrafluorides of Ce, and Tb, have been obtained. These materials were studied in preparation for examining comparable fluorides of the transplutonium elements and Pm. The experimental approach being employed is to study the temperature dependence of the congruent vaporization of the MF_3 compounds to obtain a Second-Law enthalpy for the vaporization. With the tetrafluorides, in addition to the potential congruent vaporization as MF_4 (as found with CeF_4), the decomposition of the tetrafluoride to form the trifluoride and fluorine can also occur. By measuring the fluorine vapor pressure over TbF_4 (which was in equilibrium with TbF_3) as a function of temperature, it was possible to determine the enthalpy associated with its decomposition. Studies with AmF_4 and CmF_4 are in progress. Using this approach it is possible to determine the relative stabilities of the tetra- and trifluorides. Further, since the enthalpy derived from the decomposition process represents the difference between the heats of formation of solid MF_4 and MF_3, the experimental data can be used to evaluate the thermodynamic predictions that have been made for these latter materials.

Experimental data is shown in Fig. 7.2 for the decomposition of TbF_4 with congruent vaporization of TbF_3 and F_2 evolution. The intensity of the effusate is plotted as a function of temperature. The small enthalpy for the decomposition is in accord with the modest stability of TbF_4 relative to TbF_3 and the enthalpy of vaporization for TbF_3 is in line with values for other lanthanide trifluorides.

7.1.2 Solution Thermochemical Studies[1]

(J. U. Mondal,[2] D. L. Raschella,[2] R. G. Haire, and J. R. Peterson[3])

The measurement of heat evolved from the dissolution of an actinide metal in an acid solution is a fundamental step in determining the enthalpies of formation of compounds of the metal. In previous work the enthalpies of solution of Bk and Cf metals were measured and reported. During this report period the enthalpy of solution of Am metal was measured with the intent of resolving the conflict that exists in published values for it. For the dhcp form of Am metal, a value of -620.6 kJ/mol was obtained for dissolution in 1 M HCl (see Table 7.1). This value confirmed one published value of -616.1 kJ/mol by Fuger, et al., and established which value for Am metal should be used for developing systematic trends in transplutonium metal thermodynamics.

---

1. Research sponsored by the Division of Chemical Sciences, Office of Basic Energy Sciences, U.S. Department of Energy in part under contract DE-AS05-76ER04447 with The University of Tennessee, Knoxville and in part under contract DE-AC05-84OR21400 with Martin Marietta Energy Systems.

2. Department of Chemistry, University of Tennessee, Knoxville.

3. Department of Chemistry, University of Tennessee, Knoxville, and Transuranium Research Laboratory, ORNL.

ORNL DWG 87-11651

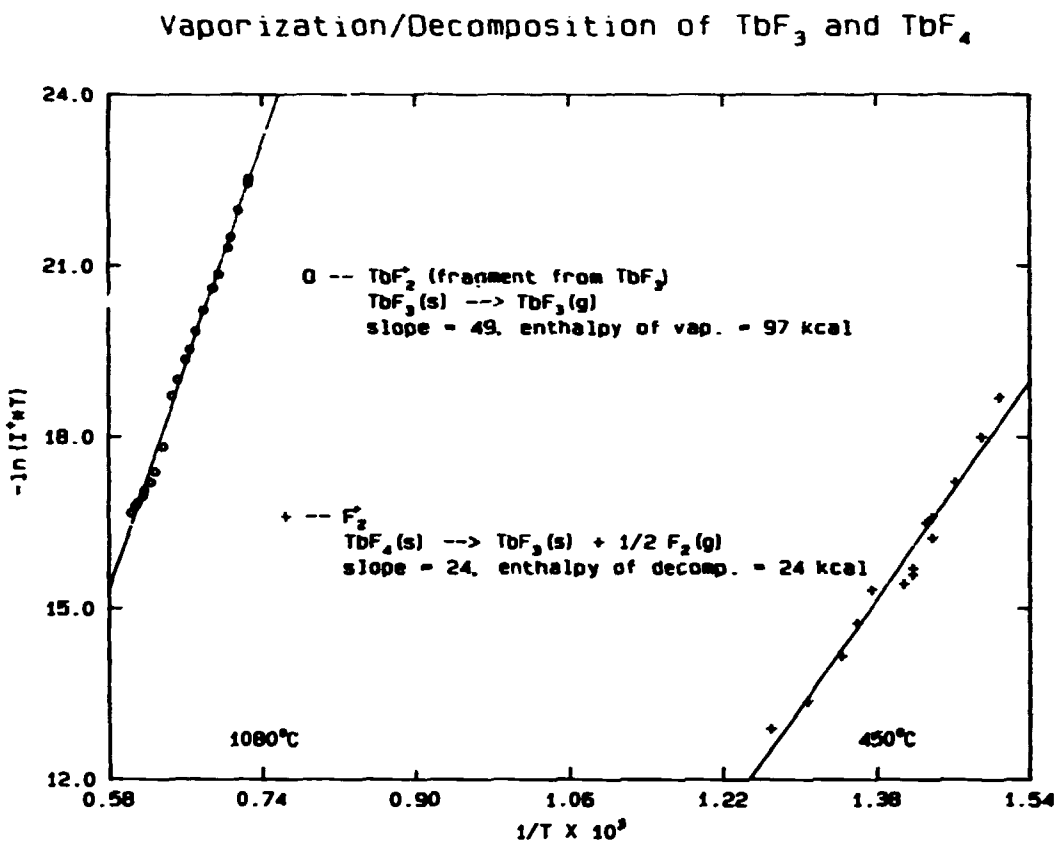

Fig. 7.2. Results of mass spectrometric studies of high temperature vaporization of TbF_3 (O) and decomposition of TbF_4 (+). The small enthalpy of decomposition of TbF_4 shows the modest stability of this compound.

7.1.3 Synthesis and Characterization of Transplutonium Monobismuthides and Monoantimonides

(J. K. Gibson and R. G. Haire)

In this period we have focused on preparing the monobismuthides of the transplutonium elements. The transplutonium monopnictides offer a group of chemically similar compounds in which the actinide-actinide separation distance may be controlled by selection of the pnictogen. The f-f and f-p interactions in the pnictinides are strongly dependent on this distance. Since bismuth is the pnictogen with the largest radius, the monobismuthides possess an unusually large actinide-actinide separation, which can be probed by magnetic and high pressure studies of these compounds.

Very few transplutonium monobismuthides have been prepared because of difficulties peculiar to bismuth that are encountered in the microscale syntheses. Past synthetic techniques for preparing the monoarsenides and monoantimonides of the transplutonium elements have relied on the ability to distill away the excess pnictogen used in the synthesis. Due to the lower vapor pressure of bismuth, this distillation was more difficult in preparing monobismuthides. For the transplutonium elements, the most difficult case encountered to date has been CfBi, since Cf metal is much more volatile

Table 7.1 Enthalpy of Solution of dhcp Americium Metal in 1 M HCl at 298.15 ± 0.5 K

Am Metal Preparation	Weight of Sample (μg)[a]	10^4 x Molarity of Am^{3+} in Solution	Heat Effect (J)[b]	$-\Delta H_{soln}$ (kJ mol^{-1})
	296.2	2.44	0.7556	620.0
	734.0	6.04	1.8775	621.7
	661.2	5.44	1.6864	619.9
I	206.6	1.70	0.5268	619.8
	624.8	5.14	1.5997	622.3
	838.5	6.90	2.1457	622.0
	517.4	4.26	1.3301	624.8
	802.4	6.60	2.0437	619.1
	416.0	3.42	1.0697	625.0
	465.1	3.83	1.1785	615.9
	296.7	2.44	0.7594	622.1
II	556.0	4.58	1.4166	619.3
	435.2	3.58	1.1053	617.3
	647.3	5.33	1.6493	619.3
	425.9	3.50	1.0860	619.8
	281.6	2.32	0.7195	621.0
Mean Value (2σ)				620.6 ± 1.3

[a]Corrected for buoyancy and known impurities.

[b]Corrected for vaporization of the solvent into the evolved hydrogen gas and into into the argon space in the sample container, known impurities, and heat of reaction initiation.

than bismuth metal. We have developed two different techniques for preparing these monobismuthides. One approach is to react the actinide metal in an atmosphere of bismuth vapor; the second is to use a molten bath of bismuth metal for the reaction and then recover the monobismuthide from it. Using these techniques it has been possible to prepare the monobismuthides of Am, Cm, and Cf. Each product has been characterized by X-ray diffraction (Fig. 7.3). All three compounds exhibited face centered cubic symmetry. The lattice parameter obtained for AmBi (a = 0.6332 nm) confirmed one of the two conflicting literature values for this compound, and is consistent with a model in which the Am in the compound is trivalent. Our data for CmBi (a = 0.6333 nm) is also consistent with such a trivalent model. Investigation of CfBi is in progress. A preliminary lattice parameter obtained for CfBi is considerably larger than anticipated based on extrapolation using the AmBi and CmBi data (see Fig. 7.3). If this parameter is confirmed, it would suggest that the Cf has a valence of less than three in this compound, a situation that would be significant to theorists as it would provide

ORNL DWG 87-11652

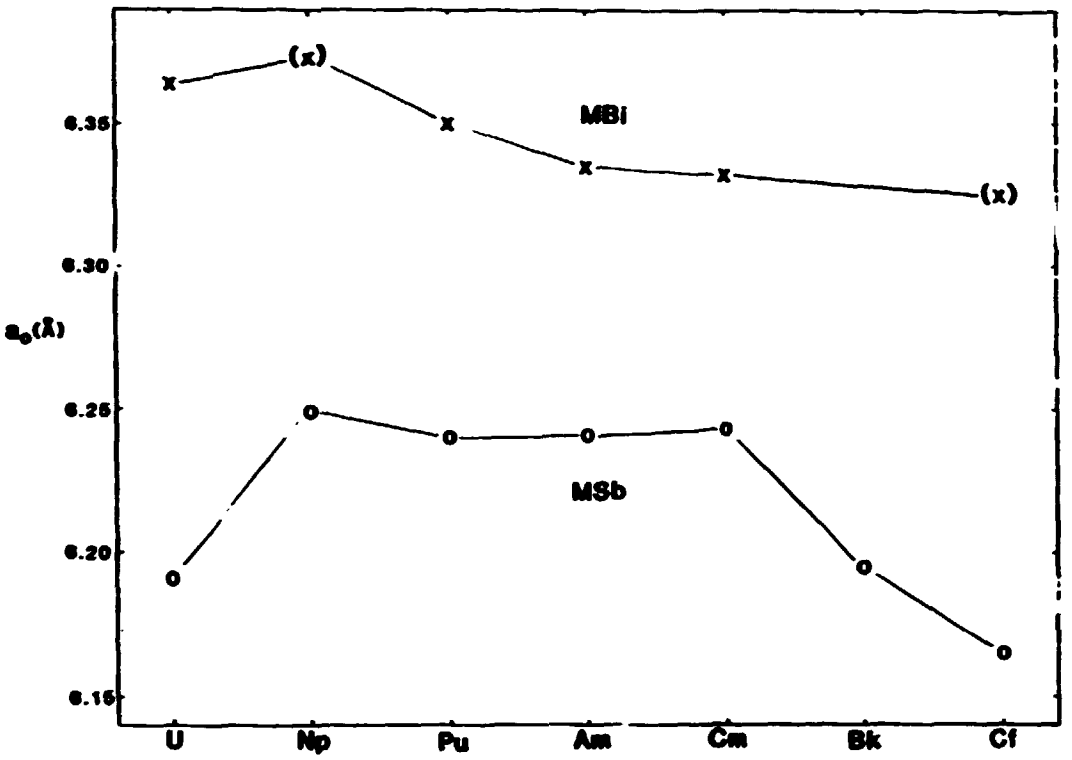

Fig. 7.3. Lattice parameters of actinide monoantimonides and monobismuthides with the NaCl-type structure: those for AmBi and CmBi and the preliminary value for CfBi are from this work.

a semimetallic compound that reflects the trend towards divalency for the second half of the series.

7.1.4 Magnetic Studies of Californium Chloride and Oxide, and Curium Bismuthide[1]

(S. E. Nave,[2] J. R. Moore,[2] R. G. Haire, J. R. Peterson,[3] J. K. Gibson)

In this report period magnetic measurements were made as a function of specific crystal axis, using a 20 μg single crystal of the hexagonal form of $CfCl_3$. The study of single crystals, as opposed to polycrystalline powders allows the determination of the magnetic properties as a function of the crystal's orientations with respect to the applied field. This permits refinement of parameters in a crystal-field model, which provide a framework for determining the effect of the anion on the f-wavefunction of the actinide. The results are shown in Fig. 7.4. In this figure the inverse susceptibility versus temperature data are given for both a polycrystalline powder and a single crystal of $CfCl_3$ with the latter oriented with an angle of 27.5° between the c-axis and the magnetic field. The dotted lines in the figure are the results of a parametric fit to the data for a crystal field model, which includes intermediate coupling and j mixing effects. With these crystal field parameters one can extrapolate to obtain the parallel and perpendicular components of the susceptibility as indicated by the solid lines. These results indicate a significant magnetic anisotropy due to the crystal field.

We have also examined the magnetic properties of polycrystalline materials. In order to separate the effects of magnetic

ORNL DWG 87-11653

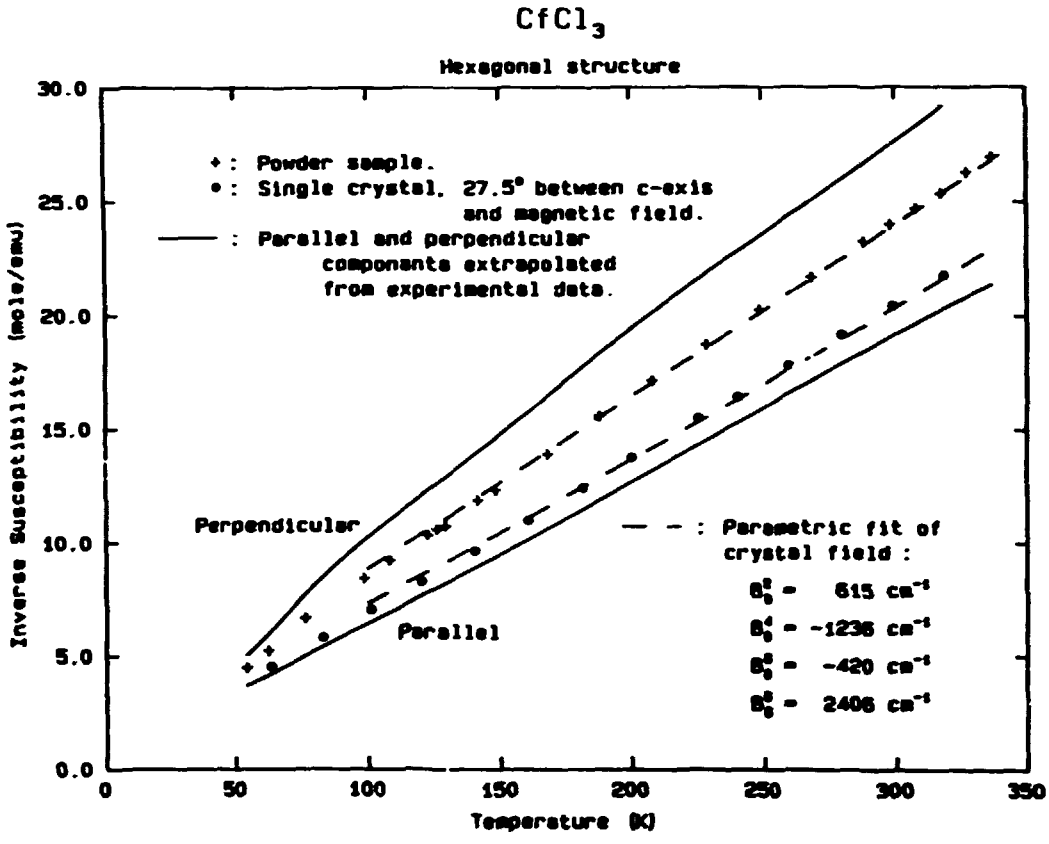

Fig. 7.4. Inverse susceptibility versus temperature for $CfCl_3$ in the form of a polycrystalline powder and a single crystal are calculated from a model which indicates a significant magnetic anisotropy arising from the crystal field.

susceptibility due to crystal fields, as opposed to those arising from direct actinide-actinide overlap (direct exchange) or actinide-anion overlap (superexchange), we have examined compounds in which the actinide is diluted in a nonmagnetic, isostructural host. Measurements on Cf_2O_3 diluted in a bcc Y_2O_3 host have indicated that the interaction parameter, theta, in a Curie Weiss fit of the data is reduced from 115 K to 25 K. This indicates that the Cf-Cf exchange interactions in these ionic-type compounds are very significant. Magnetic studies of $CfCl_3$ in a hexagonal $LaCl_3$ host indicated that a low-temperature antiferromagnetic transition exists. This transition, which is present in pure $CfCl_3$, was retained in the mixed samples. This behavior suggests that the material was a mixture of these two compounds rather than a dilute solution of the $CfCl_3$ in the host. This problem probably arose from the large difference between the trivalent ionic radii of Cf and La, which hindered formation of a true solid solution.

Magnetic studies of the actinide pnictides were extended to the compound, CmBi. These pnictides provide a group of compounds in which the effect of the actinide-actinide separation on the magnetic ordering can be determined. They also provide insight into the various electronic mechanisms reponsible for the ordering. With the Cm pnictides a minimum is observed in a plot of the ordering temperature versus actinide-actinide

separation, as seen in Fig. 7.5. This minimum occurs at an actinide-actinide separation intermediate in magnitude to values observed in CmP and CmSb. Such data suggest that the ordering temperature for CmBi would be higher than that for CmSb. The initial measurements on CmBi indicate that this is indeed the case but variations in the values observed for the ordering temperature in different samples of CmBi must be interpreted before a final conclusion can be reached.

---

1. Research sponsored by the Division of Chemical Sciences, Office of Basic Energy Sciences, U.S. Department of Energy in part under contracts DE-AS05-79ER10348 and -76ER04447 with the University of Tennessee, Knoxville and in part under contract DE-AC05-84OR21400 with Martin Marietta Energy Systems.
2. Physics Department, University of Tennessee, Knoxville.
3. Chemistry Department, University of Tennessee, Knoxville and Transuranium Research Laboratory, ORNL.

7.1.5 Behavior of Actinide Materials Under Pressure[1]

(R. G. Haire, J. R. Peterson,[2] J. P. Young,[3] U. Benedict[4])

Studies of actinide metals, alloys, and compounds under pressure have been carried

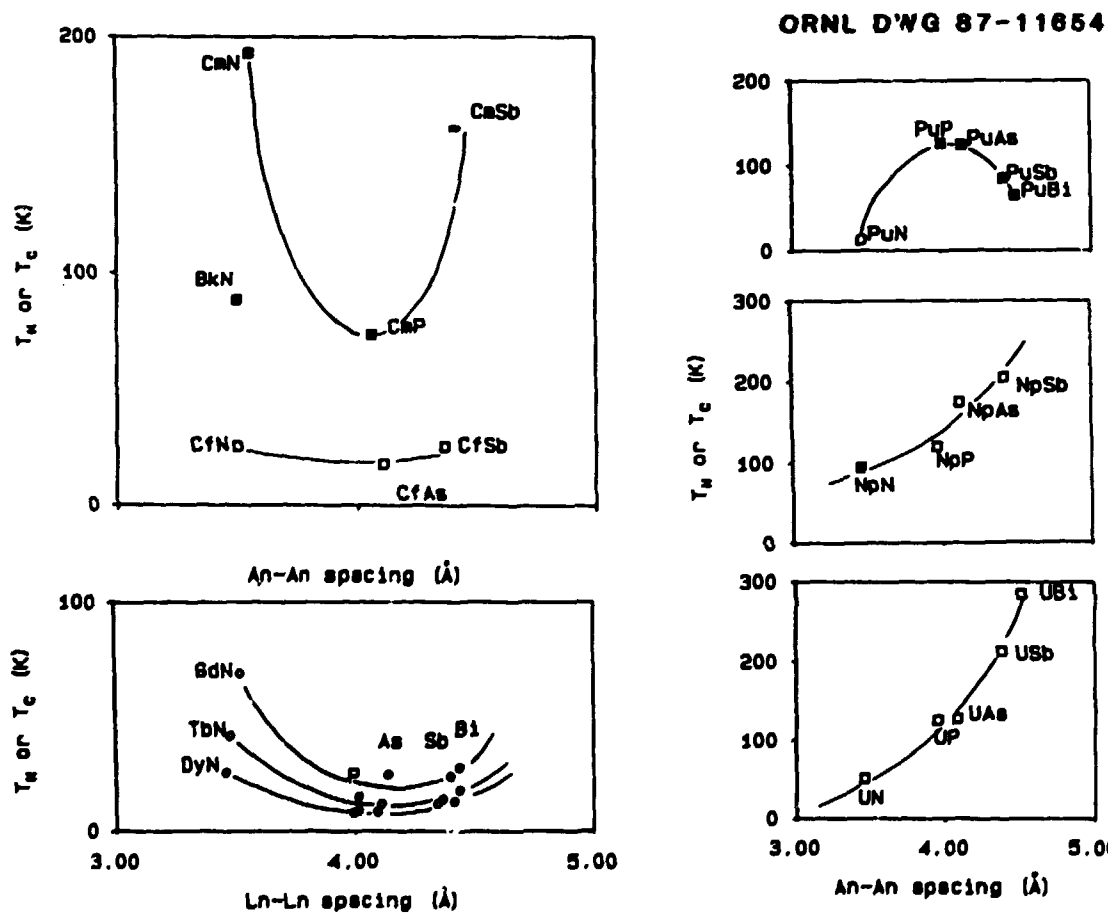

Fig. 7.5. Magnetic transition temperatures plotted versus actinide-actinide (lanthanide-lanthanide) separation indicating the approach to lanthanide like behavior with increasing atomic number of the actinide species.

out in collaboration with the European Institute for Transuranium Elements, Karlsruhe, Federal Republic of Germany. The studies employ diamond anvil pressure cells and energy dispersive X-ray diffraction analysis to measure the relative volumes (V/V_0) of the material as a function of applied pressure. Previous studies have been carried out using pure metals of Am, Cm, Bk, and Cf and alloys of Bk-Cf. One of the important findings in the studies of the pure metals was that their 5f electrons may be forced to participate in the metallic bonding by applying pressure.

One of our recent efforts has involved the study of Am-Cm alloys as a function of pressure. Important differences have been noted between the pressure behavior of pure Am metal and Cm metal, and the studies were undertaken to investigate these differences. One difference between Am and Cm metals is the absence of a trigonal high pressure phase for Cm. Another is the trend of higher pressures for comparable transitions for Cm, and a third is a much greater volume collapse for Cm (21% versus 6% for Am) at the onset of the delocalization process. It has been established in earlier work that the trigonal phase occurs only in pure Am and Cf metals (not Cm or Bk) under pressure. From these initial studies of the Am-Cm alloys, it was determined that a trigonal high pressure phase occurred in the alloy that contained up to 75 atom percent Cm. This dominance of Am in the alloy contrasts with results obtained previously with Bk-Cf alloys where the presence or absence of the trigonal high pressure phase was determined by the dominant component of the alloy. With the Am-Cm alloys, the pressures at which the different phase transitions and the delocalization of 5f electrons occurred were found to be intermediate in value to comparable transitions for the parent metals but the variances were not linear with composition. It is apparent from the data obtained in these studies of the Am-Cm alloys vs the Bk-Cf alloys that the $5f^7$ configuration (half-filled shell) had an important influence on the pressures at which the observed changes took place.

We have also studied actinide compounds under pressure during this period, using X-ray diffraction and/or absorption spectrophotometry to measure the behavior of samples as a function of pressure. The mononitrides of Cm and Cf were two compounds where it was necessary to use high-pressure X-ray diffraction in order to study them, due to their opacity to visual light. The semimetallic monopnictides are interesting compounds to study as they can be expected to exhibit valence instabilities and electronic transitions under pressure. The metal-metal distances and the f-p interactions present in these monopnictides may be altered by selection of the pnictogen. Thus a study of the different monopnictides could determine the importance of these distances and interactions on the pressure behavior of the compounds. The monopnictides of Cm and Cf have now been studied at pressures up to 50 GPa of pressure. Both nitrides as prepared exhibited a face centered cubic structure at normal pressure. Evidence for a structural change or a collapse in relative volume with the application of pressure, which would have suggested that an electronic transition or change in bonding had occurred, was not obtained. Instead, only a dynamic compression of the cell volume with pressure was observed for CmN and CfN. From their pressure-volume relationship, a bulk modulus was calculated for each compound. For CmN, a value of 150 GPa was obtained, while the modulus of CfN was determined to be 120 GPa. These values are comparable to moduli for ThN, UN, CeN, and several lanthanide/actinide oxides. In contrast, the moduli for Cm and Cf metals are only about one-third as much ranging from 40-50 GPa. Although the bulk modulus is a physical property, its value has been associated with the nature of the bonding (ionic, covalent, band structures,

etc.) in the material. For example, moduli for materials with itinerant 5f electrons will be much larger than for materials with localized electrons and fewer bonding electrons.

Several compounds under pressure have also been studied using absorption spectrophotometry. In the 8-32 x 10^3 cm^{-1} spectral region, absorption by the trivalent transuranium ions is due mainly to f-f (Laporte forbidden) transitions; and, therefore, their absorption spectra should reflect any perturbation of these 5f levels. Changes in oxidation state or electronic configuration should have major effects, but smaller perturbations can also bring about significant changes in the spectra. For example, the characteristic features of a solid state absorption spectrum can in many cases be correlated with specific properties (interatomic distances, coordination number of the metal ion, crystal field, etc.) of the crystalline matrix of the solid. This sensitivity to environment permits the use of absorption spectrophotometry for monitoring the effects of pressure on the crystal form of many actinide compounds. An important requirement for this technique is that the material being monitored should transmit adequate light during the course of the study.

In this time period we have examined PuI_3, CmI_3, and $CfCl_3$ under pressure. This work extended our earlier pressure studies on AmI_3 and $CfBr_3$. Previously, CmI_3 was known to exist only in a rhombohedral crystal form. Based on the parallel crystal behavior of the lanthanide triiodides as a function of radius, the relative trivalent ionic radii of the lanthanide and actinides, and the large difference in molecular volumes for the polymorphs of other triiodides, it was felt that applying pressure on the rhombohedral form of CmI_3 would at the very least bring about a crystal modification to a more dense orthorhombic form. Our initial efforts to study CmI_3 under pressure by absorption spectrophotometry were complicated by a shift in the absorption edge of the material to longer wavelengths at moderate pressures, which masked its major absorption peaks and prohibited spectrophotometric studies at higher pressures. In Fig. 7.6 is shown the solid state absorption spectrum of CmI_3 both at room pressure and at 10 GPa. Although an excellent spectrum can be obtained at room pressure, the shift of the absorption edge with pressure to 18 x 10^3 cm^{-1} blocks the major absorption peaks of the CmI_3 and precludes the use of absorption spectrophotometry for monitoring the effect of pressure on this compound. As in the case of AmI_3, the shifted absorption edge of CmI_3 persisted after the pressure was released, negating the hope that if a transition had occurred, it might be detected by changes in the absorption spectrum obtained subsequently at normal pressure. Thus, owing both to the nature of the absorption of CmI_3 and the irreversible shift of the absorption edge with pressure, it was evident that absorption spectrophotometry was not a viable method for monitoring this compound as a function of pressure.

A subsequent investigation of CmI_3 under pressure was carried out using X-ray diffraction. This preliminary study by X-ray diffraction has indicated that the rhombohedral form of CmI_3 does indeed convert under a pressure of about 6 GPa to form its orthorhombic polymorph, which is retained after the pressure is released. Due to experimental problems with determining a camera constant for the pressure cell during this study and the limited number of diffraction lines obtained (8), the diffraction data for CmI_3 could only be considered qualitative and hence can be used only to identify the crystal type of the CmI_3. For example, one useful difference in the diffraction patterns is the presence of a strong single line (hkl = 021) for the rhombohedral form as compared to a doublet (hkl = 112, medium intensity and hkl = 113 +

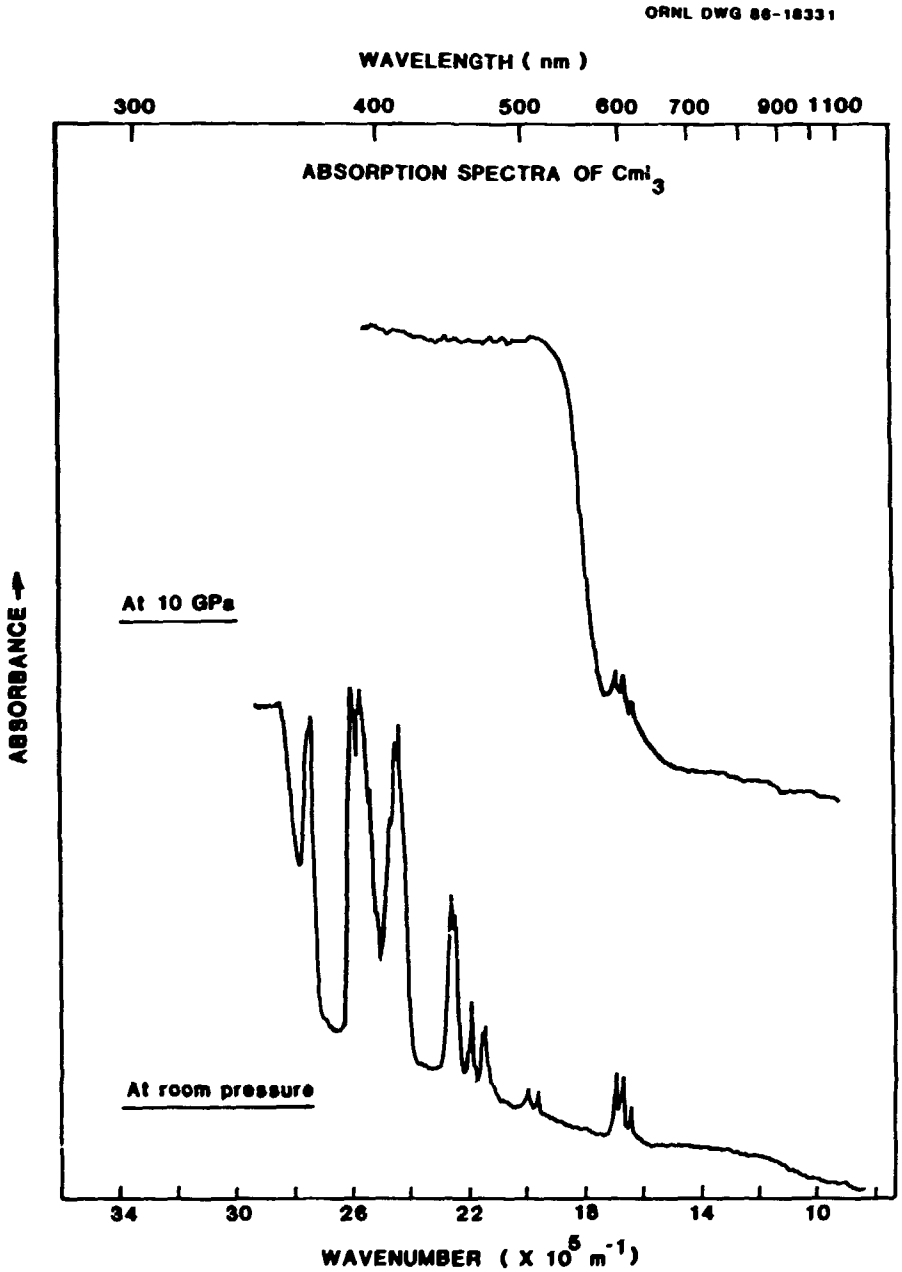

Fig. 7.6. Absorption spectra of CmI_3 at room pressure and 10 GPa showing shift of absorption edge to 18,000 cm^{-1}.

023, strong intensity) for the orthorhombic form.

An orthorhombic form of PuI_3 has been known for several years and recently a rhombohedral form has been shown to exist also. Studies of PuI_3 comparable to those described above for AmI_3 and CmI_3 have also been carried out. From such studies it has been determined that the rhombohedral form of PuI_3 under pressure also converts to an orthorhombic form, which is retained after the release of pressure. Details of these studies will be reported separately but the key results are noted here to point out that absorption

spectrophotometry was used successfully to monitor the structural changes of PuI_3 with pressure. Although the absorption edge of the PuI_3 samples also shifted to longer wavelengths with the application of pressure, a sufficient number of PuI_3 absorption peaks could be evaluated at lower frequencies (longer wavelengths) for structural analysis.

The irreversible shift in absorption edge of actinide triiodide samples (PuI_3, AmI_3, and CmI_3) under pressure is itself of interest, as it implied that some significant change is occurring (for example, electron charge transfer for small portions of the sample). If the shift resulted from a change in charge transfer bands, a decrease in the ligand-metal bond lengths, or from a compression of electron orbitals, then the shift should be reversible. The reduction of the actinide to a lower oxidation should be irreversible. The reduction of the actinide to a lower oxidation state, together with the generation of iodine, could offer one explanation for the irreversibility observed, although we were not able to obtain experimental evidence for release of iodine. In the compounds, LaI_3, GdI_3, and CmI_3, all three metal ions should be very resistant to reduction as compared to many of the other lanthanide and actinide ions. A study of the absorption edge behavior of these compounds under pressure was undertaken to better understand the darkening phenomena in the triiodide samples. It was determined that under pressure a reversible shift occurred with LaI_3, an irreversible shift was observed with CmI_3, and no shift was found with GdI_3. At the present time the reason for these changes in absorption edge under pressure is not understood. Additional studies to understand the phenomena will be carried out using CfI_3, where the reduction of the Cf ion under pressure should be more probable. If Cf^{3+} is reduced, and sufficient amounts of the divalent ion are generated, the presence of the reduced form can be determined spectrophotometrically.

A study of both the UCl_3-type hexagonal and Pu-Br-type orthorhombic forms of $CfCl_3$ samples under pressure using diamond anvil cells has also been carried out. In contrast to the actinide triiodides, the room-temperature molecular volumes of these two forms of $CfCl_3$ are essentially the same, which minimizes the effect of molecular volume on the stabilization under pressure of one form over the other. Thus, it was not possible from volume considerations to predict whether a structural transformation between these two forms would be brought about by applying pressure.

Absorption spectra obtained from orthorhombic $CfCl_3$ in the pressure range of room pressure to 35 GPa are shown in Fig. 7.7. This sample yielded particularly well resolved absorption peaks. It is apparent that individual peaks within a general absorption manifold seem to shift to longer wavelengths (lower energies) with increasing pressure. This is particularly obvious for the two absorption manifolds around 760 and 870 nm; physical compression of this crystal structure is, in a continuous way, altering the structure to make a given f→f transition more probable. The spectrum of orthorhombic $CfCl_3$ at 35 GPa is quite different from that seen for this sample at room pressure, however. Owing to the fact that these spectral changes are reversible with pressure, it seems logical to assume that no major change in crystal structure takes place; instead only a reversible compression of the orthorhombic structure with increasing applied pressure. If one speculates that a new structure is formed at very high pressure and that it transforms back to the orthorhombic form upon release of pressure, then one must also accept that such a phase transformation upon pressure release has a small activation energy, because it would have to occur without the benefit of any added energy to the system. Another possibility is that the spectra (due to f-f transitions) obtained above 30 GPa reflect

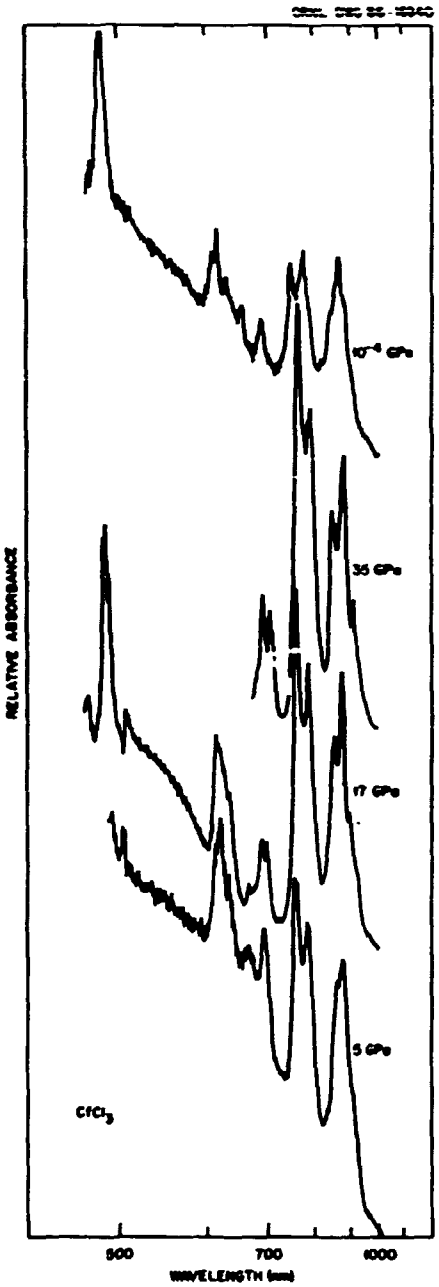

Fig. 7.7. Room temperature absorption spectra of $PuBr_3$-type orthorhombic californium trichloride showing shifts of absorption lines at 5, 17, 35 GPa from 10^{-4} GPa.

some perturbation of the 5f orbitals. Additional studies to even higher pressures, together with X-ray diffraction data for the samples under pressure, will be necessary to understand fully the above behavior of $CfCl_3$ at pressures over 30 GPa.

---

1. Research sponsored in part by the Division of Chemical Sciences, Office of Basic Energy Sciences, U.S. Department of Energy under contract DE-AC05-84OR21400 with Martin Marietta Energy Systems (R. G. Haire) and under contract DE-AS05-76ER04447 with The University of Tennessee, Knoxville (J. R. Peterson and J. P. Young) and in part by the Commission of the European Communities, Joint Research Center, Karlsruhe, FRG (U. Benedict).
2. Chemistry Department, University of Tennessee, Knoxville.
3. Analytical Chemistry Division.
4. European Institute for Transuranium Elements, Karlsruhe, FRG.

7.2 Solution Chemistry

7.2.1 Volumes of Aqua Ions from Measured Radial Distribution Functions

(R. L. Hahn[1])

In a new development in the chemistry of aqueous inorganic solutions, we have been able to use our neutron scattering data for hydrated rare-earth ions to predict and explain results obtained with the classical method of partial molal volumes. This result is important because it brings together in a consistent manner two very different approaches to the study of solutions, one that we call "macroscopic", and the other, "microscopic". To date, most experimental techniques have probed solution properties at the bulk, macroscopic level. For example, the determination of partial molal volumes of ions from solution density measurements are common. Some structural information has been derived from such experiments, but has been heavily dependent upon various assumptions and models. On the other hand, some modern diffraction and spectroscopic techniques have directly probed solution structure at the molecular or microscopic level.

Traditionally, these techniques have not provided information about bulk properties; that is, until now.

In previous work, we and others had demonstrated that the radial distribution function obtained from neutron scattering data for hydrated cations, $M(D_2O)_n^{i+}$, gives a model-free determination of the mean values and spreads of the M-O and M-D distances in the primary hydration shell and of the time-averaged value of the primary hydration number, n. In our most recent work, we have extended our treatment of hydration phenomena by developing a mathematical formalism which uses the measured structural parameters to determine in a straightforward way the effective radius of the hydrated ion, r_{eff} (for those aqua ions that, according to the neutron scattering data, have relatively well-defined spherical hydration shells). These new results are especially significant in light of the fact that other workers, in numerous studies of partial molal volumes, have also attempted to derive values for the radii of hydrated ions. However, these attempts at best have been indirect, having been based upon a variety of assumptions, some of which are clearly questionable. Also, the physical significance of the resulting radii has not been at all obvious (i.e., why should a particular aqua ion have a particular size?).

In contrast to this situation, we have been able to show that our values of r_{eff} for trivalent lanthanide cations can explain the correlations obtained from the partial molal volumes. The same treatment has also been successful for most divalent cations and for small univalent cations when reasonable values of n are assigned. Thus, the structural information obtained with a microscopic technique has been able to explain the results obtained by a bulk technique. The observed agreement strongly supports the idea that formation of the primary hydration shell is the dominant factor in determining the partial molal volume of a cation at infinite dilution.

The combined data also indicate that the molar volume of water in the first hydration shell becomes progressively smaller as the cation charge increases until, for a trivalent cation, it is only about half that of pure water. This large decrease reflects the effects of the structural alignment and loss of mobility of the water molecules induced by electrostatic bonding to the cation. Recognition of this general phenomenon has led us to suggest that published values for hydration numbers of actinide ions obtained from transport measurements are systematically low and should be corrected.

---

1. Present Address:
   Brookhaven National Laboratory,
   Chemistry Department, Upton, L.I.,
   New York.

7.3 Transeinsteinium Chemistry

7.3.1 The Search for Monovalent Mendelevium[1]

(G. F. Payne, O. L. Keller, J. Halperin, W. R. Wilmarth,[2] J. R. Peterson,[3] R. W. Lougheed,[4] E. K. Hulet,[4] R. J. Silva[4])

The experimental search for Md^{1+} was begun this year using a sample of the alpha emitting isotope $^{258}_{101}Md$ ($t_{\frac{1}{2}}$ = 55 d). This sample was prepared and separated by Ken Hulet and Ron Lougheed (Lawrence Livermore National Laboratory) and shipped to ORNL. The bombardment with a ^{13}C beam of the world's only ^{254}Es target (then about 4 micrograms) was carried out at the Lawrence Berkeley Laboratory's 88 inch cyclotron to produce the ^{258}Md as a by-product of another nuclear reaction of interest to the Livermore researchers. The ^{258}Md sample shipped to ORNL contained about 5×10^5 atoms that yielded a count rate of about 5 d/m. (About 20% of this count rate was due to a ^{254}Es contaminant from the target and from the decay of the ^{258}Md.)

The experimental plan for searching for Md^{1+} required considerable background developmental work because the oxidation state of the Md is to be determined by ion exchange chemistry in water-free (aprotic) organic solvents (such as benzonitrile or propylene carbonate). Ion exchange chemistry has never been carried out under these conditions before. All manipulations with the water-free solvents were carried out in an inert atmosphere box flushed continuously with dried argon. The water level in the box was less than 20 ppm during the experiments reported here. We have now reduced it to less than 10 ppm while physically working in the box and less than 1 ppm in a standby mode.

The experimental approach is to reduce the Md(III) in benzonitrile. Triphenyl arsine is being tested as the reductant employing Eu^{3+}/Eu^{2+} as stand-in for Md. If Mikheev and coworkers are right, under these conditions Md should be reduced to the Md^{1+}, whereas if Hulet and coworkers are right, it should be reduced to Md^{2+}. The oxidation state determination is to be made by an ion exchange technique where the log of the distribution ratio (log D) of the tracer ion is plotted vs the log of the concentration of a counterion on the resin and in the solution (such as Na^{+} or Ba^{2+}). In order to carry out these Md experiments, it must be shown that log D for Cs^{+} tracer vs log Na^{+} ion concentration gives a slope of -1 in a solution of benzonitrile containing $NaClO_4$ as the supporting electrolyte. Similarly it must be shown that Sr^{2+} tracer gives a slope of -1 in a solution of benzonitrile containing $Ba(ClO_4)_2$ as the supporting electrolyte. Thus the reduction of Md^{3+} to Md^{+} could then be established by exchanging against Na^{+} as the supporting electrolyte, and the reduction to Md^{2+} could be established by exchanging against Ba^{2+}. (The use of two different solutions with two different counterions is necessary for the oxidation state determination because we have found that in benzonitrile and propylene carbonate a divalent ion almost completely displaces a monovalent ion. So a readily interpretable slope determination cannot be reliably made except by using ions of the same charge for the supporting electrolyte and for the displacing tracer ion.) The ion exchange resins being tested are Amberlyst 15 and Nafion 117. These are both strongly acidic cation exchangers with $-SO_3H$ as the functional group. The Amberlyst resin has a polystryene backbone whereas the Nafion 117 has a perfluorinated hydrocarbon structure. Nafion will operate at higher temperatures than Amberlyst, but Amberlyst reaches equilibrium faster (at room temperature). Amberlyst 15 is a so-called reticulated resin which means it has a rigid framework that does not expand or contract with changes in the solvent as will a gel-type resin. It also has a very large surface area and high porosity. These characteristics make Amberlyst 15 a reasonable choice for applications to ion exchange in organic media. In further development of our techniques, we must reduce Eu^{3+} to Eu^{2+} in benzonitrile using triphenyl arsine and then use Amberlyst 15 ion exchange to determine the oxidation state.

In the one experiment on Md itself that we have attempted to date, we dissolved about 1/2 of the available Md sample as Md(III) in propylene carbonate and reduced it with Zn amalgam. Following the reduction step, the solution was divided into five parts (about 0.5 d/m) for evaluation of the oxidation state. Four of the aliquots were each equilibrated with the Na^{+} form of the Nafion ion exchange resin in which the substrate Na^{+} had been adjusted in the respective four solutions to 0.02, 0.03, 0.04, and 0.05 M. Following an approximate 2 day equilibration of resin and substrate, the liquid phase was separated from the resin and evaluated for

its Md content. The count rate in all 4 of the aliquots was nearly constant at about 0.1 d/m. Cs^+ tracer added as an internal standard gave a slope near -1 as expected. This result suggests that so much of the Md was in the resin that no slope for log D could be discerned at these low count rates. That is, the Md was present as +2 or +3. However, the ^{254}Es contaminant and other possible problems (such as adsorption of the Md on the glass tubes employed) add some ambiguity to these first results.

In addition to the chemical developments, nuclear counting techniques had to be adapted to our problem as well. Due to the very low concentration of Md in these solutions (0.05 - 0.2 d/m), we employed a liquid scintillation counting technique based on developments by Jack McDowell and coworkers here at ORNL. Classical counting techniques using a Si surface-barrier detector provide an approximate 30% alpha counting efficiency. This reduced efficiency together with the very low disintegration rate of these samples might very well have compromised their accurate measurement. The liquid scintillation counting techniques, on the other hand, provide 100% alpha counting efficiency. Pulse shape discrimination techniques were used to distinguish between light pulses due to alpha particles and those due to electrons in order to reduce backgrounds to the required <0.01 d/m.

In conclusion, in these preliminary experiemnts, the Md adsorption on the resin was independent of Na^+ concentrations in the supporting electrolyte (i.e., the slope of log D vs Na^+ concentration was ~0). When Cs tracer was added as an internal standard, a slope near -1 was obtained as expected. Thus the Md does not appear to have been acting as a 1+ ion in this early measurement. Further work is needed to remove ambiguities in the experimental procedures and to establish the exact state of the Md in the solutions.

---

1. Research sponsored by the Division of Chemical Sciences, Office of Basic Energy Sciences, U.S. Department of Energy in part under contract DE-AS05-76ER04447 with the University of Tennessee, Knoxville and in part under contract DE-AC05-84OR21400 with Martin Marietta Energy Systems.

2. Department of Chemistry, University of Tennessee, Knoxville.
3. Department of Chemistry, University of Tennessee, Knoxville, and Transuranium Research Laboratory, ORNL.
4. Lawrence Livermore National Laboratory, Livermore, CA.

8. SEPARATIONS CHEMISTRY

This program employs a multifaceted approach to understanding the contribution of molecular structure and bonding to the selectivity, chemistry, and physical properties of solvent-extraction and related separation systems. With present emphasis on the use of macrocyclic coordinators as extractants or as extraction synergists, promising separation systems are identified by the application of relevant molecular-design criteria and by systematic extraction testing. Selected systems are then studied in detail to elucidate the thermodynamic and structural principles underlying the separation. The techniques used include (1) measurement of extraction behavior as a function of the compositional variables followed by computer-aided data analysis to identify the reactions involved, (2) osmometry to determine association of organic-phase species, (3) calorimetric measurements to determine heats and entropies of reactions, (4) X-ray diffraction of crystalline model compounds, (5) NMR, UV/vis, and FT infrared spectral measurements to probe the bonding and structural aspects of organic-phase complexes, and (6) molecular mechanics calculations to evaluate relative energies of various known and hypothetical species and predict stable configurations. Insights gained through this approach are tested, refined, and exploited through the synthesis of innovative extraction reagents and subsequent development of novel separation systems of possible value to the Nation's energy programs.

8.1 Molecular Design and Synthesis

(R. A. Sachleben,[1] C. F. Baes, Jr., J. H. Burns, W. J. McDowell, B. A. Moyer)

The extraction of a metal cation from an aqueous solution into a non-polar organic solvent requires that the hydration sphere of the metal be replaced by a combination of neutral and anionic organophilic ligands to form an organic-phase-soluble neutral complex. Much of our research concerns the idea that macrocyclic extractants can provide high selectivity by constraining the possible orientations of donor groups to suit only certain metals. Since many useful macrocycles are neutral ligands, we have found that they may be most efficiently employed in synergistic combination with cation-exchange extractants including monofunctional organophilic carboxylic, phosphoric, and sulfonic acids. These ionizable extractants exchange protons for metal equivalents, thus eliminating the requirement that aqueous anions be co-extracted with each extracted metal cation. In addition, we are working toward the incorporation of ionizable groups into the macrocyclic molecule so that all of the coordination and charge-neutralization requirements for the selective extraction of a metal could ideally be embodied in one extractant.

Two monofunctional neo-carboxylic acids have been synthesized for testing in synergistic combination with neutral crown ethers: 2-methyl-2-heptylnonanoic acid (HMHN) and 2-methyl-2-dodecyltetradecanoic acid (HMDT) (see Section 8.3). These two examples are thought to be sufficiently branched and organophilic that they and their metal salts will be highly soluble in nonpolar organic diluents and distribute negligibly to aqueous solutions. The preparations were carried out by the following procedure:

$$R\text{-}Br + Mg \longrightarrow R\text{-}Mg\text{-}Br$$

$$CH_3CO_2C_2H_5 + 2\ R\text{-}Mg\text{-}Br \longrightarrow$$

$$CH_3\text{-}\overset{\overset{R}{|}}{\underset{\underset{R}{|}}{C}}\text{-}OH \xrightarrow[H_2SO_4]{HCO_2H} CH_3\text{-}\overset{\overset{R}{|}}{\underset{\underset{R}{|}}{C}}\text{-}CO_2H$$

A highly organophilic multidentate compound was synthesized for the synergistic extraction of Cu(II) (see Section 8.5).

The ionizable "lariat ether" sym-dibenzo-14-crown-4-oxymethylphenyl phosphinic acid was

prepared as a possible selective coordinator for Li^+ or Na^+. The preparation involved the two reactions:

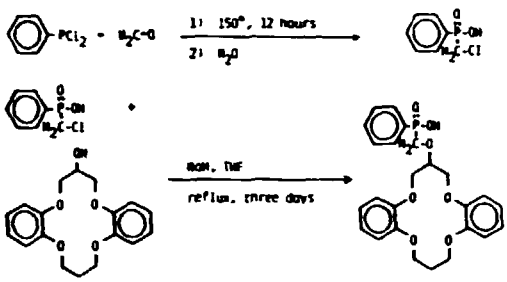

Crystals of the un-ionized lariat ether and its Li^+ and Na^+ salts have been prepared for X-ray crystallographic studies.

8.2 Synergistic Extraction of Mn(II) from Nitric Acid by Combinations of t-butylcyclohexano-15-crown-5 (tBC15C5) and t-butylbenzo-15-crown-5 (tBB15C5) with Didodecylnaphthalene Sulfonic Acid (HDDNS)

(W. J. McDowell, R. B. Chadwick,[2] C. F. Baes, Jr., G. N. Case)

The selectivity of crown ethers in reactions with metal salts has been thought to be largely dependent on the correspondence between the crown ether's cavity diameter and the metal ion diameter. In this work, the two title crown ethers, having similar cavity diameters (1.7 to 2.2 Å) but different substituent groups, have been found to differ markedly in their ability to synergize the extraction of Mn^{2+} (ionic diameter 1.4 to 2.2 Å) from aqueous nitrate solutions by HDDNS (Fig. 8.1). Under these conditions, no observable synergism of manganese occurs with the benzo-substituted crown, but the cyclohexano-substituted crown synergizes manganese strongly, resulting in a selective synergistic extraction system for manganese. Application of the least squares program SXLSQ (Section 8.12) to the extraction data obtained for mixtures of HDDNS and each of the crown ethers indicates the formation of HDDNS/crown ether intermolecular compounds in both cases

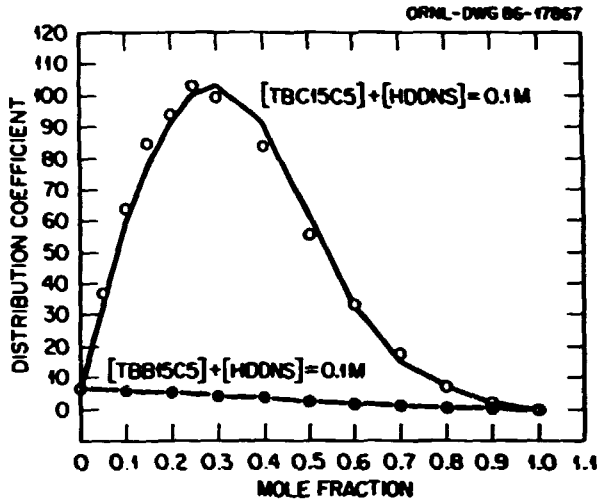

Fig. 8.1. Distribution coefficient for tracer-level managanese(II) from 0.2 M HNO_3 as a function of the ratio [crown ether]/([HDDNS] + [crown ether]) in the organic phase, the total [HDDNS] + [crown ether] being constant at 0.1 M (toluene diluent, room temperature). The curves were fit to the observed data by the program SXLSQ.

and the formation of complexes with manganese containing both HDDNS and crown ether in the case of tBC15C5. Vapor pressure data obtained thus far suggest a degree of aggregation of ca. 10 in these systems but leave a substantial uncertainty that precludes accurate definition of the stoichiometry of the organic phase species.

8.3 Radium Extraction with Dicyclohexano-21-crown-7 (DC21C7) and Neo-carboxylic Acids

(W. J. McDowell, G. N. Case)

Combinations of DC21C7 with certain high molecular weight neo-carboxylic acids in toluene have been found to be strong, selective extractants for radium. Using the proprietary neo acid, Shell Versatic-1519, or the synthesized neo-carboxylic acids, HMHN or HMDT (see Section 8.1), extraction coefficients in excess of 1000 are attainable at low aqueous ionic strength and pH > 10. These systems are selective for radium over most other elements with which it is commonly associated and form the basis for a simple and accurate analysis of radium. When naphthalene

and the scintillant, PBBO, are added to toluene containing one of the neo-carboxylic acids together with DC21C7, radium can be extracted directly into the resulting "extractive scintillator" and counted on a PERALS (Photon-Electron Rejecting Alpha Liquid Scintillation) system. Pre-concentration of radium from large-volume samples is accomplished by coprecipitation with barium sulfate. The sulfates are then converted to carbonates by metathesis with potassium carbonate. The carbonates are dissolved in acid and the solution made basic before extraction into the scintillator. Tracer ^{133}Ba may be used to correct for any chemical loss in the precipitation and conversion-to-carbonate steps although additional refinement of the procedure may make these steps quantitative. The extraction into the scintillator is quantitative, and counting on PERALS is 99.68% efficient. The approximate lower limit of detection for radium, counting only the radium alpha, is 0.01 picocuries.

8.4 Cesium Extraction with Crown Ether, Cation Exchanger Combination

(W. J. McDowell, G. N. Case, R. A. Bartsch[3])

Drawing from systematic studies of the use of crown ethers as extraction synergists completed in the last few years, it was possible to predict the type of crown ether that would strongly and selectively synergize the extraction of cesium by a cation exchanger (organophilic acid). This crown ether was synthesized (Bartsch[3]), and extraction tests have shown the compound to be as good as predicted. A disclosure for possible patent application is being made at this time.

8.5 Selective Extraction of Cu(II) and Ag(I) from Sulfuric Acid by a Synergistic Extraction System

(B. A. Moyer, C. L. Westerfield,[2] W. J. McDowell, G. N. Case, R. A. Sachleben[1])

Selected multidentate compounds have been shown to strongly and specifically synergize the extraction of Cu^{2+} and Ag^{+} from sulfuric acid by an organophilic acid (cation exchanger) in toluene diluent. Over a range of sulfuric-acid concentrations, the selectivity is given by the order $Ag^{+} > Cu^{2+} > Mn^{2+}$, Fe^{2+}, Fe^{3+}, Co^{2+}, Ni^{2+}, and Zn^{2+}, where synergism occurs only for Ag^{+} and Cu^{2+}. For Cu^{2+} extraction, a synergistic factor of 1570 was achieved with distribution coefficients more than 300 times greater than those observed for Fe^{3+} and the other first-row transition metal ions tested. Using tracer techniques, the synergistic extraction of Cu^{2+} and Ag^{+} was explored as a function of sulfuric acid concentration, relative concentration of synergist vs. cation exchanger, and loading. A recently synthesized (Sachleben) multidentate extraction synergist for Cu^{2+} has been shown to have negligible losses to the aqueous phase. A patent disclosure has been submitted to the U.S.D.O.E.

8.6 Spectral Studies and Equilibrium Analysis of the Didodecylnaphthalene Sulfonic Acid, Dicyclohexano-18-crown-6, Sr^{2+} Extraction System

(S. A. Bryan,[1] W. J. McDowell, B. A. Moyer, C. F. Baes, Jr., G. N. Case)

The species and equilibria present in the synergistic strontium extraction system, composed of didodecylnaphthalene sulfonic acid (HDDNS) and dicyclohexano-18-crown-6 (DC18C6) in CCl_4, have been studied by IR and proton NMR spectroscopies, vapor pressure osmometry (VPO), and Karl Fischer (KF) titrations. With the aid of least-squares computer methods to fit the IR and VPO results, a series of proposed equilibria and associated equilibrium constants have been shown to adequately account for all of the observed behavior. The sulfonic acid and the salt of the acid alone in CCl_4 solution form the micellar species $(HDDNS \cdot xH_2O)_{11}$ (x is in the range 7-8) and $(Sr(DDNS)_2 \cdot 11\ H_2O)_6$ respectively. The sulfonic acid alone, under conditions of intermediate loadings with Sr^{2+}, yields the predominant species $(Sr(DDNS)_2)_3(HDDNS)_5 \cdot xH_2O$. When alone in solution, DC18C6 is a monomer, but it forms

adducts with the free sulfonic acid and its strontium salt, yielding the respective product species $(HDDMS)_7 \cdot DC18C6 \cdot xH_2O$ and $Sr(DC18C6)(DDMS)_2 \cdot 2H_2O$. An excess of HDDMS or $Sr(DDMS)_2$ in the presence of $Sr(DC18C6)(DDMS)_2 \cdot 2H_2O$ yields predominantly $Sr(DC18C6)(DDMS)_2(HDDMS)_2 \cdot xH_2O$ and $(Sr(DC18C6)(DDMS)_2)_2(Sr(DDMS)_2)_3 \cdot xH_2O$, respectively.

8.7 Spectral and Equilibrium Studies of the Hydration of Crown Ethers in CCl_4

(S. A. Bryan,[1] B. A. Moyer, R. R. Willis[2])

The interaction of water with 18-crown-6 (18C6), and the cis-syn-cis and cis-anti-cis isomers of dicyclohexano-18-crown-6 (DC18C6-A and DC18C6-B, respectively) have been investigated in detail by FTIR techniques. At the concentrations used in this study ([crown] < 0.1 M and $[H_2O]$ < 0.05 M), the equilibrium behavior at 25.0 °C indicates the formation of 1:1 water-crown adducts with molar equilibrium constants of 19.9, 22.4, and 30.9 (±2.0) M^{-1}, for 18C6, DC18C6-A, and DC18C6-B, respectively. As contrasted with the known 1:1 hydrates of ethers such as diethyl ether and tetrahydrofuran, the 1:1 crown-hydrates appear to exhibit fluxional behavior involving an equilibrium between mono- and bidentate hydrogen-bonded species. For the monohydrate of 18C6, this equilibrium was probed in detail via a temperature-dependence study of the FTIR spectra as shown in Fig. 8.2. It may be seen that lowering the temperature has the effect of both increasing the total concentration of bound water as 18C6 monohydrate and increasing the relative concentration of the bidentate form. The appropriate thermodynamic parameters obtained from a least squares fit of the monodentate-bidentate hydration model to the temperature-dependent data are K_1 = 5.4 M^{-1}, ΔH_1 = -4.5 (±0.3) kcal/mol, ΔS_1 = -11.6 (±1.1) eu and K_2 = 11.1 M^{-1}, ΔH_2 = -10.9 (±0.3) kcal/mol, ΔS_2 = -31.9 (±0.9) eu for the formation of the respective monodentate and bidentate 1:1 water-crown adducts from the free crown ether and water in CCl_4 at 25 °C.

ORNL—DWG 87—9889

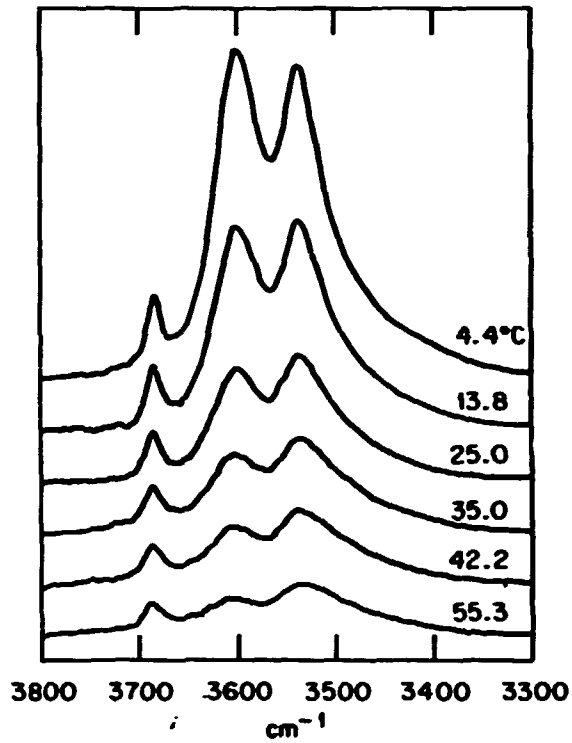

Fig. 8.2. FTIR difference spectra of the water-stretching bands of monodentate and bidentate 1:1 18C6-water adducts in CCl_4 at various temperatures. The two water-stretching bands of free water (3707 and 3618 cm^{-1}) have been subtracted out of each spectrum. Assignments: 3687 cm^{-1} (ν_{as} of monodentate water), 3600 cm^{-1} (ν_{as} of bidentate water), and 3535 cm^{-1} (superimposed ν_s peaks of monodentate and bidentate water). At 25 °C, the total H_2O and 18C6 concentrations were, respectively, 2.8×10^{-3} and 1.5×10^{-2} M (5 cm Infrasil cell).

8.8 Molecular Mechanics Studies of Crown Ether Complexes of Alkaline-Earth Metals

(J. H. Burns)

The selectivity among alkaline-earth ions by a solvent-extraction system of dibutylphosphoric acid and 18-crown-6 ether was the subject of a molecular mechanics study. Molecular structures of complexes of Sr^{2+} and Ba^{2+} with these ligands were determined by X-ray crystallography to be quite similar except for the configuration of the ether molecules. Using these structures as a starting point and employing a common set of

potential energy functions, the total molecular energies were calculated with the computer program WMIN.[4] These energies were then minimized by adjusting the structures, as were those of hypothetical complexes of the same composition but containing each of the other alkaline-earth ions; this made it possible to compare the intrinsic stabilities of the series. The energy-minimized structures are shown in Fig. 8.3.

It was found that the crown-ether ligands may be extensively distorted in order to accommodate them to ions of various sizes but, except for Mg^{2+}, the strain-energy increase is relatively small compared to the energy reduction caused by coulombic forces. That is, the crown configuration is relatively unimportant in ion selectivity. However, while the smaller cations form the intrinsically most stable complexes, the selectivity among these ions in aqueous solution also depends on the energies of hydration. When these are taken into account, the selectivities for this extraction system are estimated to be in the order Ba > Sr > Ca > Ra > Mg. This is in agreement with thermodynamic stabilities of such crown complexes for the first three ions in aqueous solution.[5]

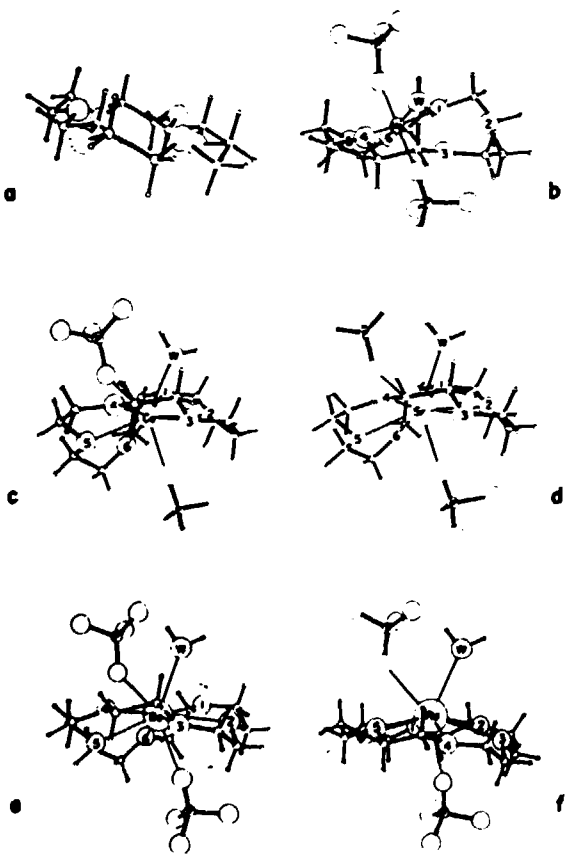

Fig. 8.3. Structures of energy-minimized actual and hypothetical molecules: (a) 18-crown-6 ligand; (b-f) $M(DBP)_2(H_2O)\cdot$18-crown-6, where M = Mg, Ca, Sr, Ba, and Ra, respectively.

8.9 Crystal Structures of $Sr((CH_3)_3C_2O_2)_2\cdot H_2O\cdot$DC-18-crown-6 and $Ba((CH_3)_3C_2O_2)_2\cdot(H_2O)_2\cdot$DC-18-crown-6$\cdot H_2O$

(J. H. Burns, S. A. Bryan[1])

The structures of the title compounds are of interest to our efforts to understand the causes for Sr^{2+} and Ba^{2+} ions being extracted differently (Sr > Ba) by mixtures of dicyclohexano-18-crown-6 (DC-18-crown-6) and long-chain neo-carboxylic acids.[6,7] Trimethylacetic (or pivalic) acid, a truncated version of these neo acids, when combined with DC-18-crown-6 ether (isomer A), forms Sr and Ba complexes which can be crystallized. X-ray diffraction analysis showed their crystal structures and stoichiometries to be quite different.

In the Sr complex, the cation is centered in the crown and has a bidentate pivalate ion attached on each side (Fig. 8.4). These complex molecules are linked in the crystal by hydrogen-bonded water molecules, but there is no water in the inner coordination sphere. The Ba complex, however, has two H_2O molecules directly bonded to the Ba^{2+} ion and only one pivalate ion attached (in a monodentate fashion) as shown in Fig. 8.5. The presence of water in this complex will contribute to its lesser tendency to be extracted into an organic phase than the Sr complex provided, of course, that these molecules are the same as the species in solution.

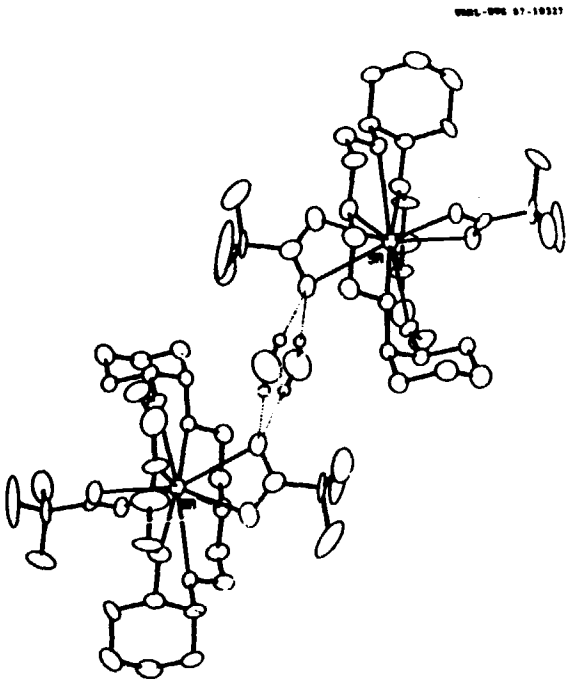

Fig. 8.4. Two molecules of $Sr(pivalate)_2 \cdot DC\text{-}18\text{-}crown\text{-}6 \cdot H_2O$ linked by hydrogen bonded water molecules.

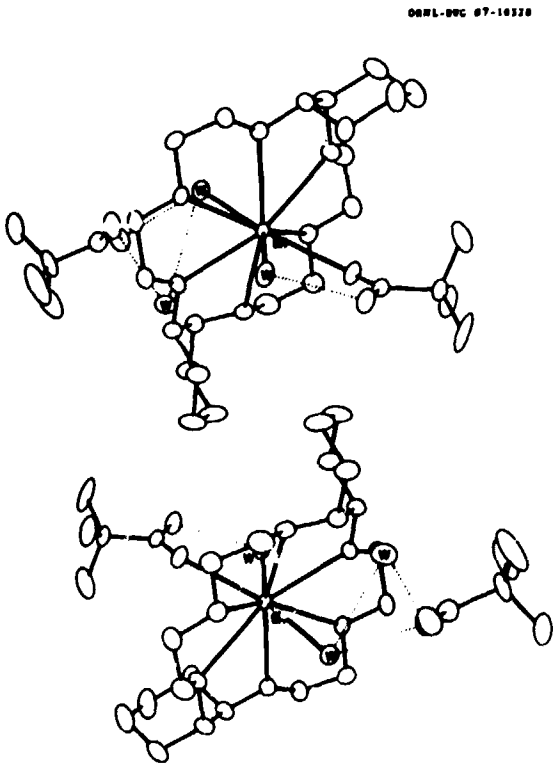

Fig. 8.5. Two molecules of $Ba(pivalate)_2 \cdot DC\text{-}18\text{-}crown\text{-}6 \cdot 3H_2O$. Oxygen atoms of the water molecules are labeled "W", and dotted lines represent hydrogen bonds.

8.10 FTIR Analysis of the Hydration of Di-2-ethylhexyl Sulfoxide (DEHSO) in Dodecane

(B. A. Moyer, C. E. Caley[3])

Our previous measurements have shown that the solubility of water in dodecane increases with increasing concentration of dissolved DEHSO.[8] Computer analysis of the water-solubility data showed that an association between water and DEHSO molecules in certain combinations can quantitatively explain the observed behavior, but it was not possible to unequivocally identify the exact species involved. Confirming proof of water-DEHSO association via hydrogen bonding has now been obtained from Fourier transform infrared (FTIR) experiments, allowing the identification of the two principle hydrated DEHSO species.

When the background FTIR spectrum of water-saturated dodecane is subtracted from the FTIR spectra of water-saturated dodecane solutions containing 0.01 to 0.4 M DEHSO, the resultant difference spectra exhibit absorption bands located in the regions associated with water stretching (3760-3200 cm^{-1}) and bending (1670-1590 cm^{-1}) vibrations. At given frequencies ν in these ranges, the absorbance (A_ν) is proportional to $[DEHSO]^x$, where $1 < x < 2$, and thus, apparent positive deviations from Beer's Law are observed. Since the observed relationship between A_ν and [DEHSO] can be mathematically modeled by the formation of both hydrated monomers and dimers of DEHSO, the experimentally observed difference spectra[8] may be deconvoluted into the two corresponding component spectra (see Fig. 8.6). From the band positions and shapes, it may be deduced that the component spectra correspond primarily to the two species $(DEHSO)(H_2O)$ (solid-line spectrum) and $(DEHSO)_2(H_2O)$ (dashed-line spectrum), where the water is hydrogen-bound respectively through one and then both of its hydrogen atoms. A corresponding shift of the S=O stretch from 1035 to 1028 cm^{-1} on hydration of DEHSO indicates that the oxygen, rather than the sulfur, atom of the sulfoxide molecule

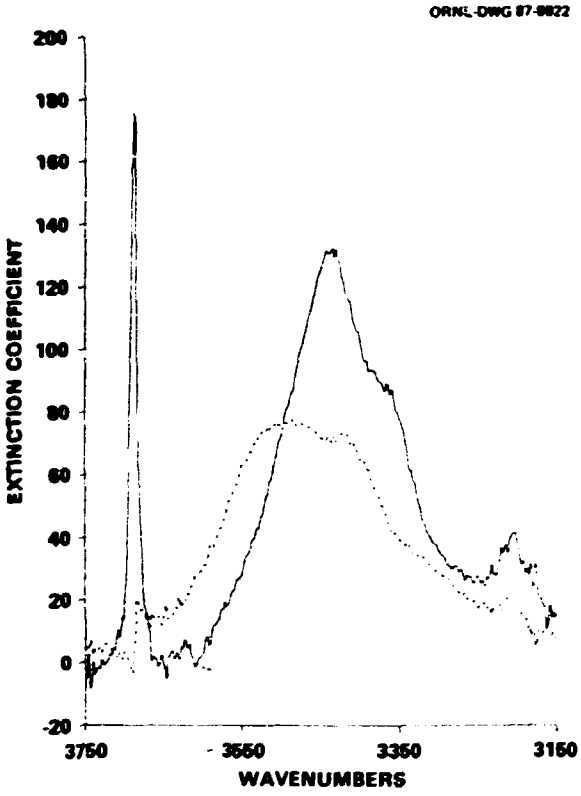

Fig. 8.6. Component FTIR spectra of hydrated monomers (——) and dimers (---) of di-2-ethylhexyl sulfoxide (DEHSO) in wet dodecane at unit water activity (25 °C).

receives the hydrogen bond. Using published spectral correlations, the magnitude of the downward shift of the stretching frequencies of the bound water in $(DEHSO)(H_2O)$ and $(DEHSO)_2(H_2O)$ compared to free, monomeric water implies (a) $R_2SO\cdots O$ bond lengths of 2.89 ± 0.03 A, (b) a slight (0.01 to 0.02 A) lengthening of the O-H bond of free water on bonding with DEHSO, and (c) an enthalpy of -18 ± 2 kJ/mol for the organic-phase reaction $DEHSO + H_2O \longrightarrow (DEHSO)(H_2O)$.

8.11 Extraction of Al(III) by Dibenzoylmethane (C. F. Baes, Jr.)

The potential of solvent extraction as a tool for characterizing metal-cation hydrolysis behavior is being examined through the analysis of the pH-dependence of the distribution of Al(III) between aqueous solutions and toluene solutions containing dibenzoylmethane (HX). In a series of equilibrations at 25 °C, the distribution of Al(III) from toluene solutions containing 0.001 M AlX_3 and 0.022 M HX to aqueous 0.1 M NaCl solutions buffered with chromate/bichromate in the pH range 4.8 to 6.8 was found to be consistent with the formation of the hydrolysis products $Al(OH)^{2+}$, $Al(OH)_2^+$, and $Al(OH)_4^-$, but not the neutral species $Al(OH)_3$. Equilibrium was apparently attained at pH values above 5 after two weeks of vigorous shaking. All of the resulting aqueous solutions were highly supersaturated with respect to $Al(OH)_3$ (Gibbsite), but there was only slight precipitation of amorphous $Al(OH)_3$ in some samples. Longer equilibration produced further precipitation, and after some six weeks, lowered the concentration of AlX_3 in the organic solutions uniformly by about 20%, suggesting that the following metastable, pH-independent equilibrium involving an active form of $Al(OH)_3$ had been reached:

$$Al(OH)_3\ (act) + 3\ HX\ (org) \rightleftharpoons AlX_3\ (org) + 3\ H_2O$$

$$K = [AlX_3]_{org}/[HX]^3_{org} \sim 80$$

If so, then precipitation may be avoided in future measurements by lowering somewhat the initial Al(III) content of the organic phase.

The study of Al(III) hydrolysis by this means has been made possible by the ion chromatograph, which under favorable conditions can yield usefully accurate analyses down to 10^{-8} M Al(III). The chromate buffer used, however, has interfered with these analyses, and another buffer may be needed for the pH range from 5 to 7. We will explore the use of carbonate buffers here. At higher pH values (7 to 9) we plan to use the Tris buffer.

The progress made in deducing the aqueous hydrolysis behavior of Al(III) from the pH dependence of its distribution to an organic phase containing dibenzoylmethane (DBM) suggests that DBM extraction may offer a much-needed tool to study the formation of mononuclear hydrolysis products of selected metal

ions at low concentrations in aqueous solution. The principal advantage is that the chemistry of the organic phase involved appears to be relatively simple and may readily be adjusted to produce equilibrium aqueous metal ion concentrations high enough to be accurately measurable but low enough to avoid hydrolytic precipitation. The principal difficulties are that non-complexing aqueous buffers are needed to control the pH, and vigorous mixing of the phases is necessary, at least for some cations, to reach equilibrium in a reasonable length of time.

8.12 Computer Modeling of Solvent Extraction Data

(C. F. Baes, Jr., W. J. McDowell, S. A. Bryan[1])

The following is an abstract of an article[9] that describes the computer program SXLSQ, currently in use to interpret various kinds of data collected in selected synergistic solvent extraction systems:

> The quantitative description of synergistic solvent extraction systems is usually a difficult problem in equilibrium analysis because a relatively large number of species can be involved. Both sophisticated methods of interpretation and extensive experimental data are required. The graphical methods of "slope analysis" and "continuous variation" provide useful guidance only when a limited number of species is present and especially when there are no competing reactions between the two synergistic extractants. A general least squares computer program (SXLSQ) is described to deal with the general case in which many possible species must be considered. It will accept six different kinds of equilibrium data for an organic solution (metal extraction, acid extraction, vapor pressure, water content, heats of mixing, and spectral absorbance) for a given system in a single data set and can be used interactively at a terminal. Analysis of data on the extraction of Mn(II) by an organophilic sulfonic acid in combination with each of two crown ethers showed that a unique identification of the species formed cannot be made without additional information about the degree of association of the sulfonic acid in the organic diluent. But narrow limits could be placed on ratios of the integers defining the principal species formed.

8.13 Improved Apparatus for Isothermal Titration Calorimetry

(S. A. Bryan,[1] R. P. Effler, Jr.[10])

The use of an isothermal titration calorimeter for the determination of thermodynamic constants (i.e., reaction equilibrium constants, K, and changes in enthalpy, ΔH, and entropy, ΔS) is hampered and often made impossible because state-of-the-art calorimetry equipment has not been able to rigorously maintain thermal equilibrium during the initial stages of the titration (see Fig. 8.7, dashed line). With the modification of an existing isothermal titration calorimeter, isothermal conditions are maintained throughout the addition of titrant to the reaction vessel (Fig. 8.7, solid line). An invention disclosure has been submitted to the U.S.D.O.E.

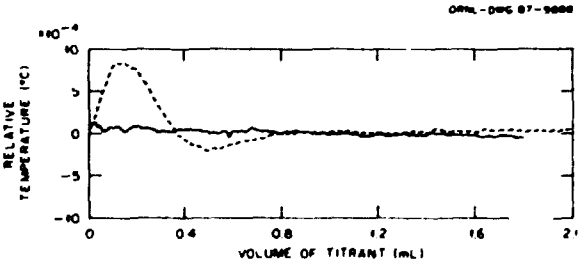

Fig. 8.7. Temperature variance observed in the reaction vessel during isothermal titration calorimetry using the improved calorimeter design (solid line) compared to the prior state-of-the-art calorimeter (dashed curve).

8.14 Dual Mechanism Bifunctional Polymers: Design, Synthesis, and Application of a New Category of Metal Ion Complexing Agents

(S. D. Alexandratos,[11] W. J. McDowell, D. R. Quillen,[11] P. T. Kaiser,[11] A. J. Walder[11])

A series of novel polymer-supported phosphinic acid extractants have been synthesized, and their extraction ability for different actinides and transition metals has been

studied. The bifunctional phosphinic acid resins, simultaneously containing both 1° and 2° phosphinic acid groups, are found to display marked metal ion selectivity in the order Fe(III) > Hg(II) > Ag(I) > Mn(II) > Co(II) > Zn(II). The distribution coefficients vary over three orders of magnitude to a high of 3000 for Fe. The commercially available sulfonic acid resin displays little selectivity; distribution coefficients for the above ions fall within the range 2-10. Two monofunctional resins have been found to display unique properties; these include a phosphonate monoester resin, which is highly reactive towards Fe, Ag, and Hg, and a phosphonate diester resin, which displays a marked affinity for Ag over Hg and Fe.

The extraction kinetics involving the bifunctional phosphinic acid resins have been studied. The introduction of macroporosity into the polymer support leads to zinc ion exchange kinetics comparable to that found with a sulfonic resin (5 min for 90% of maximum loading). The Hg redox reaction is found to require 2h for completion while that for Ag requires 9h. The faster rate for Hg is probably due to its 1:1 stoichiometry with the P-H bonds in the redox reaction while Ag, having a 2:1 stoichiometry, leads to lower redox reaction rates due to the need for termolecular organization.

Carboxylic acid ion exchange resins incorporating penta(ethylene glycol) units within the polymer support have been synthesized. It is anticipated that the glycol units will coordinate with the alkali metal ions allowing for the recovery of, for example, radioactive cesium, while the acid moieties should make the results independent of the solution anion. Limited studies to date suggest a selectivity for Cs over Na.

---

1. Post-doctoral Research Fellow with the Oak Ridge Associated Universities.
2. Undergraduate research participant in the Oak Ridge Science Semester Program.
3. Department of Chemistry, Texas Tech University, Lubbock, TX 79409.
4. W. R. Busing, WMIN, A Computer Program to Model Molecules and Crystals in Terms of Potential Energy Functions, Report ORNL-5747 (1981).
5. R. M. Izatt, R. E. Terry, B. L. Haymore, L. D. Hansen, N. K. Dalley, A. G. Avondet, and J. J. Christiansen, J. Am. Chem. Soc. 98, 7620 (1976).
6. W. J. McDowell, G. N. Case, and D. W. Aldrup, Sep. Sci. Technol. 18, 1483 (1983).
7. B. A. Moyer, W. J. McDowell, R. J. Ontko, S. A. Bryan, and G. N. Case, Solv. Extr. Ion Exch. 4, 83 (1986).
8. B. A. Moyer, C. E. Caley, W. J. McDowell, C. F. Baes, Jr., and G. N. Case, in Chemistry Division Annual Progress Report for Period Ending January 31, 1986, ORNL-6261 (May 1986), pp. 134-135.
9. C. F. Baes, Jr., W. J. McDowell, and S. A. Bryan, Solv. Extr. Ion Exch. 5, 1 (1987).
10. Instrumentation and Controls Division.
11. Department of Chemistry, University of Tennessee, Knoxville, TN 37996.

9. REACTIONS AND CATALYSIS IN MOLTEN SALTS

This research is directed at mechanistic aspe ts of molten salt catalysis and at the stabilization and characterization of reactive organic intermediates in these unusual media. Current research is centered on Friedel-Crafts catalysis in liquid chloroaluminates with high $AlCl_3$ activity and, in particular, on the respective roles of Brönsted and Lewis acidity in ionic liquids in which $Al_2Cl_7^-$ is the predominant anion. The Brönsted acidity of molecular HCl in such melts is being investigated by spectrometrically measuring the degree to which it protonates arenes to form arenium ions. Although these arenium ions are highly reactive in most media, they are for the most part quite stable in these $Al_2Cl_7^-$-rich liquids. Our investigations of reactive intermediates in molten salts make use of computer-controlled rapid spectrophotometry to follow the formation and decay of these species. During the reporting period we substantially upgraded the computer hardware and wrote a user-friendly program for measuring a series of spectra with trigger outputs to synchronize the measurements with external events such as the operation of a potentiostat-galvanostat for spectroelectrochemistry.

9.1 Protonation of Arenes in $AlCl_3$-1-Ethyl-3-Methyl-1H-Imidazolium Chloride at Ambient Temperature

(G. P. Smith, A. S. Dworkin, S. P. Zingg, R. M. Pagni)

Acidic chloroaluminates are the quintessential Friedel-Crafts (FC) catalysts that have long been used on both a laboratory and an industrial scale to carry out alkylations, acylations, transalkylations, molecular rearrangements, Scholl condensations, and related reactions. Many of the reactions that they activate are of the carbenium ion chain type. In the case of arene (ArH) substrates a key step is the partial protonation of ArH by a protic acid (HB) as shown in Eq. 1, where B^- is a generic base and ArH_2^+ is the protonated arene or arenium ion. The apparent role of the acidic chloroaluminate is the enhancement

$$ArH + HB \rightleftharpoons ArH_2^+ + B^- \qquad (1)$$

of the protonating strength of HB through the reaction of acidic chloroaluminate species, such as Al_2Cl_6, $Al_2Cl_7^-$ or $Al_3Cl_{10}^-$, with the base B^-. The simplest example of HB is HCl for which the overall protonating reaction is given in Eq. 2, where $Al_2Cl_7^-$ represents the

$$ArH + HCl + Al_2Cl_7^- \rightleftharpoons ArH_2^+ + 2AlCl_4^- \qquad (2)$$

acidic chloroaluminate.

In order to place this chemistry on a more quantitative footing we are investigating the protonation of a series of arenes by HCl in acidic mixtures of $AlCl_3$ and 1-ethyl-3-methyl-1H-imidazolium chloride (EMICl). Mixtures of $AlCl_3$ and EMICl are liquid at 25°C or less over a range of $AlCl_3$ compositions from 35 to 67 m/o. The advantage of ambient temperature chloroaluminates as opposed to the higher melting $AlCl_3$-alkali metal chloride mixtures is that they make possible the investigation of reactive species such as protonated arenes under conditions of low thermal activation. The arenes chosen for this investigation have known basicity constants (K_B) in other strong acid media, such as liquid HF, and encompass a wide range of K_B values. Thus far we have investigated nine arenes of which naphthacene is the strongest base in HF at 0°C with a log K_B of +5.8 while biphenyl is the weakest with a log K_B of -5.5. The degree to which any given arene is protonated is determined by spectroscopically measuring the concentrations of the protonated (ArH_2^+) and unprotonated (ArH)

forms in a melt containing 55 m/o or more $AlCl_3$.

The protonation of an arene by HCl in acidic $AlCl_3$-EMICl is described by Eq. 2. The equilibrium constant for this reaction (K) is given by Eq. 3 to within an approximation

$$K = \Gamma \frac{[ArH_2^+][AlCl_4^-]^2}{[ArH][Al_2Cl_7^-]P_{HCl}} \quad (3)$$

commensurate with the accuracy of our measurements, where Γ is the activity coefficient quotient, P_{HCl} is the partial pressure in atm of HCl in equilibrium with the melt and square brackets denote molar concentrations. Rearranging Eq. 3 yields Eq. 4. For melts

$$\frac{[ArH_2^+]}{[ArH]} = \left\{\frac{K\,[Al_2Cl_7^-]}{\Gamma\,[AlCl_4^-]^2}\right\} P_{HCl} \quad (4)$$

containing on the order of 55 to 60 m/o $AlCl_3$, it can be shown that the quantity in curly brackets is virtually constant at constant temperature so long as the formal concentration of arene ([ArH] + [ArH_2^+]) is small, which it is in our experiments. Thus, we anticipate that the ArH_2^+/ArH ratio will be proportional to P_{HCl}. For reasons of experimental simplicity, our initial experiments employed a very low partial pressure of HCl.

The arenes used in this investigation are listed in Table 9.1 together with their abbreviations, their basicity constants (K_B) in liquid HF, and their observed behavior in HCl-$AlCl_3$-EMICl. The greater the value of K_B the more basic the arene in liquid HF. All of the arenes listed in Table 9.1 were found to form stable solutions in acidic $AlCl_3$-EMICl melts in the absence of HCl. The spectra showed no sign of radical cation formation under conditions in which these would have been detected at the 10^{-4} M level had they been present. Furthermore, only very small amounts ($<10^{-3}$ M) of arenium ions, attributable to traces of protic impurities, were observed. Purified HCl was added at a

Table 9.1. Protonation of arenes in HCl-$AlCl_3$-EMICl with low HCl partial pressures and 55 or 67 m/o $AlCl_3$ at ambient temperatures

Arene name, abbreviation	Log K_B in HF(ℓ)	Observed behavior
Naphthacene, Nac	+5.8	Complete protonation.
Perylene, Per	+4.4	Complete protonation. Isomerization of ArH_2^+.
Anthracene, Ant	+3.8	Complete protonation. Stable ArH_2^+.
Pyrene, Pyr	+2.1	Complete protonation. Stable ArH_2^+.
Hexamethylbenzene, HMB	+1.4	Complete protonation. Stable ArH_2^+.
Pentamethylbenzene, PMB	+0.1	Complete protonation. Stable ArH_2^+.
2-Methylnaphthalene, MN	-1.4	Partial protonation. Stable ArH_2^+.
Chrysene, Chr	-1.7	Partial protonation. Stable ArH_2^+.
Naphthalene, Nap	-4.0	Partial reaction. Products unidentified.
Biphenyl, Bip	-5.5	Slight reaction. Products unidentified.

pressure of 1 atm and then pumped off leaving only a small amount in solution. As shown in Table 9.1, the six most basic arenes, Nac, Per, Ant, Pyr, HMB and PMB, were virtually completely protonated leaving no detectable trace of unprotonated arene. The protonation reactions that we are studying are, for the most part, expected to be very fast and in our experiments they appear to be limited by the rate of mixing. Once mixing is completed the resulting spectra show little or no change with time. However, in one case, perylene, the arenium ion spectrum that is initially formed very quickly, undergoes a very slow subsequent change that is reasonably attributed to a change in the ratio of perylenium isomers. Presumably, the mix of isomers formed initially is not an equilibrium mixture so that initial protonation is followed by slow isomerization reactions. The spectra of the arenium ions of the other five completely protonated arenes did not change over extended time periods, indicative of a high stability in this medium. The next two arenes, MN and Chr, underwent a partial reaction to form stable products whose spectra are probably those of the corresponding arenium ions. A more positive identification will require forcing the protonation reaction to go further at higher HCl pressures so as to yield more intense spectra. Nap underwent a partial reaction that progressed slowly to yield unidentified products. We interpret this behavior as a proton catalyzed reaction initiated by a very slight protonation of Nap. Finally, Bip, the least basic arene, showed a small amount of an unidentified stable product, possibly the protonated form of some impurity. The degree to which these arenes were protonated at low pressures of HCl in acidic $AlCl_3$-EMICl melts is not very different from the degree to which they are protonated in neat, liquid HF.

Most of the arenes that we have studied thus far are well-behaved in the sense that both the protonated and unprotonated forms are stable in acidic $AlCl_3$-EMICl mixtures at 25°, and both forms have high-quality absorption spectra that are suitable for measuring their respective concentrations. In general these UV-visible spectra are quite similar to those observed when using other media as solvents. As an example the spectrum of molecular PMB in 55-45 m/o $AlCl_3$-EMICl is shown in Figure 9.1 along with the spectrum of the pentamethylbenzenium ion formed after equilibration with HCl. The molar absorptivities of the bands used to measure concentrations are large and those for the arenium ions are usually very large so that our investigations are carried out with low substrate concentrations, on the order of 5-15 mM, and in most cases with very short optical path lengths, on the order of 100 μm or less.

The liquid mixtures used in these investigations are prepared from carefully purified materials and contain exceptionally low levels of protic and oxidizing impurities. Material transfers are carried out in Ar-atmosphere glove boxes with monitored O_2 and H_2O contents of less than 1 ppm. Highly-purified HCl at a

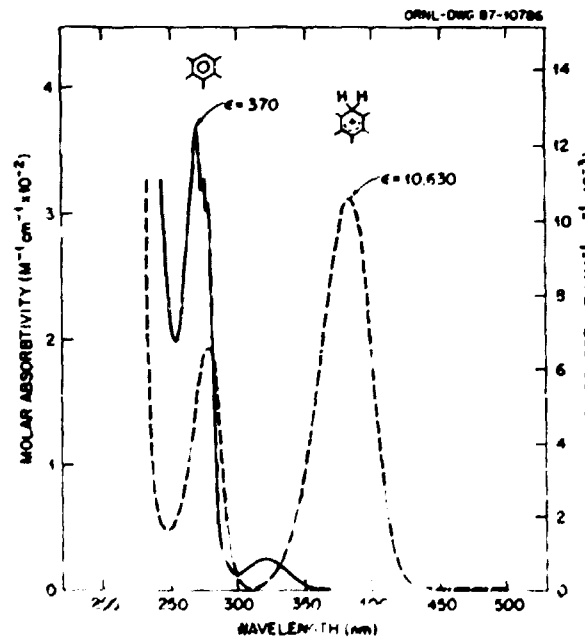

Fig. 9.1. The spectra of pentamethylbenzene and the pentamethylbenzenium ion in 55-45 m/o $AlCl_3$-EMICl at ambient temperatures.

known pressure is equilibrated with a melt contained in a gas-tight optical cell. The UV-visible spectra of easily oxidized and easily protonated arenes provide a final test of the cleanliness of the melts with respect to protic and oxidizing impurities because both the radical cations formed by oxidation and the arenium ions formed by protonation have intense visible absorption bands.

We plan to develop equipment with which we can manipulate liquid chloroaluminates under a known HCl pressure of 1 atm. This HCl pressure is much higher than that used in initial experiments and should increase the protonating power by several orders of magnitude (see Eq. 4). It will also give us a much better precision and control of the measurements. We will also carry out these measurements at HCl pressures between 0 and 1 atm which will allow us to estimate the value of K/Γ in Eq. 4. In addition we plan to add arenes to the list of those under investigation that will allow us to bracket the protonating strength more accurately.

9.2 Instrumentation for Rapid Spectrophotometry

(G. P. Smith, J. E. Coffield[1])

Reactive intermediates such as radical cations, dications and arenium ions play important roles in reactions catalyzed by molten salts. Such species commonly have intense absorption spectra so that spectrophotometry is an especially effective tool for measuring the rates at which these species are formed and decay in molten salts. Our studies of such processes have made substantial use of a computer-controlled rapid spectrometer that we designed and constructed to meet our particular needs. The heart of this instrument is its light detection system, which uses multi-element solid state detectors. For most purposes we use a linear diode array detector (Reticon) with 1024 pixels (light-measuring elements) and on occasion we use a two-dimensional detector, a 512 × 512-pixel Viticon. In a typical application we measure a series of spectra taken at intervals of 5-100s with exposure times of 50-300 ms, although, when necessary, the spectrometer can measure a large number of spectra much faster than this.

The operation of the multi-element detectors is under the control of a small computer, the detector controller, which also sends and receives signals to synchronize the measurements with the operation of other instruments. The detector controller is programmed by another small computer, the system processor, which also analyzes the data, plots or prints the results, and performs a variety of control functions. These detectors and their associated computers constitute an optical multichannel analyzer (OMA).

During the reporting period we installed state-of-the-art components that greatly enhance the capabilities of the OMA, namely, an EG&G PAR Model 1461/1463 detector controller and a Model 1460 system processor. Together, these units have three 68000 microprocessors and the system controller is capable of addressing 14M bytes of RAM, although at present we have installed only about 700K bytes. A variety of types of ports provide communication with other instruments, computers and output devices.

In order to make this equipment available to novice users we have written the first of what will be a series of user-friendly programs to carry out and analyze the results of experiments. The first program is designed for spectroelectrochemical experiments of a type frequently performed by our group. In the near future we expect to interface both the OMA and a potentiostat-galvanostat to an IBM PC so that both the spectroscopic and electrochemical instrumentation can be programmed and operated in a concerted, user-friendly manner.

---

1. Department of Chemistry, University of Tennessee, Knoxville, Tennessee.

10. SURFACE SCIENCE RELATED TO HETEROGENEOUS CATALYSIS

The purpose of this project is to study the fundamentals of surface reactivity by examining atomic and molecular interactions at well characterized solid surfaces. The goal is to obtain an increased understanding of the mechanisms by which reactions occur at surfaces which are models for industrially important heterogeneous catalysts. Two complementary tasks are defined, each focusing on different particular aspects of surface reactivity. One task is concerned with determining the structure of solid surfaces and the bonding geometry of adsorbate species. The approach is based on development and application of low energy alkali and inert gas ion scattering in combination with electron spectroscopic techniques to characterize and probe the structure of various adsorbate/-metal systems. The second task is to correlate catalytic reaction parameters with surface composition and structure as determined by various electron spectroscopies. Particular attention will be focused on model hydrodesulfurization catalysts, including bulk sulfides, sulfided metals (especially nickel and molybdenum) and supported metal complexes.

10.1 The Structure of Carburized W(001) Surface

(D. R. Mullins[1] and S. H. Overbury)

The carburized surface of W(001) has been of interest because of the moderating effect of the carbon on the catalytic properties of the W surface.[2,3] However, the structure of this surface has remained in doubt. A sequence of LEED patterns are observed with increasing carbon coverage including a c(2x2) near 0.5 ML and a p(5x1) which occurs for saturation coverage at high temperature.[4,5] It was initially proposed that the (5x1) LEED pattern arises from a hexagonal overlayer of W_2C(0001) commensurate with the W(001) substrate.[4] Variations on this model have been proposed and controversy has arisen over whether the carbon atoms are above or below the surface.[5,6]

We have studied the dissociative adsorption of ethylene on the W(001) surface using AES, LEED and alkali ion scattering. Literature LEED/AES results were reproduced. The structure of various coverages has been analyzed by ion scattering and the results for the (5x1) are not consistent with any previously proposed models. Contour maps of the Li^+ on W single scattering intensity as a function of polar and azimuthal incidence angle have been obtained for the clean and carbon covered surfaces, and an example is shown for the (5x1) surface in Fig. 10.1. From analysis of these maps and comparison

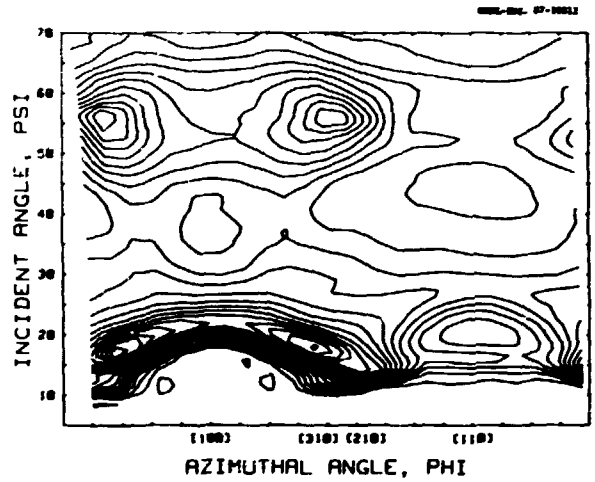

Fig. 10.1. An intensity of the Li^+ single scattering is shown as a function of polar and azimuthal incident angles for W(001) with 0.8 ML of carbon which exhibits a (5x1) LEED pattern.

with the corresponding maps for the clean and lower coverage surfaces, it is clear that the (5x1) surface is not hexagonal, and no major reconstruction of the C covered surfaces occurs. The prominent C single scattering peak observed at grazing incident angles and at all azimuths indicates that the carbon is present as an overlayer, above the plane of the first W layer. The contour maps and K^+ multiple scattering features show that the C atoms reside in four-fold hollows at all coverages. Analysis of the polar angle

associated with shadowing of W by C leads to the conclusion that the C atoms are 0.5 Å above the plane of the first layer W. The LEED (5x1) pattern is attributed to a (5x1) ordering in the C layer, which also possibly induces a periodic strain in the first layer W.

---

1. ORAU Postdoctoral Fellow.

2. E. I. Ko and R. J. Madix, J. Catal. 73 (1982) 161.
3. R. B. Levy and M. Boudart, Science 181 (1973) 547.
4. D. F. Ollis and M. Boudart, Surf. Sci. 23 (1970) 320.
5. J. B. Benziger, E. I. Ko and R. J. Madix, J. Catal. 54 (1978) 414.
6. K. J. Rawlings, S. D. Foulias and B. J. Hopkins, J. Phys. C 14 (1982) 5411.

10.2 Evidence for Sub-Surface Carbon on Mo(111)[1]

(S. H. Overbury)

The structure of carburized Mo(001) and Mo(111) surfaces have also been examined using some of the techniques described in the previous section. There are many similarities in the adsorption behavior and reactivity of Mo and W surfaces, and in the way they are affected by the presence of surface modifiers such as carbon. Both W and Mo adsorb and dissociate ethylene readily at room temperature. The resulting carburized surface show many structural similarities between corresponding faces. For example, the Mo(001) surface gives the same LEED patterns as W(001) at low carbon coverages, although the (5x1) pattern observed for W(001) at high coverages has not been observed on Mo(001). Ion scattering measurements on Mo(001) have indicated that, similar to W, the carburized surface is characterized by a carbon overlayer with adatoms located at four-fold sites of the largely unreconstructed surface.

Quite different behavior has been found on the Mo(111) surface. Ethylene was adsorbed at temperatures between 330 and 360 K and was found to saturate after about 3 L exposure according to uptake measurements made using Auger electron spectroscopy (AES). Li^+ ion scattering at grazing incidence from the saturated surface clearly shows a peak associated with surface carbon near the kinematical single scattering energy E/E_i = 0.43, as shown in Fig. 10.2. Annealing briefly to temperatures of 650 K or higher results in the irreversible disappearance of the carbon single scattering peak. The carbon Auger peak intensity, however, is not decreased by this thermal treatment, but its shape changes to that associated with a carbidic surface. These facts suggest that

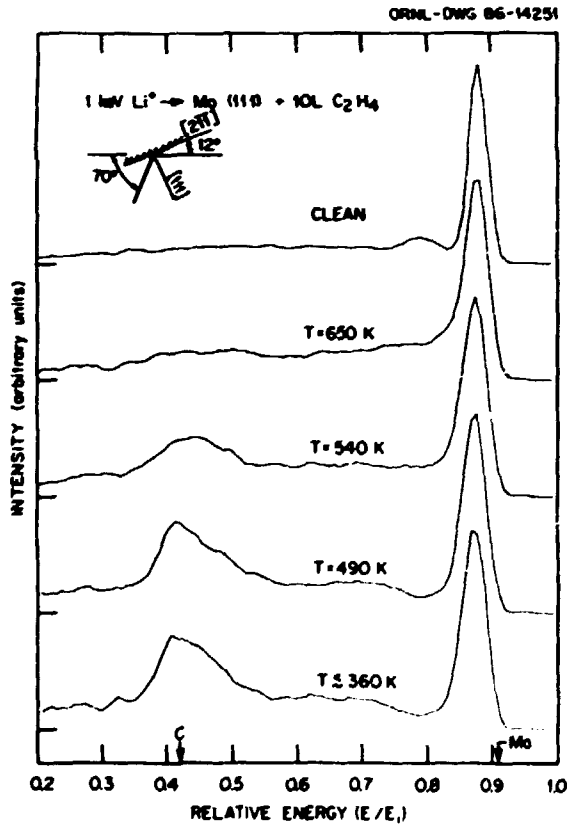

Fig. 10.2. The Li^+ ion scattering spectrum from the Mo(111) surface when clean and following saturation exposure of C_2H_4 with a 60 s anneal to the indicated temperatures.

annealing has converted the surface carbon to another state localized near but below the first layer of Mo atoms. This is in sharp contrast to the high temperature (5x1) state observed on heavily carburized W(001). Further evidence for the transition between surface and sub-surface states was provided by changes in the LEED pattern and in the shape of the incident angle dependence of the Li^+ ion scattering.

Possible chemical differences between the Mo(111) surface saturated with sub-surface vs surface carbon were probed by oxygen adsorption. Oxygen uptake was measured by AES as a function of exposure for the clean Mo(111) and for both carbon covered surfaces. It was found that the carbon reduced the oxygen sticking coefficient, but the ultimate oxygen uptake (after 20 L) is still nearly as large for either carbon covered surface as for the clean surface. Evidently neither surface nor sub-surface C substantially blocks oxygen uptake. However, during room temperature oxygen exposure the surface carbon is converted to the carbidic form associated with the sub-surface carbon as determined both by the changes in the AES C peak shape and the disappearance of the C single scattering peak in the Li^+ scattering spectrum. Annealing the co-adsorbed surface leads to rapid removal of both oxygen and carbon above 900 K due to reaction of sub-surface carbon with surface oxygen followed by desorption of CO.

---

1. Summary of paper to appear in Surface Science.

10.3 Adsorption and Reaction of Methanethiol on Ni(110)

(D. R. Huntley)

Despite the industrial importance of desulfurization catalysis, the mechanisms of the reactions are not well understood. The interactions of simple organosulfur molecules with clean and sulfided Ni(110) are being studied as models for the complex industrial hydrodesulfurization reactions. Of particular interest are factors which may affect the energy or kinetics of C-S bond scission leading to desulfurization of simple thiols. For example, it may be expected that the presence of submonolayer quantities of atomic S may passivate the surface toward desulfurization of co-adsorbed thiols through inductive effects. Alternatively, the presence of atomic sulfur may simply block adsorption sites, but not affect the desulfurization mechanism of those molecules which are adsorbed.

The approach taken in these studies is to characterize the adsorption and desulfurization pathways for methanethiol on clean and sulfided Ni(110). These experiments are done under ultra-high vacuum conditions utilizing surface sensitive techniques which include temperature programmed desorption (TPD), Auger electron spectroscopy (AES) and high resolution electron energy loss spectroscopy (HREELS). Methanethiol adsorptions are done at various temperatures above $\sim$250 K through a directed doser.

The uptake of methanethiol was measured by AES. The ratio of the intensities of the S to Ni Auger peaks was used as a measure of the S coverage. S/Ni Auger ratios (and the S peak intensity) increased linearly with exposure until the surface became nearly saturated. Coverages were estimated by assuming that the saturation coverage of S corresponds to 0.5 ML. The C/Ni ratio (and the C peak intensity) increased with exposure up to about 25% of S saturation. Above that, the C/Ni ratio appears to saturate even though the S coverage continues to increase.

The gaseous products observed in TPD from methanthiol adsorption on clean Ni(110) are methane, dihydrogen and molecular methanethiol which is desorbed at high coverages. No hydrogen sulfide or hydrocarbons other than methane were observed. The temperature corresponding to the maximum rate of methane desorption monotonically increases with coverage from about 325 K for $\approx$0.1 ML to

about 345 K for coverages near 0.5 ML. The quantity of methane desorbed is a linear function of coverage. Dihydrogen is evolved at about the same temperature as methane for all coverages less than saturation, however, for high coverages and for exposures done at higher temperatures, a second desorption feature was observed at 500 K. A plausible mechanism for the desulfurization of methanethiol involves the cleavage of the C-S bond in a methyl thiolate species to form some gaseous methane and a surface hydrocarbon species with the evolution of dihydrogen. The increase in desorption temperature of the methane with coverage of methanethiol can be explained by modification of the Ni(110) surface by the adsorbed species. Further heating to 500 K results in the decomposition of the surface hydrocarbon to form dihydrogen and adsorbed atomic C. Following TPD experiments, the surface is always contaminated with sulfur and generally with C. However, for saturation exposures of methanethiol, essentially no residual C persists following TPD experiments to 700 K. Since no unsaturated hydrocarbons (such as acetylene or ethylene) were desorbed, a possible explanation is that the C diffuses into the bulk for saturated overlayers of methanethiol.

Sulfided Ni surfaces were prepared by heating the methanethiol overlayers to 700 K which was well above the desorption temperature of methane. For S coverages of less than about 0.5 ML, some C (roughly 0.05 - 0.10 ML) was also present. The desorption products from methanethiol adsorption on these modified surfaces were methane, dihydrogen and methanethiol at high coverages. The presence of atomic sulfur (and carbon) caused an enhancement of the methane yield. The desorption temperature of the methane increased with the initial coverage of atomic S. These results indicate that these atomic overlayers may passivate the surface toward methanethiol desulfurization by stabilizing the C-S bond. These results are preliminary and will need further verification on surfaces where the C coverage can be more carefully controlled (i.e., on sulfided surfaces prepared by the decomposition of hydrogen sulfide). In addition, spectroscopic characterization of the adsorbates by HREELS is in progress.

10.4 Structure and Composition of the Surface of NiAl(110) and NiAl(100)

(D. R. Mullins[1] and S. H. Overbury)

The surface of NiAl alloy has been studied by low energy alkali ion scattering, Auger electron spectroscopy and LEED. The incident angle dependence of Li^+ scattering from NiAl(110) indicates that the structure of this surface is approximately that expected for a bulk termination, with a small rippling in the first layer as reported in previous LEED studies. The position of the critical angles associated with shadowing of first layer atoms by other first layer atoms were measured for both the Ni and Al single scattering peaks. In the [001] and [1$\bar{1}$0] azimuths these positions correspond to the known Ni-Ni and Al-Al interatom spacings and allow calibration of the Li/Ni and Li/Al scattering potentials. The derived potentials were then used to determine the extent of rippling, i.e., the spacing between the planes of first layer Ni and Al atoms. This was done by measuring the position of the Ni and Al critical angles along the [1$\bar{1}$3] azimuth where Ni and Al atoms alternate in the surface chains. The critical angles for Ni and Al yield a spacing of 0.22 and 0.20 A respectively, in excellent agreement with the LEED result of 0.20 A.

The scattering from the NiAl(110) surface, in azimuths where Ni and Al atoms contribute equally, was also used to obtain the ratio of the Ni to Al scattering cross sections. These values qualitatively agree with the values calculated from the scattering potentials. The cross section ratio was then used to determine the surface composition of the NiAl(100) surface. On this surface it is

possible, in principle, for the surface to terminate on either the Ni or the Al sub-lattice. It is found that the top layer of the surface is principally Al, as determined from scattering along the [1$\bar{1}$0] azimuth under conditions where scattering from only the first layer is expected. Along the [100] azimuth, where focused scattering from second layer atoms occurs, a strong Ni peak is observed. The results indicate that the bulk ordering persists up to the surface with alternate (100) layers of Ni and Al. Furthermore, there is a strong tendency for the surface to arrange itself so as to terminate on the Al sub-lattice. However, the first layer Al may contain a small fraction of Ni or of vacancies.

---

1. ORAU Postdoctoral Fellow.

11. ELECTRON SPECTROSCOPY

Photoelectron dynamics of free molecules and atoms are being studied over a wide photon energy range with the aid of synchrotron radiation, coupled to angle resolved Auger and photoelectron spectroscopy. Molecules under investigation range from the simple diatomic to the more complex transition metals compounds. In several instances, the data are sufficient for systematic comparisons among homologous series of molecules. Atoms include a variety of metal vapors throughout the periodic table. Both open and closed shell atoms have been studied with particular attention to the behavior of d and f subshells. Multiplet effects in the outermost shell of open-shell atoms are examined in detail. Both molecular and atomic studies have revealed a number of phenomena requiring special attention, such as autoionization, the Cooper minimum, core-shell threshold effects, multichannel interactions, multiple excitation processes, shape resonances and pre-ionization resonances. Essential to this program has been the close interaction with coordinated theoretical calculations, which have yielded fundamental insights into the dynamics of the photoionization process, a basis on which to test molecular orbital theory, and a number of critical tests of many-body theory. Besides providing fundamental information in atomic and molecular science, the research supplies data and ideas for studying molecules adsorbed on surfaces, a clarification for solid state properties in metals, and an understanding of clusters.

11.1 Electronic Structure and Dynamics of Free Atoms

(M. O. Krause, P. Gerard,[1] J. Jiménez-Mier,[2] T. A. Carlson, C. D. Caldwell,[3] B. H. McQuaide,[4] M. S. Banna[4])

The many-body aspects of the electronic structure of atoms are still a largely unexplored phenomenon. This holds especially true for the outer electrons which are chemically important and for electrons in open-shell atoms which constitute the major part of the periodic table. We have been using the photoelectron as a probe of the many-body aspects which influence, sometimes dramatically, the electronic structure and, in particular, the dynamics of the electrons under the action of an electromagnetic perturbation.

The experimental apparatus employed in our studies is an electron spectrometer specially designed and built at ORNL. This spectrometer is operated in conjunction with a synchrotron radiation source, usually the Wisconsin light source. The partial photoionization cross sections σ_i and the photoelectron angular distributions, characterized by a parameter β_i, are measured as a function of photon energy. At the present time, studies emphasize the energy range from 5 to 1000 eV.

During this period, several new and exciting developments occurred. First, the many-electron effects in the outermost shell of the Pb atom were delineated and compared with the theoretical multiconfiguration state predictions.[5] Second, a preliminary ion detector was successfully operated allowing us to expand our measurement capabilities and correlate the electron and ion signals. Third, the new 800 MeV Aladdin storage ring in Wisconsin has come on line; as a result we can extend our measurements to 1 keV photon energy. Important many-electron interactions in the lightly bound inner subshells of Mn could be closely investigated for the first time. Finally joint studies with faculty members and students from several university chemistry and physics departments have been undertaken or are underway. This collaboration has greatly increased the value and effectiveness of our program within the general setting of atomic, molecular, and solid state science.

In addition to Pb and Mn, four more atoms were studied, namely Ga, Zn, Cd, and Hg. In Zn, the dynamic parameters for the 3d

subshell were determined and in Ga, Cd, and Hg, the autoionization resonances in the outer regions of the atoms were characterized by both the cross section and the β parameter.

The multiconfiguration state for the 6p subshell of Pb. In contrast to the single-particle model in which the two 6p valence electrons are placed into the $6p_{1/2}$ level, the many-particle theory places the electrons in the multiconfiguration state $c_1 6p_{1/2}^2 + c_2 6p_{3/2}^2$, thereby allowing for an occupation of the excited, or admixed, $6p_{3/2}$ level. We experimentally delineated the importance of the admixed state by studying the near threshold region, and we determined its relative occupation amplitude c_1^2/c_2^2 to be about 7% from the photoelectron cross sections at higher energies, $h\nu \gtrsim 40$ eV. As seen from Fig. 11.1, the partial cross section for the $6p_{1/2}$ level, $\sigma(6p_{1/2})$, is very weak near its own threshold, but gains enormous strength, when the $6p_{3/2}$ threshold is reached. This shows that the sparsely occupied $6p_{3/2}$ level plays a dominant role, by interchannel coupling, in the dynamic response of the electrons under photon excitation. The unusual behavior of the $6p_{1/2}$ electrons close to threshold excitation additionally demonstrates a relativistic effect. Instead of a large σ at and above 7.4 eV, as characteristic for p electrons, a small σ is observed, as characteristic for s electrons. However, relativistically $p_{1/2}$ electrons behave like s electrons due to their near-spherical charge distribution, and this effect appears to be present in our measured $\sigma(6p_{1/2})$.

Figure 11.1 also displays the total cross section σ_{tot} as obtained from (a) the sum of the partial σ's, $\sigma(6p_{1/2}) + \sigma(6p_{3/2})$, and (b) a measurement of the Pb^+ ion current. A good accord can be seen to exist between the two different determinations. With this work we have now covered the entire photon range from threshold at 7.4 eV to 110 eV for the heaviest element that can conveniently be studied in the free-atom state.[5-8]

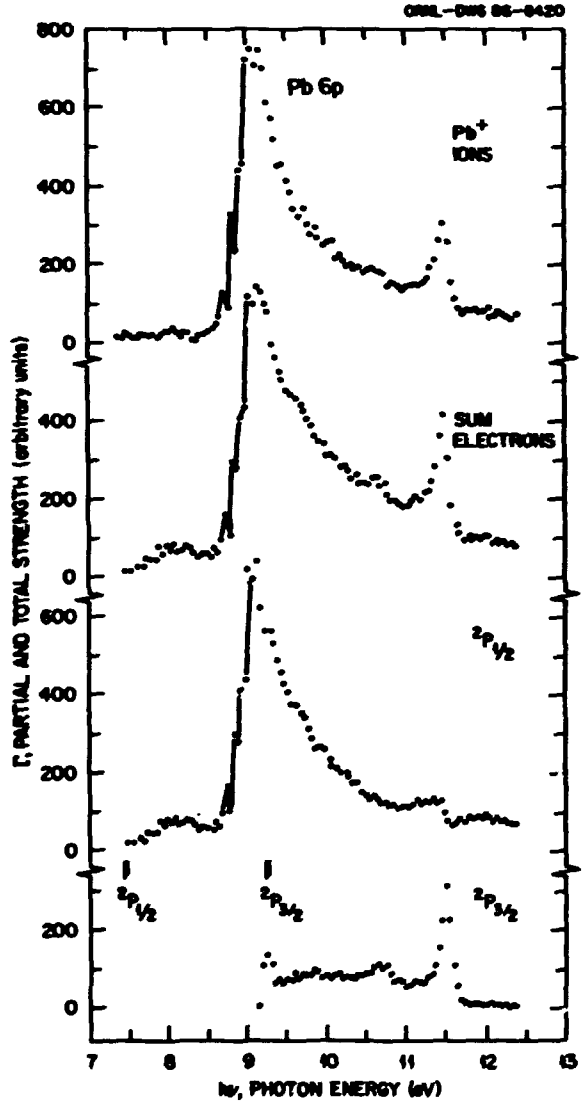

Fig. 11.1. Photoionization of atomic Pb. The two lower spectra show the partial strengths or cross section of the two channels that leave the ion in the $^2p_{3/2}$ and $^2p_{1/2}$ states, respectively. Also shown are the sum of these two partial strengths and the intensity of ions measured as a function of photon energy. The electron sum spectra and the ion spectrum are both proportional to the total photoionization cross section.

The 3s and 3p multiplet structure in Mn. The higher photon energies now available to us at the Aladdin Storage Ring allowed us to penetrate deeper into the electronic structure of Mn and to examine the multiplet

structure within the 3s and 3p levels. This is the first time that the coupling of these inner shells with the half-filled 3d shell could be measured. We found a good overall agreement of the multiplet splitting with theory, which previously could only be compared with results obtained from solid MnF_2. Our results demonstrated unambiguously the purely atomic nature of level splittings. In addition, we showed in a joint effort with C. S. Fadley and B. H. Hermsmeier of the University of Hawaii that the multiplet components, because of their different multiplicity, can be used as probes for the spin orientation in magnetic materials. This collaboration with individuals working in solid state science demonstrated, once again, the importance of understanding the purely atomic characteristics underlying the properties of condensed matter.

Autoionization in Hg. The autoionization resonances associated with 5d → nf or n'p, n ≥ 5 or n' ≥ 6, are of particular interest because of the possibly large differences between the different series and because calculations are feasible in the jj coupling scheme which is a quite good approximation for this heavy element. We measured both σ and β for the 6s → εp photoelectron which provides the deexcitation pathway (exit channel) for the resonances. The range from the ionization threshold at 10.4 eV to the $5d6s^2(^2D_{3/2})$ threshold at 16.7 eV was covered continuously in small, 3-meV steps by the constant-ionic-state (CIS) method described earlier.[9] A photon bandpass of 1.6 Å was sufficient to faithfully trace the resonance contours of the low lying np resonance states, but not those of the higher np states and the very narrow nf states. The data up to 14.2 eV could be compared with a theoretical close-coupling calculation[10] for both σ and β. As seen from the small interval presented in Fig. 11.2, there is a qualitative agreement between theory and experiment. An analysis of our Hg data is underway; this analysis is being done in context with the results on Cd, for which we have recently obtained analogous data.

---

1. Postdoctoral Fellow, Orsay, France.
2. Postdoctoral Fellow, Mexico City, Mexico.
3. University of Central Florida, Orlando, Florida.
4. Vanderbilt University, Nashville, TN.
5. M. O. Krause, P. Gerard and A. Fahlman, Phys. Rev. A 34, 4511 (1986), Rapid Communication.
6. M. O. Krause, P. Gerard, A. Fahlman, T. A. Carlson and A. Svensson, Phys. Rev. A 33, 3146 (1986).
7. M. O. Krause, F. Cerrina, A. Fahlman and T. A. Carlson, Phys. Rev. Lett. 51, 2093 (1983).
8. M. O. Krause, A. Svensson, A. Fahlman, T. A. Carlson and F. Cerrina, Z. Phys. D 2, 327 (1986).
9. M. O. Krause, F. Cerrina and A. Fahlman, Phys. Rev. Lett. 50, 1118 (1983).
10. K. Bartschat and P. Scott, J. Phys. B 18, L 191 (1985).

11.2 Photoelectron Dynamics of Free Molecules

(T. A. Carlson, M. O. Krause, P. Gerard,[1] J. Jimenez-Mier,[2] T. Rosseel,[3] G. VonWald,[4] B. Yates,[4] J. W. Taylor,[4] F. A. Grimm,[5] B. P. Pullen[6])

Last year was a particularly exciting one because of the startup of the new Synchrotron Storage Ring at Wisconsin (Aladdin). During our first run on the new ring in the fall of 1986, data were obtained on a number of core shells. Studies included shape resonances in gases such as N_2O and angular distribution from solids. The most interesting investigation was the application for the first time of angle resolved electron spectroscopy to the problem of pre-ionization resonances for core shells. Earlier in the year on the older storage ring (Tantalus) important studies were completed on the

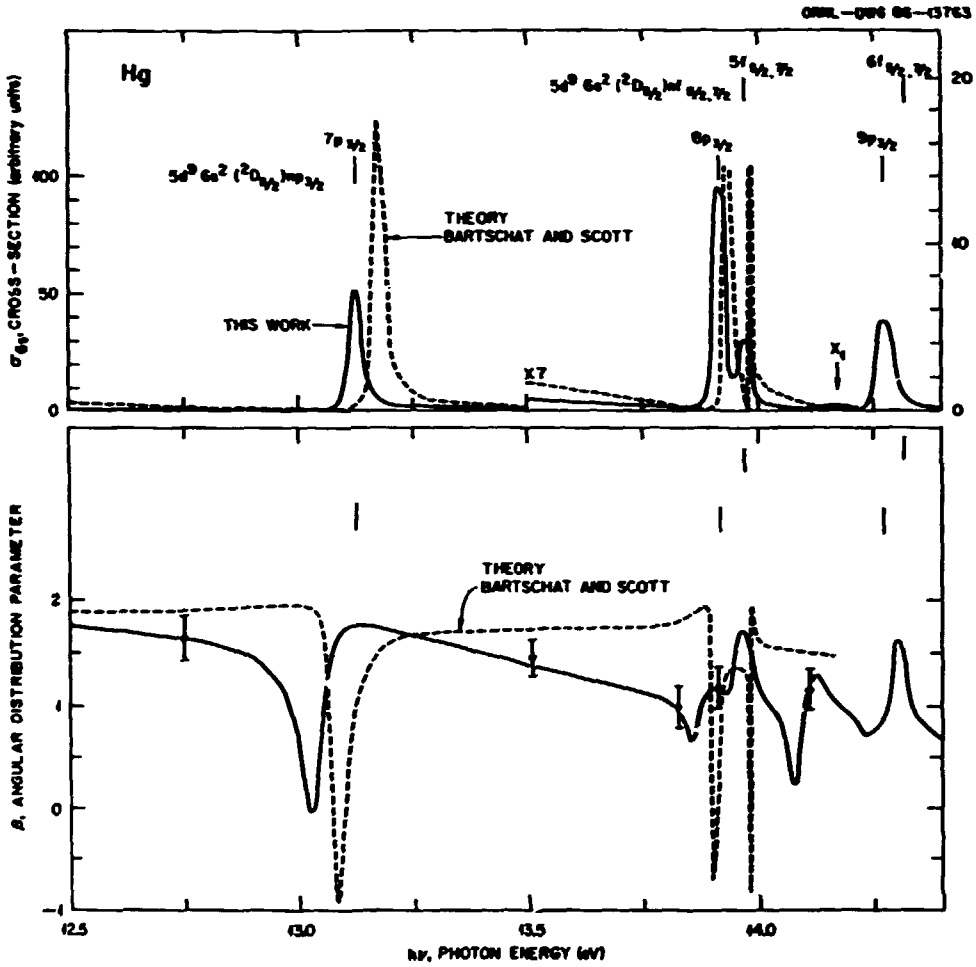

Fig. 11.2. Autoionization profiles in the 5d → np resonance region of Hg as observed by way of the 6s photoelectron. Experiment (solid lines with diamond calibration points) is compared with the theory (dash line) of Ref. 10.

autoionization of iodine compounds and the comprehensive survey of the valence shells of benzene.

Pre-Ionization Resonances for Core Shells

When one scans the photon energy range just before the ionization potential of a core shell electron of a molecule, resonance occurs by which a core shell electron is excited to a virtual but bound state. If the radiative yield is small, the core vacancy is usually filled by a non-radiative process. Either the excited electron refills the core hole with ejection of an outer shell electron (autoionization) or the excited electron remains intact as a spectator with the outer shell electrons undergoing an Auger process. In a molecule the processes are most interesting when the outer shell electrons are the valence shell electrons.

Angle-resolved electron spectroscopy has been carried out as a function of photon energy, using synchrotron radiation, for processes near the 2p core shell of silicon, sulfur, and chlorine for CS_2, OCS, $SiCl_4$, and the chloro methanes. The Auger spectra can be disentangled from valence shell photoelectron spectra by observing that the

photoelectron processes far above valence shell threshold have a high angular distribution parameter, β, while the Auger processes are more isotropic. Typical spectra are illustrated in Fig. 11.3. It is found that spectator Auger processes are more dominant than direct participation of the excited electron by autoionization. The shift in

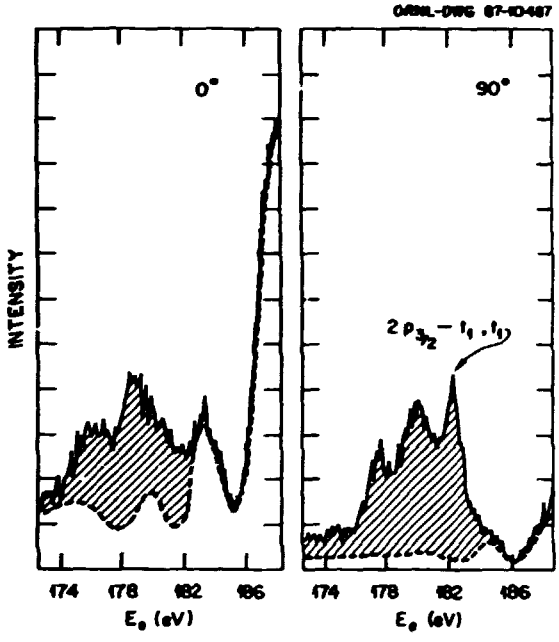

Fig. 11.3. Electron spectra from the first preionization resonance in CCl_4 taken at a photon energy of 202 eV. The dashed lines represent contributions from the photon electron spectra of the valence shell or determined from data just below the resonance; the striped areas are due to Auger processes. It can be seen that the corrections due to photoelectron processes are much smaller when the polarization is perpendicular (90°) to the direction of the ejected electron. The first band of the Auger processes can be identified as a $2p_{3/2} - t_1t_1$ transition following excitation to the first resonant state with a $2p_{3/2}$ vacancy. The resolution of the electron spectrometer is 0.6 eV, the resolution of the monochromator is 2 eV.

energy for the Auger processes has been related to the resonance energy by means of a model in which the spectator electron is treated like an electron in a Bohr atom. As expected, the model is not unreasonable for the higher Rydberg states but fails for the more molecular states. The field of preionization core shell resonances as examined by electron spectroscopy appears to be a very rich one, both from the knowledge gained regarding the dynamics of ionization and the nature of molecular orbitals.

Autoionization in Iodine Substituted Molecules We have expanded our previous successful study of autoionization between the spin-orbit split lone-pair orbitals of iodine in HI to other molecules: CH_3I, C_2H_5I, C_3H_7I and I_2. The principal structure of Rydberg states converging to the ionization potential of the orbital with $\frac{1}{2}$ spin is remarkably similar for the mono-substituted iodides. This is indicative of a super atomic-like behavior. The most notable difference between the molecules is the increasing background with increasing complexity of the polyatomic structure. This background is probably due to a high density of closely spaced unresolved resonances derived from a complexity of vibrational and electronic states and is of great importance to our understanding of photoionization of polyatomic molecules. In sharp contrast to the mono-substituted iodine molecules, I_2 showed a completely different autoionization spectrum, indicative of the strong perturbation between the lone pair orbitals of adjacent atoms.

Photoelectron Dynamics of Benzene Data were obtained on the partial cross sections and angular distribution parameters for all ten of the valence orbitals, except the most tightly bound $2a_{1g}$. Most important, calculations were also made that were used to compare with the experimental data. The comparison between experiment and calculations, based on the multiple scattering X_α method, offers one of the most ambitious

evaluations, to date, for the photoelectron dynamics of a relatively complex polyatomic molecule. Though there remains much room for improvement, many of the observed features including a variety of shape resonances were correctly described by the calculations.

---

1. Postdoctoral Fellow, Orsay, France.
2. Postdoctoral Fellow, Mexico City, Mexico.
3. ORNL Analytical Chemistry Division.
4. University of Wisconsin, Madison, WI.
5. University of Tennessee, Knoxville, TN.
6. Southeastern Louisiana University, Hammond, LA. Leave funds have been provided by Research and Grant Committee, Southeastern Louisiana University and ORAU.

12. CHEMISTRY RELATED TO NUCLEAR WASTE DISPOSAL

Several research topics in the Chemistry Division are directly related to chemical problems of high-level radioactive waste disposal. Safety analyses of radioactive waste disposal depend upon reliable prediction of radionuclide migration in the event of penetration of the nuclear waste repository by groundwater and flow of the groundwater to the accessible environment. Prediction of the migration rates of nuclides within host geological formations is dependent upon knowledge of sorption properties and chemical speciation of the nuclides. In Sections 12.1 and 12.3, programs are described for evaluation of the parameters affecting the sorption of Tc, Np, U, Sr, Eu, and Cs. Knowledge of the solubilities of nuclides, especially for reducing repository environments, is necessary for prediction of maximum concentrations of nuclides in the groundwaters. In Section 12.2, solubility studies of Tc(IV) oxides are summarized. In Sections 12.4 and 12.5, other types of chemical support for assessment and evaluation activities are presented.

12.1 An Evaluation of Retardation Parameters for Nuclide Migration in Geological Media

(R. E. Meyer, W. D. Arnold, J. G. Blencoe, F. I. Case, and J. F. Land)

The objective for this program is to evaluate for the U. S. Nuclear Regulatory Commission critical retardation parameters given by the site contractors of the Department of Energy with respect to their adequacy and pertinence in high-level waste repository safety assessment. In the event of a breach of a repository by groundwater, the nuclides may be mobilized and transported to the environment. Safety analyses must demonstrate that the quantity of nuclides released from the repository and transported be maintained within acceptable limits. During the past year, particular emphasis has been given to sorption of cesium, strontium, europium, technetium, neptunium, and uranium on various samples of tuff from the Yucca Mountain proposed site in Nevada for a high-level waste repository.

Sorption onto the tuff samples was studied first with batch experiments in which crushed tuff was shaken with the groundwater for a specified period of time and the amount of sorption determined by measuring the reduction of the radionuclide concentration in the groundwater. Small columns of the tuff were then constructed, and sorption was studied by injecting spikes of the radionuclides into the entrance to the column and determining the elution peaks from the columns. From the shapes and position of the peaks, information on the extent of sorption and on the type of sorption process was extracted. This information was then compared to the results of the batch experiments. For some, but not all, radionuclides the results of the column tests could be predicted from the results of the batch sorption experiments.

These results provide information concerning the applicability of DOE sorption data for prediction of radionuclide transport at DOE candidate sites for high-level waste repositories. Details of our experiments and comparisons of our results to DOE results are presented in NUREG annual, semiannual, and quarterly reports.[1-4]

---

1. A. D. Kelmers, F. G. Seeley, W. D. Arnold, J. G. Blencoe, R. E. Meyer, G. K. Jacobs and S. K. Whatley, Progress in Evaluation of Radionuclide Geochemical Information Developed by DOE High-Level Nuclear Waste Repository Site Projects: Report for Jan-Mar 1985, NUREG/CR-4236 ORNL/TM-9614/V2.
2. A. D. Kelmers, W. D. Arnold, J. G. Blencoe, R. E. Meyer, G. K. Jacobs and S. K. Whatley, Progress in Evaluation of Radionuclide Geochemical Information Developed by DOE High-Level Nuclear Waste Repository Site Projects: Report for

April-June 1985, NUREG/CR-4236 ORNL/TM-9614/V3.

3. R. E. Meyer, W. D. Arnold, J. G. Blencoe, G. K. Jacobs, A. D. Kelmers, F. G. Seeley and S. K. Whatley, Progress in Evaluation of Radionuclide Geochemical Information Developed by DOE High-Level Nuclear Waste Repository Site Projects: Annual Report for Oct 1984 - Sept 1985, NUREG/CR-4236 ORNL/TM-9614/V4.
4. R. E. Meyer, W. D. Arnold, J. G. Blencoe, G. D. O'Kelley, F. I. Case, J. F. Land and G. K. Jacobs, Progress in Evaluation of Radionuclide Geochemical Information Developed by DOE High-Level Nuclear Waste Repository Site Projects: Semiannual Report for Oct 1985-Mar 1986, NUREG/CR-4708 ORNL/TM-1014/V1.

12.2 Solubility and Electrochemical Studies of Tc(IV) Oxides

(R. E. Meyer, W. D. Arnold, F. I. Case, J. F. Land)

Based upon current knowledge of technetium chemistry, it is generally predicted that some form of Tc(IV) oxide would be formed if reducing conditions exist in a repository environment and Tc is released from the stored waste by a groundwater-intrusion event. The solubility of Tc(IV) oxides is one of the parameters necessary for the calculation of the transport rate of technetium for the case of solubility-limited transport. However, technetium has an unusually complicated redox chemistry, and much is unknown about the chemistry of reduced valence states of technetium. In particular, little is known about the solubilities of Tc(IV) oxides. Solubilities of technetium (IV) oxides were therefore determined in solutions of NaCl, HCl, and synthetic basalt groundwaters in the pH range 0 to 10.

The technetium (IV) oxides were prepared either by electroreduction from Tc(VII) solutions onto platinum electrodes or by precipitation of Tc from Tc(VII) solutions using hydrazine. In some of the determinations, the oxide was precipitated onto purified sand by use of hydrazine. The oxide-covered sand was then placed into a column and the test solution continuously recirculated through the column. The oxide-covered platinum electrode was placed into a small cell and the test solution stirred. Solubilities were determined by counting the beta radiation of ^{99}Tc in the stirred or circulated solution in contact with the oxide. In the pH range 3 to 10, solubilities were in the range 3×10^{-9} to 5×10^{-8} mol/L. In acid solutions, the solubilities were generally higher for hydrazine-precipitated oxides than for electrodeposited oxides, and they increased as the pH was lowered. For electrodeposited oxides, solubilities were generally lower for oxides deposited from basic solutions compared to those deposited from acid solutions. By carefully weighing the electrodeposited oxides, the oxides were found to be hydrated with the formula $TcO_2 \cdot nH_2O$ where n was found to average 1.63. Electrochemical studies of the potential as a function of concentration and pH were also carried out to verify the relation for the Tc(VII) - Tc(IV) couple

$$TcO_2 + 2H_2O = TcO_4^- + 4H^+ + 3e^-.$$

Solubilities of Tc(IV) oxides will be useful for calculation of transport rates of technetium for the case of solubility-limited transport in nuclear waste repository environments. Details of these measurements are described in NUREG reports.[1-2]

1. R. E. Meyer, W. D. Arnold and F. I. Case, Valence Effects on Solubility and Sorption: The Solubility of Tc(IV) Oxides, NUREG/CR-4309 ORNL-6199, 1986.
2. R. E. Meyer, W. D. Arnold and F. I. Case, The Solubility of Electrodeposited Tc(IV) Oxides, NUREG/CR-4865 ORNL-6374, 1987.

12.3 Sorption of Radionuclides on Shales

(P. C. Ho, W. D. Arnold, F. I. Case, R. E. Meyer)

The Sedimentary Rock Program (SERP) is investigating shales in the United States for their potential suitability as host rocks for the disposal of high-level radioactive waste. In support of this program, preliminary studies were carried out of sorption of Cs, Sr, Tc, U, and Np onto Nolichucky, Green River, Pumpkin Valley, Chattanooga Upper Dowelltown, and Pierre Shales under oxic (air-present) conditions. One of the groundwaters used is a synthetic groundwater made up to simulate highly saline groundwaters in the Conasauga shale formation. The other two groundwaters are a 100/1 dilution of this groundwater and 0.03 M $NaHCO_3$. Moderate to significant sorption was observed under most conditions for all the tested radionuclides except technetium. Moderate sorption of technetium was observed on Chattanooga Upper Dowelltown shale, and essentially no sorption was observed on the other tested shales. Little sorption of strontium onto the shales was observed from the concentrated groundwater. Sorption tests were also run on shales that had been heated at 250°C for six months. Except for the Green River Shale, heating the shales resulted in an increase of sorption for Cs. Heating also destroyed what little ability the shales had for sorbing technetium. For the other radionuclides, the results of heating produced no clear patterns in the effect of heating on sorption. The results of these experiments have been published in an annual report.[1] These data will be used to help select the potentially most favorable shales for detailed site-specific characterization from among those currently being considered.

One of the questions regarding the sorption ability of shales is the effect of the organic content of the shales which for some shales is significant. As a first step in this study, an extensive literature review of the organic content of shales was completed.[2] This review will serve as a basis for initiation of experimental studies on the effects of the organic content on the sorption ability of the shales.

---

1. P. C. Ho, R. E. Meyer, W. D. Arnold and F. I. Case, Sorption of Np, U, Tc, Sr and Cs onto Shales, ORNL/CF-86/321, (1986).
2. P. C. Ho and R. E. Meyer, A Review of the Organic Geochemistry of Shales, ORNL/CF-86/359, (1986).

12.4 Review and Evaluation of Literature on Geochemical Issues Pertinent to the Disposal of High-Level Radioactive Wastes: Technical Assistance to Geotechnical Staff of the Nuclear Regulatory Commission (NRC)

(J. G. Blencoe)

This project focuses on compiling and evaluating various geochemical data/information pertinent to the licensing of a geologic repository for high-level radioactive waste (HLW). Project activities include, but are not restricted to, the following tasks: (1) assemble and assess key geochemical data for candidate repository sites; (2) evaluate DOE programs for determining the geochemical characteristics and radionuclide-containment performances of potential repository sites; (3) review and evaluate reports, journal articles, and the parts of DOE site-characterization plans that deal with geochemical issues; and (4) review draft technical material written by NRC geochemistry personnel for inclusion in NRC documents. The results of these various activities are usually transmitted to the NRC in the form of reports that identify and attempt to resolve particular geochemical issues and concerns. Examples of documents written for the project include "topical review" papers[1,2,3] and evaluations of reports and journal articles that deal with issues pertinent to the candidate-repository sites at Hanford, Washington, and Yucca Mountain, Nevada.

Project staff also have the responsibility to attend meetings, symposia, workshops, etc. that deal with geochemical aspects of the disposal of HLW. After attending such a meeting, a staff member must prepare a trip report in which he outlines the agenda of the meeting, the most important new information that was present at the meeting, and his general impressions of the usefulness of the meeting. This trip report is then sent to appropriate NRC geotechnical staff for their examination and evaluation.

---

1. J. G. Blencoe, Review and Assessment of DOE-Hanford information on the Solubilities/Concentrations of Radionuclide-Analog Elements in the Systems - Simulated Waste Form ± Uranium Basalt + Grande Ronde Groundwater, NUREG/CR-4024, ORNL/TM-9415, (1987).
2. J. G. Blencoe, Review and Assessment of Information on Geochemical Conditions at the Hanford, Washington, Candidate High-Level-Radioactive-Waste Repository Site (in preparation).
3. G. E. Grisak and J. G. Blencoe, Matrix Diffusion of Radionuclides in Rock/Groundwater systems (in preparation).

12.5 Solubility Issues Related to the Performance of a High-Level Nuclear Waste Repository in Bedded Salt: A Survey of Data Needs on Solubilities and Aqueous Species of Radium, Technetium and Iodine

(G. D. O'Kelley)

It has been recognized for some time that, as part of a licensing strategy for a nuclear waste repository, it will be necessary to consider solubilities of the radionuclide compounds in making conservative estimates of concentrations in aqueous solution. For relatively insoluble species, solubilities are the sink terms for leaching calculations and the source terms for the mass transport of radionuclides through the packing material.

As provided in the Nuclear Waste Policy Act of 1982, the U.S. Department of Energy (DOE) has reduced the five sites originally proposed for a nuclear waste repository to three: Hanford, Washington; Yucca Mountain, Nevada; and Deaf Smith County, Texas. Use of the Deaf Smith County site would involve emplacing the wastes in bedded salt, a geologic setting with novel implications for nuclear waste chemistry. Additionally, it was recognized that defensible solubility data were lacking for a number of key elements under conditions expected in a salt repository. Water providing the means for mobilizing wastes in such a setting is expected to be present as brine with very high ionic strength, which led to concern that there needed to be a careful evaluation of published solubility data to identify relevant data and to identify areas of deficiency requiring new experimental measurements.

The program concerned with the Deaf Smith County site is managed by the Office of Nuclear Waste Isolation (ONWI), Project Management Division, Battelle, Columbus, Ohio, for the DOE Salt Repository Project Office. The literature review summarized here was performed for ONWI as part of a study which involved several laboratories and which emphasized a search for published solubility data for radium, technetium, and iodine, both in dilute solutions and in solutions of high ionic strength, and at temperatures ranging from room temperature to more than 100°C. However, it was recognized in carrying out this survey that thermodynamic data on solid radionuclide compounds and on the aqueous species in equilibrium with the solid phases will be needed for calculating the concentrations of species in the liquid phase.

The procedure developed for the review primarily made use of thermodynamic databases and associated references assembled by the European NEA committee and a similar, though less complete, database for the Lawrence

Livermore National Laboratory (LLNL) program EQ3/6. Computer searches of Chemical Abstracts On-Line and the ORNL Waste Management Database were used to augment the resources of the NEA and EQ3/6. Key references and reviews were also helpful. It was also decided that, at the outset, a comprehensive table of all possible solid compounds would be compiled for each element, together with an equally comprehensive table of all aqueous species. A uniform procedure for screening the data in the first two tables was agreed upon between the laboratory representatives participating in the various surveys, and this procedure then was employed to generate final tables of solid compounds and aqueous species which appeared to require further study.

On the logic flowchart used by the authors of the literature reviews, the first critical decision concerned whether solubility and/or thermodynamic data were available. This report used a very strict interpretation of the term "data." In general, data were considered available for a given chemical species only if the particular quantities were determined by direct measurement. Many of the thermodynamic data quoted in reviews and in the NEA database are calculated or estimated values. Of course, even estimated values for thermodynamic parameters were very valuable in deciding whether the particular compound or aqueous species was of sufficient importance in the salt repository brines to require future measurements. If experimental data were available, then a series of objective culling criteria were applied to decide whether additional information was needed.

The results and recommendations of this literature review will be published in a forthcoming ORNL report.

13. COMPUTATIONAL MODELING OF SECURITY DOCUMENT PRINTING

The U.S. Bureau of Engraving and Printing (BEP) produces approximately 40 billion security documents annually with currency and postage stamp production accounting for 93% of the total. The seven billion banknotes are printed in sheets, inspected by human examiners, and passed in sheets to overprinting, cutting, and packaging equipment. In the next few years the BEP will be switching to a web oriented operation requiring new web printing presses, an automated inspection system for examining the printed web, and new overprinting, cutting, and packaging equipment to handle web input. We are assisting BEP by building a prototype Web Currency Inspection System (WCIS) to be installed at BEP in 1990. We are also assisting BEP with a systems analysis for a Web Currency Finishing System for overprinting, cutting, and packaging, and another systems analysis for automatic stamp inspection.

The world's currencies and postage stamps reflect the cultural heritage of the issuing nations and are a source of national pride. It is essential that high quality products of consistent uniformity be produced so that the citizens of the country become very familiar with the items and can differentiate the real items from counterfeits. Tight quality control is essential for this goal to be accomplished. A major source of security document variability is the presence of printing flaws introduced in the manufacturing process. Quantification of printing flaws is needed because of the future use of machine inspection for automatic detection and elimination of flawed specimens. We have carried out an extensive survey on human perception of currency flaw severity and have derived a model which relates that severity to physically measurable quantities. A related task on postage stamp flaws is underway.

For machine inspection, detailed guidelines must be established to properly differentiate between objectionable flaws which should be rejected and minor variations which should not cause rejection. The differentiation between good and bad is often a flexible operational threshold which must accommodate the sometimes conflicting goals of production time schedules and uniform high quality. We have derived a Flaw Specification Language to aid in this task.

During the past year we have carried out an extensive survey of the chemical literature on Hansen solubility parameters and their applicability to ink formulation. An extensive experimental design for analysis of the Hansen parameters for BEP ink components was derived but not carried out since BEP recently decided to reduce their internal ink production and rely more on commercially formulated printing inks. However, Hansen parameters can provide useful quality control measures as well as guidelines for formulation. A method for the testing of ink adhesion through image analysis of crumpled currency was derived and is being implemented.

Two international conferences and an international workshop were organized by ORNL in collaboration with BEP during the past year.

13.1 Web Currency Inspection And Finishing Systems

(C. K. Johnson, Project Leader, D. McDonald, Chief Engineer[1])

Quality assurance and economics motivate the major upgrading in currency production facilities at BEP. Web printing technology allows the printing of both front and back sides of currency in a single pass through the press at top speeds up to 600 feet per minute (180 notes per second). On-press inspection of the printed currency for paper and printing flaws is highly desirable to allow immediate corrective measures during periods of high flaw rates to minimize currency spoilage. The principal on-press inspection requirement is to warn the operator when unacceptable flaw rates occur. Process control to automatically correct certain press problems may also be feasible.

At present, sheet currency printed with four columns by eight rows of notes is split into half-sheets of two columns by eight rows and examined visually by trained currency examiners who manually remove flawed half-sheets for shredding. A conveyor belt system called the mechanical examination device is used to transport the half-sheets past the examiners. Even though a single flawed note on a half-sheet requires destruction of the entire half sheet, flawed note removal is fairly straightforward in sheet oriented currency production.

13.1.1 Web Currency Inspection System (WCIS)

(C. K. Johnson, D. McDonald,[1] D. McCue,[1] B. Jetko,[1] M. Burnett)

In the web process, the continuous web, which is several thousand feet long, presents complications in manual identification and removal of

flawed sections. Automatic machine vision identification of flaws with marking for removal, either as sections of the web when flaw rate is severe or as single notes when the flaw rate is less severe, is essential for optimal utilization of the web production process. The prototype Web Currency Inspection System (WCIS) under development by our group is designed to identify and mark the flawed currency which is to be removed.

We are also doing a systems analysis of a completely web-oriented production train. This system study will investigate three production train configurations. The first configuration mimics the existing sheet oriented production train with a separate press, mechanical automatic inspection station, and web finishing system. The second configuration will consist of an integral press and inspection system with a separate finishing machine. The final configuration will consist of a second generation fully integrated machine which takes in blank rolls of paper and produces inspected packaged currency as its output.

If the comprehensive inspection system can be made fast enough, the complete inspection task can be carried out by a single inspection system located on-line at the web currency press. If that speed cannot be obtained, it will be necessary to have a simpler Web Press Printing Monitor (WPPM) capable of detecting unacceptable rates of severe flaw occurrences on-line at the web press for warning and process control purposes. The comprehensive flaw inspection system could then be placed on the Web Finishing press or in a stand-alone web-to-web operation between the web currency and web finishing presses. Multiple stand-alone inspection systems could be used to handle the work load from the web currency press.

The decision about where to place the comprehensive flaw detection unit will depend on the technical capabilities of the prototype inspection system. A fail-safe strategy is to build first a stand-alone system with capability for attachment to both the web currency and web finishing presses for production testing in all three scenarios. Controlled testing of the inspection system can most easily be accomplished in the stand-alone configuration. This is the approach we are following in our procurement and integration of the prototype WCIS.

---

1. I&C Division, ORNL.

13.1.2 Web Currency Finishing System

(C. K. Johnson, D. Richards,[1] D. Thomas,[2] C. Harrison,[2] M. Durnett)

The Web Currency Finishing System represents the final component in the web currency production train. It will be used to (a) add serial numbers and Federal Reserve Bank seals to blank engraved notes, (b) cut the web into individual notes, (c) remove flawed notes from the final production stream, (d) package product notes for shipment, and (e) maintain records for security accountability purposes. The flawed currency to be removed will have been previously identified and marked by WCIS. A systems analysis on feasible designs for the Web Finishing System is being carried out by our group.

A key factor in the conceptual design will be the speed capability of the web finishing system relative to the speed capability of the web press and the WCIS. If the systems are eventually to operate in a single web stream, they must have comparable speeds; otherwise, they must operate independently. Four key engineering issues are present for the web finishing system: (a) what printing technology will be employed for overprinting, (b) how will defective notes be detected and eliminated, (c) how will the final product be inspected, and (d) what packaging and accounting procedures are required. A major requirement is to maintain sequential runs of serial numbers in the final currency bricks of 4000 notes. Skipping the overprinting of bad notes or not advancing the serial number for a bad note to be discarded are possible approaches. We are currently carrying out conceptual designs and

discrete event simulations on a number of alternatives.

1. Engineering Division, ORNL.
2. University of Tennessee.

13.2 Printing Flaw Characterization

(C. K. Johnson, M. Burnett, R. Sherrod,[1] C. Goodman,[1] R. Schmoyer[2])

At the highest level, most printing flaws fall into one of two categories: ink where it should not be (an excess-of-ink flaw, EOIF) or no ink where it should be (a dearth-of-ink flaw, DOIF). At a lower level, there are several ways to classify a printing flaw. For example, a flaw might in some way be correlated with the printed image while others are not. The four main categories of flaws are (a) Excess ink or discoloration uncorrelated with engraving pattern, (b) Excess ink correlated with opposite side engraving pattern, (c) Deficiency of ink uncorrelated with engraving pattern, and (d) Deficiency of ink correlated with engraving pattern.

With respect to time, printing flaws may occur at totally random times, at regular repeat intervals, or continuously. For example, a little ink might not get totally wiped off the printing roller, resulting in a spot on the paper. Such events would be expected to occur at random times. On the other hand, if the ink supply should become low on the press, all printing will get lighter until the ink supply is replenished. The third situation is exemplified by a crack in an engraving. At present, the printing roller on an intaglio press has four engraved plates around its circumference. If one of these should develop a crack, the resulting flaws will occur on every fourth sheet to come off the press.

One way to view flaw origins is through a flowchart of the printing process that indicates the positions in the overall scheme where flaws are introduced. Allegorically, flaws may be described as being due to a collection of spoilage demons whose sole purpose is to ruin currency. Each demon has a personality of its own and does its evil deed in its own peculiar but characteristic way. Figure 13.1 depicts the more common flaw demons. A symbolic representation of this sort is particularly useful in machine reasoning about diagnosis and ultimately process control.

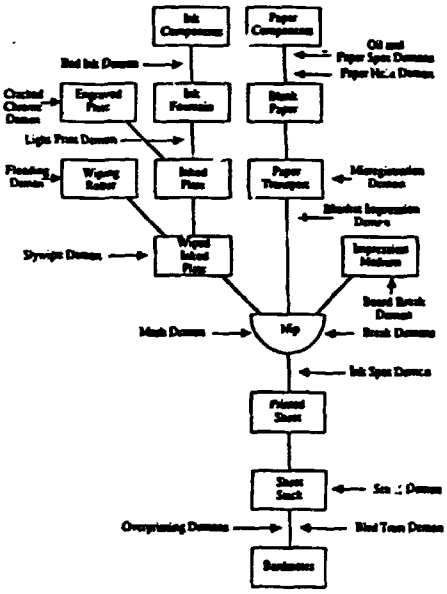

Figure 13.1. Flaw demon causal network.

1. University of Tennessee.
2. Engineering Physics Division, ORNL.

13.2.1 Flaw Specification Language

(C. K. Johnson, M. Burnett, R. Blake,[1] R. Cockett,[1] R. Sherrod,[1] C. Goodman[1])

Figure 13.2 gives the schematic overview of a hypothetical currency inspection system and provides the focus for this section. The characteristic features of primary interest in currency examination are the topological and human factor attributes shown at the top of the figure.

In this hypothetical automated currency inspection system, a flaw specification language has been created to provide a flexible means of communication between the operator and the system. The language permits the operator

to alter system default flaw acceptance levels, to instruct the system to search specific regions of notes for particularly troublesome features, or to change the way the system reacts to a particular occurrence of flaws. Using familiar terms and a simple, straight-program" which is translated by the

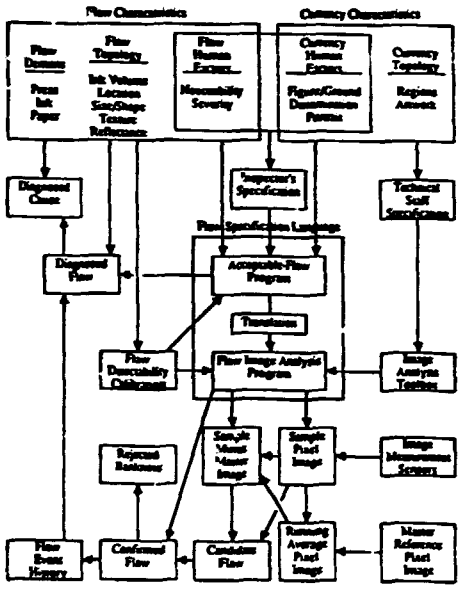

Figure 13.2. Idealized inspection system.

forward syntax, the operator writes an "acceptable-flaw system into the necessary image processing and machine operations. When writing the program, the operator will be concerned primarily with the human factors of Figure 13.2 but must also be concerned with the specifics of flaw types, note regions, and flaw susceptible artwork components.

The formality of a programming language is utilized to structure the acceptable-flaw programs that can be written and to direct an orderly consideration of flaws relative to note topology. The language is distinctly "Pascal-like." Pascal is a widely used computer programming language and has a clear formal definition, making it a good model for the flaw specification language.

1. University of Tennessee.

13.2.2 Currency Flaw Severity Survey and Model

(C. K. Johnson, M. Burnett, R. Sherrod,[1] C. Goodman,[1] R. Schmoyer[2])

A survey of opinion on currency flaws was carried out primarily at the BEP to establish flaw acceptance/rejection criteria to be used in an automated currency inspection system. Thirty-seven judges, representing several different occupational categories inside and outside of the BEP including management, press operators, currency inspectors, quality assurance personnel, engravers, and research scientists, participated in the flaw survey.

Each judge sorted 300 currency samples into five groups, based on his or her opinion of the flaw severity on each sample: (1) always accepted; a threshold acceptance/rejection range with three subdivisions based on printing quality: (2) good, (3) fair, and (4) poor; and finally, (5) always rejected. The 300 specimens covered 31 graded series of typical flaws.

Over two-thirds of the notes were found absolutely acceptable by the most liberal judge whereas over two-thirds were absolutely unacceptable to the most conservative judge. The remaining judges were fairly evenly spaced between these extremes. This "judges' bias" trend was at first rather disturbing until it was realized that a person's opinion on currency flaws is fully as subjective as his opinions on politics or art appreciation and that most people have very narrow regions which they consider "marginal." Internal consistency seems unrelated to the liberal/conservative bias.

In spite of the wide variety in judges' individual biases and the fact that the judges were not given the opportunity to compare individual notes in a series side by side, the population of judges as a whole produced average severity measures which ranked the notes in series very similarly to a carefully arbitrated independent ranking of the 31 different series at Oak Ridge.

Determination of which of the survey data should be included in the model required an

analysis of two populations -- the sampled population of flawed notes and the sampled population of biased judges. Outlier notes were found through a statistical analysis of voting histogram bimodality. By examining these notes in some detail it was possible to explain discrepancies quite well with factors such as camouflage and multiple flaws. Another indicator of both the judge's consistency and the specimen note's suitability was derived through a singular-value decomposition of the complete survey data matrix. For fitting of the model described below, it was advantageous to use the results from a subset of judges with the highest internal consistency.

Flaw density was estimated by using a graduated half-tone overlay that had been created for and used in an earlier flaw study conducted by quality assurance at the BEP. Area was estimated by measuring the approximate width and length of the flaw. In cases where a flaw had a complex shape and/or varied in density, the flaw was subdivided into more easily measured components approximating rectangles.

The region of flaw location was also recorded as shown in Figure 13.3.

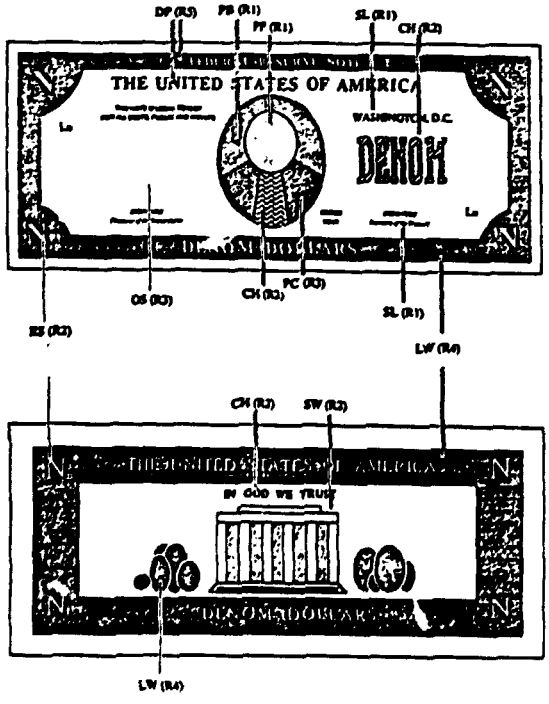

Figure 13.3. Currency regions.

The following model has been derived to correlate the flaw severity grades obtained in the survey with the physical parameters of the flaws. The unknown parameters were obtained by nonlinear least-squares refinement using observations from 175 notes flawed with sly-wipes and breaks. The flaw model has the form

$$F_c = B_i \cdot (T+\Sigma\Sigma[R_j\, D_{jk}{}^{u} A_{jk}{}^{v}])^{1/w} \qquad (13.1)$$

where the calculated flaw severity for a note is a function of the note's denomination and the summation of all flaw components on the note. The symbols in the model are defined as follows:

D_{jk}	measured density for flaw component k in region j
A_{jk}	measured area for flaw component k in region j
B_i	scale factor for note denomination i
R_j	scale factor for region j
T,u,v,w	parameters for entire data set

The refined parameters gave a remarkably good fit to the experimental flaw severity observations with a mean deviation of roughly 0.4 units on the observation scale of 1 (always acceptable) to 5 (never acceptable).

Prior to our work, it appears that such an analytical methodology has not been used extensively in flaw severity characterization. Dr. John Rolfe, the chairman of the Committee on Flaw Severity Perception at the workshop described in Section 13.2.4, discusses our results in his paper presented there on User's Perception of Printing Flaws and concludes his paper, "Finally one more tribute to the ORNL team for blazing a trail and allowing the likes of me to walk along their trail and criticize it. Let us not forget that the ranking of flaw severity is only the first step along the path to machine examination. I am confident that subsequent steps will be even more difficult."

1. University of Tennessee.
2. Engineering Physics Division, ORNL.

13.2.3 Postage Stamp Flaws

(C. K. Johnson, R. Sherrod,[1] C. Goodman,[1] M. Burnett, R. Schmoyer[2])

The fact that currency has printing on both sides simplified the characterization of flaws since front and back could be considered at the same time. Postage stamps, on the other hand, have gummed backs which introduce additional flaw possibilities. The use of multiple printing methods such as intaglio, gravure and offset lithography and the multicolor nature of stamps further complicates the analysis. For postage stamps, we have identified ten major categories of defects.

Due to the complexity of stamp defects, several different severity surveys may be required to characterize the flaw categories. The stamp survey currently being conducted focuses on defects of the type found in currency. We are utilizing one-color intaglio stamps and the threecolor intaglio flag stamp. Based on our success in quantifying similar flaws in our currency flaw survey, we can now determine how the parameters differ between currency and postage stamps and evaluate the perceptual differences between the miniature artwork of postage stamps and the larger more complex artwork of currency.

The stamp survey has two components, the first to estimate thresholds between philatelic select (PS) and field grade (FG) stamps and between FG and rejects (R), as indicated by judges, and the second to assess more generally the functional relationship between quantified characteristics of stamp flaws and their appraisals by the judges.

The threshold component of the survey utilizes overlays containing designed flaws of progressive severity, superimposed on two-dimensional arrays of stamps. Different overlays enable comparisons of attributes that may be considered discrete, such as shape, (intaglio) colors, regions of the same or even different stamps, and perhaps multiplicity. Our early results indicate that the perceptual aspects of shape differences for circles and 3/1 rectangles are unimportant.

The functional relationship component of the survey will be more like the currency survey and will use designed and real flaws on blocks of nine stamps fixed to cards. The judges will be asked to sort the stamps into PS, FG, and R groupings, and within the FG group to further sort them into high, mid, and low range subgroups. This sorting scheme gives five individual stacks which can be assigned grades as in the currency survey.

---

1. University of Tennessee.
2. Engineering Physics Division, ORNL.

13.2.4 International Workshop

(C. K. Johnson, M. Burnett, C. Goodman,[1] D. McDonald[2])

A two-and-one-half day international workshop on Printing Flaw Standards for Machine Inspection was sponsored by the Bureau of Engraving and Printing and organized by the Oak Ridge National Laboratory in cooperation with the Technical Association for the Graphic Arts (TAGA). The workshop was held in parallel with the annual meeting of TAGA scheduled for the same two-and-one-half days (March 30 through noon of April 1, 1987) at the U. S. Grant Hotel in San Diego.

The main purpose of the workshop was to initiate the establishment of international flaw standards which can facilitate the specification of functional requirements for machine inspection equipment. The workshop participants were from the international community of security printers with extensive experience in the production of printed security documents and from the international community of industrial machine inspection. Nineteen countries - Australia, Austria, Canada, Chile, China, Denmark, Finland, England, Germany, Italy, Japan, Korea, Mexico, Spain, Sweden, Switzerland, Thailand, and the United States - were represented by the sixty participants.

Each workshop participant served on one of six committees, each with a specific subtask of the overall flaw standards problem. The workshop chairman was Carroll Johnson of ORNL.

The findings of the workshop are addressed to the international community of security printers and will be published as part of the proceedings of the International Conference for Security Documents for the 21st Century described in Section 13.4.

---

1. University of Tennessee.
2. Engineering Physics Division, ORNL.

13.3 Printing Ink Chemistry and Technology

13.3.1 Ink Formulation

(C. K. Johnson, B. K. Williams,[1] M. Burnett, R. Cockett[1])

The problem of formulating an ink resembles at first sight the art of cooking. It is replete with heuristics, tricks of the trade, and highly specialized knowledge. Much of the knowledge behind the formulation and use of an ink is almost intuitive to the ink chemists, who know the characteristics of the press and process in which the formulation will be applied, the abilities of the press operators to make the ink "work," and a myriad of other incidentals. Based on this characterization, our initial approach to the ink formulation problem was to use Artificial Intelligence (AI) Expert Systems methodology.

Recently, the main project emphasis has switched from the use of Artificial Intelligence as the principle methodology to its use in more of a supporting role. The reason for the change is that we were unable to accumulate sufficiently robust heuristics (i.e., empirical rules of experience) to provide comprehensive reasoning on ink printability. We found that more analytical modeling was required based on physical chemistry principles and have selected mixture dispersion and solubility, modeled via Hansen parameters, as the principle representation.

Hansen parameters describe nonpolar, polar and hydrogen-bond interactions between molecules. These parameters may be interpreted as a three dimensional geometric space with different molecules lying at their characteristic points in this space. The Hansen parameters do not represent a rigorous modeling of chemical principles, and reasoning based upon Hansen parameter geometry will be less valid in some situations than in others. Aqueous solutions may be particularly troublesome for the Hansen theory. Various extensions of Hansen parameter formulation are given in the literature and it may eventually be necessary to use one of the more comprehensive treatments.

Our working hypothesis about interpretation of ink formulas in the 3-dimensional Hansen parameter space is that the configuration of points representing the components for a "good ink" of a certain type will be "isomorphic" to the configuration of points for other good inks of that type. The term isomorphism in mathematics means that a one-to-one correspondence exists between the elements of two sets such that the results of an operation on elements of one set corresponds to the result of the analogous operation on their images in the other set. The basis for this hypothesis is that the distances between points in Hansen space reflect the mutual solubility of the compounds represented. The solubilities in turn reflect rheological behavior which influence printing properties.

The isomorphism mainly involves distance geometry. In a three component system with two of the components fixed, we can rotate the third point about an axis through the two fixed points and generate a circle. Any compound with Hansen parameters on or near that circle should act as a substitute for the third member of the original series. In a four component system with three of the components fixed, a mirroring of the fourth point through the plane through the first three points also should produce an isomorphic configuration. Once the locus of equivalent points is determined, chemical group additivity relationships for Hansen parameters can be applied to generate candidate chemical structures. A more general description of the mapping is rigid-body

movement of the arbitrarily complex configuration of points, or rigid-body motion combined with the mirroring operation.

1. University of Tennessee

13.3.2 Ink Adhesion Determination

(C. K. Johnson, M. Burnett, C. Harrison,[1] R. Sherrod,[1] B. Jatko,[2] R. Schmoyer[3])

Ink durability, printability, and color are all of primary consideration in ink formulation. Although we have mainly concentrated on the color and printability aspects to date, we must now also consider durability. Durability includes resistance of ink loss to crumpling, abrasion, and common chemicals such as laundry detergent and bleach.

Crumpling resistance appears to be the most important test which must be met for satisfactory currency ink durability. The testing procedure used at the Bureau requires rolling a 2.5" square sample of printed currency into a cylinder with roughly the diameter of a cigarette and then compressing the cylinder end-on to about the size of a cigarette filter. The crumpled sample is then opened and flattened out, rerolled at 90 degrees to the previous rolling direction, and compressed end-on again. This process is normally repeated until a note undergoes 4, 8, 12, 16, 24, or 32 crumplings.

In our research on measuring ink loss from crumpled currency samples, we have collected digitized image data from currency and processed that data into histograms containing pixel count as a function of gray level intensity. We have been successful in fitting the data to a model consisting of two overlapping Gaussian density functions. In this model, parameters of interest are amplitude (i.e., area inclosed), position (i.e., center of peak along the X axis), and band width (i.e., full width at half maximum). Comparison of these parameters from series of banknotes with different degrees of crumpling provides calibration curves interpretable in terms of ink redistribution and ink lost due to crumpling.

During initial experimentation, we digitized note samples and applied a nonlinear least-squares refinement method to exhibit the usefulness of the model. This series of tests showed the model would work, even in further tests where we performed region-averaging tests to simulate the effect of data collection at different pixel-to-pixel resolution values.

The focus of our research now is to develop a stand-alone system for automatic collection of histogram data and automatic analysis of that data with minimal operator intervention. We currently have two machines which could possibly be used for further development and production work. The first is a Sun workstation with a Data Cube image processor attached, which is located at our facility in Oak Ridge, and the second is a Rank Videometrix system located at the BEP. It has not yet been determined which system would be better for actual data collection and analysis since neither machine is configured optimally for this task at present. Both machines are currently being upgraded.

Preliminary experiments required handguided refinement in which parameters were estimated, refined, and re-estimated until suitable initial estimates were found. For the final system, a robust method of data analysis without operator intervention is necessary. We are experimenting with different procedures to circumvent some of the nonlinear least squares problems.

1. University of Tennessee.
2. I&C Division, ORNL.
3. Engineering Physics Division, ORNL.

13.4 International Conference Organization

(C. K. Johnson, M. Burnett, C. Goodman,[1] C. Steele, B. Reesor[2])

Two international conferences and an international workshop (see 13.2.4) were organized and carried out during the past year. Organizing and conducting three international meetings held within a six month period can be

rather hectic. During the month of February 1987, 300 letter, cable and telex communications were sent by ORNL to prospective attendees in preparation for the March workshop and April conference.

---

1. University of Tennessee.
2. F&M Division, ORNL.

13.4.1 Machine Inspection of Printed Security Documents

The first International Conference on Machine Inspection of Printed Security Documents (MIDSP) was held on September 25-26, 1986, in Long Beach, California. The conference was sponsored by the Bureau of Engraving and Printing (BEP) and organized by the Oak Ridge National Laboratory (ORNL) and the Machine Vision Association (MVA) of the Society of Manufacturing Engineers (SME) which conducted their own conference, VISION WEST, on September 23-24. Both conferences were held in the newly opened Ramada Renaissance Hotel. The conference was attended by 147 participants representing 16 countries.

The first day was chaired by Milton Seidel, Assistant Director of Research and Engineering at the BEP. In his opening remarks Mr. Seidel outlined the objectives of the conference as two-fold. The BEP hopes first "..to generate an interest in machine inspection of security documents by potential suppliers"; and second, to provide a forum for the exchange of information on the current state-of-the-art of machine inspection systems (either already in operation or in the process of development) for the examination of currency and postage stamps.

Twenty speakers from Canada, Denmark, France, Italy, Japan, Sweden, Switzerland, and the United States discussed their experience and plans for automated inspection.

13.4.2 Security Documents For The 21st Century

The two-and-one-half day International Conference on Security Documents for the 21st Century was sponsored by the Bureau of Engraving and Printing and organized by the Oak Ridge National Laboratory in cooperation with the Technical Association of the Graphic Arts (TAGA). The conference followed the annual meeting of TAGA scheduled for March 30 through noon of April 1 at the same location. The opening session of the conference on Wednesday, April 1, 1987, was in the Grand Ballroom of the U. S. Grant Hotel. The conference sessions on Thursday and Friday, April 2 and 3, were at the Convention and Performing Arts Center in San Diego.

The objective of the conference was to establish a 10- to 15-year perspective on the requirements and technology for printed security documents having monetary or importance value and for high technology complements and alternatives to printed documents. In addition to currency and postage stamps, these include documents with creditorship, ownership, authorization, or identification functions as well as items such as optically variable devices and SmartCards.

There were 173 attendees from 20 countries. The speakers were from Australia, Canada, England, France, Germany, Italy, Japan, Netherlands, Spain, Sweden, Switzerland, Thailand, and the United States. The proceedings of the conference will be edited and published by ORNL and should be available in July.

14. SPECIAL TOPICS

14.1 Conservation Programs

The work summarized in this section provides physicochemical support to programs in the Engineering Technology Division (14.1.1 and 14.1.3) and in the Energy Division (14.1.2). The heat storage alloy work (14.1.1) is sponsored by the Department of Energy through its Office of Energy Storage and Distribution. The Thermal Energy Storage Program of this Office is managed by Oak Ridge National Laboratory, and has as its objectives the identification and development of thermal storage technologies which, when implemented, will increase the efficiency of heating and cooling systems for buildings or provide a mechanism for use of waste energy in industrial processes. The work on absorption heat pumps (14.1.2) is sponsored by the Department of Energy's Office of Industrial Programs. The Chemical Heat Pump Program has as its aim the recovery of waste heat at intermediate temperatures in industrial processes by means of heat pumps driven by chemical reactions (CHP) or by sorption/desorption processes (AHP). Consultation is provided on solution thermodynamics and thermochemistry for use in the identification of fluid pairs capable of providing higher coefficients of performance at higher temperatures than those in use currently can provide. The work on LiH properties (14.1.3) is in support of SDI programs and is sponsored by the Air Force Wright Aeronautical Laboratories, Aeropropulsion Laboratory.

14.1.1 Hypereutectic Heat Storage Alloy
(M. R. Bennett and J. Braunstein)

Si-encapsulated Al-Si alloys have been proposed[1] for phase-change heat storage to recover industrial waste heat. Experiments were done to determine the stability of the interface between silicon metal and an eutectic alloy of aluminum and silicon to thermal cycling.[2] Silicon bars in contact with bars of Al-Si eutectic (577°C) were thermally cycled between 530°C and 600, 650 or 700°C, sectioned, and the interface examined by photomicrography and by scanning electron microscopy. At 650°C and above, wetting and interpenetration occur, as seen in the photomicrograph and in the electron micrographs in Fig. 14.1. Such "roughening" of the interface, of the order of 0.15 - 0.25 mm thick, suggests that application of Si-encapsulated Al-Si shot probably is not feasible for temperatures of 700°C and above, where extensive degradation occurs. Application at temperatures up to 600°C probably is feasible if the somewhat reduced storage capacity is acceptable and if temperature excursions can be avoided. There is then little advantage to Siencapsulation over encapsulation by an inert material, as the latent heat available would be primarily that of the eutectic core, with little contribution from a partially dissolving and reprecipitating shell.

---

1. C. E. Mobley and R. A. Rapp (Principal Investigators) "Hypereutectic Heat Storage Shot," Research proposal submitted by Ohio State University Research Foundation, OSURF #17062-55-00, Aug. 10, 1983.
2. M. R. Bennett and J. Braunstein, "Silicon Integrity in Molten Al-Si Eutectic," ORNL/TM-10380, in preparation.

14.1.2 Solution Thermodynamics for Modeling Ideal Absorption Heat Pump Fluids[1]
(J. Braunstein)

The aim of this work is to represent thermodynamic properties of mixtures in a computer optimization program for characterizing fluids with improved coefficient of performance (COP) in absorption heat pump (AHP) cycles.[2-4] A compromise with few enough parameters to be manageable, but sufficient to represent variations of sign,

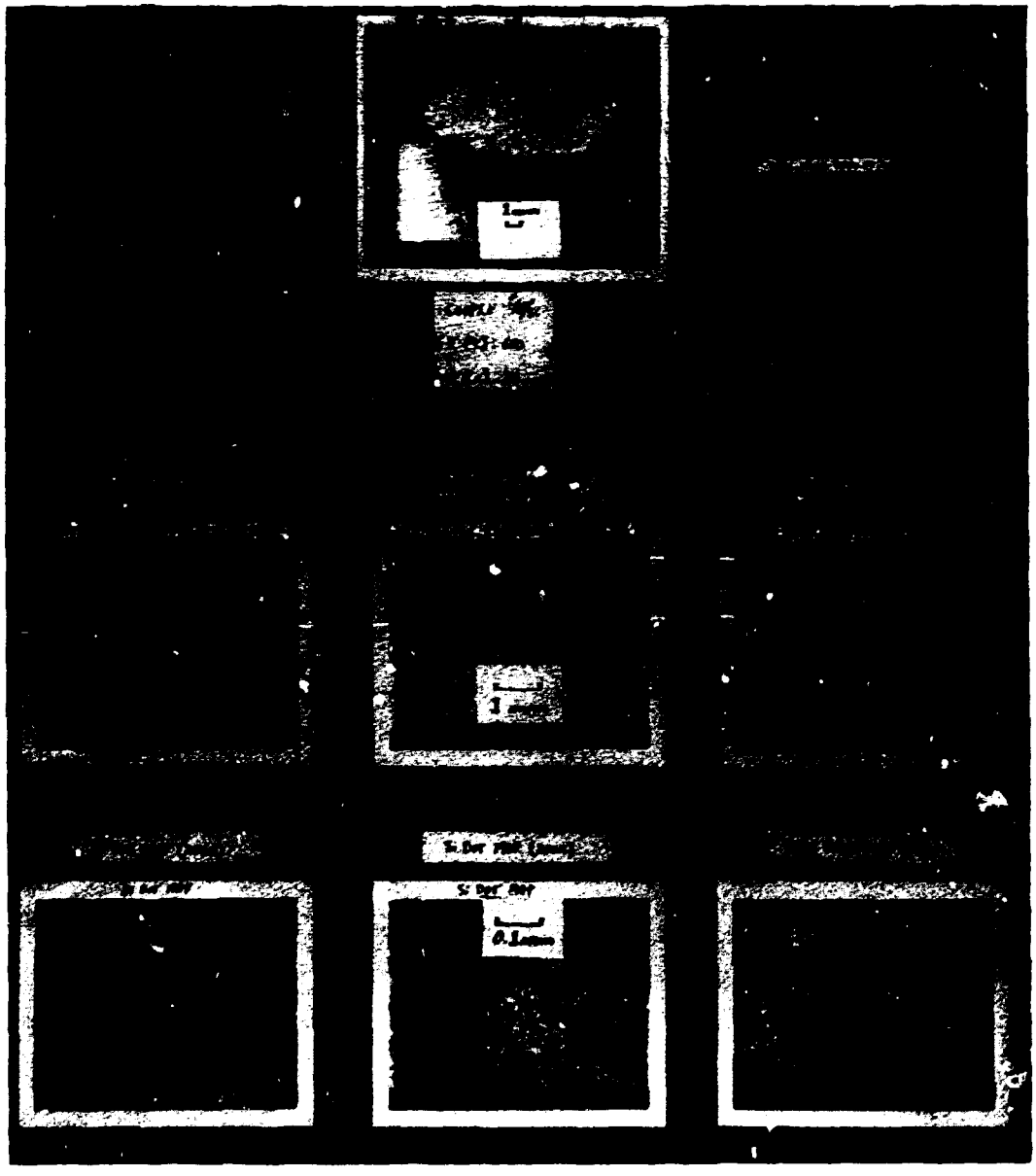

Fig. 14.1. Photomicrograph (top) and electron micrographs at two magnifications showing: (left) Al dots maps, (center) Si dot maps, and (right) electron backscattering micrographs.

magnitude and forms of composition and temperature dependence of the excess free energies and heats of mixing is the molal excess free energy function $G^E = \alpha_F\{1+(\beta-1)x\}x(1-x)$; $\alpha_F = [K-MT+LT(1-\ln T)]$; x is the mole fraction of one component, T the temperature.[1] The derivatives with respect to temperature and composition give partial excess enthalpies with Margules type composition dependence and linear temperature dependence, Margules type activity coefficients, and nonzero excess entropy. Other parameters optimized are the vapor pressures, heats of vaporization and heat capacities at a reference temperature. Thermodynamic relations then give vapor pressure, heat of vaporization and heat of mixing at temperatures and compositions in the heat pump

cycle. Figure 14.2 shows vapor pressure-temperature plots for hypothetical refrigerant solutions that would provide a coefficient of performance 90% of Carnot efficiency. The results demonstrate that the ideal fluid model approach can be a useful guide in the search for fluid pairs giving improved COPs in AHPs[1] and suggest additional steps required in matching the parameters to those of real systems.

1. H. Perez-Blanco, M. R. Patterson and J. Braunstein, Ideal Fluid Properties for Optimizing Absorption Heat Pump Performance, ORNL/TM-10315 (1987).
2. S. I. Kaplan et al., A Survey and Assessment of Chemical Heat Pumps, ORNL/TM-9544 (Dec. 1985).
3. H. Perez-Blanco, "Working Mixtures for Industrial Chemical Heat Pumps," Proceedings of Second BHRA International Symposium on the Large-Scale Applications of Heat Pumps, York, England, 1984.
4. M. R. Ally, Thermodynamic Properties of Aqueous Ternary Solutions Relevant to Chemical Heat Pumps, ORNL/TM-10258, 1987.

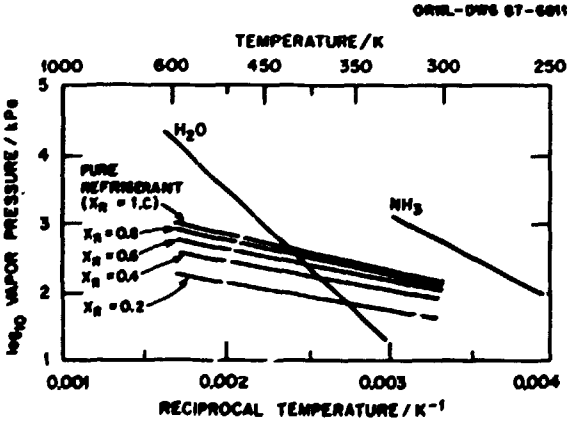

Fig 14.2. Vapor pressure (logarithmic) versus reciprocal temperature for optimized refrigerant-absorbent mixtures for absorption heat pump cycle. Plots for pure H_2O and pure NH_3 are included for comparison.

14.1.3 Lithium Hydride Properties for Thermal Energy Storage

(J. Braunstein)

Because of its high molar heat of fusion and low formula weight, encapsulated LiH is a candidate for thermal energy storage at temperatures in the vicinity of 1000 K.[1] The capsules of LiH would be packed in a bed through which a heat exchange fluid is passed. Proper design requires an extensive knowledge of the thermophysical properties and of the effects of impurities, dissociation products and corrosion products. Container materials must have resistance to fracture and corrosion, and low hydrogen permeability. The calculated[2] partial predominance area diagram in Fig. 14.3, for the

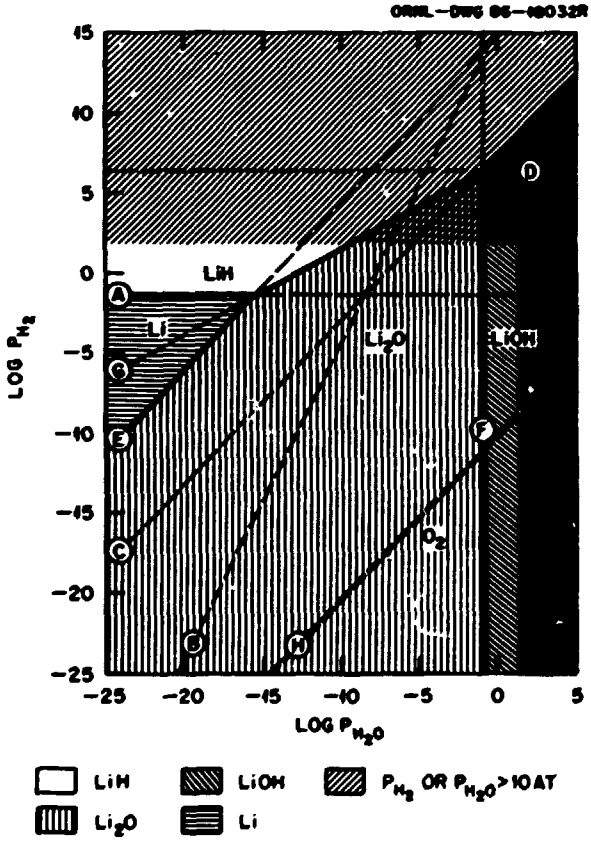

Predominance Area Diagram for LiH, Li, Li_2O, LiOH, H_2O, H_2 at 1000 K.

Fig. 14.3. Pressures of H_2 and of H_2O at which condensed phases of LiH, Li, Li_2O and LiOH are stable at unit activity at 1000 K.

phases Li, LiH, Li_2O and LiOH, suggests the complexity of the system. Because many metals are permeable to hydrogen, and many ceramics are unstable to lithium, the dissociation of LiH poses conflicting demands on containment materials. A survey is in progress of phase diagrams, dissociation pressure, heat capacity, heat of fusion, thermal conductivity, viscosity, surface tension, wetting angle, and isotope effects. Because of the small molecular Li isotope effect, the enthalpy of fusion per unit mass and the transport properties, such as fluidity and thermal conductivity, may show significant enhancement with ^{6}LiH over ^{7}LiH.

1. D. G. Morris, J. P. Foote and M. Olszewski, Development of Encapsulated Lithium Hydride Thermal Energy Storage for Space Power Systems, ORNL/TM-10413 (in preparation).
2. I. Barin, O. Knacke and O. Kubaschewski, Thermochemical Properties of Inorganic Substances, Springer Verlag, Berlin, 1973 and Supplement 1, 1977.

14.2 Regeneration of Spent Activated Carbon (P. C. Ho)

The U.S. Army Toxic and Hazardous Materials Agency (USATHAMA) and the U.S. Environmental Protection Agency (EPA) have undertaken a joint effort to determine the feasibility of using the EPA mobile carbon regenerator at U.S. Army installations to regenerate spent activated carbon laden with explosives. ORNL, with the Engineering Technology Division having the lead role, is assisting the USATHAMA in assessing methods for regenerating carbons saturated with explosive wastes. The Chemistry Division is involved in two of the project tasks. The first is to evaluate the technical and safety aspects of the present methods (mostly thermal) used to regenerate spent explosive-contaminated carbons. The second is to characterize the chemicals adsorbed in the spent carbon. To date, the technique most frequently used to clean explosive-contaminated (mostly nitro organic compounds) waste water in military munition facilities is by adsorption on granular activated carbon. When the activated carbon becomes exhausted, the spent carbon is either incinerated or buried. This is not only costly but also leads to air and water pollution. The object of the present study is to develop an effective, safe, and economical method to regenerate the spent carbon and, at the same time, destroy the hazardous chemicals sorbed by the carbon.

During this reporting period, studies were made on the adsorption of a model compound explosive 2,4-dinitrotoluene (DNT) on two Calgon granular activated carbons (Filtrasorb FS300 and FS400). Both carbons proved to be excellent adsorbers for the removal of DNT from aqueous solution. Regeneration of spent FS300 and FS400 was performed by desorption of the adsorbed chemicals using solvent extraction. The solvents tested were water, acetone, methanol, and acetone/water and methanol/water mixtures. Acetone, methanol and their 1:1 mixtures with water proved to be effective solvents. In most cases, the regeneration was greater than 85% effective. Analysis of the solvent extracts revealed that, in the solution, besides DNT several other chemicals were present as well. Three of the chemicals (or byproducts) were identified by GC/MS and HPLC as 2,4-dinitrobenzyl alcohol, 2,4-dinitrobenzaldehyde and 2,4-dinitrobenzoic acid.[1] This suggests that after DNT was adsorbed by the carbon, chemical reactions (such as oxidation) occurred. This could be expected as it is well known that activated carbons are highly porous materials with a large surface area containing various chemically reactive groups such as radicals, carbonyl groups, and oxides, etc.[2]

Solvent regeneration of explosive-contaminated carbons is an attractive and promising process. Not only is the extent of regeneration high, but the process is also safe and economical. Solvent regeneration can be done in situ, and the solvent used for regeneration

can also be recovered for reuse. In addition, the desorbed chemicals can be refined for reuse or simply destroyed. In contrast, when the concentration of explosive in the carbon is high (sometimes the concentration of explosive is higher than 50%), the inherent violent nature of the explosive can cause problems when the spent carbon is treated by the conventional thermal processes.

1. P. C. Ho, Environ, Sci. & Technol. 20, 260 (1986).
2. J. B. Bonnet, Carbon 6, 161 (1968).

14.3 Microemulsion Fuels

(A. L. Compere, W. L. Griffith, J. S. Johnson, Jr.[1])

Incorporation of fuel additives in microemulsion dispersions provides wider options of modifying compositions without degrading engine performance from inhomogeneity than one has when the additives have to be hydrocarbon soluble. For example, aqueous microemulsions in diesel fuel have been shown to affect substantially NOX, SOX, particulates, hydrocarbon, and CO emissions. However, reports conflict on the extent, and even the direction, of effects of water and other additives. To resolve some of the discrepancies, we have been investigating the size and structure of dispersions by small-angle neutron scattering. These will be correlated with engine tests performed by a cooperative program.

In last year's report and in a journal publication,[2] we presented results for several compositions, comprised of potassium oleate, 1-pentanol or 1-hexanol, hexadecane, and water; various contrasts in scattering power were achieved by using deuterated components. Reasonably satisfactory fits to the patterns were achieved by postulating monodisperse oblate ellipsoids of axial ratio about a half, with an aqueous core surrounded by a shell of surfactant and alcohol - hydrocarbon, penetrated to an extent by hydrocarbon of solvent or of other particles. The dimension of the cores, in terms of radii of spheres of equivalent volume, increased from about 18 to 38 Å as the volume fraction of water increased from 10 to 30%, the ratios of other components being approximately constant.

For quantitative interpretation, one must use, as we do here, model compositions of pure compounds. Qualitatively, we have observed similar patterns with practical components, for example, with diesel fuel as hydrocarbon and vegetable oils as surfactants. We have further confirmed pertinence by extending compositional range to an ashless surfactant counterion (ethanolamine), to partial neutralization of the surfactant, and to an aromatic hydrocarbon (toluene).

Substitution of ethanolamine for potassium-oleate did not cause drastic changes in the patterns for a given composition when the surfactant was fully neutralized. Decreasing the degree of neutralization increased the size of the particles (Fig. 14.4). To a rather good approximation, half of a reference concentration of fully neutralized

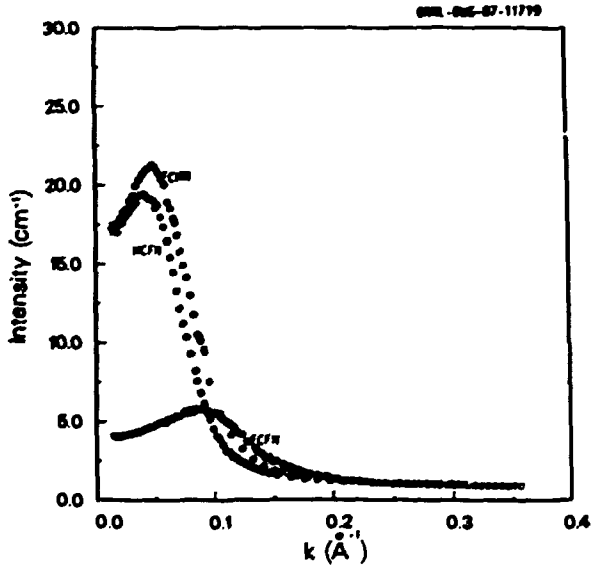

Fig. 14.4. SANS scattering patterns of FCFN, FCHN, and HCFN ethanolamine oleate microemulsions in hexadecane.

(HCFN) gave the same pattern as the reference concentration half neutralized (FCHN).

In contrast to our prior procedure of fitting individual patterns, we have now developed programs which simultaneously fit patterns of the same chemical composition but with components of different isotopes. Although the fits are not expected to be as close because of minor variations between compositions and experimental conditions, as well as deuterium/hydrogen isotope effects, simultaneous fits are more convincing evidence of the validity of models. Figure 14.5 is an example. The parameters obtained are close to those previously reported for a similar potassium oleate composition (A of reference 2).

Our analysis of the toluene formulations is as yet preliminary. To obtain stable microemulsions, we used tertiary butyl alcohol as cosolvent and a higher water content; the composition (volume fractions) is similar to that of solution B of the potassium oleate study (44 moles of water/mole ETA oleate). The same structural

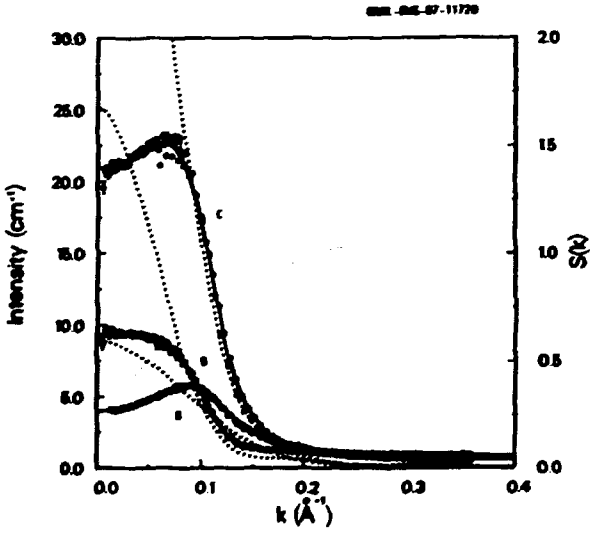

Fig. 14.5. SANS pattern from ethanolamine oleate microemulsion in hexadecane showing the contrast provided by selected isotope labeling of different components: (B) D2O, hexadecane; (C) H2O, hexadecane-d34; (D) D2O, hexadecane-d34. FCFN.

model appears to be applicable, and the dimensions are similar to those of B. In this case, we also varied the isotope labeling of the alcohol, by using fully deuterated and protonated butanol. The patterns indicated clearly that alcohol was distributed between core, shell, and continuous phase, rather than only between shell and solvent as in the case of pentanol and hexanol.

---

1. Consultant.
2. E. Caponetti, L. J. Magid, J. B. Hayter and J. S. Johnson, Jr., Langmuir 2, 722 (1986).

14.4 The Expert System for Chemistry: Planning Syntheses and Polymer Degradation

(W. E. Thiessen, J. D. Allen, Jr.[1])

In this report, we describe the continuation of our effort to develop Artificial Intelligence techniques for application to organic chemical syntheses, the work to date on a new project (sponsored by ECUT) whose focus is the extension of our previously developed AI methods to the domain of polymer conversion and degradation, and lastly, the exploration of the utility of neural net technology in capturing the methodology of the synthetic organic chemist.

Our recent work on the OPS-5 synthesis programs has focused on implementing more effective techniques for deciding which of several potentially applicable retro-synthetic steps should be invoked. Central to this task has been the introduction into the programs of even more abstract representational schemes not only for the molecules of interest, but for properties of chemical importance in terms of which decisions should be made. Of these schemes, the "vertex" based representation of chemical structure and the canonical tree representation of vertex relationships have proved of primary importance.

For our purposes, the vertices are carbon-, oxygen-, or nitrogen-centered descriptions of the chemical environment immediately surrounding the center. A body of a few hundred rules has

the task of discovering all vertices in a molecule, noting the associated atoms and the bonding structure, and naming the vertices by type and class. Type names are sufficiently specific that detailed molecular structure is apparent, whereas class names are intended to capture the essential chemical characteristics of the vertex.

The programs build two new representations of a molecule based on the vertices, the first, a "vertex connectivity," the second a "canonical tree" representation which captures in a collection of ordered trees the chemical environments relative to all the points in the molecule which the program considers "interesting." The principal utility of the vertex connectivity representation lies in its support of the construction of very general chemical transformation rules (the target sites to which we have referred in previous reports). In fact, it is our plan to express most, if not all, of the older, and generally too specific, target sites in this new mode. It is probably obvious that constraining the application of rules of such a general nature will require more care than the constraining of those of the earlier form. However, it appears that the constraints themselves can be represented in the new form as well and may prove both easier to formulate and more economical of code than was previously the case.

The property of the canonical tree representation which so excites us is its apparent capacity to produce from two similar (but not necessarily identical) molecules, perspectives which are computationally easy to identify as similar. We anticipate that we will be able to write code capable of comparing an unfamiliar molecule with a set of known molecules whose properties (among them, synthesis methods) are known and thus quickly to generate an approximate synthesis plan for the unknown entity.

The polymer conversion work began as a two-phase attempt to construct one or more Expert Systems capable of suggesting single- or multi-step degradation schemes for polymers and mixtures of polymers of industrial importance. The first (and still ongoing) phase involved exhaustive application of modified (direction reversed) versions of our existing synthesis programs to the codification of our knowledge of known polymer reactions. Although this phase was to serve as much to further educate us as to refine the programs, some interesting reaction possibilities have emerged. Nevertheless, it was clear from the beginning that even with massive modifications, the original programs were unlikely to produce novel chemistry with any regularity and that only programs capable of capturing and applying with intelligence the essence of chemical mechanisms were likely to be adequately inventive. Production rule programs embodying these capabilities are the focus of the present second phase task, some features of which we discuss briefly below.

One of the important components of the new programs is a body of rules intended to capture the general notion of the "reactive intermediate." It is our goal to produce code so complete that when it operates on a polymer molecule, it will be capable of proposing (within specified constraints on potential reaction conditions, reagents, and the like) all mechanistically possible reactive intermediates. A second (suitably constrained) body of rules must capture knowledge about the transition between reactive intermediates and final states. Although examples of the reactive intermediate generation rules are in place, we are only beginning to consider the codification of constraint knowledge. This is intentional, for we have found in every previous case that it is useful to produce an essentially constraint free system, study its behavior, and construct the constraint knowledge base in a manner suggested by results of our study. We have begun to formalize the chemical characteristics which these constraints should take, but will write code only after extended observation of the unconstrained system at work.

We have noted elsewhere that one of the long range goals of any Artificial Intelligence work involving production rule programs should be the development of a system capable of independent

learning of, and analogical thought about, the tasks which comprise the domain of the work. Among other things, such a system should be characterized by a constantly evolving understanding of both its successes and its failures, should be capable of developing a variety of representations or perceptions of relations among the constituents of its domain, and should be able to make deductions and predictions in the absence of complete, or completely accurate information about the entities (in our case molecules) which it is asked to consider. Although it is possible to construct production rule systems of sufficient complexity and depth to exhibit some of these characteristics to a limited degree, the incompleteness inherent in the very act of representing expert knowledge as productions inevitably limits the flexibility the resulting systems can exhibit in dealing with the unfamiliar.

Over the last year, we have begun to explore the possibility of employing neutral net technology for the development of systems for learning about and reasoning by analogy about organic chemical synthesis. The ultimate system would be capable of learning by example (we would teach it by "flash cards"), reasoning by analogy about unfamiliar syntheses problems, developing a variety of chemical "perspectives" of a molecule, explaining its behavior, even a sort of "AH HA" insight into the clever special cases which characterize so many of the great syntheses. Clearly, it will be some time before such a competent system can be fully operational. In fact, so considerable will be the number of neurons in such a system (at least millions) that dedicated architectures will surely be required for realizing acceptable speeds of execution. We are, in fact, pursuing two such architectures (a dedicated neural net processor for a PC host and a custom VLSI based neural net machine). There are several preliminary tasks which can (indeed must) be addressed on a smaller scale before a full system is constructed. The simplest of these involves building a neural net system capable of accepting molecular structures in normal graphical form and transforming these into coordinate free, orientation independent, canonical representations. We have produced neural net code capable of performing this task quite efficiently. In order to acquire some understanding of the relationships between task definition and network complexity, we are building a small neural system which we will try to teach to recognize molecules, if not by name, at least (and indeed more interestingly) by class. Since such a system, if complete, would need to understand most of the concepts in terms of which general chemical descriptions are constructed, we shall for the present concern ourselves with a limited set of quite small molecules spanning not more than a few classes.

---

1. Consultant, Instrumentation and Controls Division, ORNL.

14.5 Development of DNA-Specific Cytochemical Stains for Electron Microscopy

(S.-H. Kim,[1] B. A. Moyer, D. P. Allison,[2] A. L. Olins[3])

In spite of remarkable growth in the use of electron microscopy (EM) in the life sciences, a reliable DNA-specific cytochemical stain for EM has not been developed. Our goals in this 1-year Seed Money project are to (1) synthesize and chemically characterize useful DNA-specific stains, (2) demonstrate selective DNA staining, and (3) initiate studies of the chemical mechanism involved in the staining procedure.

Using a previously reported synthetic method,[4] we have found that the crude product of the reaction of $Na_2[Os^{IV}Cl_6]$ with aqueous ammonia at 100 °C for 12 h in a closed system behaves as an effective DNA-specific stain for EM using a Feulgen[5] staining procedure on a thin section of epoxy-embedded rat liver. The advantages of this stain over a previously reported[5] ill-defined and difficult-to-use "osmium amine" material include good staining reproducibility and low stain consumption; e.g., 5-10 mg of the new stain is enough for the procedure whereas 50-100 mg of "osmium

amine" was typically employed. Using cation exchange chromatography, we have separated the crude stain into three components, which are currently being examined individually to determine staining ability and chemical identity. Analytical and spectroscopic results show that one of the components is a previously reported compound (A) postulated[4,6] to be a nitrido-bridged Os(IV) dimer with the structure

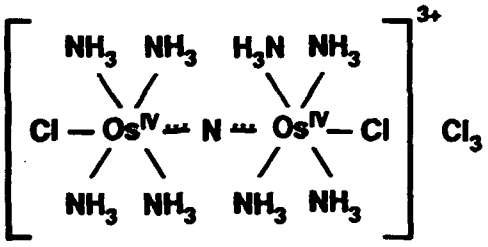

A

μ - Nitrido Dimer

Under modified reaction conditions (150 °C, 72 h, Ar atmosphere), we have found that A becomes the dominant reaction product and may be isolated directly from the reaction mixture in improved yield (65%) without the need for chromatographic purification. The IR spectrum of one of the other components (B) of the crude stain suggests that it, too, is a nitrido-bridged dimer, but chemical analysis shows that it contains a higher chloride:ammonia ratio than A. Synthetic work in progress shows that the anaerobic reaction of $Na_2[Os^{IV}Cl_6]$ with liquid ammonia for 12 h at -33 °C gives a product spectroscopically identical to B and may be a convenient alternate preparative route.

---

1. Oak Ridge Associated Universities Postgraduate Research Fellow.
2. Biology Division, ORNL.
3. University of Tennessee, Knoxville, TN.
4. M. J. Cleare and W. P. Griffith, J. Chem. Soc. (A), 1117 (1970).
5. R. Cogliati and A. Gautier, C. R. Acad. Sci. Paris 276, 3041 (1973).
6. F. P. Dwyer and J. W. Hogarth, Proc. Roy. Soc. of N. South Wales 84, 117 (1951).

PUBLICATIONS, PRESENTATIONS, AND PATENTS

COAL CHEMISTRY

Publications

B. M. Benjamin and E. C. Douglas, "New Chemical Structural Features of Coal. The Structure of Coal Products," Fuel 65, 1735 (1986).

B. M. Benjamin, E. C. Douglas, and E. W. Hagaman, "New Chemical Structural Features of Coal. Reactions of Some Components of a Texas Lignite," Energy and Fuels 1, 187 (1987).

A. C. Buchanan, III, T. D. J. Dunstan,[1] E. C. Douglas, and M. L. Poutsma, "Enhancement of Free-Radical Chain Rearrangement, Cyclization, and Hydrogenolysis During Thermolysis of Surface-Immobilized Bibenzyl: Implications for Coal Chemistry," J. Am. Chem. Soc. 108, 7703 (1986).

A. C. Buchanan, III and M. L. Poutsma, "Organic Chemistry of Coal," ORNL Review, No. 3, 181 (1986).

A. C. Buchanan, III and C. A. Biggs, "Thermolysis of Surface-Attached 1,3-Diphenylpropane. Impact of Surface Immobilization on Thermal Reaction Mechanisms," Preprints, Am. Chem. Soc., Div. Fuel Chem. (in press).

R. R. Chambers, Jr., E. W. Hagaman, and M. C. Woody, "Selective Functionalization of Coal Model Compounds Based on Benzylic Hydrogen pK_a Differences: Alkylation," Fuel 65, 895 (1986).

R. R. Chambers, Jr., E. W. Hagaman, and M. C. Woody, "Selective Methylation of Hydroaromatic Sites in Coal: The Importance of Fluorene-Like Structural Units in Bituminous Coals," Preprints, Am. Chem. Soc., Petr. Div. 31, 803 (1986).

R. R. Chambers, Jr., E. W. Hagaman, and M. C. Woody, "Selective Methylation of Hydroaromatic C-H Sites in Coal: The Importance of Fluorene-Like Structural Units in Bituminous Coals," Chemistry of Polynuclear Aromatic Compounds, ACS Symposium Series (in press).

E. W. Hagaman, R. R. Chambers, Jr., and M. C. Woody, "Determination of the Fraction of Organic Carbon Observable in Coals and Coal Derivatives Measured by High-Resolution Solid-State Carbon-13 Nuclear Magnetic Resonance Spectrometry," Anal. Chem. 58, 387 (1986).

J. S. Johnson,[2] C. G. Westmoreland, F. H. Sweeton,[2] K. A. Kraus,[2] E. W. Hagaman, W. P. Eatherly,[3] and H. R. Child,[4] "Modification of Cation-Exchange Properties of Activated Carbon by Treatment with Nitric Acid," J. Chromatography 354, 231 (1986).

G. Wulfsberg,[5] A. C. Buchanan, III, I. Rubin,[6] A. Weiss,[7] D. A. Davis,[5] K. Bass,[5] R. W. Todd,[5] and C. Jui,[5] "Studies of Fluxionality in Pentachlorocyclopentadienylmercurials $RHgC_5Cl_5$ by Solution and Solid State ^{13}C NMR and by ^{35}Cl NQR Spectroscopy," Z. Naturforsch. 41, 175 (1986).

Presentations

R. R. Chambers, Jr., E. W. Hagaman, and M. C. Woody, "Selective Methylation of Hydroaromatic C-H Sites in Coal: The Importance of Fluorene-Like Structural Units in Bituminous Coals," Division of Petroleum Chemistry, American Chemical Society National Meeting, Anaheim, CA, Sept. 7-12, 1986.

---

1. US DOE Postgraduate Research Training Participant.
2. Consultant.
3. Metals & Ceramics Division.
4. Solid State Division.
5. Middle Tennessee State University, Murfreesboro, TN.
6. Analytical Chemistry Division.
7. Technische Hochschule, Darmstadt, FRG.

AQUEOUS CHEMISTRY AT HIGH TEMPERATURES AND PRESSURES

Publications

H. F. Holmes and R. E. Mesmer, "Isopiestic Studies of Aqueous Solutions at Elevated Temperatures. VIII. The Alkali Metal Sulfates," J. Chem. Thermodyn. 18, 263 (1986).

H. F. Holmes and R. E. Mesmer, "Thermodynamics of Aqueous Solutions of the Alkali Metal Sulfates," J. Solution Chem. 15, 495 (1986).

H. F. Holmes, R. H. Busey,[1] J. M. Simonson, R. E. Mesmer, D. G. Archer,[2] and R. H. Wood,[3] "The Enthalpy of Dilution of HCl(aq) to 648 K and 40 MPa. Thermodynamic Properties," J. Chem. Thermodyn. (in press).

M. H. Lietzke[1] and W. L. Marshall, "Sodium Sulfate Solubilities in High Temperature Aqueous Sodium Chloride and Sulfuric Acid Solutions — Predictions of Solubility, Vapor Pressure, Acidity, and Speciation," J. Solution Chem. 15, 903 (1986).

W. L. Marshall, "Electrical Conductance of Liquid and Supercritical Water Evaluated from 0°C and 0.1 MPa to High Temperatures and Pressures. Reduced State Relationships," J. Chem. Eng. Data (in press).

W. L. Marshall, "High Temperature Aqueous Solutions and Energy Considerations — Physical Chemical Studies," chapter in International Association for the Properties of Steam, Tenth Conference, Moscow, 1984, 1987.

W. L. Marshall, "Modified Raoult's Law Including the Solvent Structural Constant and Solute Solvation; Aqueous Sodium Chloride Solutions, 25 to 300°C; Other Electrolytes and Urea, 25°C," J. Solution Chem. 15, 439 (1986).

W. L. Marshall, "Reduced State Relationship for Limiting Electrical Conductances of Aqueous Ions Over Wide Ranges of Temperature and Pressure," J. Chem. Phys. (in press).

W. L. Marshall, "Solvent Structural Constant and Solvation Behavior Applied to the Description of Aqueous Electrolytes at 25-300°C," J. Chem. Soc., Faraday Transactions I 82, 2283 (1986).

W. L. Marshall and J. D. Frantz,[4] "Electrical Conductance Measurements of Dilute, Aqueous Electrolytes at Temperatures to 800°C and Pressures of 400 bars; Techniques and Interpretations," chapter in Research Techniques for High Pressure and High Temperature, Revised, ed. H. L. Barnes and G. C. Ulmer, in press.

R. E. Mesmer and W. L. Marshall, "Research on High-Temperature Water Solutions," ORNL Quarterly Review 3 (1986).

D. A. Palmer and R. van Eldik[5], "The Spectral Characterization and Kinetics of Formation of Hypoiodous Acid in Aqueous Solution," Inorg. Chem. 25, 928 (1986).

D. A. Palmer and S. E. Drummond, "Thermal Decarboxylation of Acetate. Part I. The Kinetics and Mechanism of Reaction in Aqueous Solution," Geochim. Cosmochim. Acta. 50, 813 (1986).

D. A. Palmer, D. Wesolowski, and R. E. Mesmer, "Potentiometric Investigation of the Hydrolysis of Chromate(VI) Ion in Sodium Chloride Media to 175°C," J. Solution Chem. (in press).

D. A. Palmer and D. Wesolowski, "The Acid Association Quotients of Tris(hydroxymethyl)aminomethane in Aqueous Sodium Chloride Media to 200°C," J. Solution Chem. (in press).

K. S. Pitzer[6] and J. M. Simonson, "Thermodynamics of Multicomponent, Miscible Ionic Systems: Theory and Equations," J. Phys. Chem. 90, 3005 (1986).

R. W. Ramette[7] and D. A. Palmer, "Thermodynamics of Tri- and Pentabromide Anions in Aqueous Solution," J. Solution Chem. 15, 397 (1986).

J. M. Simonson, R. N. Roy,[8] and J. J. Gibbons,[8] "The Thermodynamics of Aqueous Mixed Potassium Carbonate, Bicarbonate, and Chloride Solutions to 368 K," J. Chem. Eng. Data 32, 41 (1987).

J. M. Simonson and K. S. Pitzer,[6] "Thermodynamics of Multicomponent, Miscible, Ionic Systems: the System $LiNO_3$-KNO_3-H_2O," J. Phys. Chem. 90, 3009 (1986).

J. M. Simonson, R. N. Roy,[8] J. Connole,[8] L. N. Roy,[8] and D. A. Johnson,[8] "The Thermodynamics of Aqueous Borate Solutions I. Mixtures of Boric Acid with Sodium or Potassium Borate and Chloride," J. Solution Chem. (in press).

J. M. Simonson, R. N. Roy,[8] D. Mrad,[8] P. Lord,[8] L. N. Roy,[8] and D. A. Johnson,[8] "The Thermodynamics of Aqueous Borate Solutions II. Mixtures of Boric Acid with Calcium or Magnesium Borate and Chloride," J. Solution Chem. (in press).

J. M. Simonson, D. J. Bradley,[9] and R. H. Busey,[1] "Excess Molar Enthalpies and the Thermodynamics of (Methanol + Water) to 573 K and 40 MPa," J. Chem. Thermodyn. (in press).

Presentations

H. F. Holmes and R. E. Mesmer, "Thermodynamics of HCl(aq) to High Temperatures and Pressures," 69th Canadian Chemical Conference, Saskatoon, Saskatchewan, Canada, June 1-4, 1986.

W. Marshall, "Electrical Conductance of Liquid and Supercritical Water Evaluated from 0°C and 1 Bar to High Temperatures and Pressures," 193rd American Chemical Society National Meeting, Denver, Colorado, April 5-10, 1987.

R. E. Mesmer, "Aqueous Chemistry and Thermodynamics to High Temperatures and Pressures," Brigham Young University, Provo, Utah, April 3, 1986; Whiteshell Nuclear Research Establishment, Pinawa, Manitoba, May 15, 1986; 41st Calorimetry Conference, Annadale, NJ, August 17, 1986.

D. A. Palmer, "A Potentiometric Investigation of the Hydrolysis of Chromium(VI) in NaCl Solution to 175°C," 69th Canadian Chemical Conference: Symposium on "Chemical-Physical Properties of Electrolytes and Surfactants," Saskatoon, Saskatchewan, Canada, June 1-4, 1986.

D. A. Palmer, "Formation Constants for Ferrous Acetate Complexes in Aqueous Solution from 100 to 250°C and 250 to 1250 Bars," 69th Canadian Chemical Conference: Symposium on "Chemical-Physical Properties of Electrolytes and Surfactants," Saskatoon, Saskatchewan, Canada, June 1-4, 1986.

D. A. Palmer, "Metal Complexation from Solubility Measurements: Ferrous Acetate Complexation," NATO Advanced Study Institute on "Advances in High Pressure Studies of Chemical and Biochemical Systems," September 28 through October 11, 1986, Corfu, Greece.

D. A. Palmer, "Ferrous-Acetate Complexation in Aqueous Solutions to 250°C and 1250 Bars," Institute of Physical Chemistry, Karlsruhe University, F.R.G., Colloquium, October 15, 1986.

J. M. Simonson, D. J. Bradley,[9] and R. H. Busey,[1] "Enthalpies of Mixing and the Thermodynamics of (Methanol + Water) Solutions to 573 K," The 41st Calorimetry Conference, Annadale, NJ, August 18-21, 1986.

J. M. Simonson and R. E. Mesmer, "Enthalpies of Dilution of Aqueous Sodium Hydroxide to 673 K and 40 MPa," The 41st Calorimetry Conference, Annadale, NJ, August 18-21, 1986.

---

1. Retired (ORNL).
2. National Institute for Petroleum and Energy Research, Bartlesville, OK.
3. University of Delaware, Newark, DE.
4. Carnegie Institution of Washington, Washington, DC.
5. University of Frankfurt, FRG.
6. University of California, Lawrence Berkeley Laboratory, Berkeley, CA.
7. Carleton College, Northfield, MN.
8. Drury College, Springfield, MO.
9. Montana College of Mineral Science and Technology, Butte, MT.

GEOCHEMISTRY OF CRUSTAL PROCESSES TO HIGH TEMPERATURES AND PRESSURES

Publications

D. R. Cole and S. E. Drummond, "The Effect of Transport and Boiling on Ag/Au Ratios in Hydrothermal Solutions: A Preliminary Assessment and Possible Implication for the Formation of Epithermal Precious-Metal Ore Deposits," Exploration for Ore Deposits of the North American Cordillera, ed. C. E. Nichols, J. Geochem. Explor. 25, 45 (1986).

D. R. Cole and H. Ohmoto,[1] "Kinetics of Isotopic Exchange at Elevated Temperatures and Pressures," Stable Isotopes in High Temperature Geological Processes, ed. J. W. Valley, H. P. Taylor, Jr., and J. R. O'Neil, Reviews in Mineralogy 16, 41 (1986).

D. R. Cole, M. Mottl,[2] and H. Ohmoto,[1] "Isotopic Exchange in Mineral-Fluid Systems. II. Oxygen and Hydrogen Isotopic Investigation of the Experimental Basalt-Seawater System," Geochim. Cosmochim. Acta (in press).

M. S. Drummond,[3] P. C. Ragland,[4] and D. Wesolowski, "An Example of Trondhjemite Genesis by Means of Alkali Metasomatism: Rockford Granite, Alabama Appalachians," Contributions to Mineralogy and Petrology 93, 98 (1986).

S. E. Drummond and D. A. Palmer, "Thermal Decarboxylation of Acetate: Part II. Boundary Conditions for the Role of Acetate in the Primary Migration of Natural Gas and the Transportation of Metals in Hydrothermal Systems," Geochim. Cosmochim. Acta 50, 825 (1986).

S. E. Drummond, "Gas Solubility Experiments: Analysis of Error and Techniques," in Hydrothermal Experimental Techniques, ed. H. L. Barnes and G. C. Ulmer, John Wiley and Sons, New York, in press.

M. D. Dyar,[5] M. T. Maney, and S. E. Swanson,[6] "Effects of Quench Methods on Fe^{3+}/Fe^{2+} Ratios: A Mössbauer and Wet Chemical Study," Am. Min. (in press).

M. T. Maney and F. H. Ward,[7] "Sample Manipulator and Quenching Apparatus for High Temperature, 1 Atm Experiments," Am. Min. 71, 837 (1986).

D. Wesolowski, J. J. Cramer,[8] and H. Ohmoto,[1] "Scheelite Mineralization in Skarns Adjacent to Devonian Granitoids at King Island, Tasmania," CIM Bulletin, Special Conference Volume #39, Recent Advances in the Geology of Granite-Related Mineral Deposits, in press.

Presentations

D. R. Cole, "Stable Isotope Geochemistry of Hydrothermally Altered Rocks from Geothermal Systems in Iceland," Geol. Soc. Amer. Annual Mtg., San Antonio, TX, November 10-13, 1986.

D. R. Cole and H. Ohmoto,[1] "Kinetics of Isotopic Exchange Reactions at Elevated Temperatures and Pressures," Presentation at short course on "Stable Isotopes in High Temperatures Geological Processes," sponsored by the Min. Soc. Amer., San Antonio, TX, November 7, 1986.

P. G. Feiss[9] and D. Wesolowski, "Oxygen Isotopic Evidence for the Interaction of Meteoric-Hydrothermal Waters with Granites and Subaerial Volcanics in Pyrophyllite/Au Deposits of the Carolina Slate Belt," Geological Society of America Annual Meeting, San Antonio, TX, November 10-13, 1986.

D. Wesolowski, "Hydrothermal Fluids Associated with Major Thrust Faults in the Southern Appalachians," ORNL Chemistry Division Annual Information Meeting, June 23-25, 1986.

---

1. Pennsylvania State University, University Park, PA.
2. Hawaii Geophysical Institute.
3. University of Alabama in Birmingham, Birmingham, AL.
4. Florida State University, Tallahassee, FL.
5. University of Oregon, Eugene, OR.
6. University of Alaska, Fairbanks, AK.
7. Plant & Equipment Division.
8. Whiteshell Nuclear Research Establishment, Pinawa, Manitoba, Canada.
9. University of North Carolina, Chapel Hill, NC.

CHEMISTRY OF ADVANCED INORGANIC MATERIALS

Publications

C. E. Bamberger and G. M. Begun, "Synthesis of BN Using BPO_4 as the Boron Source," J. Am. Ceram. Soc. 69, C-95 (1986).

C. E. Bamberger, "Reaction of Silicon Dioxide with Sodium Cyanide at 1000°C," React. of Solids 2, 277 (1986).

C. E. Bamberger, G. M. Begun, and H. W. Dunn,[1] "The System TiO_2-$Bi_2Ti_4O_{11}$," J. Am. Ceram. Soc. 69, C-93 (1986).

C. E. Bamberger and G. M. Begun, "Sodium Titanates; Stoichiometry and Raman Spectra," J. Am. Ceram. Soc. (in press).

C. E. Bamberger, G. M. Begun, and D. E. Heatherly, "The Reaction of Titanium Dioxide with Sodium Cyanide at 1000°C," React. of Solids (in press).

C. E. Bamberger and G. M. Begun, "Synthesis and Characterization of Titanium Phosphates, TiP_2O_7 and $(TiO)_2P_2O_7$," J. Less-Common Metals (in press).

P. F. Becher[2] and G. M. Begun, "Transformation Toughening Behavior in Ceramics," in Science and Technology of Zirconia, Advances in Ceramics, Vol. 3, The American Ceramics Society, in press.

G. M. Begun, P. F. Becher,[2] and E. F. Funkenbusch,[3] "Raman Microprobe Study of Phase Transformations in Ceria Stabilized Zirconia," pp. 11-48 in Proceedings of the Tenth International Conference on Raman Spectroscopy, University of Oregon Press, 1986.

H. G. Bohn,[4] J. M. Williams,[5] C. J. McHargue,[2] and G. M. Begun, "Recrystallization of Ion Implanted α-SiC," J. Mater. Res. (in press).

Gilbert M. Brown, "The Reduction of Chlorate and Perchlorate Ions at an Active Titanium Electrode," J. Electroanal. Chem. 198, 313 (1986).

Gilbert M. Brown and L. Maya, "Ammonolysis Products of the Dialkylamides of Titanium, Zirconium, and Niobium as Precursors to Metal Nitrides," Inorg. Chem. (in press).

C. B. Finch,[5] P. F. Becher,[2] P. Angelini,[2] S. Baik,[2] C. E. Bamberger, and J. Brynestad, "Effect of Impurities on the Densification of Submicrometer TiB_2 Powders," Adv. Ceram. Mater. 1, 50 (1986).

E. J. Kelly, p. 281 in Contemporary Classics in Engineering and Applied Science, ed. E. Garfield, ISI Press, Philadelphia, PA, 1986.

E. J. Kelly, D. E. Heatherly, C. E. Vallet, and C. W. White,[5] "Application of Ion Implantation to the Study of Electrocatalysis. I. Chlorine Evolution at Ru-implanted Titanium Electrodes," J. Electrochem. Soc. (in press).

T. B. Lindemer[6] and J. Brynestad, "Review and Chemical Thermodynamic Representations of $\langle U_{1-x}Ce_xO_{2\pm x}\rangle$ and $\langle U_{1-x}Ln_xO_{2\pm x}\rangle$; Ln = Y, La, Nd, Gd," J. Am. Ceram. Soc. 69, 867 (1986).

L. Maya, "Synthetic Approaches to Aluminum Nitride via Pyrolysis of a Precursor," Adv. Ceram. Mater. 1, 150 (1986).

L. Maya, "A Mixed Valence Ti(III)-Ti(IV) Amido Bridged Tetramer and Related Compounds," Inorg. Chem. 25, 4213 (1986).

L. Maya, "Precursors of Titanium Carbonitride," Mat. Res. Soc. Symp. Proc. 73, 401 (1986).

L. Maya, "Use of Ammonolytic Intermediates for the Synthesis of Nitrides and Carbonitrides," Proceedings NATO Advanced Research Workshop, Cape d'Agde, France, Sept. 1986, in press.

L. Maya, "The Ammonolysis of Niobium V Bromide," Inorg. Chem. (in press).

C. J. McHargue,[2] G. C. Farlow,[2] G. M. Begun, J. M. Williams,[5] C. W. White,[5] B. R. Appleton,[5] P. S. Sklad,[2] and P. Angelini,[2] "Damage Accumulation in Ceramics During Ion Implantation," Nucl. Instru. and Methods in Phys. Research B16, 212 (1986).

S. A. Sherrow,[6] L. M. Toth,[6] and G. M. Begun, "Raman Spectroscopic Studies of UO_2^{2+} Association with Hydrolytic Species of Group IV(4) Metals," Inorg. Chem. 25, 1992 (1986).

Presentations

P. F. Becher[2] and G. M. Begun, "Transformation Toughening Behavior in Ceramics," International Conference on Science and Technology of Zirconia, Tokyo, Japan, Sept. 9-11, 1986.

G. M. Begun, P. F. Becher,[2] and E. F. Funkenbusch,[3] "Raman Microprobe Study of Phase Transformations in Ceria Stabilized Zirconia," Tenth International Conference on Raman Spectroscopy, Eugene, Oregon, Aug. 31 - Sept. 5, 1986.

L. Maya, "Precursors of Titanium Carbonitrides," Materials Research Society, Palo Alto, CA, April 15-19, 1986.

L. Maya, "Use of Ammonolytic Intermediates for the Synthesis of Nitrides and Carbonitrides," NATO Advanced Research Workshop, Cape d'Agde, France, Sept. 1-5, 1986.

---

1. Analytical Chemistry Division.
2. Metals and Ceramics Division.
3. 3M Company, Saint Paul, MN 55101.
4. Institut für Festkörperforschung, Jülich, Federal Republic of Germany.
5. Solid State Division.
6. Chemical Technology Division.

STRUCTURE AND DYNAMICS OF ADVANCED POLYMERIC MATERIALS

Publications

P. A. Agron and W. R. Busing, "Calcium and Strontium Dichloride Hexahydrates by Neutron Diffraction," Acta Cryst. C42, 141 (1986).

J. B. Delos,[1] S. K. Knudson,[1] and D. W. Noid, "Bound State Semiclassical Wave-function," J. Chem. Phys. 84, 6886 (1986).

J. B. Drake,[2] S. K. Knudson,[1] E. Johnson, D. W. Noid, G. A. Pfeffer,[3] and S. Thompson,[2] "Molecular Dynamics of a Model Polymer on a Hypercube Parallel Computer," Computers and Chemistry (in press).

S. K. Gray,[4] S. A. Rice,[4] and D. W. Noid, "The Classical Mechanics of Vibrational Predissociation: A Model Based Study of Phase Space Structure and Its Influence on Fragmentation," J. Chem. Phys. 84, 3745 (1986).

A. Habenschuss[5] and A. H. Narten, "X-Ray Diffraction Study of Liquid Propane at 92 and 228 K," J. Chem. Phys. 85, 6022 (1986).

E. Johnson, "Two and Three Particle Distribution Functions for Lattice Fluids from Ornstein-Zernike Equations," J. Chem. Phys. (in press).

M. L. Koszykowski,[6] G. A. Pfeffer,[3] and D. W. Noid, "Applications of the Semiclassical Spectral Method to Nuclear, Atomic, Molecular and Polymeric Dynamics," in Chaotic Phenomena in Astrophysics, ed. J. R. Buchler and H. Eichorn, New York Academy of Science, in press.

P. Lamparter,[7] A. Habenschuss,[5] and A. H. Narten, "Neutron and X-Ray Diffraction Study of the Ti84-Si16 Metallic Glass," J. Non-Cryst Solids 86, 109 (1986).

W-K. Liu,[8] W. H. Fletcher,[9] and D. W. Noid, "Laser Induced Dissociation Dynamics in Triatomic Molecules," p. 331 in Adv. Laser Sci., ed. W. C. Stwalley and M. Lapp, AIP Conf. Proc. 146 (1986).

W.-K. Liu,[8] A. F. Turfa,[10] W. H. Fletcher,[9] and D. W. Noid, "A Classical Trajectory Study of Laser Induced Dissociation Dynamics in Triatomic Molecules," J. Phys. Chem. (in press).

A. H. Narten, "Diffraction Studies of Liquids," Acta. Chim. Hung. 121, 173 (1986).

J. W. Neuberger[11] and D. W. Noid, "Numerical Calculation of Eigenvalues for the Schrodinger Equation III," J. Comp. Chem. (in press).

D. W. Noid, S. K. Gray,[4] and S. A. Rice,[4] "Fractal Behavior in Collisional Energy Transfer," J. Chem. Phys. 84, 2649 (1986).

D. W. Noid and R. A. Marcus,[12] "Semiclassical Calculation of Eigenvalues for Higher Order Resonances in Non-Separable Oscillator Systems," J. Chem. Phys. 85, 3305 (1986).

D. W. Noid, S. K. Knudson,[1] M. L. Koszykowski,[6] and R. J. Renka,[11] "Semiclassical Calculation of Molecular Vibrations from ab initio Potentials Using Splines: Ozone," J. Phys. Chem. 90, 6135 (1986).

D. W. Noid, F. X. Hartman,[13] and M. L. Koszykowski,[6] "Classical and Semiclassical Calculation of Nuclear Electron Coupling," in Advances in Laser Science II, ed. W. C. Stwalley and M. Lapp, AIP Conf. Proc., in press.

D. W. Noid, S. K. Knudson,[1] and M. L. Koszykowski,[6] "Semiclassical Calculation of Stretching Frequencies in Non-Bending Ozone," J. Phys. Chem., in press.

D. W. Noid, F. X. Hartman,[13] and M. L. Koszykowski,[6] "Classical and Semiclassical Calculation of Nuclear Electron Coupling," J. Phys. Chem., in press.

B. G. Sumpter[14] and D. W. Noid, "Method for Semiclassical Calculation of A Grid of Eigenvalues," Chem. Phys. Lett. 84, 3745 (1986).

B. G. Sumpter,[14] D. L. Thompson,[14] and D. W. Noid, "The Effect of Resonances on Collisional Energy Transfer," J. Chem. Phys. (in press).

Presentations

W. R. Busing, "History of Computers in Crystallography," American Chemical Society National Meeting, Anaheim, CA, September 9, 1986.

S. Z. D. Cheng,[15] B. Wunderlich,[15] D. W. Noid, and G. A. Pfeffer,[3] "Computer Simulation of Motion on Crystal Surfaces and Molecular Nucleation of Macromolecules," American Physical Society National Meeting, New York, NY, March 1987.

J. B. Delos,[1] S. K. Knudson,[1] and D. W. Noid, "Quantum Wavefunctions from Classical Trajectory Manifolds," American Physical Society National Meeting, Washington, DC, April 1986.

J. B. Delos,[1] S. K. Knudson,[1] and D. W. Noid, "Quantum Wave Functions from Classical Trajectory Manifolds," Joint DEAP and DCP Meeting of the American Physical Society, Eugene, OR, June 1986.

E. Johnson, "Thermodynamics of Polymer Mixtures from Lattice Fluid Models," Thirteenth Annual Meeting of the National Organization of Black Chemists and Chemical Engineers, Atlanta, GA, April 22-25, 1986.

S. K. Knudson,[1] D. W. Noid, and M. L. Koszykowski,[6] "Semiclassical Determination of Vibrational Frequencies in Non-Bending Ozone," Joint DEAP and DCP Meeting of the American Physical Society, Eugene, OR, June 1986.

A. H. Narten, "Structural Studies of Polymers by Wide-Angle Neutron and X-Ray Scattering," Meeting on Materials Science and Engineering, Oak Ridge National Laboratory, May 14-16, 1986.

A. H. Narten, "Chemical Applications of Neutron Scattering," Brookhaven National Laboratory, October 7, 1986.

A. H. Narten, "Mechanism of Conductivity in Polyaniline," American Physical Society National Meeting, New York, NY, March 1987.

D. W. Noid, "Quasiperiodic and Chaotic Behavior in Molecular Spectra," Workshop on Chaotic Phenomena in Astrophysics, Gainesville, FL, October 1986.

D. W. Noid, F. X. Hartmann,[13] and M. L. Koszykowski,[6] "Classical and Semiclassical Calculation of Nuclear-Electron Coupling," International Laser Science Conference, Seattle, WA, October 1986.

D. W. Noid, "Quasiperiodic and Chaotic Dynamics in Atoms and Molecules," Department of Chemistry, University of Alabama, Huntsville, AL, November 1986.

D. W. Noid, G. A. Pfeffer,[3] S. Z. D. Cheng,[15] and B. Wunderlich,[15] "Computer Simulation of 2-D Polymer Crystal Melting," American Physical Society National Meeting, New York, NY, March 1987.

G. A. Pfeffer,[3] D. W. Noid. S. Z. D. Cheng,[15] and B. Wunderlich,[15] "Static Simulation of Macromolecular Conformation on 2-D Polymer Crystal Surface," American Physical Society National Meeting, New York, NY, March 1987.

---

1. College of William and Mary, Williamsburg, VA.
2. Engineering Physics and Mathematics Division.
3. University of Nebraska, Omaha, NE.
4. University of Chicago, Chicago, IL.
5. Oak Ridge Associated Universities, Oak Ridge, TN.
6. Sandia National Laboratory, Livermore, CA.
7. Max Planck Institute for Metals Research, Stuttgart, FRG.
8. University of Waterloo, Waterloo, Ontario, Canada.
9. University of Tennessee, Knoxville, TN.
10. Temple University, Philadelphia, PA.
11. North Texas State University, Denton, TX.
12. California Institute of Technology, Pasadena, CA.
13. Institute for Defense Analysis, Alexandria, VA.
14. Oklahoma State University, Stillwater, OK.
15. Rensselaer Polytechnic Institute, Troy, NY.

CHEMISTRY OF TRANSURANIUM ELEMENTS AND COMPOUNDS

Publications

C. W. Alexander,[1] J. Halperin, J. B. Knauer,[1] and R. L. Walker,[2] "The Thermal Neutron Capture Cross Sections and Resonance Integrals of ^{144}Sm and ^{145}Sm," Nucl. Sci. and Eng. 95, 194 (1987).

J. K. Gibson and R. G. Haire, "Preparation and X-Ray Diffraction Studies of Californium Dihydride: A Possible Indication of Divalent Character of Californium," Radiochim. Acta 38, 193 (1985).

J. K. Gibson and R. G. Haire, "Preparation and Lattice Parameters of Bismuthides of Am and Cm," J. Less-Common Metals 132, 149 (1987).

R. G. Haire, "Californium," pp. 1025-1071 in The Chemistry of the Actinide Elements, 2d ed., ed. J. J. Katz, G. T. Seaborg, and L. R. Morss, Chapman and Hall Ltd., London, Chapter Ten, 1986.

R. G. Haire, U. Benedict,[3] J. R. Peterson,[4] C. Dufour,[3] and S. Dabos,[3] "A New Look at the Atomic Volumes of the β-Form of the Transplutonium Metals," Physica 1448, 19 (1986).

R. G. Haire, "Preparation, Properties, and Recent Studies of the Actinide Metals," J. Less-Common Metals 121, 379 (1986).

R. G. Haire, J. P. Young, J. R. Peterson,[4] and U. Benedict,[3] "Studies of Selected Transuranium and Lanthanide Triiodides Under Pressure Using Absorption Spectrophotometry," J. Less-Common Metals 133, 167 (1987).

R. L. Hahn, A. H. Narten, and B. K. Annis, "Neutron Scattering from Solutions: The Hydration of Lanthanide and Actinide Ions," J. Less-Common Metals 122, 233 (1986).

R. L. Hahn, "Volumes of Aqua Ions from Measured Neutron Radial Distribution Functions," J. Phys. Chem. (in press).

R. L. Hahn, K. S. Toth,[5] Y. LeBeyec,[6] B. Lagarde,[6] and M. W. Guidry,[5] "Reactions of Ar-40 and Kr-84 Leading to the Same Compounds Nucleus, Po-200," Phys. Rev. C (in press).

J. Halperin, J. H. Oliver, and W. J. McDowell, "A Micro Mixer-Settler for the Rapid Solvent Extraction of Radioactive Nuclides," Lanthanide Actinide Research 1, 179 (1986).

D. E. Hobart[7] and J. R. Peterson,[4] "Berkelium," pp. 989-1024 in The Chemistry of The Actinide Elements, 2d ed., ed. J. J. Katz, G. T. Seaborg, and L. R. Morss, Chapman and Hall Ltd., London, Chapter Ten, 1986.

D. E. Hobart[7] and J. R. Peterson,[4] "The Chemistry of Berkelium: A Review," J. Less-Common Metals 121, 645 (1986).

E. K. Hulet,[8] J. F. Wild,[8] R. J. Dougan,[8] R. W. Lougheed,[8] A. D. Dougan,[8] M. Schadel,[9] R. L. Hahn, P. A. Baisden,[8] C. M. Henderson,[8] R. J. Dupzyk,[9] K. Summerer,[9] and G. R. Bethune,[8] "Bimodal Symmetric Fission Observed in the Heaviest Elements," Phys. Rev. Lett. 56, 313 (1986).

E. K. Hulet,[8] R. W. Lougheed,[8] J. F. Wild,[8] R. J. Dougan,[8] K. J. Moody,[10] R. L. Hahn, C. M. Henderson,[8] R. J. Dupzyk,[9] and G. R. Bethune,[8] "Z and A Identification of 370-μs Fm-258," Phys. Rev. C 34, 1394 (1986).

O. L. Keller, "Californium-252: Properties and Production," Nucl. Sci. Applic. 2, 263 (1986).

J. V. Kratz,[11] W. Bruchle,[9] H. Folger,[9] H. Gaggeler,[9] M. Schadel,[9] K. Summerer,[9] G. Wirth,[9] W. Brulich,[9] G. Herrmann,[11] U. Hickmann,[11] P. Peuser,[11] N. Trautmann,[11] E. K. Hulet,[8] R. W. Lougheed,[8] J. M. Nitschke,[10] R. L. Ferguson,[5] and R. L. Hahn, "Search for Superheavy Elements in Damped Collisions Between U-238 and Cm-248," Phys. Rev. C 33, 504 (1986).

R. W. Lougheed,[8] E. K. Hulet,[8] R. J. Dougan,[8] J. F. Wild,[8] R. J. Dupzyk,[9] C. M. Henderson,[8] K. J. Moody,[10] R. L. Hahn, K. Summerer,[9] and G. Bethune,[8] "The Discovery of Md-260 and the Decay Properties of Fm-258, Md-258M,g and Md-259," J. Less-Common Metals 122, 461 (1986).

J. U. Mondal,[4] D. L. Raschella,[4] R. G. Haire, and J. R. Peterson,[4] "The Enthalpy of Solution of ^{243}Am Metal and the Standard Enthalpy of Formation of Am^{3+} (aq)," Thermochimica Acta (in press).

S. E. Nave,[4] J. R. Moore,[4] R. G. Haire, J. R. Peterson,[4] D. A. Damien,[12] and P. G. Huray,[4] "Magnetic Susceptibility of CfN, CfAs, and CfSb," J. Less-Common Metals 121, 319 (1986).

S. E. Nave,[4] J. R. Moore,[4] and R. G. Haire, "Magnetic Susceptibility of Cf Oxides," J. Less-Common Metals 121, 379 (1986).

S. E. Nave,[4] J. R. Moore,[4] J. R. Peterson,[4] and R. G. Haire, "Magnetic Susceptibility of $CfCl_3$ and Its Dependence on Crystal Structure," J. Less-Common Metals 127, [illegible] (1987).

G. F. Payne and J. R. Peterson,[4] "Spectroscopic and Electrochemical Studies of Tri- and Tetravalent Cerium and Americium with Triphenylarsine Oxide in Acetonitrile," Radiochim. Acta 39, 155 (1986).

G. F. Payne and J. R. Peterson,[4] "Oxidation Studies of Selected Lanthanides in Acetonitrile," J. Less-Common Metals 126, 371 (1986).

G. F. Payne and J. R. Peterson,[4] "Oxidation Studies of the Plutonium(VI)/(IV) Couple with Triphenylarsine Oxide in Acetonitrile," Radiochim. Acta 40, 1 (1986).

J. R. Peterson,[4] J. P. Young,[2] R. G. Haire, and U. Benedict,[3] "Absorption Spectrophotometric Studies of Some Lanthanide and Actinide Halides Under Pressure," Physica 144B, 85 (1986).

J. R. Peterson,[4] U. Benedict,[3] J. P. Young,[2] R. G. Haire, and G. M. Begun, "A Diamond Anvil Cell for Absorption Spectral Studies of Actinides to 30 GPa," Microchemical Journal 34, 76 (1986).

J. R. Peterson,[4] J. P. Young,[2] D. D. Ensor,[13] and R. G. Haire, "Absorption Spectrophotometric and X-Ray Diffraction Studies of the Trichlorides of Berkelium-249 and Californium-249," Inorg. Chem. 25, 3779 (1986).

J. R. Peterson,[4] R. G. Haire, U. Benedict,[3] and J. P. Young,[2] "Experimental Studies at Karlsruhe and Oak Ridge of Transplutonium Metals and Compounds Under Pressure," J. Less-Common Metals (in press).

R. R. Ryan,[7] E. M. Larson,[7] G. F. Payne, and J. R. Peterson,[4] "The Structure of fac-$Ce(OAsPh_3)_3Cl_3 \cdot CH_3CN$ and $Ce(OAsPh_3)_3(NO_3)_3$. Evidence for a Structural Trans Influence," Inorg. Chim. Acta (in press).

M. Schadel,[9] W. Bruchle,[9] M. Brugger,[9] H. Gaggeler,[9] K. J. Moody,[10] D. Schardt,[9] K. Summerer,[9] E. K. Hulet,[8] A. D. Dougan,[8] R. J. Dougan,[8] J. H. Landrum,[8] R. W. Lougheed,[8] J. F. Wild,[8] G. D. O'Kelley, and R. L. Hahn, "Heavy Isotope Production by Multinucleon Transfer Reactions with Es-254," J. Less-Common Metals 122, 411 (1986).

G. T. Seaborg[10] and O. L. Keller, "Future Elements," pp. 1629-1647 in The Chemistry of the Actinide Elements, 2d ed., ed. J. J. Katz, G. T. Seaborg, and L. R. Morss, Chapman and Hall Ltd., London, Chapter Ten, 1986.

J. C. Spirlet,[3] J. R. Peterson,[4] and L. B. Asprey,[7] "Preparation and Purification of Actinide Metals," pp. 1-41 in Advances in Inorganic Chemistry and Radiochemistry, ed. H. J. Emeleus and A. G. Sharpe, Academic Press, Orlando, Florida, Volume 31, 1987.

Presentations

J. K. Gibson and R. G. Haire, "Preparation and Solid State Properties of Americium and Curium Bismuthides," 192nd American Chemical Society Meeting, Anaheim, CA, Sept. 7-12, 1986.

J. K. Gibson and R. G. Haire, "Preparation and X-Ray Diffraction Studies of the Hydrides of Curium, Berkelium, and Californium," 17th Rare Earth Research Conference, Hamilton, Canada, June 8-12, 1986.

R. G. Haire, J. R. Peterson,[4] J. P. Young,[2] U. Benedict,[3] C. Dufour,[3] and S. Dabos,[3] "Studies of Transuranium Elements and Compounds Under Pressure," Second International Workshop on Actinides Under Pressure, Karlsruhe, Federal Republic of Germany, June 2-3, 1986.

R. G. Haire, J. P. Young,[2] J. R. Peterson,[4] and U. Benedict,[3] "Studies of Plutonium and Curium Triiodides Under Pressure," 192nd American Chemical Society Meeting, Anaheim, CA, Sept. 7-12, 1986.

J. Halperin and O. L. Keller, "Chemical Separations Techniques in Studies of Transfermium Elements," American Chemical Society Meeting, New York, NY, April 13-18, 1986.

D. E. Hobart,[7] D. E. Morris,[7] P. Palmer,[7] R. G. Haire, and J. R. Peterson,[4] "Synthesis and Raman Spectral Characterization of Lanthanide and Actinide Oxalates," 2nd International Conference on the Basic and Applied Chemistry of f-Transition and Related Elements, Lisbon, Portugal, April 6-10, 1987.

O. L. Keller, G. F. Payne, J. Halperin, R. L. Hahn, J. R. Peterson,[4] E. K. Hulet,[8] R. J. Silva,[8] and R. W. Lougheed,[8] "Search for the Monovalent Species: Mendelevium 1+," 32nd Research Materials/Transplutonium Program Committee Meeting, Anaheim, CA, Sept. 11-12, 1986.

S. E. Nave,[4] J. M. Moore,[4] J. R. Peterson,[4] and R. G. Haire, "Magnetic Susceptibility of $CfCl_3$ and Its Dependence on Crystal Structure," 17th Rare Earth Research Conference, Hamilton, Canada, June 8-12, 1986.

S. E. Nave,[4] J. R. Moore,[4] W. R. Wilmarth,[4] J. R. Peterson,[4] and R. G. Haire, "Magnetic Properties of Polycrystalline Samples of Cf^{3+} in $LaCl_3$ and Synthesis of Single Crystals," 32nd Research Materials/Transplutonium Program Committee Meeting, Anaheim, CA, Sept. 11-12, 1986.

G. F. Payne and J. R. Peterson,[4] "Oxidation Studies of Selected Lanthanides and Actinides in Acetonitrile," 17th Rare Earth Research Conference, Hamilton, Canada, June 8-12, 1986.

G. F. Payne and J. R. Peterson,[4] "Stabilization of the Tetravalent Oxidation State of Selected Lanthanides and Actinides in Acetonitrile with Triphenylarsine Oxide," 2nd International Conference on the Basic and Applied Chemistry of f-Transition (Lanthanide and Actinide) and Related Elements, Lisbon, Portugal, April 6-10, 1987.

J. R. Peterson,[4] J. P. Young,[2] R. G. Haire, and U. Benedict,[3] "Absorption Spectrophotometric Studies of Some Actinide Halides Under Pressure," Second International Workshop on Actinides Under Pressure, Karlsruhe, Federal Republic of Germany, June 2-3, 1986.

J. R. Peterson,[4] R. G. Haire, U. Benedict,[3] and J. P. Young,[2] "Experimental Studies of Transplutonium Metals and Compounds Under Pressure," 192nd American Chemical Society Meeting, Anaheim, CA, Sept. 7-12, 1986.

J. R. Peterson,[4] "Research and Opportunities with the Transplutonium Elements," Transuranium Processing Plant (TRU), Oak Ridge, TN, Feb. 20, 1986.

J. R. Peterson,[4] "Chemical and Physical Consequences of Radioactive Decay in Transcurium Halides," Swarthmore College, Swarthmore, PA, March 25, 1986.

J. R. Peterson,[4] "Chemical and Physical Consequences of Radioactive Decay in Transcurium Halides," Washington and Lee University, Lexington, VA, March 27, 1986.

J. R. Peterson,[4] "The Transuranium Elements: On the Edge of Matter," Ecole Nationale Superieure de Chimie de Strasbourg, Strasbourg, France, June 6, 1986.

J. R. Peterson,[4] "Determination and Interpretation of Some Physical and Chemical Properties of the Transuranium Elements," Ecole Nationale Superieure de Chimie de Strasbourg, Strasbourg, France, June 7, 1985.

J. R. Peterson,[4] "The Transuranium Elements: On the Edge of Matter," The University of Tennessee, Knoxville, TN, Aug. 12, 1986.

J. R. Peterson,[4] "Chemical and Physical Consequences of Alpha and Beta Decay in the Solid State," East Tennessee State University, Johnson City, TN, Oct. 10, 1986.

J. R. Peterson,[4] "The Transplutonium Elements: On the Edge of Matter," University of Alabama, Tuscaloosa, AL, Oct. 23, 1986.

J. P. Young,[2] R. G. Haire, J. R. Peterson,[4] G. M. Begun, and U. Benedict,[3] "Absorption Spectrophotometric Study of Selected Actinide Halides Under Pressure," European Study Group on Solid State Spectroscopy of the Parliamentary Assembly of the Council of Europe, London, England, April 17-18, 1986.

J. P. Young,[2] R. G. Haire, and J. R. Peterson,[4] "Spectrophotometric Studies Applied to Transplutonium Chemistry," ORNL Analytical Chemistry Division Information Meeting, Oak Ridge, TN, Feb. 18-20, 1987.

---

1. Chemical Technology Division.
2. Analytical Chemistry Division.
3. European Institute for Transuranium Elements, Karlsruhe, FRG.
4. University of Tennessee, Knoxville, TN.
5. Physics Division.
6. Institut de Physique Nucleaire, Orsay, France.
7. Los Alamos National Laboratory, Los Alamos, NM.
8. Lawrence Livermore National Laboratory, Livermore, CA.
9. Gesellschaft fur Schwerionenforschung, Darmstadt, West Germany.
10. Lawrence Berkeley Laboratory, Berkeley, CA.
11. Institut fur Kernchemie, Universitat Mainz, Mainz, Federal Republic of Germany.
12. Centre d'Etudes Nucleaires, Fontenay-aux-Roses, France.
13. Tennessee Technological University, Cookeville, TN.

SEPARATIONS CHEMISTRY

Publications

S. D. Alexandratos,[1] D. L. Wilson,[1] P. T. Kaiser,[1] and W. J. McDowell, "Dual-Mechanism Bifunctional Polymers: Phosphinic Acid Ion-Exchange/Redox Resins and the Kinetics of Metal Ion Complexation," Reactive Polymers 5, 23 (1987).

S. D. Alexandratos,[1] D. R. Quillen,[1] and W. J. McDowell, "Dual Mechanism Bifunctional Polymers for the Complexation of Lanthanides and Actinides," Sep. Sci. Technol. 22, 983 (1987).

C. F. Baes, Jr. and D. J. Pruett,[2] "Separation Science and Technology," ORNL Review, Vol. 19, No. 3, Special Issue, Basic Physical Sciences at ORNL, 1986, pp. 162-172.

C. F. Baes, Jr., W. J. McDowell, and S. A. Bryan,[3] "The Interpretation of Equilibrium Data from Synergistic Solvent Extraction Systems," Solv. Extr. Ion Exch. 5, 1 (1987).

J. H. Burns, "Structural Chemistry," pp. 1417-1479 in The Chemistry of the Actinide Elements, 2d ed., ed. J. J. Katz, G. T. Seaborg, and L. R. Morss, Chapman and Hall, Ltd., London, Chapter 20, 1986.

J. H. Burns and R. M. Kessler,[3] "Structural and Molecular Mechanics Studies of Bis(dibutylphosphato)-aquastrontium-18-crown-6 and Analogous Alkaline-Earth Complexes," Inorg. Chem. (in press).

W. J. McDowell, Alpha Counting and Spectrometry Using Liquid Scintillation Methods, Nuclear Science Series, Radiochemistry Techniques, sponsored by the National Academy of Science/National Research Council, Office of Scientific and Technical Information, U. S. Department of Energy, 1986, 117 pp.

W. J. McDowell, B. A. Moyer, G. N. Case, and F. I. Case, "Selectivity in Solvent Extraction of Metal Ions by Organic Cation Exchangers Synergized by Macrocycles: Factors Relating to Macrocycle Size and Structure," Solv. Extr. Ion Exch. 4, 217 (1986).

W. J. McDowell, B. A. Moyer, S. A. Bryan,[3] R. B. Chadwick,[4] and G. N. Case, "Selectivity and Equilibria in Extraction with Macrocycles in Synergistic Combination with Organophilic Acids," pp. 477-482 in Proc. Internat. Solv. Extr. Conf. (ISEC '86), Munchen, FRG, Sept. 11-16, 1986, Vol. I, Deutsche Gesellschaft fur Chemisches Apparatewesen, Chemische Technik und Biotechnologie e.V., Frankfurt am Main, 1986.

W. J. McDowell, G. N. Case, R. A. Bartsch,[5] and B. P. Czech,[5] "Solvent Extraction of Radium and Barium Cations into Chloroform by a Lipophilic Acyclic Polyether Dicarboxylic Acid," Solv. Extr. Ion Exch. 4(3), 411 (1986).

B. A. Moyer, "Alkane-Insoluble Trialkylammonium Double Salts Involving the Dodecamolybdophosphate Anion. III. Nature of a Liquid Third Phase," Solv. Extr. Ion Exch. 5, 195 (1987).

B. A. Moyer and W. J. McDowell, "Alkane-Insoluble Double Salts Involving the Dodecamolybdophosphate Anion. II. Effect of Amine Structure on Third-Phase Formation," Sep. Sci. Technol. (in press).

B. A. Moyer, C. O. Price,[6] and W. J. McDowell, "Alkane-Insoluble Double Salts involving the Dodecamolybdophosphate Anion. I. Model Studies Using Trioctylamine in Dodecanol-Modified Nonane," Hydrometallurgy 16, 177 (1986).

B. A. Moyer, W. J. McDowell, R. J. Ontko,[4] S. A. Bryan,[3] and G. N. Case, "Complexation of Strontium in the Synergistic Extraction System Dicyclohexano-18-Crown-6, Versatic Acid, Carbon Tetrachloride," Solv. Extr. Ion Exch. 4, 83 (1986).

E. H. Nordlander[4] and J. H. Burns, "Structure of a Hydrogen-Bonded Lattice Compound Between Phosphoric Acid and 18-Crown-6: $H_3PO_4 \cdot 0.5(C_{12}H_{24}O_6) \cdot 3H_2O$," Inorg. Chim. Acta 115, 31 (1986).

Presentations

S. A. Bryan,[3] W. J. McDowell, and B. A. Moyer, "Complex Characterization Studies in the Didodecylnaphthalene Sulfonic Acid, Dicyclohexano-18-Crown-6, Sr^{2+} Extraction System," 191st American Chemical Society National Meeting, New York, NY, Apr. 16-18, 1986.

J. H. Burns and S. A. Bryan,[3] "Strontium Dipivalate Dicyclohexano-18-crown-6 Hydrate: Molecular and Crystal Structure," Ann. Mtg. Amer. Cryst. Assoc., Austin, TX, March 15-20, 1987.

J. H. Burns, "A Molecular Mechanics Study of the Stabilities of Crown-Ether Complexes with Alkaline-Earth Metals," 192nd American Chemical Society National Meeting, Anaheim, CA, Sept. 7-12, 1986.

W. J. McDowell, B. A. Moyer, S. A. Bryan,[3] R. B. Chadwick,[4] and G. N. Case, "Selectivity and Equilibria in Extraction with Macrocycles in Synergistic Combination with Organophilic Acids," International Solvent Extraction Conference, Munich, FRG, Sept. 11-16, 1986.

B. A. Moyer, "Interfacial Emulsion Formation in Tertiary-Amine Solvent Extraction," 191st American Chemical Society National Meeting, New York, NY, April 16-18, 1986.

---

1. Department of Chemistry, University of Tennessee, Knoxville, TN 37996.
2. Chemical Technology Division.
3. Post-Doctoral Research Fellow with the Oak Ridge Associated Universities.
4. Undergraduate research participant in the Oak Ridge Science Semester Program.
5. Department of Chemistry, Texas Tech University, Lubbock, TX 79409.
6. Undergraduate research participant in the Cooperative Education Program sponsored by Union Carbide Nuclear Division.

REACTIONS AND CATALYSIS IN MOLTEN SALTS

Publications

D. M. Chapman,[1] A. C. Buchanan, III, G. P. Smith, and G. Mamantov,[1] "Bonded Versus Non-Bonded Electron Transfers in Molten Salts: Characterization and Rates of Formation of the Radical Cations and Dications of Phenoxazine and Phenothiazine and Behavior of the M(2,2′-bipyridine)$_3^{2+/3+}$ (M = Fe, Ru, Os) Complexes in $SbCl_3$-Rich Media," J. Am. Chem. Soc. 108, 654 (1986).

D. M. Chapman,[1] G. P. Smith, A. C. Buchanan, III, and G. Mamantov,[1] "Effect of Melt Composition on the Reactions of the Anthracene Radical Cation in $SbCl_3$-Rich Melts: Chlorination Versus Aryl-Aryl Coupling," p. 498 in Proc. Fifth Inter. Symp. Molten Salt Chem., ed. M.-L. Saboungi et al., Proceedings Series, Vol. 86-1, The Electrochemical Society, Princeton, N.J., 1986.

G. P. Smith, "Application of Optical Electronic Absorption Spectroscopy to Chemical Reactions in Melts," in Molten Salt Chemistry. An Introduction and Selected Applications, ed. G. Mamantov and R. Marassi, D. Reidel Publishing Co., in press.

G. P. Smith, "Molten Salt Hydrocracking Catalysis," Molten Salts Bulletin Sels Fondus, No. 32, ed. M. Gaune-Escard, Univ. des Provence, 1987, p. 3.

G. P. Smith and R. M. Pagni,[1] "Homogeneous Organic Reactions in Molten Salts. Selected Topics," in Molten Salt Chemistry. An Introduction and Selected Applications, ed. G. Mamantov and R. Marassi, D. Reidel Publishing Co., in press.

Presentations

G. P. Smith, "Application of Optical Electronic Absorption Spectroscopy to Chemical Reactions in Melts," NATO Advanced Study Institute, Camerino, Italy, Aug. 1986.

G. P. Smith, "Catalytic Chemistry of Arenes in Molten $SbCl_3$: An Account of a Decade of Research at the Oak Ridge National Laboratory," EUCHEM Conference on Molten Salts, Geiranger, Norway, Aug. 1986.

G. P. Smith and R. M. Pagni,[1] "Homogeneous Organic Reactions in Molten Salts. Selected Topics," NATO Advanced Study Institute, Camerino, Italy, Aug. 1986.

S. P. Zingg, "The Generation of Radical Cations in Molten Salt Media," Exxon Research Corp., Clinton, NJ, March 1986.

S. P. Zingg, "The Generation of Radical Cations in Molten Salt Media," ORAU Traveling Lecture Series, Lehigh University, Bethlehem, PA, March 1986.

S. P. Zingg, "The Generation of Radical Cations in Molten Salt Media," ORAU Traveling Lecture Series, Mississippi State University, Starkville, MS, Feb. 1986.

S. P. Zingg, "Reaction Pathways of Substituted Anthracene Radical Cations in $SbCl_3$-Rich Melts," 191st American Chemical Society Meeting, New York, NY, April 1986.

S. P. Zingg, "Spectroscopic and Electrochemical Investigations of Some Arenes and Heteroaromatics in Aluminum Chloride – 1-Ethyl-3-methyl-1H-imidazolium Chloride at Ambient Temperatures," EUCHEM Conference on Molten Salts, Geiranger, Norway, Aug. 1986.

---

1. Department of Chemistry, University of Tennessee, Knoxville, TN.

SURFACE SCIENCE RELATED TO HETEROGENEOUS CATALYSIS

Publications

H. Derks,[1] H. Hemme,[1] W. Heiland,[1] and S. H. Overbury, "Low Energy Ion Scattering from the Au(110) Surface - Structural Results," Nucl. Instr. Meth. B (in press).

D. R. Huntley, S. H. Overbury, D. M. Zehner,[2] J. D. Budai,[2] and W. E. Brower, Jr.,[3] "Surface Characterization of Amorphous and Crystallized $Fe_{80}B_{20}$," Applied Surface Science 27, 180 (1986).

F. W. Meyer,[4] C. C. Havener,[4] S. H. Overbury, K. J. Snowdon,[1] D. M. Zehner,[2] W. Heiland,[1] and H. Hemme,[1] "Charge Exchange Processes Between Highly Charged Ions and Metal Surfaces," Nucl. Instr. Meth. B. (in press).

F. W. Meyer,[4] C. C. Havener,[4] and K. J. Snowdon,[1] "Observation of the Neutralization of Highly Charged Ions Interacting with a Metal Surface," Phys. Rev. A, 35 (1987).

S. H. Overbury, "Surface Layer Relaxation on Mo(111) Measured by Low Energy Alkali Ion Scattering," Surface Science 175, 123 (1986).

S. H. Overbury, "Evidence for Sub-Surface Carbon on Mo(111) by Low Energy Alkali Ion Scattering," J. Vac. Sci. Technol. (in press).

S. H. Overbury, "The Use of Low Energy Alkali Ion Scattering as a Probe of Surface Structure," Nucl. Instr. Meth. B (in press).

S. H. Overbury, "The Adsorption of Ethylene on Mo(111): Evidence for a Sub-Surface Carbon," Surface Science (in press).

D. M. Zehner,[2] S. H. Overbury, C. C. Havener,[4] F. W. Meyer,[4] and W. Heiland,[1] "Electron Emission from the Interaction of Multiply Charged Ions with an Au(110) Surface," Surface Science 178, 359 (1986).

Presentations

S. H. Overbury, "Evidence for Sub-Surface C Adsorption on Mo(111) by Low Energy Alkali Ion Scattering and AES," 10th International Vacuum Congress/33rd National Symposium of the American Vacuum Society, Oct. 27-31, 1986, Baltimore, MD.

S. H. Overbury, "The Use of Low Energy Alkali Ion Scattering to Probe Surface Structure and Adsorbate Geometry," 6th International Workshop on Inelastic Ion Surface Collisions, Aug. 25-29, 1986, Argonne, IL.

S. H. Overbury, "Studies of Clean and S-Covered Mo(111) by Low Energy Alkali Ion Scattering," 46th Annual Conference of Physical Electronics, June 16-18, 1986, Austin, TX.

S. H. Overbury, "Determination of Surface Structure by Low Energy Alkali-Metal Ion Scattering," ORAU Traveling Lecture Program, May 8, 1986, Auburn University, Auburn, AL.

---

1. University of Osnabruck, Osnabruck, FRG.
2. Solid State Division.
3. Southern Illinois University, Carbondale, IL.
4. Physics Division.

ELECTRON SPECTROSCOPY

Publications

P. A. Agron, T. A. Carlson, W. B. Dress,[1] and G. L. Nyberg,[2] "Angle-Resolved Polarization-Dependent Photoemission Spectra of Benzenethiol Adsorbed on Cu(110)," J. of Elect. Spectrosc. (in press).

T. A. Carlson, W. A. Svensson,[3] M. O. Krause, T. A. Whitley,[4] F. A. Grimm,[4] G. VonWald,[5] J. W. Taylor,[5] and B. P. Pullen,[6] "Shape Resonances in the Angle-Resolved Photoelectron Spectroscopy of the Si 2p Shell of $SiCl_4$," J. Chem. Phys. 84, 122 (1986).

T. A. Carlson, A. Fahlman,[7] M. O. Krause, T. A. Whitley,[4] F. A. Grimm,[4] M. N. Piancastelli,[5] and J. W. Taylor,[5] "Angle-Resolved Photoelectron Spectroscopy of the Valence Orbitals of $SiCl_4$ as a Function of Photon Energy from 14 to 80 eV," J. Chem. Phys. 84, 641 (1986).

T. A. Carlson, P. Gerard, M. O. Krause, G. VonWald,[5] J. W. Taylor,[5] and F. A. Grimm,[4] "Autoionization Between the Ionization Thresholds for the $^2\pi_{3/2}$ and $^2\pi_{1/2}$ States of HI^+," J. Chem. Phys. 84, 4755 (1986).

T. A. Carlson, M. O. Krause, W. A. Svensson,[3] P. Gerard, F. A. Grimm,[4] T. A. Whitley,[4] and B. P. Pullen,[6] "Photoelectron Dynamics of the Cooper Minimum in Free Molecules," Z. Physik D 2, 309 (1986).

T. A. Carlson, P. Gerard, M. O. Krause, F. A. Grimm,[4] and B. P. Pullen,[6] "Photoelectron Dynamics of the Valence Shells of Benzene as a Function of Photon Energy," J. Chem. Phys. (in press).

P. Gerard, M. O. Krause, and T. A. Carlson, "Photoelectron Study of the 4d Subshell of Atomic Tin Between 35 and 115 eV," Z. Physik D 2, 123 (1986).

M. O. Krause, P. Gerard, A. Fahlman,[7] T. A. Carlson, and A. Svensson,[3] "Photoeffect in the 5d, 6s and 6p Subshells of Atomic Lead Between 25 and 110 eV," Phys. Rev. A 33, 3146 (1986).

M. O. Krause, A. F. Starace,[8] J. A. R. Samson,[8] P. W. Langhoff,[9] A. C. Parr,[10] and B. Crasemann,[11] "Atomic and Molecular Science," Lawrence Berkeley Laboratory Report, PUB-5154, Dec. 1985, Section 3-1.

M. O. Krause, "Current Status and Future Directions of Atomic ESSR Studies," Austr. J. Phys. 39, 601 (1986).

M. O. Krause, A. Svensson,[3] A. Fahlman,[7] T. A. Carlson, and F. Cerrina,[5] "Autoionization Resonances in Atomic Ga, In, and Pb," Z. Physik D 2, 327 (1986).

M. O. Krause, P. Gerard, and A. Fahlman,[7] "Effects of the Admixed State on the Photoionization in the 6p Subshell of Pb," Phys. Rev. A 34, 4511 (1986).

B. H. McQuaide,[12] M. S. Banna,[12] P. Gerard, and M. O. Krause, "Photoelectron Spectrometry of Mercury in the 17 to 40 eV Photon-Energy Range," Phys. Rev. A 35, 1603 (1987).

T. M. Rosseel,[13] T. A. Carlson, R. E. Megri,[5] C. E. Beall,[5] and J. W. Taylor,[5] "Synchrotron Radiation as a Source for Quantitative X-Ray Photoelectron Spectroscopy: Advantages and Consequences," J. Vac. Soc. Tech. (in press).

Presentations

T. A. Carlson, "Photoelectron Dynamics of Molecules Using Synchrotron Radiation," Seminar at Chemistry Department, University of Western Ontario, March 14, 1986.

T. A. Carlson, "The Study of Preionization Resonances in the Core Shells of Molecules by Means of Angle-Resolved Electron Spectroscopy," Workshop on New Directions in Soft X-Ray Near Threshold Phenomena, Asilomar, CA, March 1-4, 1987.

T. A. Carlson, P. Gerard, B. P. Pullen,[6] F. A. Grimm,[4] and M. O. Krause, "Autoionization from the Lone Pair Orbitals of Molecules Containing Iodine," Gordon Research Conference on Electron Spectrometry, Wolfeboro, NH, July 1986.

T. A. Carlson, P. Gerard, M. O. Krause, B. P. Pullen,[6] and F. A. Grimm,[4] "Autoionization in Alkyl Iodides and Iodine," Users Meeting, Synchrotron Radiation Center, Stoughton, WI, Oct. 20-22, 1986.

P. Gerard, M. O. Krause, T. A. Carlson, B. McQuaide,[12] and M. S. Banna,[12] "Autoionization Resonances in the Hg-$6s^2$ Photoionization," Gordon Research Conference on Electron Spectrometry, Wolfeboro, NH, July 1986.

M. O. Krause, P. Gerard, T. A. Carlson, B. H. McQuaide,[12] and M. S. Banna,[12] "Autoionization Resonances in the Outer Regions of the Pb and Hg Atoms," Users Meeting, Synchrotron Radiation Center, Stoughton, WI, Oct. 1986.

M. O. Krause, "Present and Future Directions in ESSR Studies," US-Australian Joint Seminar — Workshop on Excited and Ionized States of Atoms and Molecules, Hobart, Tasmania, Feb. 2-7, 1986.

M. O. Krause, "Autoionization Resonances in Open-Shell Atoms," US-Australian Joint Seminar — Workshop on Excited and Ionized States of Atoms and Molecules, Hobart, Tasmania, Feb. 2-7, 1986.

M. O. Krause, "Autoionization Resonances in Open-Shell Atoms," Fourth Australian Conference on Atomic and Molecular Physics and Quantum Chemistry, University of Tasmania, Hobart, Australia, Jan. 28-31, 1986.

M. O. Krause, "Current Status and Future Directions of ESSR Studies of Atoms," Seminar at LURE and Physics Department of the Universite Paris-Sud, Orsay, France, Feb. 17, 1986.

M. O. Krause, "Trends in ESSR Studies of Atoms," VUV-8 International Conference in Lund, Sweden, Aug. 4-8, 1986.

M. O. Krause, "Future Capabilities Offered by Advanced Synchrotron Radiation Sources," Review at the Workshop on New Directions in Soft X-Ray Near Threshold Phenomena, Asilomar, CA, March 1-4, 1987.

M. O. Krause, "Electron Spectrometry with the Use of Synchrotron Radiation," Colloquium at the University of Central Florida, Orlando, FL, March 11, 1987.

G. VonWald,[5] T. A. Carlson, J. W. Taylor,[5] and F. A. Grimm,[4] "Gas Phase Photoelectron Dynamics of Core Level Ionization," Users Meeting, Synchrotron Radiation Center, Stoughton, WI, Oct. 20-22, 1986.

---

1. Instrumentation and Controls Division.
2. Chemistry Department, LaTrobe University, Bundoora, Australia.
3. Daresbury Laboratory, Warrington WA4 4AD, England.
4. University of Tennessee, Knoxville, TN.
5. University of Wisconsin, Madison, WI.
6. Southeastern Louisiana Univ., Hammon, LA.
7. Linkoping Institute of Technology, Linkoping, Sweden.
8. Department of Physics, University of Nebraska, Lincoln, NE.
9. Department of Chemistry, Indiana University, Bloomington, IN.
10. National Bureau of Standards, Gaithersburg, MD.
11. Physics Department, Univ. of Oregon, Eugene, OR.
12. Vanderbilt University, Nashville, TN.
13. Analytical Chemistry Division.

CHEMISTRY RELATED TO NUCLEAR WASTE DISPOSAL

Publications

J. G. Blencoe, Review and Assessment of DOE-Hanford Information on the Solubilities/Concentrations of Radionuclide-Analog Elements in the Systems — Simulated Waste Form ± Untanum Basalt + Grande Ronde Groundwater, NUREG/CR-4024, ORNL/TM-9415 (1987).

P. C. Ho and R. E. Meyer, A Review of the Organic Geochemistry of Shales, ORNL/CF-86/359 (1986).

P. C. Ho, R. E. Meyer, W. D. Arnold, and F. I. Case, Sorption of Np, U, Tc, Sr and Cs onto Shales, ORNL/CF-86/321 (1986).

A. D. Kelmers,[1] F. G. Seeley,[1] W. D. Arnold, J. G. Blencoe, R. E. Meyer, G. K. Jacobs,[2] and S. K. Whatley,[1] Progress in Evaluation of Radionuclide Geochemical Information Developed by DOE High-Level Nuclear Waste Repository Site Projects: Report for Jan-Mar 1985, NUREG/CR-4236, ORNL/TM-9614/V2.

A. D. Kelmers,[1] W. D. Arnold, J. G. Blencoe, R. E. Meyer, G. K. Jacobs,[2] and S. K. Whatley,[1] Progress in Evaluation of Radionuclide Geochemical Information Developed by DOE High-Level Nuclear Waste Repository Site Projects: Report for April-June 1985, NUREG/CR-4236, ORNL/TM-9614/V3.

R. E. Meyer, W. D. Arnold, J. G. Blencoe, G. K. Jacobs,[2] A. D. Kelmers,[1] F. G. Seeley,[1] and S. K. Whatley,[1] Progress in Evaluation of Radionuclide Geochemical Information Developed by DOE High-Level Nuclear Waste Repository Site Projects: Annual Report for Oct. 1984 - Sept. 1985, NUREG/CR-4236, ORNL/TM-9614/V4.

R. E. Meyer, W. D. Arnold, J. G. Blencoe, G. D. O'Kelley, F. I. Case, J. F. Land, and G. K. Jacobs,[2] Progress in Evaluation of Radionuclide Geochemical Information Developed by DOE High-Level Nuclear Waste Repository Site Projects: Semiannual Report for Oct. 1985-Mar. 1986, NUREG/CR-4708, ORNL/TM-1014/V1.

R. E. Meyer, W. D. Arnold, and F. I. Case, Valence Effects on Solubility and Sorption: The Solubility of Tc(IV) Oxides, NUREG/CR-4309, ORNL-6199 (1985).

R. E. Meyer, W. D. Arnold, and F. I. Case, The Solubility of Electrodeposited Tc(IV) Oxides, NUREG/CR-4865, ORNL-6374 (1987).

---

1. Chemical Technology Division.
2. Environmental Sciences Division.

HEURISTIC MODELING

Presentations

C. K. Johnson, "Artificial Intelligence Applications in Security Document Production," International Conference on Security Documents for the 21st Century, April 2, 1987, San Diego, CA.

C. K. Johnson, "Artificial Intelligence Research and Applications at ORNL," Association for Energy Systems Operations and Programming (AESOP) XXVII, Nov. 7, 1986, San Diego, CA.

C. K. Johnson, "Machine Intelligence Applications in Counterfeit Deterrence," Panel on Human Perception and Counterfeit Deterrence, Third Annual Document Security Conference (DOCSEC) '86, June 11, 1986, Washington, DC.

C. K. Johnson, "The ORNL/BEP Currency Flaw Survey and Flaw Severity Model," Workshop on Printing Flaw Standards for Machine Inspection, March 30, 1987, San Diego, CA.

SPECIAL TOPICS

Publications

E. Caponetti,[1] R. Triolo,[1] P. C. Ho, J. S. Johnson, Jr.,[2] L. J. Magid,[3] P. Butler,[3] and K. A. Payne,[3] "A Small Angle Neutron Scattering (SANS) Study of Micellar Structure and Growth of a Straight-Chain Benzene Sulfonate: Comparison with an Isomeric Branched Chain Surfactant," J. Coll. Interface Sci. 116, 200 (1987).

A. L. Compere, W. L. Griffith, and J. M. Googin,[4] "Stability and Composition of Palm, Coconut and Soy Oil Fatty Acid Microemulsion Diesel Fuels," pp. 355-360 in Alternative Energy Sources VII, Vol. D, ed. T. N. Veziroglu, Hemisphere Press, Inc., Washington, DC, 1986.

W. L. Griffith, J. M. Googin,[4] and A. L. Compere, "Effects of Alcohols, Ketones and Sodium Salts on the Extraction of 1-Butanol from Aqueous Solution by the Ethyl Ester of Soybean Oil Fatty Acids," Sep. Sci. and Tech. 22(2,3), 373 (1987).

W. L. Griffith, R. Triolo,[1] and A. L. Compere, "Analytical Structure Function of a Polydisperse Percus-Yevick Fluid with Schulz (Gamma) Distributed Diameters," Phys. Rev. A33, 2197 (1986).

W. L. Griffith, R. Triolo,[1] and A. L. Compere, "Analytical Scattering Function of a Polydisperse Percus-Yevick Fluid with Schulz (Gamma) Distributed Diameters," Phys Rev. A35, 2200 (1987).

P. C. Ho, "Photooxidation of 2,4-Dinitrotoluene in Aqueous Solution in the Presence of Hydrogen Peroxide," J. Environ. Sci. Tech. 20, 260 (1986).

P. C. Ho and J. B. Ramsey,[5] "Tetramethylammonium Perchlorate: Ion Size Parameters in Solution and in the Solid State," J. Chem. Eng. Data 31, 430 (1986).

P. C. Ho, "Evaluation of Ultraviolet Light/Oxidizing Agent as a Means for the Degradation of Toxic Organic Chemicals in Aqueous Solutions," in Proc. Recent Advances in the Management of Hazardous and Toxic Wastes in the Process Industries Intern. Congress, Vienna, March 1987, in press.

M. R. Patterson,[6] M. R. Ally,[7] J. Braunstein, and S. I. Kaplan,[7] Modeling of an Ideal Working Fluid for a Temperature-Amplifier Absorption Heat Pump, ORNL/TM-10360 (in press).

H. Perez-Blanco,[7] M. R. Patterson,[6] and J. Braunstein, Ideal Fluid Properties for Optimizing Absorption Heat Pump Performance, ORNL/TM-10315 (March 1987).

Presentations

P. C. Ho, "Evaluation of Ultraviolet Light/Oxidizing Agent as a Means for the Degradation of Toxic Organic Chemicals in Aqueous Solutions," Intern. Congress on Recent Advances in the Management of Hazardous and Toxic Waste in the Process Industries, Vienna, Austria, March 8-13, 1987.

---

1. Instituto Chimica Fisica, University of Palermo, Palermo, Italy.
2. Consultant, Chemistry Division.
3. Department of Chemistry, University of Tennessee, Knoxville, TN.
4. Y-12 Development Division.
5. Deceased; formerly Professor of Chemistry, University of California, Los Angeles.
6. Computing and Telecommunications Division.
7. Energy Division.

DIVISIONAL STAFFING AND FINANCIAL SUMMARY
FY 1986

Funding source	Financial plan ($K)	Direct scientific and technical staff (full-time equivalents)
DOE PROGRAMS		
Basic Energy Sciences		
Nuclear Sciences	1165	5.2
Materials Sciences	2191	14.1
Chemical Sciences	3399	23.8
Geosciences	528	3.5
Conservation	134	1.0
Defense Waste	85	0.7
Geothermal	69	0.5
TOTAL DOE PROGRAMS	7571	48.8
WORK FOR OTHERS PROGRAMS		
Nuclear Regulatory Commission	722	5.8
Department of Treasury	580*	1.0
University of Tennessee	206*	
Department of Defense	64*	
TOTAL WORK FOR OTHERS	1572	6.8
TOTAL PROGRAMS	9143	55.6

Divisional staff	Number (full-time equivalents)
Scientific and technical	
Direct	55.6
Indirect	2.7
On loan to other Divisions and institutions	7.0
Support	8.5
TOTAL	73.8

*Significant subcontracting component

CHEMISTRY DIVISION

May 1, 1987

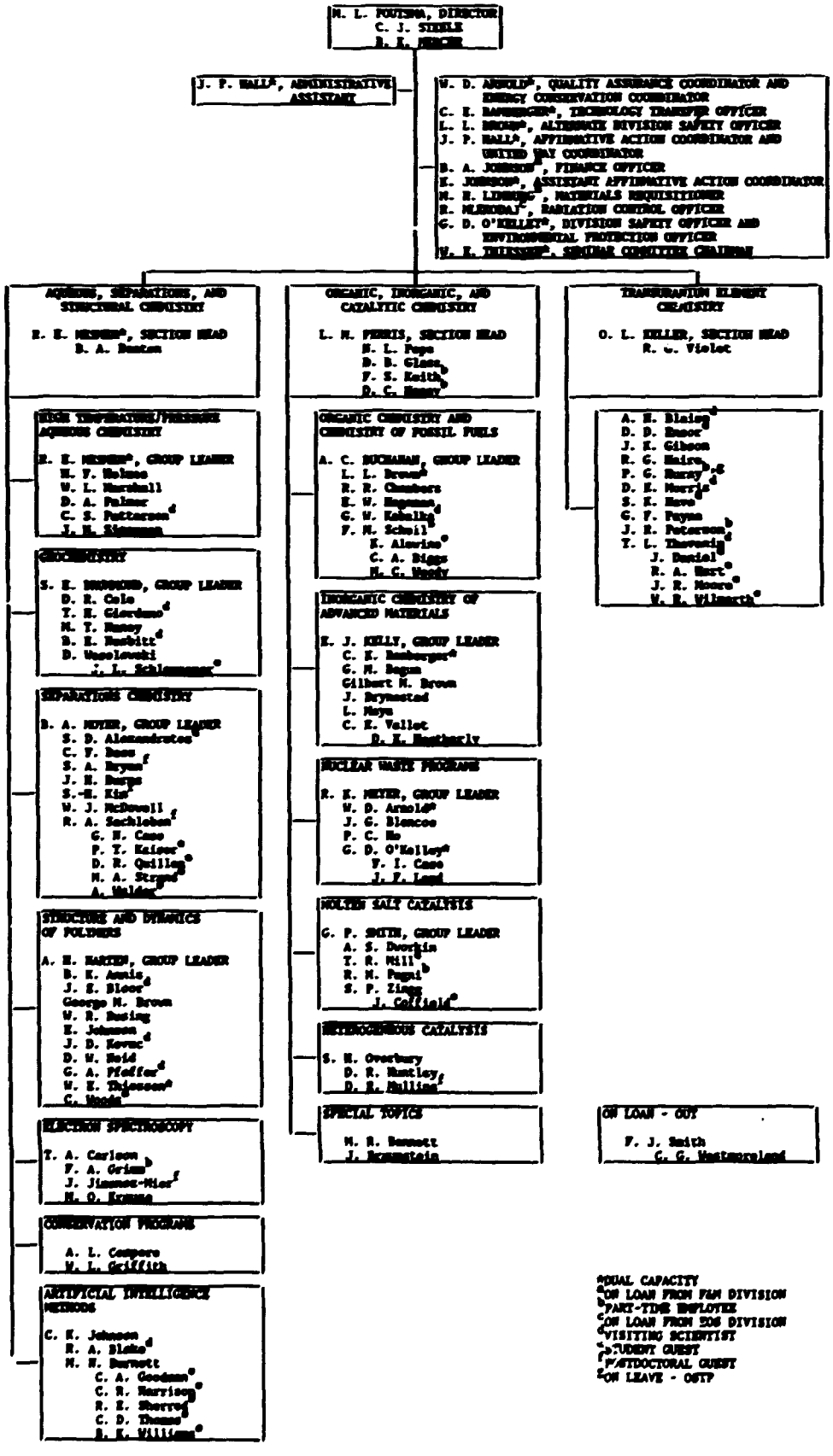

[a]DUAL CAPACITY
[b]ON LOAN FROM F&M DIVISION
[c]PART-TIME EMPLOYEE
[d]ON LOAN FROM ESH DIVISION
[e]VISITING SCIENTIST
[f]STUDENT GUEST
[g]POSTDOCTORAL GUEST
[h]ON LEAVE - OSTP

ORNL-6385
Distribution Category UC-4

INTERNAL DISTRIBUTION

1. Biology Library
2-3. Central Research Library
4. Laboratory Shift Supervisor
5. ORNL-Y-12 Technical Library
Document Reference Section
6-8. Laboratory Records Department
9. Laboratory Records, ORNL R.C.
10-12. Technical Publications Department, ORNL
13. T. D. Anderson
14. B. R. Appleton
15. J. T. Atherton
16. J. B. Ball
17-18. V. B. Baylor
19. A. C. Buchanan
20. R. S. Carlsmith
21. T. A. Carlson
22. S. E. Drummond
23. B. G. Eads
24-28. L. M. Ferris
29. J. R. Hightower
30. D. W. Jared
31-35. O. L. Keller, Jr.
36. F. C. Maienschein
37. A. P. Malinauskas
38-42. R. E. Mesmer
43. R. E. Meyer
44. B. A. Moyer
45. A. H. Marten
46. S. H. Overbury
47. D. C. Parzyck
48-148. M. L. Poutsma
149. D. E. Reichle
150. C. R. Richmond
151. W. D. Shults
152. G. P. Smith
153. E. J. Soderstrom
154. V. J. Tennery
155. B. J. Williams
156. R. G. Wymer
157. A. Zucker

EXTERNAL DISTRIBUTION

158. F. L. Culler, Office of the President, Electric Power Research Institute, P. O. Box 10412, 3412 Hillview Avenue, Palo Alto, CA 94303
159. J. R. Peterson, Department of Chemistry, University of Tennessee, Knoxville, TN 37916
160. P. L. Johnson, Executive Director, Oak Ridge Associated Universities, P. O. Box 117, Oak Ridge, TN 37831
161. L. C. Ianniello, Office of Basic Energy Sciences, DOE, Washington, DC 20545
162. A. H. Peters, Director, Savannah River Laboratory, Aiken, SC 29801
163. D. A. Shirley, Director, LBL, Berkeley, CA 94720
164. E. Steinberg, Chemistry Division, ANL, 9700 South Cass Avenue, Argonne, IL 60439
165. A. Wolf, Chairman, Chemistry Department, BNL, Upton, NY 11973
166. Gleb Mamantov, Head, Chemistry Department, University of Tennessee, Knoxville, TN 37916
167. M. J. Steindler, Chemical Technology Division, ANL, 9700 South Cass Avenue, Argonne, IL 60439
168. C. J. Hardy, Australian Atomic Energy Commission, Lucas Heights, Sydney, Australia
169. John L. Burnett, Division of Chemical Sciences, Office of Basic Energy Sciences, DOE, Washington, DC 20545
170. Office of Assistant Manager for Energy Research and Development, DOE-ORO
171. Harry B. Gray, Gates and Crellin Laboratories of Chemistry, California Institute of Technology, Pasadena, CA 91125
172. A. Schriesheim, Director, ANL, 9700 South Cass Avenue, Argonne, IL 60439
173. F. D. Stevenson, Division of Chemical Sciences, Office of Basic Energy Sciences, DOE, GTN, Washington, DC 20545
174. G. A. Kolstad, Division of Engineering and Geosciences, Office of Basic Energy Sciences, DOE, Washington, DC 20545
175. Oak Ridge Associated Universities, MERT Division Library, P. O. Box 117, Oak Ridge, TN 37831
176. R. S. Marianelli, Division of Chemical Sciences, Office of Basic Energy Sciences, DOE, GTN, Washington, DC 20545
177. Director, Office of Basic Energy Sciences, DOE, Washington, DC 20545
178. A. Laufer, Division of Chemical Sciences, Office of Basic Energy Sciences, DOE, Washington, DC 20545
179. J. W. Nehls, DOE-ORO, Oak Ridge, TN 37831
180. I. L. Thomas, Division of Materials Sciences, Office of Basic Energy Sciences, DOE, GTN, Washington, DC 20545

181. D. L. Hildenbrand, SRI International, 333 Ravenswood Ave., Menlo Park, CA 94025
182. Beth Jinkerson, Oak Ridge Associated Universities, University Programs Division, P. O. Box 117, Oak Ridge, TN 37831
183. J. S. Coleman, Division of Engineering, Mathematical and Geosciences, Office of Basic Energy Sciences, DOE, Washington, DC 20545
184. R. Hirsch, Division of Chemical Sciences, Office of Basic Energy Sciences, DOE, GTN, Washington, DC 20545
185. D. M. Chapman, Union Carbide Corporation, Old Saw Mill River Road, Tarrytown, NY 10591
186. R. Kelley, Division of Chemical Sciences, Office of Basic Energy Sciences, DOE, Washington, DC 20545
187. C. Gilbert, Division of Engineering and Geosciences, Office of Basic Energy Sciences, DOE, Washington, DC 20545
188. T. Cooper, 234-5 Bldg., 200 West Area, Rockwell Hanford Operations, Richland, WA 99352
189-268. John Haffey, Office of Information Services, Oak Ridge Associated Universities, P. O. Box 117, Oak Ridge, TN 37831
269-371. Given distribution as shown in TID-4500 under Chemistry Category (25 copies - NTIS).